HELLENIC REPUBLIC
UNIVERSITY OF IOANNINA
SCHOOL OF SCIENCES
DEPARTMENT OF MATERIALS SCIENCE AND ENGINEERING

Development of a methodology for evaluating the structural integrity of reinforced concrete elements and other building materials

ANASTASIOS C. MPALASKAS
DIPL. CIVIL ENGINEER

Thesis for the degree of
DOCTOR OF PHILOSOPHY

IOANNINA 2016

ΕΛΛΗΝΙΚΗ ΔΗΜΟΚΡΑΤΙΑ
ΠΑΝΕΠΙΣΤΗΜΙΟ ΙΩΑΝΝΙΝΩΝ
ΣΧΟΛΗ ΘΕΤΙΚΩΝ ΕΠΙΣΤΗΜΩΝ
ΤΜΗΜΑ ΜΗΧΑΝΙΚΩΝ ΕΠΙΣΤΗΜΗΣ ΥΛΙΚΩΝ

Ανάπτυξη μεθοδολογίας για την αξιολόγηση της δομικής ακεραιότητας στοιχείων από οπλισμένο σκυρόδεμα και άλλα δομικά υλικά

ΑΝΑΣΤΑΣΙΟΣ Χ. ΜΠΑΛΑΣΚΑΣ
ΔΙΠΛ. ΠΟΛΙΤΙΚΟΣ ΜΗΧΑΝΙΚΟΣ

ΔΙΔΑΚΤΟΡΙΚΗ ΔΙΑΤΡΙΒΗ

ΙΩΑΝΝΙΝΑ 2016

«Η έγκριση της διδακτορικής διατριβής από το Τμήμα Μηχανικών Επιστήμης Υλικών της Σχολής Θετικών Επιστημών του Πανεπιστημίου Ιωαννίνων δεν υποδηλώνει αποδοχή των γνωμών του συγγραφέα Ν. 5343/32, άρθρο 202, παράγραφος 2».

Application date of Mr Anastasios Mpalaskas: 14/02/2008
Designation date of the three member advising committee: 28/05/2008
Advising committee:
Supervisor
Theodore Matikas, Professor at the Department of Materials Science and Engineering, University of Ioannina
Members
Alkiviadis Paipetis, Professor at the Department of Materials Science and Engineering, University of Ioannina
Haris Apostolopoylos, Assistant Professor at the Department of Mechanical Engineering and Aeronautics, University of Patra

Designation date of thesis subject: 28/05/2008

Develop a methodology for evaluating the structural integrity of reinforced concrete elements

Designation date of modified thesis subject: 30/03/2016

Develop a methodology for evaluating the structural integrity of reinforced concrete elements and other building materials

Designation date of the seven member examining committee:07/10/2015

Theodore Matikas	Professor at the Department of Materials Science and Engineering, University of Ioannina
Alkiviadis Paipetis	Professor at the Department of Materials Science and Engineering, University of Ioannina
Haris Apostolopoylos	Assistant Professor at the Department of Mechanical Engineering and Aeronautics, University of Patra
Aggelis Dimitris	Professor at the Department of Mechanics of Materials and Constructions Vrije Universiteit Brussel
Nektaria-Marianthi Barkoula	Assistant Professor at the Department of Materials Science and Engineering, University of Ioannina
Konstantinos Dassios	Assistant Professor at the Department of Materials Science and Engineering, University of Ioannina
Leonidas Gergidis	Assistant Professor at the Department of Materials Science and Engineering, University of Ioannina

Doctor of philosophy certificate awarded with «HONOURS» on: 05/04/2016

Head of the Materials Science Engineering Department of the College of Sciences and Technologies:

Department Secretariat

Karakassides Michael
Professor

Xanthi Toutountzoglou

Ημερομηνία αίτησης της/του κ. Μπαλάσκα Αναστάσιου: 14/02/2008
Ημερομηνία ορισμού Τριμελούς Συμβουλευτικής Επιτροπής: 28/05/2008
Μέλη Τριμελούς Συμβουλευτικής Επιτροπής:
Επιβλέπων
Θεόδωρος Ματίκας, Καθηγητής Τμήματος Μηχανικών Επιστήμης των Υλικών του Πανεπιστημίου Ιωαννίνων
Μέλη
Αλκιβιάδης Παϊπέτης, Καθηγητής Τμήματος Μηχανικών Επιστήμης των Υλικών του Πανεπιστημίου Ιωαννίνων
Χάρης Αποστολόπουλος, Επίκουρος Καθηγητής Τμήματος Μηχανολόγων Μηχανικών και Αεροναυπηγικής Π. Πατρών

Ημερομηνία ορισμού θέματος: 28/05/2008

Ανάπτυξη μεθοδολογίας για την αξιολόγηση της δομικής ακεραιότητας στοιχείων από οπλισμένο σκυρόδεμα

Ημερομηνία τροποποίησης θέματος: 30/03/2016

Ανάπτυξη μεθοδολογίας για την αξιολόγηση της δομικής ακεραιότητας στοιχείων από οπλισμένο σκυρόδεμα και άλλα δομικά υλικά

ΗΜΕΡΟΜΗΝΙΑ ΔΙΟΡΙΣΜΟΥ ΕΠΤΑΜΕΛΟΥΣ ΕΞΕΤΑΣΤΙΚΗΣ ΕΠΙΤΡΟΠΗΣ:07/10/2015

Ματίκας Θεόδωρος	Καθηγητής Τμήματος Μηχανικών Επιστήμης των Υλικών του Πανεπιστημίου Ιωαννίνων
Παϊπέτης Αλκιβιάδης	Καθηγητής Τμήματος Μηχανικών Επιστήμης των Υλικών του Πανεπιστημίου Ιωαννίνων
Αποστολόπουλος Χάρης	Επίκουρος Καθηγητής Τμήματος Μηχανολόγων Μηχανικών και Αεροναυπηγικής Π. Πατρών
Αγγέλης Δημήτριος	Καθηγητής Τμήματος Μηχανικών Υλικών και Κατασκευών Vrije Universiteit Brussel
Μπάρκουλα Νεκταρία-Μαριάνθη	Επίκουρη Καθηγήτρια Τμήματος Μηχανικών Επιστήμης των Υλικών του Πανεπιστημίου Ιωαννίνων
Δάσσιος Κωνσταντίνος	Επίκουρος Καθηγητής Τμήματος Μηχανικών Επιστήμης των Υλικών του Πανεπιστημίου Ιωαννίνων
Γεργίδης Λεωνίδας	Επίκουρος Καθηγητής Τμήματος Μηχανικών Επιστήμης των Υλικών του Πανεπιστημίου Ιωαννίνων

Έγκριση Διδακτορικής Διατριβής με βαθμό «ΑΡΙΣΤΑ» στις: 05/04/2016

Πρόεδρος του Τμήματος Μηχανικών Επιστήμης Υλικών της Σχολής Επιστημών & Τεχνολογιών

Η Γραμματέας του Τμήματος

Καρακασίδης Μιχαήλ
Καθηγητής

Ξανθή Τουτουνζόγλου

TO MY FAMILY

Περίληψη

Οι κατασκευές από Σκυρόδεμα αποτελούν τη βάση του σύγχρονου τεχνικού πολιτισμού. Υποστηρίζουν τις συγκοινωνίες, την αποθήκευση πρώτων υλών και προϊόντων και προσφέρουν κατάλυμα σε ανθρώπους σε ευρεία κλίμακα. Η άποψη ότι οι κατασκευές από οπλισμένο σκυρόδεμα παρουσιάζουν υψηλή ανθεκτικότητα στο χρόνο έχει εγκαταλειφθεί προ πολλού. Είναι κατασκευές οι οποίες υπόκεινται σε συνθέτες καταπονήσεις λόγω: μακροχρόνιας φόρτισης από το ίδιο βάρος, δυναμικών σεναρίων φόρτισης συμπεριλαμβανομένων των σεισμών, καθώς και υποβάθμισης της δομικής ακεραιότητας λόγω περιβαλλοντικών συνθηκών. Οι κατασκευές από σκυρόδεμα πρέπει να υποβάλλονται σε επιθεώρηση και αξιολόγηση της κατάστασης της δομικής τους ακεραιότητας, ενώ θα πρέπει παράλληλα να προτείνονται κατάλληλες ενέργειες συντήρησης. Για να παραταθεί η ωφέλιμη διάρκεια ζωής τους, θα πρέπει να εφαρμόζεται μια αξιόπιστη μεθοδολογία παρακολούθησης της εναπομένουσας αντοχής και γενικότερα της δομικής ακεραιότητας των επιμέρους δομικών στοιχείων. Αρχικά βασικές πληροφορίες της μηχανικής τους απόδοσης εξάγονται από την οπτική επιθεώρηση, ωστόσο, αυτές αφορούν μόνο τις επιφανειακές ενδείξεις αποσάθρωσης και αστοχιών. Οι βλάβες μπορεί να ξεκινούν την εμφάνιση τους από το εσωτερικό του εκάστοτε δομικού στοιχείου για το λόγο αυτό και η αξιολόγηση της δομικής ακεραιότητας που βασίζεται μόνο στην οπτική επιθεώρηση είναι ατελής και πρόχειρη. Η ακουστική εκπομπή (AE) είναι εκείνη από τις μεθοδολογίες μη καταστρεπτικού ελέγχου που αξιολογούν τον πλήρη όγκο της δομής, η οποία έχει αρχίσει να εφαρμόζεται σε ευρεία βάση. Η (AE) είναι μια παθητική τεχνική μη καταστροφικής αξιολόγησης (NDE), που προσφέρει ιδιαίτερα πλεονεκτήματα, όπως η σε πραγματικό χρόνο παρακολούθηση της προόδου της βλάβης, η οποία είναι σε θέση να επιτρέπει τον χαρακτηρισμό του κρίσιμου χρόνου για την δομή σε σχέση με το εφαρμοζόμενο λειτουργικό φορτίο.

Ο στόχος της παρούσας διατριβής είναι η ανάπτυξη και εφαρμογή μιας νέας μεθοδολογίας συνδυασμού τεχνικών NDE, ειδικότερα της ακουστικής εκπομπής (AE) και των υπερήχων (Ultrasound Pulse Velocity UPV), για την αξιολόγηση και την παρακολούθηση της βλάβης που προκαλείται στα στοιχεία της δομής. Η πρόβλεψη της υπολειπόμενης διάρκειας ζωής μιας δομής επικουρείται από τον

χαρακτηρισμό του είδους θραύσης. Ανάλογα με τον τύπο θραύσης παρατηρείται διαφορετική κίνηση των πλευρών της ρωγμής κατά την δημιουργία της βλάβης, με συνέπεια η ελαστική ενέργεια που εκπέμπεται να παράγει κυματομορφές με διαφορετικά χαρακτηριστικά, οι οποίες καταγράφονται από τους αισθητήρες ακουστικής εκπομπής και αναλύονται ως προς την συχνότητά καθώς και άλλες παραμέτρους. Με αυτόν τον τρόπο επιτυγχάνεται ο προσδιορισμός του είδους θραύσης στα δομικά υλικά, χρησιμοποιώντας ελαστικές κυματικές μεθόδους. Τέλος, αναπτύσσεται μια καινοτόμος μεθοδολογία για τη διερεύνηση της βλάβης (τεχνητή και φυσική) σε δομικά στοιχεία με βάση το τσιμέντο, χρησιμοποιώντας ελαστικές κυματικές μη καταστρεπτικές μεθόδους .

Abstract

Concrete structures are the basis of contemporary technical civilization. They support transportation, storage of goods and shelter humans in large numbers. Despite their endurance, they have ceased to be considered as maintenance-free. They are subject to long-term loading due to own weight, dynamic loading scenarios including earthquakes, as well as environmental degradation. Concrete structures need to undergo inspection and evaluation of their health condition while proper maintenance actions should be proposed. In order to prolong their useful life span, a robust monitoring methodology should be applied. The first and basic information is extracted from visual inspection. However, this concerns only the surface distress indications. Defects may start to grow from the interior and therefore, an assessment based solely on visual observation would not be complete. Among monitoring methodologies that assess the full volume of the structure, acoustic emission (AE) has started to be applied in a wide basis. AE is a passive nondestructive evaluation (NDE) technique that offers specific advantages like real time monitoring of defects propagation, which enables to characterize the critical moments of the structure in relation to the applied operational load.

The objective of this thesis is the development and application of a novel methodology with NDE techniques, especially acoustic emission (AE) and ultrasonic (Ultrasound Pulse Velocity UPV), for the evaluation and monitoring of induced damage in the elements of the structure. The prediction of the remaining life of a structure can be assisted by the characterization of the current cracking mode. Usually, tensile phenomena precede shear fracture. Due to the different movement of the crack sides according to the dominant mode, the emitted elastic energy possesses waveforms with different characteristics. These are captured by acoustic emission sensors and analyzed for their frequency content and waveform parameters.

Therefore, identification of the mode of fracture in building materials using elastic wave methods has been achieved. Finally, an innovative methodology for damage investigation cement-based structural elemens, using elastic wave approaches has been developed.

Acknowledgements

Firstly, I would like to express my sincere gratitude to my advisor Theodore Matikas Professor of the Materials Science Engineering (MSE) Department, for the continuous support of my PhD study and related research, for his patience, motivation, and immense knowledge. His guidance helped me in all the time of research and writing of this thesis. I could not have imagined having a better advisor and mentor for my PhD study. Without his continuous encouragement and endless support, this thesis would not have been completed and I would be more than glad to continue working in his team.

I wish to thank Alkiviadis Paipetis, Professor of MSE for being a member of the advisory committee. I am grateful for his insightful comments, his encouragement and potent guidance during the conduction of my study.

I wish to thank Haris Apostolopoulos, Assistant Professor at the Dept of Mechanical Engineering and Aeronautics, University of Patras for being a member of my advisory committee. I am thankful for his help and support in as many ways as possible during my studies

I wish to thank Aggelis Dimitris Professor at the Department of Mechanics of Materials and Constructions VUB for being a member of the committee. Without his continuous encouragement, guidance and endless support, this thesis would not have been completed. Except for our scientific collaboration, a friendship was born escorting our collaboration for the past 5 years.

I wish to thank Nektaria-Marianthi Barkoula, Assistant Professor, of MSE for being a member of the committee. I am thankful for her help and support in as many ways as possible during my studies.

I wish to thank Konstantinos Dassios, Assistant Professor, of MSE for being a member of the committee. I am thankful for his help and support.

Furthermore, I would like to thank Leonidas Gergidis Assistant Professor of MSE,

for being a member of the committee.

Working in “Mechanics, Smart Structures & NDE” laboratory, I have been assisted in many ways by my colleagues. First and foremost, I am more than thankful to Exarchos Dimitris, an efficient PhD researcher and “master” in the field of thermography.

To continue, many thanks to all of the rest of my colleagues and friends Dr. Evangelos Kordatos, Dr. Dimitra Soulioti, Eftymis Tatsis, Anna Tsoumani, Panagiwta Aikaterinh Dalla, Panagiwta Alafogiannh, Hlias Tragazikhs, Doti Kordatoy, Sotirhs Grammatikos, Nikolaos Vlachas, Dimosthenhs Paterousis, Ioannhs Papastayros, Evi Aggelh, Nikolaos Zwidis.

Last but not least, I wish to thank my family members, my parents Christos and Panagiwta as well as my brother Dimitris. They have been helping me and supporting me in many ways. They kept providing me all the psychological and financial support in order to achieve the maximum in my life.

Τέλος, ένα πολύ μεγάλο ευχαριστώ στην οικογένεια μου, στους γονείς μου Χρήστο και Παναγιώτα και στον αδερφό μου Δημήτρη, που με την αδιάλειπτη συμπαράσταση, υποστήριξη και κυρίως την κατανόηση τους σε ηθικό αλλά και υλικό επίπεδο μου δίνουν δύναμη και πυγμή ώστε να ανταπεξέρχομαι και να αποδίδω τα μέγιστα σε ότι πραγματεύομαι.

TABLE OF CONTENTS

TABLE OF FIGURES

ΚΑΤΑΛΟΓΟΣ ΠΙΝΑΚΩΝ

Chapter 1. Introduction

1.1. Introduction - Overview

Nondestructive evaluation methods are a wide group of analysis techniques used in science and industry to evaluate the properties of a material, component or system without causing damage [1].

The aim of the current thesis is the development and use of a methodology with NDE techniques especially acoustic emission (AE) and ultrasonics (Ultrasound Pulse Velocity UPV) for the evaluation and monitoring of induced damage in the elements of the structure.

The process of implementing a damage detection and characterization strategy for engineering structures is referred to as Structural Health Monitoring (SHM) [2]. The SHM process involves the observation of a system over time using periodically sampled dynamic response measurements from an array of sensors, the extraction of damage-sensitive features from these measurements, and the statistical analysis of these features to determine the current state of the system's health. For long-term SHM, the output of this process is periodically updated information regarding the ability of the structure to perform its intended function in light of the inevitable aging and degradation resulting from operational environments. After extreme events, such as earthquakes or blast loading, SHM is used for rapid condition screening and aims to provide, in near real time, reliable information regarding the integrity of the structure [3].

Reinforced concrete (RC) structures are no longer maintenance free. Especially, damage due to salt attack in RC structures is considered to be one of the most critical deteriorations in concrete engineering. In the concrete structures, reinforcing steel-bars (rebars) normally do not corrode because of a passive film nucleated on the surface of rebar in concrete of high PH. When chloride concentration at the level of rebar in concrete, however, exceeds the threshold value for corrosion, the passive film is destroyed and corrosion is initiated in rebar. The electro-chemical reaction continues with supplying oxygen and water. Then, due to expansion of corrosion products, corrosion-induced cracks are generated in concrete. Accordingly, development of non-destructive evaluation (NDE) techniques for detection of the corrosion in RC structures at early stage is urgently important. So far, electrochemical techniques of half-cell potential and polarization resistance are widely employed. These techniques estimate corroded conditions of rebars from electrical data [4]. The phenomenon evolution period (steel corrosion) associates with apparent increase in steel volume and loss of bonding (thus increasing the local component deformations or even their deflection etc.). It is possible to detect (ie record and evaluate) the development period of the phenomenon of corrosion by the acoustic emission sensors

The AE technique has been widely used in the field of civil engineering for monitoring of corrosion. The advantage of the AE technique is that can be used without intruding into any of the processes associated with the Reinforced concrete structures [5]. There are two different approaches in analyzing AE data, one is the classical or parameter-based AE technique and the second is the quantitative or signal-based AE technique [6,7]

As far as the parameter- based AE technique AE hits is one of the most crucial AE parameters used to study the onset of corrosion and the nucleation of crack in Reinforced concrete structures [8,11]. Yoon et al. [8] carried out AE monitoring in Reinforced concrete beams subjected to four different degrees of corrosion. It was observed that AE hits increased with an increase in the degree of corrosion. This trend could provide important information for estimating the degree of corrosion. Ohtsu and Tomoda [11,12] investigated AE hits of Reinforced concrete specimens in sodium chloride (NaCl) concentration. Corresponding to two high AE activities, two periods of onset of corrosion and nucleation of cracks were observed [5].

The results of the current thesis will be presented in the form of different research works witch discuss: First the identification of the mode of fracture in different building materials using elastic wave methods and second the effect of artificial damage in the form of nearly spherical expanded PS inclusion and real damage in the form of fire on the mechanical and combined elastic wave behavior in cement based elemens. Thus the current thesis includes the following chapters:

Part A of the thesis **which includes Chapters 2,3 and 4** thesis concern with the identification of the mode of fracture in building materials using elastic wave methods. The fracturing behavior of materials can be nondestructively monitored by the acoustic emission (AE) technique, using sensors that detect the transient elastic waves after any crack propagation event. In addition to the information relatively to the total activity and the location of the cracks, certain waveform features supply detailed information on the type of cracking. The waveform of the emitted AE signal depends on the relative motion of the crack sides and therefore, it carries information on the mode of cracks. Therefore, AE is used for classification of the active cracking mode. This enables characterization of the current fracturing condition within the material and warning before final failure.

Chapter 2 is adapted from "Effect of wave distortion on acoustic emission characterization of cementitious materials", published in Construction and Building Materials, Volume 35, October 2012, Pages 183-190

This Chapter deals with the effect of wave distortion on acoustic emission characterization in cementitious materials. In most cases wave propagation from the crack to the sensor is attenuative and dispersive. This results in signal distortion which is enhanced by geometry restrictions and material or damage-induced inhomogeneity. This results in strong change of the waveform shape and the calculated AE parameters. This effect is stronger as the propagation distance increases rendering crack classification troublesome for structures where the separation distance between sensors is long. In the present study, fracture experiments were conducted in cementitious specimens in order to investigate the influence of distance on the AE parameters as measured by sensors at different distances from the source. Numerical simulations based on the finite difference method are also used to enlighten the problem and expand to different material conditions..

Chapter 3 deals with the determination of fracture mechanism under Flexural load in building materials

The 3.1 Section adapted from "Investigation of different fracture modes in cement-based materials by acoustic emission" published in Cement and Concrete Research, Volume 48, June 2013, Pages 1-8

In this section fracture experiments on cementitious specimens (mortar) are conducted. The fracture mode is controlled by modifying the experiment geometry and the process is monitored by acoustic emission. The distinct signature of the cracking modes is reflected on acoustic waveform parameters like the amplitude, RA-value and peak frequency.

The 3.2 Section adapted from "Acoustic emission signatures of damage modes in concrete" Proc. SPIE 9062, Smart Sensor Phenomena, Technology, Networks, and Systems Integration 2014, 90620P (22 April 2014); doi: 10.1117/12.2044750, ISBN 9780819499882.

In this section fracture experiments on concrete beams are conducted. The aim is to examine the typical acoustic signals emitted by different fracture modes (namely tension due to bending and shear) in a concrete matrix.

The 3.3 Section adapted from "Acoustic signature of different fracture modes in marble and cementitious materials under flexural load" published in Mechanics Research Communications, Volume 47, January 2013, Pages 39-43

This section deals with the examination of the acoustic emission signatures of distinct fracture modes. Tensile and mixed mode cracking is excited in specimens of marble and cement mortar and the acoustic emission behavior is monitored and compared.

The 3.4 Section adapted from "Acoustic emission signatures of damage modes in structural materials" Proc. SPIE 8694, Nondestructive Characterization for Composite Materials, Aerospace Engineering, Civil Infrastructure, and Homeland Security 2013, 86940T (16 April 2013); doi: 10.1117/12.2008942

Again in this section Acoustic emission signatures of different fracture modes are examined. The building materials tested and compared this time are cement mortar, as a material with microstructure, and granite as representative of more homogeneous materials. The goal is to check the typical acoustic signals emitted by different modes as well as to estimate the effect of microstructure in the emitted wave as it propagates from the source to the receivers.

The 3.5 Section adapted from "Acoustic signatures of different damage modes in plain and repaired granite specimens" Proc. SPIE 9439, Smart Materials and

Nondestructive Evaluation for Energy Systems 2015, 94390L (March 27, 2015); doi:10.1117/12.2085040

In this section bending and shear fracture experiments on healthy and adhesively repaired granite samples with concurrent acoustic emission (AE) monitoring are discussed.

Chapter 4 is adapted from "Monitoring of the fracture mechanisms induced by pull-out and compression in concrete" Engineering Fracture Mechanics, Volume 128, September 2014, Pages 219-230

This Chapter deals with the study of the mechanism of fracture induced by Pull- Out and Compression in concrete.

More specifically acoustic emission (AE) is applied during both compression and pull-out experiments on concrete cubes. Results show that the two damage modes emit different AE signatures, with compression leading to higher frequencies and pull-out to longer signal durations, while the finite element method (FEM) is used to analyze the stress field.

The **Part B** of the thesis which includes **Chapters 5 and 6** expands on the use of damage investigation of Cement – based Elements applying elastic wave approaches.

Chapter 5 is adapted from "Mechanical and fracture behavior of cement-based materials characterized by combined elastic wave approaches" Construction and Building Materials, Volume 50, 15 January 2014, Pages 649-656

This Chapter deals with the effect of artificial damage in the form of nearly spherical expanded PS inclusion in the mechanical and fracture properties of cementitious material (mortar). Different volume contents of light nearly-spherical grains are included to simulate micro-cracking that could be the result of thermal damage. Nondestructive monitoring techniques are applied in an effort to establish or improve correlations with the simulated damage content and the failure load. Specifically, the specimens are ultrasonically interrogated before fracture, while during fracture their behavior is monitored by acoustic emission.

Chapter 6 deals with the mechanical behavior of concrete after extensive thermal damage. After being exposed to direct fire action at temperatures of 700^{o}C and 850^{o}C, specimens were subjected to bending and compression in order to determine the loss of strength and stiffness in comparison to intact specimens. Nondestructive monitoring techniques were also applied in the form of ultrasonics (i.e. ultrasonic pulse velocity, UPV) and acoustic emission (AE).

Chapter 7 deals with the mechanical behavior of Reinforced concrete after extensive thermal damage. After being exposed to direct fire action at temperatures of 700^{o}C and 850^{o}C, specimens were not been able to subject to bending and compression in order to determine the loss of strength and stiffness in comparison to intact specimens, because of extensive damage in the shape of the fired damaged specimens. The Nondestructive monitoring techniques were not been able to apply too because of extensive damage in the shape of the fired damaged specimens.

Final conclusions and suggestions for future work are presented in the **8th Chapter**.

1.2. Reference

[1] Cartz, Louis (1995). Nondestructive Testing. A S M International. ISBN 978-0-87170-517-4.

[2] Dawson, Brian (1976). "Vibration condition monitoring techniques for rotating machinery". The Shock and Vibration Digest (London: SpingerLink) 8 (12): 3. Doi: 10.1177/058310247600801203.

[3] A Review of Structural. Health Monitoring Literature: 1996–2001. LA-13976-MS:5

[4] Yuma Kawasaki a,*, Yuichi Tomoda b, Masayasu Ohtsu c ,AE monitoring of corrosion process in cyclic wet–dry test, Construction and Building Materials, Volume 24, Issue 12, December 2010, Pages 2353–2357

[5] Ahmad Zaki,1 Hwa Kian Chai,1,* Dimitrios G. Aggelis,2 and Ninel Alver3, Non-Destructive Evaluation for Corrosion Monitoring in Concrete: A Review and Capability of Acoustic Emission Technique, Sensors (Basel). 2015 Aug; 15(8): 19069–19101.

[6] Ohno, K.; Ohtsu, M. Crack classification in concrete based on acoustic emission. Constr. Build. Mater. 2010, 24, 2339–2346

[7] Shiotani, T.; Ohtsu, M.; Ikeda, K. Detection and evaluation of AE waves due to rock deformation. Constr. Build. Mater. 2001, 15, 235–246..

[8] Yoon, D.J.; Weiss, W.J.; Shah, S.P. Assessing damage in corroded reinforced concrete using acoustic emission. J. Eng. Mech. 2000, 126, 273–283.

[9] Kawasaki, Y.; Wakuda, T.; Kobarai, T.; Ohtsu, M. Corrosion mechanisms in reinforced concrete by acoustic emission. Constr. Build. Mater. 2013, 48, 1240–1247.

[10] Kawasaki, Y.; Tomoda, Y.; Ohtsu, M. AE monitoring of corrosion process in cyclic wet–dry test. Constr. Build. Mater. 2010, 24, 2353–2357. Sensors 2015, 15 19100

[11] Ohtsu, M.; Tomoda, Y. Acoustic emission techniques for rebar corrosion in reinforced concrete. In Advances in Construction Materials 2007; Springer-Verlag: Berlin, Germany, 2007.

[12] Ohtsu, M.; Tomoda, Y. Phenomenological model of corrosion process in reinforced concrete identified by acoustic emission. ACI Mater. J. 2008, 105, 194–199.

PART A IDENTIFICATION OF THE MODE OF FRACTURE IN BUILDING MATERIALS USING ELASTIC WAVE METHODS

Chapter 2. Effect of wave distortion on acoustic emission characterization of cementitious materials[1]

2.1 Purpose

The fracture behavior of materials can be nondestructively monitored by the acoustic emission (AE) technique, using sensors that detect the transient elastic waves after any crack propagation event. In addition to the information relatively to the total activity and the location of the cracks, certain waveform features supply detailed information on the type of cracking. The waveform of the emitted AE signal depends on the relative motion of the crack sides and therefore, it carries information on the mode of cracks. Therefore, AE is used for classification of the active cracking mode. This enables characterization of the current fracturing condition within the material and warning before final failure. Tension-related cracks, which in most materials and loading conditions are nucleated first, emit signals with higher frequency content and shorter rising time than shear cracks. However, in most cases wave propagation from the crack to the sensor is attenuative and dispersive. This results in signal distortion which is enhanced by geometry restrictions and material or damage-induced inhomogeneity. This results in strong change of the waveform shape and the calculated AE parameters. This effect is stronger as the propagation distance increases rendering crack classification troublesome for structures where the separation distance between sensors is long. In the present study, fracture experiments were conducted in cementitious specimens in order to investigate the influence of distance on the AE parameters as measured by sensors at different distances from the source. Numerical simulations based on the finite difference method are also used to enlighten the problem and expand to different material conditions. This is one of the first studies of wave dispersion examined not from the classical ultrasonics point of view of phase velocity dependence on frequency but from the AE view, where specific waveform

[1] *Adapted from "Effect of wave distortion on acoustic emission characterization of cementitious materials", published in Construction and Building Materials, Volume 35, October 2012, Pages 183-190*

parameters are of interest. Experimental and numerical results show that the influence of the propagation path is crucial and should be taken into consideration for AE characterization of large structures, while it should not be neglected even in small-scale laboratory studies in order to improve crack characterization.

2.2 Introduction

Acoustic emission (AE) is a nondestructive inspection technique utilizing the transient elastic energy which results mainly from crack propagation events inside a material [1,2]. The dislocation created at the tip of the crack excites elastic waves which propagate outwards and can be captured by sensors on the surface of the material. Acoustic emission is studied in relation with the damage evolution under dynamic loading or relatively to crack propagation rate [3-5]. It is reasonable that the number of recorded signals during loading can be correlated with the actual number of active cracks within the material [6,7]. For certain structures, the rate of incoming activity is a stand-alone criterion on which engineering decisions are based concerning safety, while strict standardization has been applied internationally. Apart from the cumulative AE activity, each signal carries raw information from its source, concerning the severity (the amount of displacement of the crack sides under the specific load) and the mode of fracture (opposing movement of the crack sides or parallel). Therefore, the qualitative characteristics of the waveform, like the amplitude, duration and main frequency may reveal crucial information on the damage mode and fracture intensity inside a material [8,9]. The main benefit of this approach is based on the fact that for most materials and loading conditions, shear types of failure follow tensile [10,11]; therefore, the classification of cracks according to their mode would indicate the current fracturing stage and provide an early warning of final failure. Controlled laboratory studies in different material systems shed light into the correlation of AE characteristics with the cracking mode. The connection between the mode of crack and the wave recorded at a specific point is a very complicated subject depending on the motion of the crack tip, as well as to geometry factors like orientation of the crack relatively to the receiver and propagation distance. While the present experimental and numerical study aims to enlighten aspects of the problem, some simple remarks concerning the excited wave modes can be stated.

When a dislocation occurs inside a material, both modes of bulk waves (longitudinal and shear) are reasonable to be emitted. However, it is also reasonable that a tensile (or mode I) cracking incident excites a large part of the elastic energy in the form of longitudinal waves, due to the transient volumetric change near the vicinity of the crack tip. On the contrary, when shear cracking develops, the percentage of energy is shifted in favor of the shear waves due to the shape distortion that shear action induces in the vicinity of the crack tip. In the first case, the main energy carrier is also the fastest wave type leading to waveforms with short rise time (RT), see Figure 2.1, top. RT is the delay between the onset of the waveform (practically the first threshold crossing) and the moment of peak amplitude. Correspondingly, the rise angle of the waveform is high, as calculated by the Amplitude, A over RT. Recently in the field of concrete, the inverse of the rising angle is studied, namely RA in μs/V [10]. In the case of shear incident, the main part of energy travels with the shear waves which are slower, leading to longer RT and lower rise angle, (see Figure 2. 2, bottom).

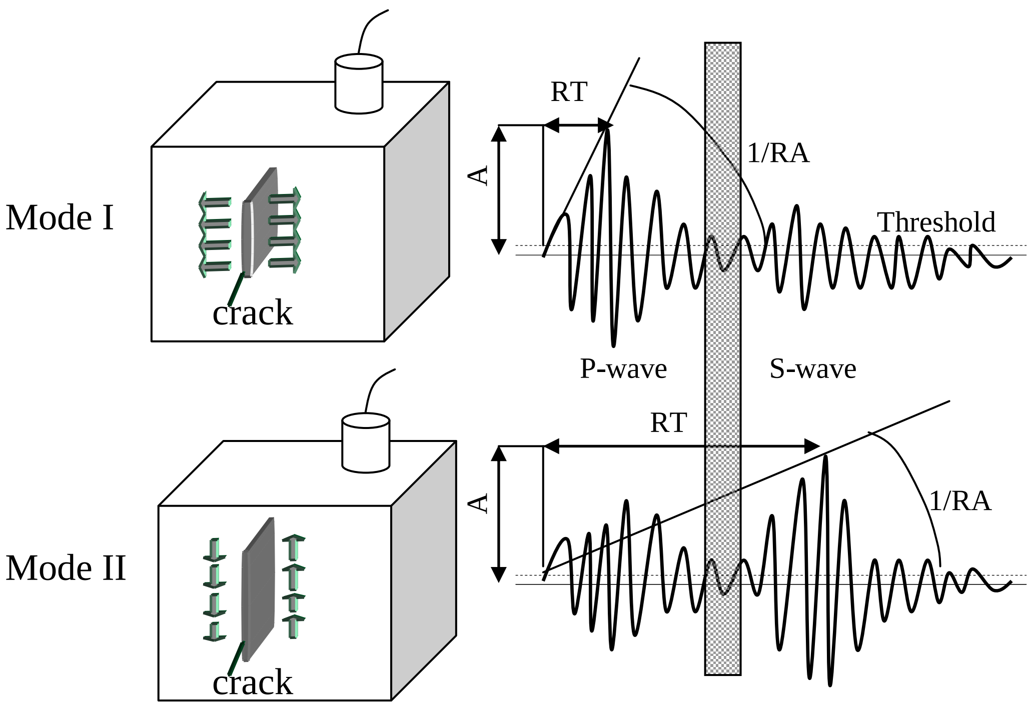

Figure 2. 1 *Cracking modes and recorded AE waveforms*

The validity of these general remarks is very sensitive to geometric conditions, relative orientation and the propagation characteristics of the medium, as will be discussed in the text. However, these assumptions have been examined in several experimental studies. Some main points on a literature review are introduced in this section in order to establish the parameters that are measured and discussed throughout the text. The AE waveform parameters which have been correlated with the fracture mode are mainly the RA value and the frequency content expressed by the number of threshold crossings over the duration of the waveform (average frequency, AF) [10]. It has been found that the RA value increases, while the average frequency decreases as damage is being accumulated in bending experiments in steel- and vinyl-fiber reinforced concrete [12,13]. Additionally, these parameters undergo a great change at the moment of the main crack formation, which indicates the shift of the dominant failure mechanism from matrix cracking to fiber pull-out [14,15]. This kind of analysis has also proven useful in rock failure [16], fracture of composite laminates [17-19] which exhibit matrix cracking (mode I) and delaminations (mode II), corrosion cracking in concrete [20] and damage evaluation on reinforced concrete panels subjected to seismic load [21]. The mutual trend in all studies is that despite differences in material, propagation path length or specimen size, the shear type of damage usually results in waveforms with longer rise time, duration, high RA and lower frequency than tensile.

The shifting trends of these parameters during fracture in concrete have been proven quite reliable in several laboratory studies. Consequently, classification of AE signals concerning the mode of the original crack has proven quite successful, based on AE parameters like AF and RA [15,20,22]. However, the application of the same laboratory criteria to real structures is not straightforward. This is mainly due to intrinsic problems that usually hinder the exploitation of this kind of information. Some of the factors complicating the assessment are the specimen or structure’s size and geometry, the heterogeneity of the material and the sensor’s response as explicitly explained in [19]. These factors render the results case-specific and prevent from general application, especially when the goal is other than simply crack location. As a consequence, any attempt of AE material characterization, would greatly benefit by the complementary study of the influence of the propagation path on the signal acquired at different surface measurement points. In this study cementitious mortar specimens were fractured under bending while their AE activity was monitored by two sensors. The sensors were placed at different distances from the notch which enabled acquiring the transient wave from the same fracturing event at two distinct points and evaluating the effect of distortion and attenuation based on the separation distance. The problem was also numerically simulated by an available finite differences code, which gave the opportunity to include different contents of simulated cracks and to expand to frequencies other than the experimental. The numerical and experimental results show that the effect of waveform distortion is strong and it should not be neglected in laboratory. Furthermore, it should certainly be taken into consideration in-situ in order to expand the use of simple crack classification schemes to real structures.

It is mentioned that the acquired experimental and numerical waveforms were analyzed for their acoustic emission parameters. Therefore, the analysis is not based on a typical ultrasonic approach, which usually employs calculations of wave speed and attenuation. The investigation involves parameters of the AE waveforms, like RT, RA and AF, which although carry information on the mode of the cracking event they suffer strong changes due to propagation through an inhomogeneous medium like concrete. This discussion is particularly important in the field of concrete where standardization is currently attempted [10], while it also applies in thin-walled structures due to plate wave dispersion [23,24].

2.3 Limitations for AE characterization

When the specimen's dimensions are finite, reflections from the edges interfere with the original AE waves. However, this is not the only complication met in AE measurements. Almost the total number of AE applications concern either piezoelectric sensors attached on the surface, or in some cases non-contact measurements, based on laser interferometry [25]; in both cases the information comes from the transient displacement of the surface. This introduces the effect of geometry even in large structures, when reflections from other sides are not expected. The reason is that as the primary wave front of the emitted AE signal impinges on the surface, mode conversion occurs and a Rayleigh wave is continuously excited. Since the propagation velocity of Rayleigh is lower, the shape of the pulse is automatically influenced, causing distortion and changing crucial waveform parameters like duration and rise time..

Apart from the waveform distortion caused by the differential velocity of the wave modes, excessive dispersion is caused depending on the heterogeneity of the material. It is mainly attributed to scattering which redirects the wave energy each time the wave front impinges on a scatterer [26]. Dispersion applies to inhomogeneous materials, like concrete [27-29], or other particulate and fiber composites [30,31] and suspensions [32] and is enhanced by the presence of damage in the form of micro-cracks and microstructure [33-35]. It is reasonable that the characteristics of a wave emitted by a crack are severely distorted while propagating through a heterogeneous system containing numerous other cracks which act as scatterers. The interaction between the microstructure and the propagating elastic wave has been correlated to the damage degree and typical size, mainly through measurements of attenuation and phase velocity in the several ultrasonic studies [29, 31, 36]. It is reasonable that the effect of inhomogeneity on the transient AE signal (which is in fact an ultrasonic wave) is equally important. Therefore, the signal’s shape and main characteristics, as quantified by AE analysis, also changes for different measurement locations. The evaluation of this distortion is the primary aim of this work.

2.4 Experimental details

Two different mortar mixtures were produced consisting of six specimens each. One was plain mortar (PM) and the other included 0.5% (vol.) of straight steel fibers (steel fiber reinforced mortar, SFRM). Their length was 25 mm, their diameter 0.6 mm, their density 7.85 kg/dm3 and were supplied by CHIRCU PROD-IMPEX COMPANY SRL, Romania. The aggregates consisted of 100% crushed sand with maximum aggregate size 4.75 mm and fineness modulus 2.93, while water/cement ratio was 0.55 by mass. The density and the water absorption of the sand were 2500 kg/m3 and 2.44 % respectively. The exact mix proportions were as follows: cement (type II) 440 kg/m3, water 242 kg/m3, sand 1529 kg/m3, super-plasticizer 4.5 kg/m3. For the fiber reinforced mortar the mix proportions were the same with the addition of

39.3 kg/m3 of steel fibers and modification of sand amount to 1517 kg/m3. The specimens were cured in water for 28 days prior to testing.

The specimens were 40x40x160 mm in size. They were subjected to three-point bending according to EN 13892-2:2002 [37](Figure 2. 3).

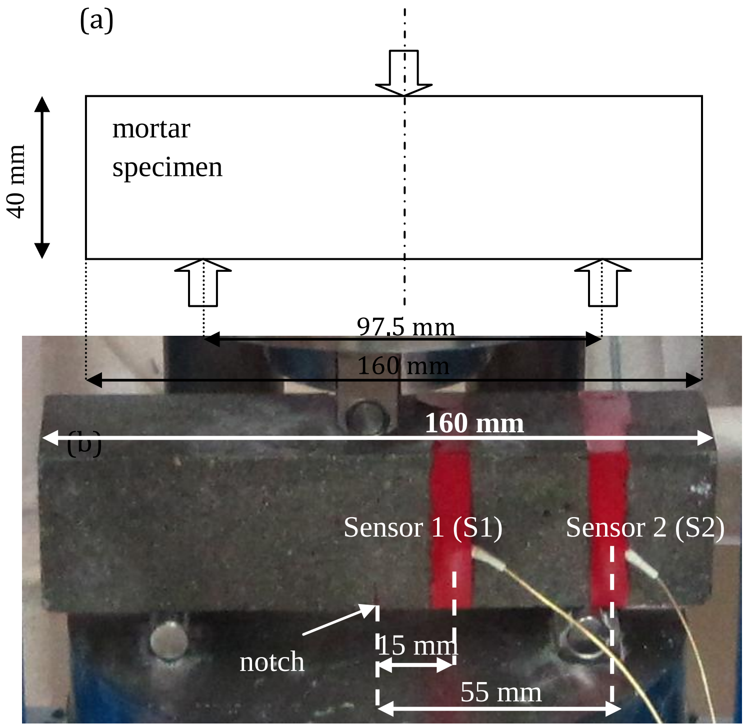

Figure 2. 2 *(a) Schematic representation of three point bending test, (b) photo of the specimen with AE sensors.*

In order to secure that the crack would initiate at the center of the specimen a notch was created by inserting a small wooden stick in the midspan of the side to be placed at the bottom during bending (tensile side). The load was applied at a constant rate of 50N/s until fracture and the loading was automatically terminated at the moment of load drop. As to AE monitoring, two AE sensors (Pico, PAC) were attached to the side of the specimen as seen in Figure 2. 4(b). They are considered quite broadband with central frequency of 500 kHz. Roller bearing grease was used for acoustic coupling, while the sensors were secured by the use of tape during the experiment (see Figure 2. 5(b)). The horizontal distance between the sensors was 40 mm and the first was placed at the horizontal distance of 15 mm from the notch, as seen in Figure 2.1.1. 1(b). The signals were recorded in a two-channel monitoring board PCI-2, PAC with a sampling rate of 5 MHz. The threshold was set to 40 dB in order to avoid ambient noise and the acquired signals were pre-amplified by 40 dB.

2.5 Results

2.5.1. Total activity

The small size of the specimen results in relatively small level of AE activity. Typical graphs of cumulative AE activity for PM and SFRM are depicted in Figure 2. 3a and b respectively.

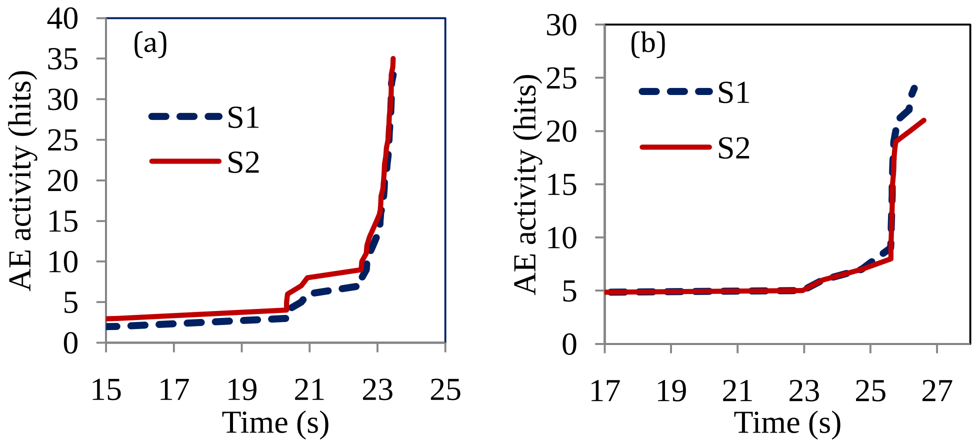

Figure 2. 3 *Typical cumulative AE activity of (a) PM and (b) SFRM.*

The activity of each sensor (S1 near the crack, and S2 away from the crack) is presented separately. The number of signals is generally less than 100 in total and the population is divided almost evenly in both receivers. This shows that despite the inherent attenuation, that will also be discussed later, the small separation distance enables capturing the fracture events by both sensors. The largest percentage of AE hits is received at the end of the experiment indicating that serious cracking processes take place only at the latest stages of loading, just before the maximum load has been reached. The almost vertical increase of the AE activity at the moment of fracture is preceded by small number of few signals approximately 2 s before final fracture, most likely due to fast-developing micro-cracking just before final failure.

It is interesting to observe qualitative characteristics of the AE waveforms as captured by the two receivers. Figure 2. 4 shows the time histories of AF of the AE signals of the same specimens as recorded by the two sensors separately.

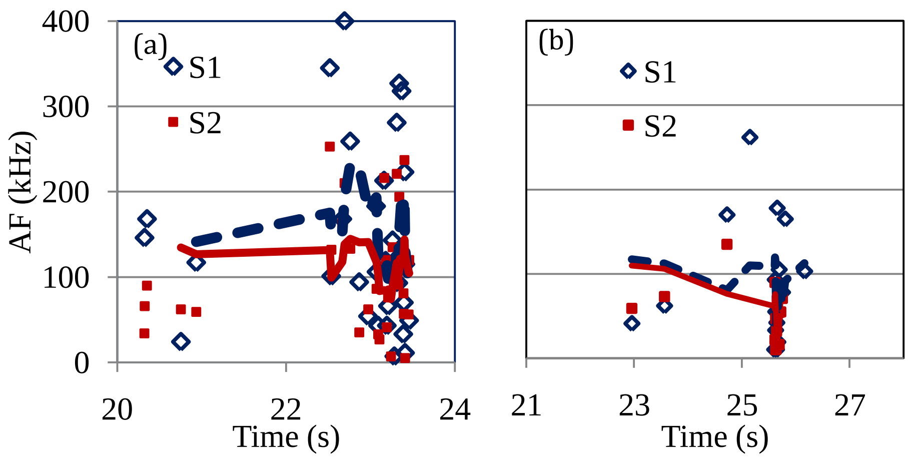

Figure 2. 4 *AF history for typical (a) PM and (b) SFRM specimen as obtained by the two sensors*

The symbols represent the AF of each signal, while the lines stand for the moving average of the recent 5 hits, in order to demonstrate the trends more clearly. For both cases, after some fluctuations, AF is decreased at the moment of final failure, which is typical for cementitious materials [10, 12, 14, 38]. Although the differences in average values are discussed in the next section, it is evident that generally S1 records signals with higher AF than S2 (see Figure 2. 7a). The same holds for the case of (Figure 2. 8b) for a typical SFRM specimen. Additionally, in the case of SFRM the frequency indicator is in general at lower level compared to plain mortar, which will be discussed along with the average results.

Figure 2. 5, shows the time history of RA for the same specimens.

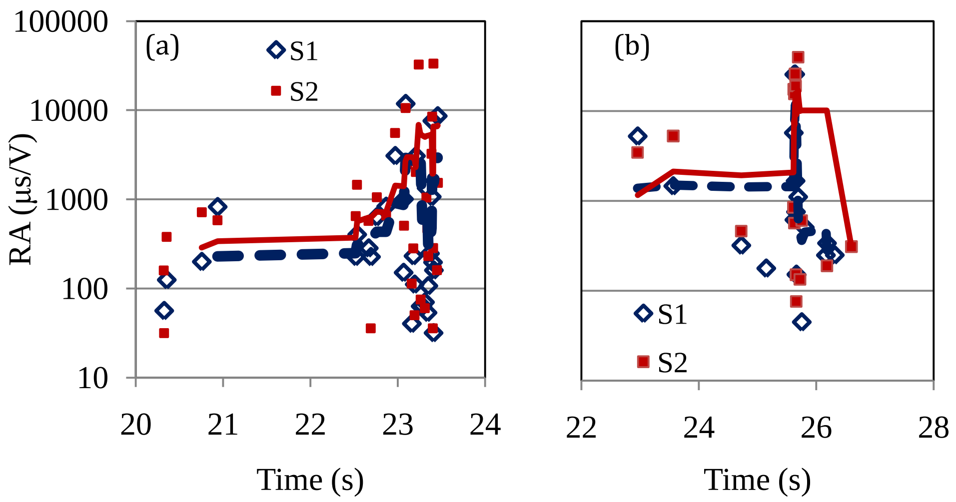

Figure 2. 5 *RA history for typical (a) PM and (b) SFRM specimen as obtained by the two sensors*

In both cases, RA increases sharply just before the termination of the experiment as is typical for materials at the onset of macrofracture [10, 38]. For the plain mortar the initial RA values are below 1 ms/V, while as main fracture approaches, values higher than 10 ms/V are depicted. Again a distinct difference is seen between the two sensors, with the sensor closest to the crack (S1) exhibiting lower values for both specimens.

Correspondingly, in this case SFRM exhibits higher RA than PM, which is again attributed to the fiber action as was the behavior in AF.

2.5.2. AE Events

The above indicative curves are based on the total number of signals received by each sensor, including any possible source, even though it is reasonable that the main source is the notch at the center. Although the trends would still be clear, in order to exclude any random signals, the data were strictly limited to the “AE events”. An AE event is the source incidence that releases elastic energy and is captured by both receivers within a short time window. This secures that each signal recorded by the first receiver can be compared to the same source signal as captured by the other receiver after traveling an additional propagation path. For each specimen, the values of the AE parameter recorded during failure by the first sensor were averaged and compared to the corresponding average value of the second sensor. Figure 2. 6(a) shows the average RA values as captured by the two sensors (S1 at horizontal distance of 15 mm and S2 at 55 mm from the notch).

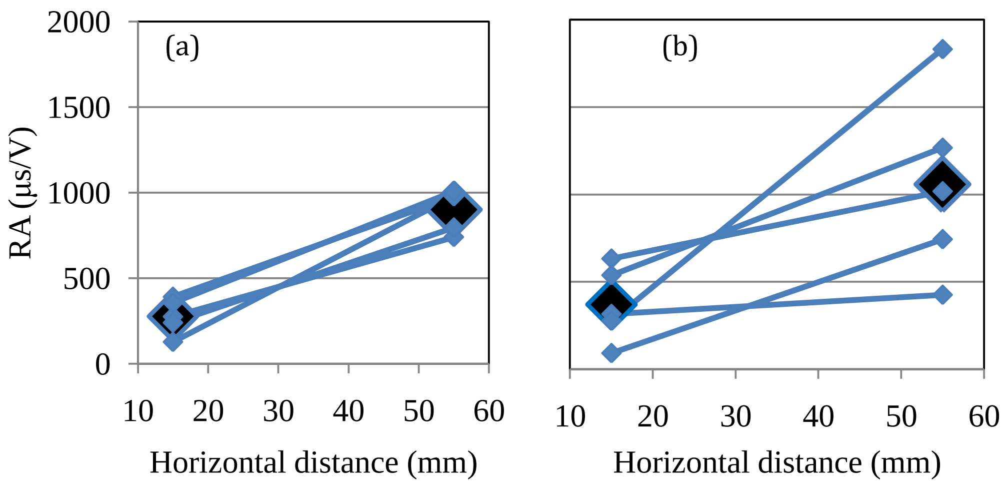

Figure 2. 6 *RA values for all (a) PM and (b) SFRM specimens for two propagation distances. Small symbols represent average values for individual specimens while large symbols stand for the average of all corresponding points.*

Each point typically represents the average of approximately 20 individual values which was a usual number of identified AE events during the bending test of a specimen. The symbols corresponding to each specimen are connected by a straight line, while the large symbols are the average of the individual points for each distance. The RA values captured from S1 are between 130 and 390 μs/V. For all the specimens there is an almost uniform increase in the RA for S2 (between 740 and 1010 μs/V). In average, the RA of the second receiver is increased by more than 3 times (901 μs/V) compared to the first (278 μs/V). This is a definite indication of distortion that occurs for the same signals, for the short additional propagation distance between S1 and S2. This indicates how important the propagation length is for AE analysis even in laboratory scale. Figure 2. 9(b) shows the corresponding graph for SFRM. The trend is similar, with S2 exhibiting 1057 μs/V, almost three times higher than the RA of S1 (371 μs/V). Though distance is equally critical for these measurements as well, a slightly higher value of RA is exhibited for SFRM, while the variability seems much stronger.

The other basic feature of interest in crack classification schemes is AF which is a rough but very indicative expression of the frequency content, as explained in the introduction. It is generally well known that when a pulse propagates through an inhomogeneous medium its main frequency is downshifted [30,36], due to scattering. In each specific specimen, AF decreases between the first and second receiver. Results for plain mortar (Figure 2. 7a) and SFRM (Figure 2. 7b) share approximately similar trends for the average value of AF.

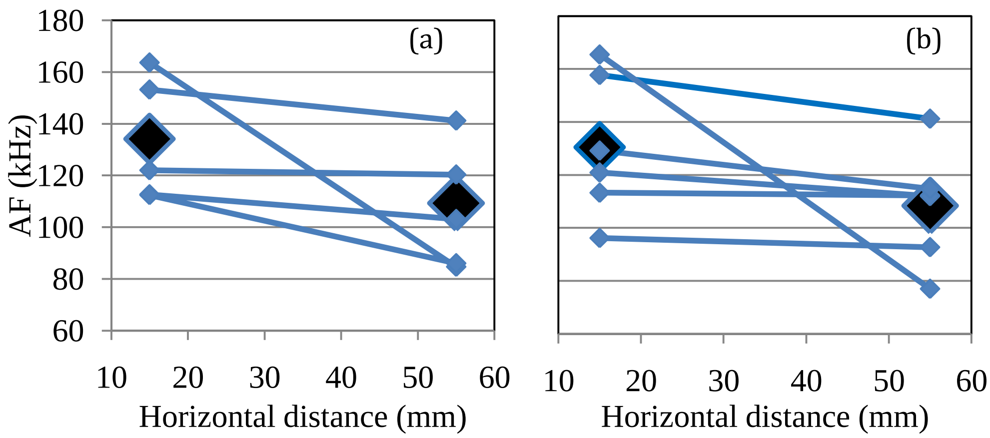

Figure 2. 7 *AF values for all (a) PM and (b) SFRM specimens for two propagation distances. Small symbols represent average values for individual specimens while large symbols stand for the average of all corresponding points.*

The decrease is of the order of 20%. This change in the additional propagation of approximately 40 mm is indicative of attenuation and distortion mechanisms that can influence basic AE parameters even in laboratory scale.

Figure 2. 8 (a) and (b) focus on the central and the peak frequency of the hits as monitored by th e different sensors for plain mortar.

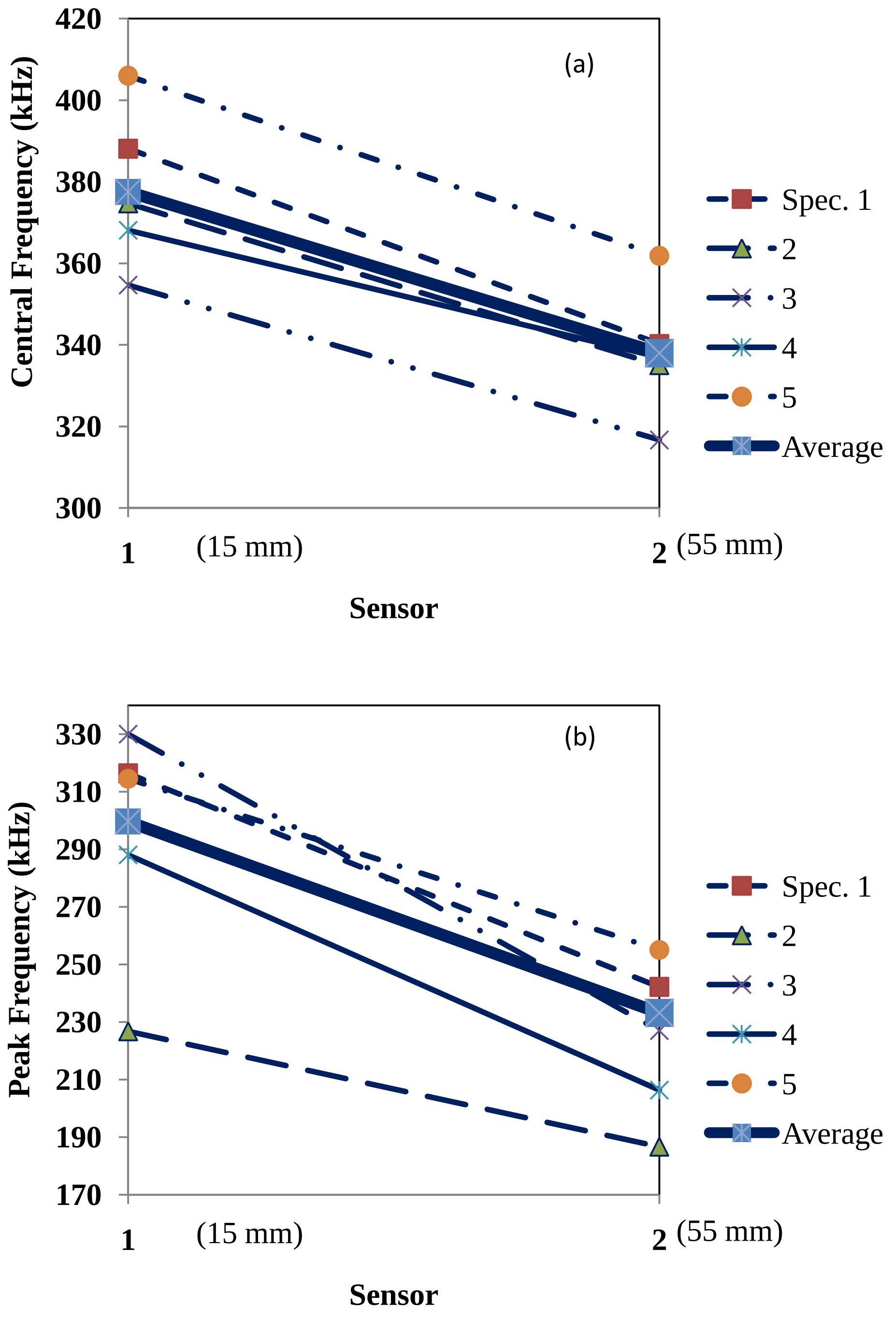

Figure 2. 8 *(a) Central and (b) Peak frequency for both sensors and different plain mortar specimens*

A similar decreasing trend is seen again both for central and peak frequencies. The trends are decreasing and repeatable for each of the specimens. CF decreases by about 11% (from 380 kHz to 340 kHz) between the two sensors. PF which corresponds to the frequency with the maximum magnitude, exhibits more or less the same trend. A strong decrease is noted for all specimens, resulting in an average drop of 23%. This decrease of frequency descriptors is again attributed to the microstructure and mainly scattering of the sand grains, pores and cavities of the cementitious material. Again it is understandable that if a separation distance of 40 mm is responsible for a change of 10 to 25% in an AE parameter, one should be definitely very careful in application of any laboratory characterization scheme [43] in a real structure.

Concerning the wave amplitude it is expected that energy-related parameters are downgraded as the wave propagates through cementitious material due to damping and scattering. Amplitude is a crucial parameter of the waveform. Not only because it is directly connected to the cracking intensity [7,8], but because it also influences most of the rest waveform parameters. Higher amplitude, results in larger number of oscillations above the threshold (counts), influencing therefore, the duration, RT, AF and most of the calculated AE features. This is of paramount importance in actual structures, where long distances impose severe attenuation in the signal. The exact results for both types of specimens are seen in Figure 2. 9 (a) and (b).

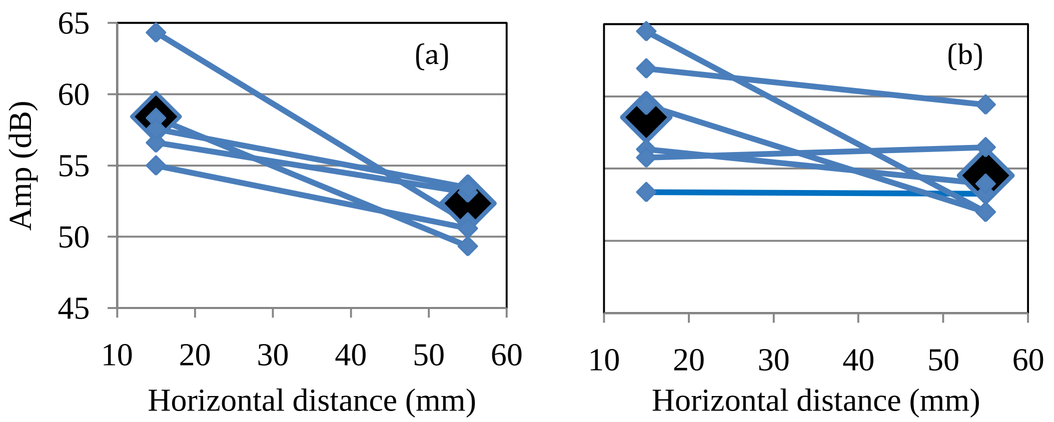

Figure 2. 9 *Amplitude values for all (a) PM and (b) SFRM specimens for two propagation distances. Small symbols represent average values of individual specimens while large symbols stand for the average of all corresponding points.*

For PM, the amplitude received by the nearest sensor is 58.4 dB in average. Inherent attenuation imposes a decrease of approximately 6 dB for the second receiver. For SFRM the decrease is 4 dB in average, still as seen by Figure 2. 9 b, noticeable and repeatable decrease of amplitude is exhibited even in laboratory scale.

Another energy related parameter that is downgraded as the wave propagates through cementitious material due to damping and scattering is the AE energy. For the whole number of events (typically around 20 for each test), the values of selected AE features were averaged for each sensor. Figure 2. 10, shows the average energy of the hits for both sensors for plain mortar.

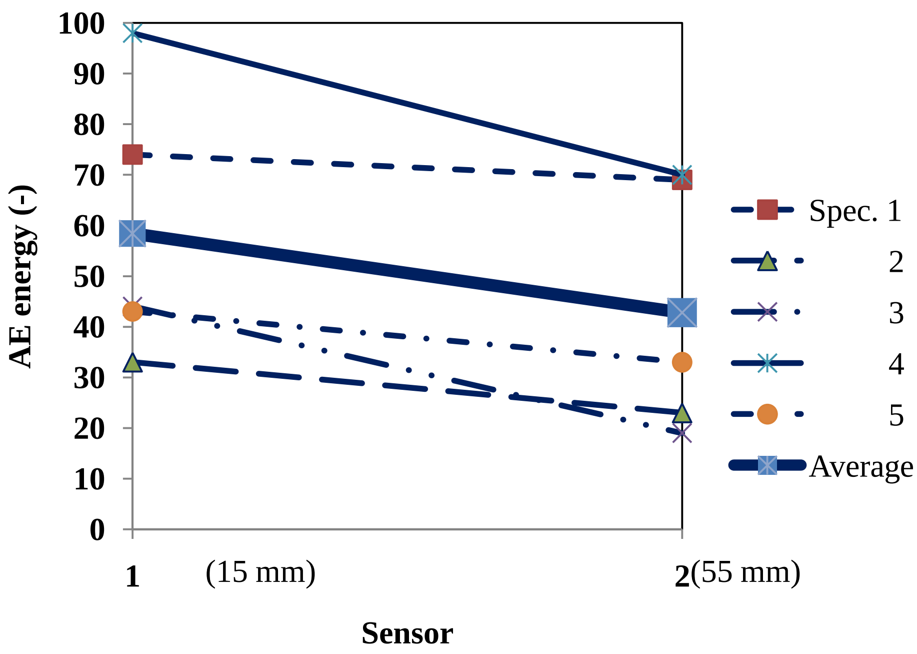

Figure 2. 10 *AE energy for both sensors and different plain mortar specimens*

It is seen that for the first sensor, the AE energy ranges between 30 and 100 units. The recorded energy at the 2nd sensor ranges from 20 to 70. It is noteworthy that for each one of the five specimens there is a decreasing trend for AE energy between the 1st and 2nd sensor. As an average for the whole number of specimens the energy reduces from 58.4 to 42.8 units between the 1st and 2nd sensor. Therefore, an additional propagation distance of roughly 40 mm reduces the acquired energy by approximately 27%. The reduction seems normal considering attenuation mechanisms. However, the amount of energy drop in such a small distance shows that the specimen size and sensor separation distance are crucial when quantitative AE is undertaken. This implies how important the propagation length is for AE analysis even in laboratory scale.

A final example of distortion of AE signal between the two sensors for plain mortar specimens is included in Figure 2. 11.

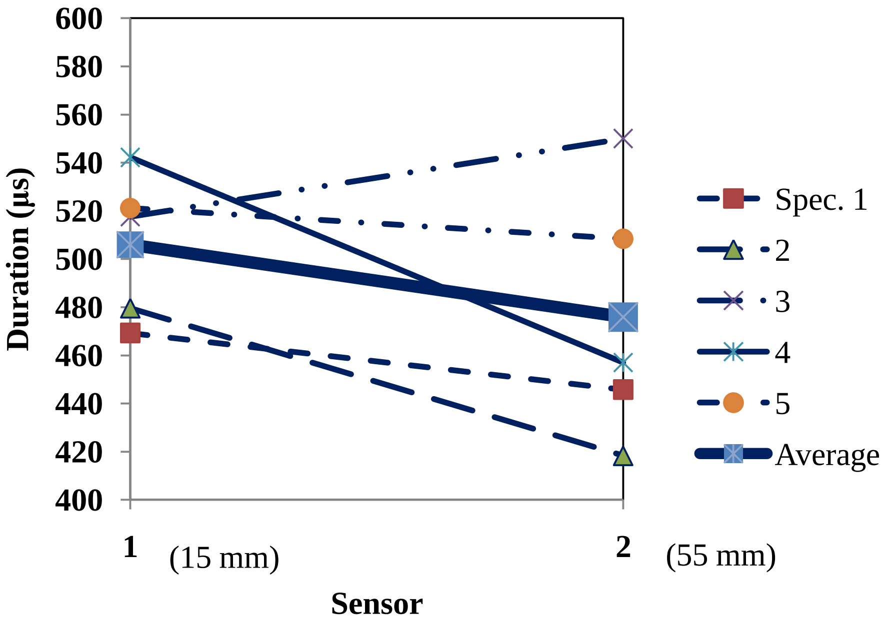

Figure 2. 11 *AE duration for both sensors and different plain mortar specimens*

There, the duration of the waveforms is depicted for the two sensors and the different specimens. With just one exception (specimen 3) the duration of the signals drops considerably between the two sensors. It is reminded that the duration of an AE waveform is calculated based on a user-defined threshold. When the material is attenuative (like mortar in the present case) it is reasonable that less peaks of the waveform will exceed the threshold level as the wave is propagating away from the source, hence leading to acquisition of shorter waveforms. The average reduction of duration is about 6% from 506 μs to 475 μs. Different AE characteristics based on the waveform shape exhibit similar change between the two sensors as was reported recently [44].

The three kinds of features (energy-, frequency- and waveform shape- related) that were analyzed in this section show how propagation of a few additional mm attenuates and distorts the signals. The differences between the sensors are quite strong especially taking into account that the two sensors are separated only by 40 mm. This distortion would reduce the accuracy of any crack classification scheme unless the exact experimental conditions are applied. In laboratory, the distance between the cracking source and the sensor is limited due to the limited size of the specimens. Therefore, although the effect of distortion and attenuation is evident, still it does not hinder the establishment of classification rules. However, in real structures the cracking event may occur just a few mm away from the sensor or several meters away. The interchangeable accumulated effect of inhomogeneity that would be different for events coming from different locations would definitely mask the results and make derivation of reliable conclusions troublesome [45].

2.5.3. Numerical simulations

2.5.3.1 Model

Numerical simulations are generally used in order to increase the understanding of wave propagation in specific problems. They enable recognition of wave modes and reflections in complicated geometries. Additionally, they can be used to expand to different geometries and cases that are not experimentally tested. In this case indicative two-dimensional simulations were conducted on the specific geometry of the experimental test including different cases of material texture, namely homogeneous (simulating cement paste), matrix with round scatterers (paste with sand grains, mortar), and three different contents of thin cracks. The fundamental equation governing the two-dimensional propagation of elastic waves in a perfectly elastic medium, is seen below:

$$\rho \frac{\partial^2 \underline{u}}{\partial t^2} = \mu \nabla^2 \underline{u} + (\lambda + \mu) \nabla \nabla \cdot \underline{u} \tag{1}$$

where $\underline{u}$ =u(x,y,t) is the time-varying displacement vector, ρ is the mass density, λ and μ are the first and second Lame constants respectively, while t is time. The simulations were conducted with commercially available software [39] that solves the above equation in time domain with the finite difference method in the plane strain case. Equation (1) is solved with respect to the boundary conditions of the object, which include the input source that has pre-defined time-dependent displacements at a given location and a set of initial conditions [40]. For heterogeneous media, propagation in each distinct homogeneous phase is solved according to Eq. (1), while the continuity conditions for stresses and strains must be satisfied on the interfaces. In this case, the propagation of an elastic wave in mortar is simulated. The aim is mainly to study the influence of cracks and sand grains scattering on the propagating wave. Different excitation types could be used to create this transient wave, such as force, velocity or displacement. In cases of crack propagation, where a permanent dislocation occurs, the magnitude of crack displacement and the AE wave motion are commonly modeled [41]. Since the source of the elastic wave in this simulation is supposed to be a crack propagation event, a short displacement excitation was also used as a conventional way to excite the transient pulse.

The basic geometry of the model is shown in Figure 2. 12.

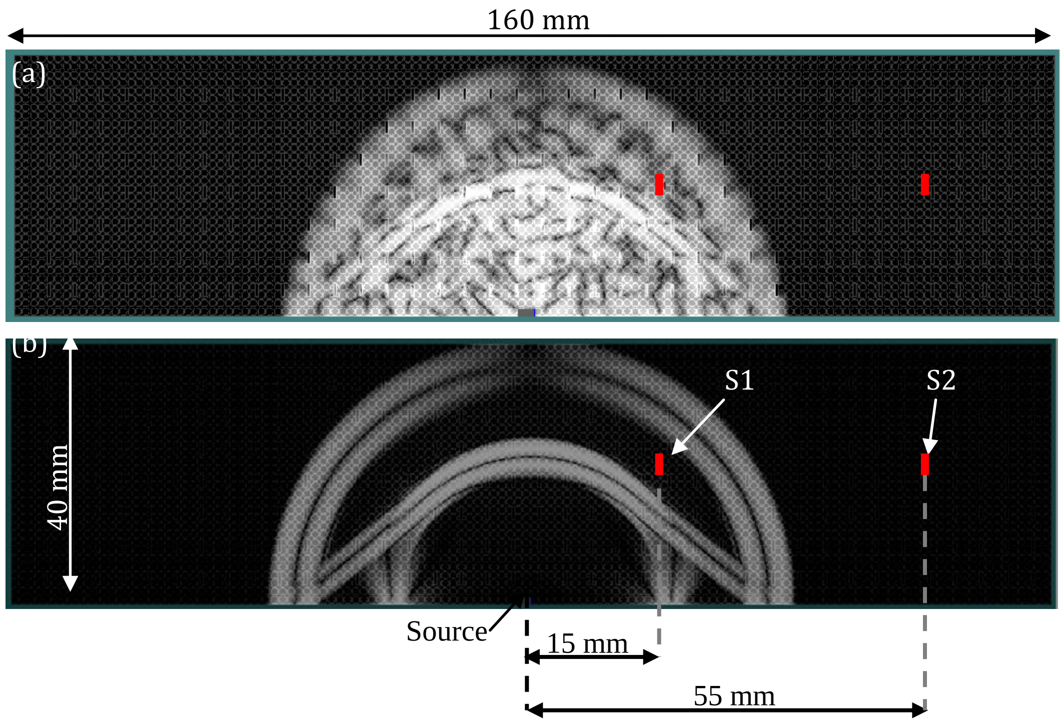

Figure 2. 12 *Geometrical model and displacement field 10 μs after excitation for material with 50% sand grains and 5% cracks (a), and homogeneous matrix (b).*

The "source" is placed at the bottom of the mid span, at the position of the notch in the actual specimen with a length of 1 mm. It introduces one cycle of 500 kHz in the longitudinal mode. This frequency is the resonant frequency of the sensors used in the experimental section and was indicatively selected among many other possible values since in AE the major frequency is not known a priori. Two receiving sensors (S1 and S2) are placed in the middle of the height, with horizontal distance of 15 mm and 55 mm on the right side from the excitation point (see Figure 2.10). The receivers are simulated by straight lines. In order to better simulate the experimental case their length was set to 5 mm which is the diameter of the specific AE transducers used. Considering the grid of 0.2 mm, the sensor length includes 25 nodes. The sensor's calculated response is the average of the displacement of these nodes either in the direction vertical to their length or parallel. Since, the experimental transducers record motion components vertical to their surface, the same response was also selected to be analyzed from the simulation results.

Materials were considered elastic without viscosity components. Different cases were simulated, namely homogeneous elastic matrix, matrix with 50% stiff elastic scatterers simulating sand grains, and matrix with sand grains and different contents of crack, namely 1%, 5% and 10% by cross section area. The properties of the different materials are seen in Table 2. 1.

Table 2. 1 *Properties of the materials used for the simulation model*

Material	**λ (GPa)**	**μ (GPa)**	**ρ (kg/m³)**	**C_p (m/s)**
Cement matrix	8.3	12.5	2100	3984
Sand grains	15.3	18.5	2600	4486
Air	10^{-4}	10^{-6}	1.2	316

The sand grains were simulated by circles of 1 mm diameter and the cracks by thin inclusions of size 0.5x2 mm assigned the properties of air. It is mentioned that the above described model is indicative of concrete-like materials and by no means is the only appropriate case for studying the problem in hand.

The focus, from the engineering point of view is given on simulating the actual geometry examined experimentally and not on the numerical method itself. However, certain prerequisites should be followed in order for the analysis to lead to reliable results. Concerning the mesh size, a preliminary evaluation took place to select a suitable value for accurate as well as time-efficient simulation. Different values of mesh size were applied, namely from 1 mm down to 0.1 mm and the corresponding wave flight times to the 2nd receiver were calculated. As the mesh became finer, the calculated transit time increased slightly, as seen in Figure 2. 13.

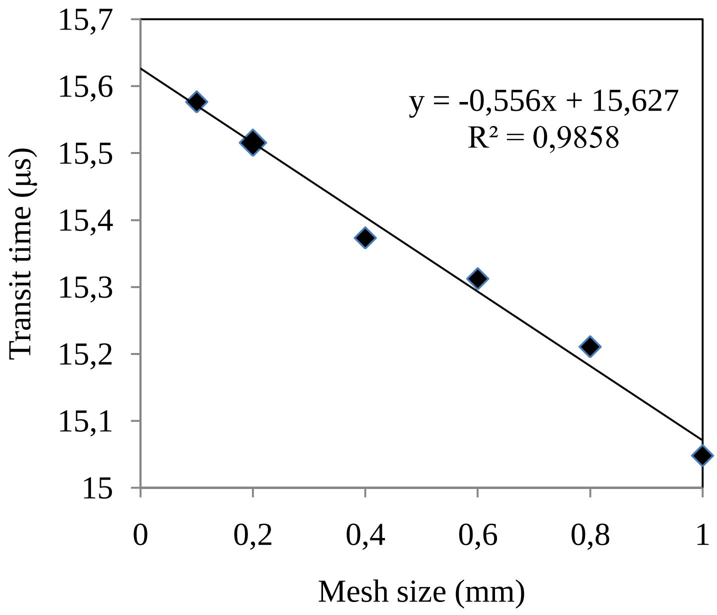

Figure 2. 13 *Transit time between excitation point and the 2nd receiver of the model of Fig. 9 vs. mesh size.*

This dependence seems quite linear and projecting the value of the linear fit for infinitesimally small grid, the transit time would be 15.627 μs. For grid of 0.2 mm, the result was 15.5156 μs, resulting in an error of 0.7% and in quite reasonable calculation time. Indeed, for a basic frequency of 500 kHz, the major wave length is about 8 mm resulting in 80 points per wave length. Concerning the time sampling, the time step was set at the value of 0.0182 μs. Considering that the basic period was 2 μs, it is clear that the number of points representing one cycle are higher than 100, while in similar studies the numbers of 20 points per wavelength and cycle are considered adequate [42]. The total simulation time window was 100 μs.

2.5.3.2 Simulation results

Figures 2. 12 a and b depict the displacement field at approximately 10 μs after excitation for the case of material with 50% grains and 5% cracks and for homogeneous material respectively. The distortion of the wave field is evident for the heterogeneous case and is accumulating as the wave propagates away from the excitation. The waveforms received by the two sensors for the first case are seen in Figure 2. 14.

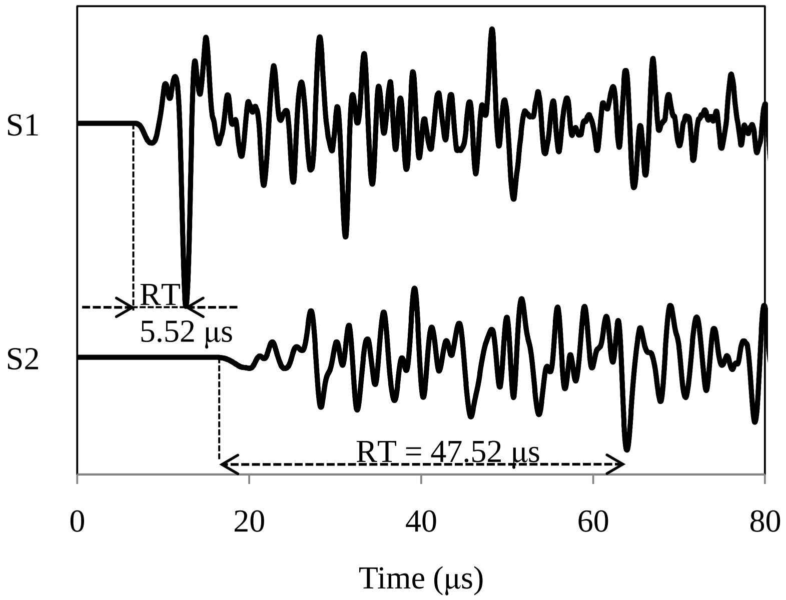

Figure 2. 14 *Simulation waveforms for the two sensors for material with 50% grains and 5% crack content.*

Despite the short initial excitation of one cycle, both sensors record a long waveform due to the multiple scattering of the wave on the several heterogeneities either in the form of grains or in the form of cracks. One of the distinct differences between the two waveforms concerns the rise time (the delay of the maximum peak compared to the onset). For S1, RT equals 5.5 μs, while for S2 the maximum peak delays considerably resulting in a RT of almost 48 μs. It is mentioned that the onset of the waveform was defined by the first threshold crossing, the threshold being 2% of the maximum amplitude of the waveform of S1, while 5% has also been checked without serious change in the resulting trends. Additionally, the oscillations are less dense in the case of S2, implying a downshift in the basic frequency. The exact values of RA and AF as measured from the simulation waveforms are presented in Figure 2. 15 for both receivers (S1 at 15 mm, S2 at 55 mm).

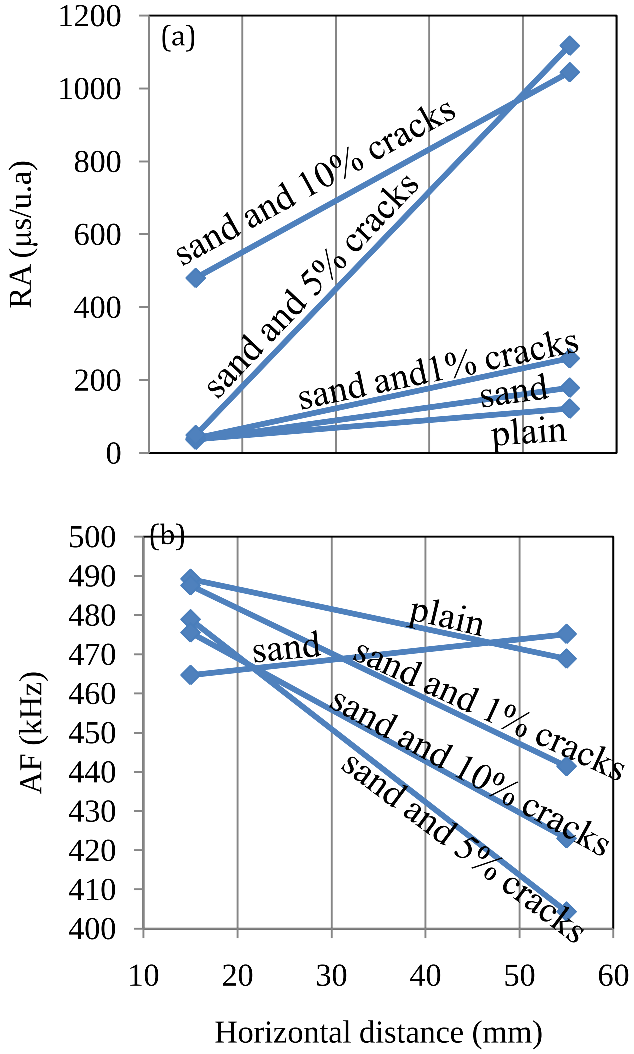

Figure 2. 15 *RA (a) and AF (b) for the two sensors and different material conditions.*

Concerning RA (Figure 2. 15 a) there is a certain increase for the second receiver, from three to six times between homogeneous material and material with 1% of cracks. For 5% cracks the increase for the 2nd receiver is explosive (23 times higher than the 1st sensor). Finally for 10% cracks the RA is quite high from the first receiver (480 μs/unit amplitude, [u.a.]), showing the heavy influence of heterogeneity on the shape of the waveform. It is reminded that the RA of the excited pulse is 0.5 μs/u.a. (one fourth of the period of 2 μs over the unity excitation amplitude). Through the propagation distance of 58 mm, which is the straight distance between the excitation point and 2nd receiver, this value becomes approximately 2000 times higher (1045 μs/u.a.) due to distortion of the pulse on the cracks and aggregates. It is easily realized that the original information of the pulse is heavily masked and that any classification approach based on the waveform as received by the sensor would most likely be misleading.

(Figure 2. 15 b) presents the values of AF. Since the basic frequency of the excitation is 500 kHz, reasonably the first sensor acquires frequencies close to the original pulse (465 - 490 kHz) for all cases. With the only exception of the geometry with aggregates, the frequency is downshifted for the second receiver in all the models. Especially for the cases of 5% and 10% cracks, AF decreases by 16% and 11% respectively. The above simulations confirm that even for such short distances of a few cm, the signal distortion is dominant owing only to elastic scattering excluding viscosity effects.

2.6 Discussion

The above experimental and numerical results taken from small geometries enable drawing of conclusions towards the improvement of signals classification schemes based on simple AE features. Table 2. 2, summarizes the average values of basic AE parameters as experimentally measured by both sensors.

Table 2. 2 *Experimental AE parameters*

	Dist. from notch (mm)	**AMP (dB)**		**RA (µs/V)**		**AF (kHz)**	
		Aver.	St. dev.	Aver.	St. dev.	Aver.	St. dev.
Plain	15 (Sensor 1)	58.4	5.0%	278.4	33.2%	134.1	14.8%
	55 (Sensor 2)	52.3	4.5%	900.7	12.2%	109.3	18.5%
SFRM	15 (Sensor 1)	58.5	6.5%	371.2	51.9%	130.5	18.6%

	55 (Sensor 2)	54.5	4.9%	1056.9	45.2%	108.3	18.4%

The decrease of AF by almost 20% and the increase of RA by more than 3 times for the 2nd sensor (55 mm from the notch), shows that the position of the sensors with respect to the crack location is crucial. The results, even in such close quarters include the effect of dissipation and scattering and differ significantly from the original pulse, as emitted by the source. Since the pulse suffers substantial changes for a short additional distance of 40 mm between the receivers, it is understandable that the effect in actual structures would be even stronger. In real-size structures, a finite number of sensors are placed in order to cover as large volume of the material as possible. Therefore, a cracking incidence may have its source just millimeters beneath the sensor or at a distance of several meters away. Although the signal may be acquired in both cases (provided that its energy is high enough), its characteristics should definitely differ at various measurement points. Therefore, the event location relatively to the sensor is crucial in order to evaluate how much the signal has been distorted while propagating. As already mentioned, in the engineering use of AE, crack characterization is important since it gives insight in the fracture stage. In laboratory scale, assuming that distortion and attenuation are limited, classification criteria have been studied based on specific values of RA and AF [15,22]. As an example from [15], tensile matrix cracking in steel fiber reinforced concrete under bending was characterized by an average AF of 400 kHz and RA less than 1 ms/V, while mixed-mode fracture (macro-cracking with fiber pull-out) by AF of 150 kHz and RA of 4 ms/V, as seen also in Figure 2. 16.

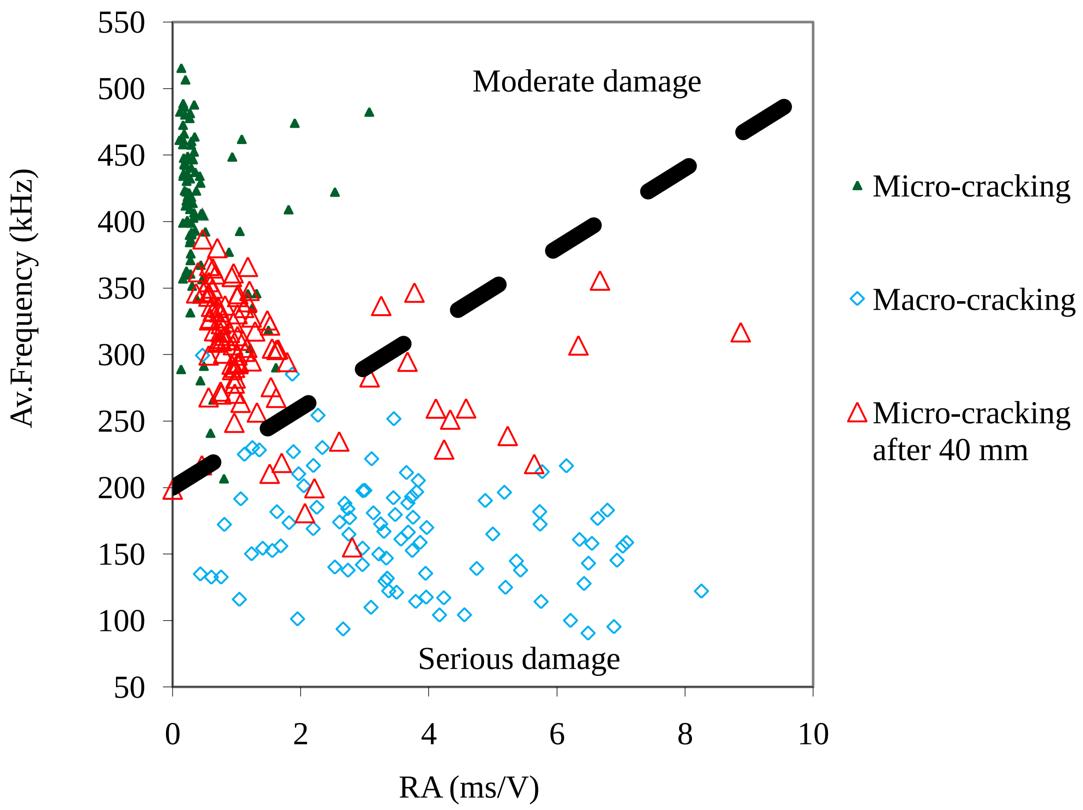

Figure 2. 16 *Cracking mode classification for steel fiber reinforced concrete beams of 400 mm size under bending.*

This classification produced very accurate results (less than 1% overlapping points) in beam specimens of 400 mm length and sensors placed nominally 50 mm away from either side of the expected crack. However, if the same criteria were to be used in-situ for different conditions and sensor separation distances, the classification would not necessarily be equally accurate. Under the light of the experimental results of the present study it is understood that the RA of a tensile event after propagation through a few cm of heterogeneous cementitious material would increase by about 3 to 4 times, as was seen in Table 2. 2. Simulations at higher frequencies indicate a much stronger increase of RA (from five to twenty five times depending on the material’s condition). Similarly the frequency content would decrease by more than 20% for propagation of a few additional cm, as was seen in (Figure 2. 7). When this distortion effect is incorporated in the values of the micro-cracking population of Figure 2. 16 (small solid green triangles) by multiplying the RA of each point by 3.5 and decreasing AF by 25%, the new set of data (larger open red triangles) it results in much stronger overlap with the original macro-cracking (20% of the population). Therefore, the influence of distance may easily lead to misclassification of a tensile event located away from the receiver, as a shear event located close to the receiver. It is evident, that any crack characterization scheme in real structures should include certain waveform correction procedures in order to lead to meaningful results. Concerning laboratory specimens which are commonly used for fracture characterization purposes, the effect of distortion is limited due to smaller dimensions and short propagation distances. However, as the results of the present study show, distortion does exist and although it does not prevent from the establishment of simple classification schemes, characterization would certainly benefit in terms of accuracy by taking out the effect of propagation distance.

The specific problem is quite complicated and further numerical and experimental efforts should be undertaken. Experiments of different fracturing modes should be conducted, while the number of sensors must be increased in order to monitor AE signals for longer distance. Concerning simulations, these should be expanded in three dimensions in order to more realistically simulate the exact geometry and orientation of the sensors' surface relatively to the AE wave directions.

Without being the target problem of the present study, a few comments can be pointed at the comparison between the AE parameters of different materials (plain and fiber reinforced). Apart from matrix cracking, failure in steel fiber materials includes another fracture mechanism due to the fiber pull-out. For the case of straight fibers when the material is being cracked, friction between the fibers and the surrounding matrix occurs, which resembles shear. As mentioned in the experimental section, the loading automatically stops at the first load drop; therefore, it is not possible to monitor sufficient number of pull-out events. However, it is certain that the fibers located at the center of the specimen are instantaneously involved in pull-out events when the main crack is formed. This contribution of the steel fibers' friction with the cement matrix is bound to be responsible for this slight increase of the average RA value for SFRM (371 μs/V) compared to 278 μs/V for plain mortar, as seen in (Table 2. 2) for sensor 1. For the same reason the AF is slightly decreased for SFRM. This has been experimentally seen in concrete studies [13, 14, 38] with extensive pull-out stage. In this case the contribution of pull-out is instantaneous, but still its influence is evident on the average values. On the other hand it is interesting to comment on the variation of the measurements, which is certainly higher for SFRM. (Table 2. 2) includes the standard deviation of the AE parameters as a percentage of the average. It can be seen that, especially for RA, the scatter of the different specimens is much higher for SFRM (approximately 50% compared to 30% or less for the plain material). This is also evident in (Figure 2. 6 b), where the scatter of experimental points is larger than (Figure 2. 6 a). This is particularly interesting because it shows that the increased inhomogeneity of the steel fiber material is reflected in variability of the fracturing properties along with other physical properties, variability in which would be certainly expected.

2.7 Conclusions

The present study deals with the propagation of elastic wave pulses within a material with a specific microstructure. The investigation includes AE parameters which are used for characterization of the fracture properties of the material, instead of the classical method of monitoring the wave velocity and attenuation, which are related to the mechanical and physical properties. These AE parameters are mainly the average frequency and the inverse of the rising angle of the waveform (RA value), which under controlled conditions are used for crack classification purposes. Due to the heterogeneity of concrete, the waveforms are continuously distorted as the wave propagates away from the source. This results in significant shift of the original content when the pulses are recorded by the receiver. Experiments in specimens of mortar show that an additional propagation distance of a few centimeters affects the calculated values by orders of magnitude. The RA increases by three to four times, while frequency decreases by about 30%. This strong influence would not allow the use of any laboratory-based criterion in-situ. Simulations were also conducted in order to expand this methodology to different materials and higher frequencies. Results showed even higher influence of inhomogeneity on the propagating wave. Therefore, it is evident that the AE waveform as received by the sensor should not be directly used for crack classification purposes; instead the original waveform characteristics, as emitted by the crack, should be sought for in order to exclude the distortion that propagation in a heterogeneous medium induces.

2.8 References

[1] Grosse, C. U., Ohtsu, M., 2008. Acoustic Emission Testing, Springer, Heidelberg.

[2] Mindess S., 2004. Acoustic Emission Methods. In CRC Handbook of Nondestructive Testing of Concrete, Editors Malhotra V.M., Carino N. J., CRC, Boca Raton, FL.

[3] Gudmundson, P., 1999. Acoustic emission and dynamic energy release rate for steady growth of a tunneling crack in a plate in tension, J. Mech. Phys. Solids 47, 2057-2074.

[4] Carpinteri, A., Cardone, F., Lacidogna, G., 2010. Energy Emissions from Failure Phenomena:Mechanical, Electromagnetic, Nuclear. Experimental Mechanics 50, 1235–1243.

[5] Moura, A., Lei, X., Nishisawa, O., 2005. Prediction scheme for the catastrophic failure of highly loaded brittle materials or rocks, Journal of the Mechanics and Physics of Solids 53, 2435–2455.

[6] Suzuki, T., Ogata, H., Takada, R., Aoki, M., Ohtsu, M., 2010. Use of acoustic emission and X-ray computed tomography for damage evaluation of freeze-thawed concrete, Construction and Building Materials 24, 2347–2352.

[7] Kurz, J.H., Finck, F., Grosse, C.U., and Reinhardt, H.W., 2006. Stress drop and stress redistribution in concrete quantified over time by the b-value analysis. Structural Health Monitoring, 5, 69-81.

[8] Shiotani T, Fujii K, Aoki T, Amou K., 1994. Evaluation of Progressive Failure using AE Sources and Improved B-value on Slope Model Tests. Progress in Acoustic Emission 7, 529-534.

[9] Watanabe, T., Hosomi, M., Yuno, K., Hashimoto, C., 2010. Quality evaluation of shotcrete by acoustic emission. Construction and Building Materials, 24, 2358–2362.

[10] Ohtsu M., 2010. Recommendation of RILEM TC 212-ACD: Acoustic emission and related NDE techniques for crack detection and damage evaluation in concrete: Test method for classification of active cracks in concrete structures by acoustic emission, Materials and Structures, 43(9), 1187-1189.

[11] Yuyama, S., Li, Z., Ito, Y., Arazoe, M., 1999. Quantitative analysis of fracture process in RC column foundation by moment tensor analysis of acoustic emission. Constr. Build. Mater. 13, 87–97.

[12] Soulioti, D., Barkoula, N.M., Paipetis, A., Matikas, T.E., Shiotani, T., Aggelis D.G., 2009. Acoustic emission behavior of steel fibre reinforced concrete under bending. Construction and Building Materials, 23, 3532-3536.

[13] Aggelis, D.G., Shiotani, T., Momoki, S., Hirama, A., 2009. Acoustic emission and ultrasound for damage characterization of concrete elements. ACI Materials J. 106(6), 509-514.

[14] Grosse, C.; Reinhardt, H.; and Dahm, T., 1997. Localization and Classification of Fracture Types in Concrete with Quantitative Acoustic Emission Measurement Techniques," NDT&E International, 30(4), 223-230.

[15] Aggelis, D.G., 2011. Classification of cracking mode in concrete by acoustic emission parameters, Mechanics Research Communications 38, 153–157.

[16] Shiotani, T., 2006. Evaluation of long-term stability for rock slope by means of acoustic emission technique, NDT&E Int, 39(3), 217-228.

[17] Anastassopoulos, A., and Philippidis, T. P., 1995. Clustering methodology for evaluation of acoustic emission from composites, J. Acoust. Emiss. 13, 11–22.

[18] Philippidis, T. P., Assimakopoulou, T. T., 2008. Strength degradation due to fatigue-induced matrix cracking in FRP composites: An acoustic emission predictive model, Composites Science and Technology 68, 3272–3277.

[19] Scholey, J. J., Wilcox, P. D., Wisnom, M. R., Friswell, M. I., 2010. Quantitative experimental measurements of matrix cracking and delamination

using acoustic emission, Composites: Part A 41, 612–623.

[20] Ohtsu, M., Tomoda, Y., 2008. Phenomenological model of corrosion process in reinforced concrete identified by acoustic emission, ACI Mater J. 105(2), 194–200.

[21] Lu, Y., Li, Z., Liao, W. I., 2011. Damage monitoring of reinforced concrete frames under seismic loading using cement-based piezoelectric sensor, Materials and Structures, 44(7) 1273-1285.

[22] Ohno, K., Ohtsu, M., 2010. Crack classification in concrete based on acoustic emission. Construction and Building Materials 24(12), 2339-2346.

[23] Hamstad MA, O'Gallagher A, Gary J. A wavelet transform applied to acoustic emission signals: part 1: source identification. J Acoustic Emission 2002;20:39–61.

[24] Aggelis, D. G., Matikas, T. E. Effect of plate wave dispersion on the acoustic emission parameters in metals, Computers and Structures, doi:10.1016/j.compstruc.2012.01.014

[25] Tsuda, H., Koo, J.-H., Kishi, T., 2001. Detection of simulated acoustic emission with Michelson interferometric fiber-optic sensors, Journal of Materials Science Letters 20(1), 55-56.

[26] Waterman, P.C., Truell, R. 1961. Multiple scattering of waves. J Math Phys 2, 512–37.

[27] Chaix, J.F., Garnier, V., Corneloup, G., 2006. Ultrasonic wave propagation in heterogeneous solid media: theoretical analysis and experimental validation. Ultrasonics, 44, 200–210.

[28] Punurai, W., Jarzynski, J., Qu, J., Kurtis, K.E., Jacobs, L.J. 2006. Characterization of entrained air voids in cement paste with scattered ultrasound. NDT&E INT, 39(6), 514–524.

[29] Aggelis, D. G., Polyzos, D., Philippidis, T.P., 2005. Wave dispersion and attenuation in fresh mortar: theoretical predictions vs experimental results. J

Mech Phys Solids, 53, 857–883.

[30] Kinra, V. K., Day, N.A. Maslov, K., Henderson, B.K., Diderich, G., 1998. The transmission of a longitudinal wave through a layer of spherical inclusions with a random or periodic arrangement, J. Mech. Phys. Solids 46(1), 153-165.

[31] Tsinopoulos, S. V., Verbis, J. T., and Polyzos, D., 2000. An iterative effective medium approximation for wave dispersion and attenuation predictions in particulate composites, Adv. Composite Lett. 9, 193–200.

[32] Cowan, M. L., Beaty, K., Page, J. H., Zhengyou, L., Sheng, P., 1998. Group velocity of acoustic waves in strongly scattering media: Dependence on the volume fraction of scatterers,’’ Phys. Rev. E 58, 6626–6636.

[33] Yang, L., and Turner, J. A., 2003. Scattering of elastic waves in damaged media, J. Acoust. Soc. Am. 113 (6), 2992-3000.

[34] Littles Jr., J. W., Jacobs, L.J., Qu, J., 1995. Experimental and theoretical investigation of scattering from a distribution of cracks. Ultrasonics, 33(1), 37-43.

[35] Papargyri-Beskou S., Polyzos D. and Beskos D. E., 2009. Wave dispersion in gradient elastic solids and structures: A unified treatment, International Journal of Solids and Structures, 46, 3751-3759.

[36] Aggelis, D. G., Shiotani, T. 2007. Experimental study of surface wave propagation in strongly heterogeneous media. Journal of the Acoustical Society of America, 122(5), EL 151-157.

[37] EN 13892-2:2002, Methods Of Test For Screed Materials - Part 2: Determination Of Flexural And Compressive Strength

[38] Aggelis, D.G., Soulioti, D.V., Sapouridis, N., Barkoula, N.M., Paipetis, A.S., and Matikas, T.E., 2011. Acoustic emission characterization of the fracture process in fibre reinforced concrete, Construction and Building Materials, 25,4126-4131.

[39] Wave2000, Cyber-Logic, Inc, NY /http://www.cyberlogic.org

[40] Kaufman, J.J., Luo, G., Siffert, R.S., 2008. Ultrasound simulation in bone. IEEE Transactions on Ultrasonics, Ferroelectrics and Frequency Control 55(6),1205–18.

[41] Uddin, F. A. K. M, Shigeishi, M., Ohtsu M., 2006. Fracture Mechanics of Corrosion Cracking in Concrete by Acoustic Emission, Meccanica 41, 425-442.

[42] Moser F, Jacobs LJ, Qu J., 1999. Modeling elastic wave propagation in waveguides with finite element method. NDT&E Int. 32, 225–34.

[43] Aggelis, D.G., 2011. Classification of cracking mode in concrete by acoustic emission parameters. Mechanics Research Communications 38, 153–157.

[44] Aggelis, D. G., Mpalaskas A. C., Ntalakas D., Matikas T. E., Effect of wave distortion on acoustic emission characterization of cementitious materials, Construction and Building Materials 35 (2012) 183-190.

[45] A. Carpinteri, G. Lacidogna, F. Accornero, A. Mpalaskas, T.E. Matikas, D. G. Aggelis, Influence of damage in the acoustic emission parameters, Cement and Concrete Composites 44 (2013) 9-16

Chapter 3. Determination of Fracture Mechanism under Flexural Load in Building materials

3.1. Mortars[2]

3.1.1. Purpose

Characterization of the cracking mode in cementitious materials allows evaluations concerning the remaining life of the structure since in general, shear-like phenomena occur after tensile cracking. Individual modes of cracking cause different motion of the crack tip dictating the waveforms emitted after cracking events. In this study, fracture experiments on cementitious specimens are conducted. The fracture mode is controlled by modifying the experiment geometry and the process is monitored by acoustic emission. The distinct signature of the cracking modes is reflected on acoustic waveform parameters like amplitude, RA-value and peak frequency. Signals emitted by the shear testing exhibit longer waveforms and lower frequency than the tensile tests. The influence of inhomogeneity is also evident as signals acquired at different distances exhibit distinct characteristics. Results show that AE leads to the characterization of the dominant fracture mode using only two AE descriptors and offer the potential for in-situ application.

3.1.2. Introduction

Characterization of the fracture mode in engineering materials is a task concentrating a lot of effort in the engineering community. This is particularly important since during the fracture process, a sequence of fracturing modes is generally followed. Therefore, characterization of the dominant mode highlights the stage of failure

[2] Adapted from "Investigation of different fracture modes in cement-based materials by acoustic emission" published in Cement and Concrete Research, Volume 48, June 2013, Pages 1-8

(initial, intermediate or final). Specifically for concrete, a lot of work has been done showing that shear phenomena dominate at the last stages of failure, while initially, tensile mode is mostly active [1-5]. A method that is suitable for the monitoring of the fracture phenomena is acoustic emission (AE). AE gives the opportunity to highlight the moments of major or minor fracture occurrences and follow the procedure until final failure. Information of the population of the AE signals, as well as specific indices enlighten the understanding of the fracture process and enable the evaluation of the general condition of the material each moment. Concerning the fracture mode characterization, moment tensor analysis (MTA) has been developed and successfully applied in laboratory experiments [6]. The fracture mode is evaluated and reasonably correlated with the observation of the location of the cracks after failure [1,6]. However, the use of MTA is not easy in real structures due to practical limitations. The most important is that each AE event needs to be recorded by as many as eight individual sensors in order to supply enough information on the directionality of the acoustic wave. In large structures the sensors are distributed in relatively long distances in order to cover as much volume of the structure as possible and enable evaluations on the whole scale. Therefore, when using sensor separation distances of several meters [7,8] it is highly unlikely to record the transient waves of the same event with the required number of sensors due to inherent material attenuation. Under the light of the above, a reliable characterization scheme that requires less number of sensors is desirable which however, can provide useful and reliable information on the material's damage status.

The problem of accurate characterization of the cracking condition in a material is a nearly impossible task. In order to fully describe the damage condition within a material, several parameters should be evaluated. These include the size, shape and orientation of each crack, the fracture mode under which it propagates as well as its propagation rate under a specific loading pattern. Considering that any large concrete structure includes numerous cracks either from construction or function loads, one realizes that successfully dealing with the problem of damage status characterization in its absolute form is highly unlikely. Still, information on the general condition is vital. If this information derived by NDT monitoring is the basis for a maintenance procedure that potentially extends the safe service life for decades, it is understood that even rough evaluations attain great significance. Additionally, indices obtained as a function of time, enable comparisons between the behavior and performance of the structure before and after sustaining additional loading. An effort has been undertaken in order to monitor damage of cementitious materials based on the recording of simple AE parameters. A description of AE monitoring and the main signal descriptors follows.

AE allows monitoring of crack growth using transducers placed on the material. These transducers record the transient response of the surface after each cracking event (similar to seismic activity) and transform it into electrical voltage due to their piezoelectric nature [9]. The information that can be drawn concerns the cracks' location and the total activity, which is related to the number and the nature of cracking events [10,11]. Detailed study of qualitative parameters of the received waveforms leads to characterization of the fracture process [1-6] and sustained damage assessment [10,12,13]. Certain AE features have been successfully correlated to the fracture process. One is the maximum amplitude (A) of the waveform that depends on the intensity of the cracking source, see Figure 3.1. 1 (a).

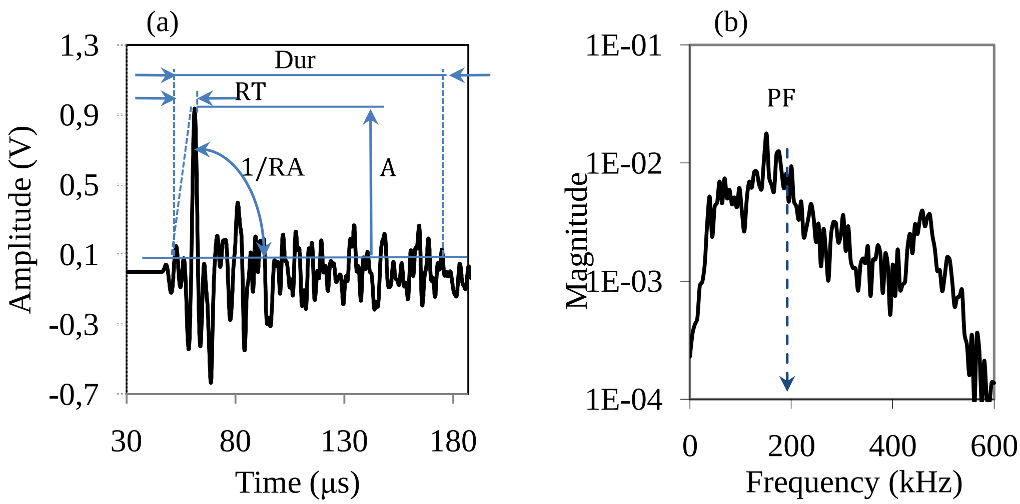

Figure 3.1. 1 *(a) Typical AE waveform with main parameters, (b) typical frequency spectrum*

Another important descriptor is "RA value" which is the duration of the first, rising part of the waveform (rise time, RT) over A measured in μs/V, and has been shown very sensitive to the fracture mode [4,14,15]. Frequency parameters like the "average frequency", AF, are also important. AF is the number of threshold crossings over the duration of the signal, measured in kHz. Another important frequency feature is the peak frequency, PF, which is the frequency with the maximum magnitude after fast Fourier transformation of the waveform [16], see Figure 3.1. 1 (b). The individual modes of failure, lead to wave emissions with different characteristics allowing characterization of cracks based on their mode [17]. Several studies have shown that tensile cracks lead to AE with higher frequency characteristics and lower RA values than shear cracks [1-4,14,15]. Apart from damage, AE parameters have also been used to highlight other processes like self-healing in concrete [18,19], melting of particles in a matrix [20] or correlate with strength and particle/inclusion size [11,21].

In most of the above works tensile and shear phenomena are successfully distinguished by their AE behavior. However, the distinct fracture signatures are exhibited by various kinds of phenomena and not by the different fracture mode of the material itself. As an example, in steel fiber reinforced concrete [3,4] under bending, tensile cracks are related to matrix cracking. On the other hand shear phenomena are associated with fiber-pull out. The first depends on the strength and quality of the concrete matrix, while the second on the interfacial shear strength between the matrix and the fibers. Similarly matrix cracking and delaminations are monitored in laminated composites [11,22,23]. The first are basically associated to the tensile strength of the off-axis layers, while delaminations depend again on the interfacial shear strength between successive layers. In the present study the modes of fracture are associated with the core material itself (cement based matrix), without other sources of inhomogeneity like fibers or laminas. The geometry of the testing experiment was slightly modified in order to excite different fracture modes as expressed by the dominant normal or shear stresses developed at the position of cracking as also suggested by finite element simulation. The material was cementitious mortar with small aggregates (sand) which is considered homogeneous relatively to concrete that includes large aggregates. AE was monitored during fracture and the differences between the typical signals received during shear and tension are highlighted. It is seen that, at least in laboratory conditions, characterization of fracture mode can be reliably conducted based on the results of just two AE receivers. This is the continuation of a study concerning the effect of propagation distance on the acquired AE parameters of pure bending [24].

3.1.3. Experimental details

3.1.3.1. Materials

Two similar mortar mixtures were produced consisting of six specimens each. The specimen size was 40x40x160 mm as typically used for three-point bending. The aggregates consisted of 100% crushed sand with maximum aggregate size 4.75 mm and fineness modulus 2.93, while the water/cement ratio was 0.55 by mass. The density and the water absorption of the sand were 2500 kg/m3 and 2.44 % respectively. The exact mix proportions were as follows: cement (type II 42.5N) 440 kg/m3, water 242 kg/m3, sand 1529 kg/m3, super-plasticizer 4.5 kg/m3.

Six of the specimens were subjected to three-point bending according to EN 13892-2:2002 [25], see Figure 3.1. 2 (a).

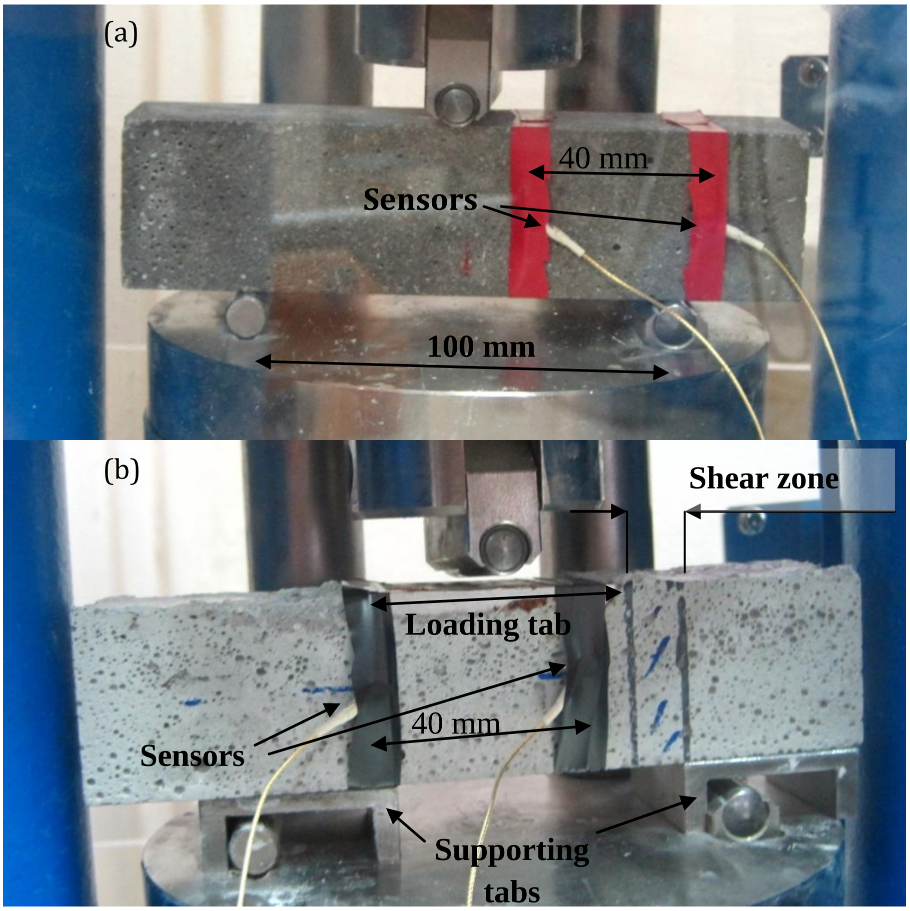

Figure 3.1. 2 *Experimental setup for (a) three-point bending and (b) shear mode with AE sensors*

A notch was created at the mid span of the bottom (tensile) side in order to secure that the crack would initiate at the center of the specimen. The load was applied at a constant rate of 50N/s and the loading was automatically terminated at the moment of load drop. A slight modification was done in the molding of the other six specimens that were intended for study of the shear fracture mode. Specifically, a metal tab of length of 50 mm and width of 40 mm was placed inside the specimen just after molding at the center of the top side (Figure 3.1. 2b). This modification of the geometry in combination with the support altered considerably the stress field as will be discussed in a later section.

3.1.3.2. Acoustic emission

Concerning AE monitoring, two broadband AE sensors with maximum sensitivity at 500 kHz (Pico, PAC) were attached to the side of the specimen as seen in Figure 3.1. 2(a) and (b). Roller bearing grease was used to promote acoustic coupling, while the sensors were secured by tape (see again Figure 3.1. 2). The horizontal distance between the sensors was 40 mm and the first was placed at the horizontal distance of 15 mm from the expected location of the crack which was secured by small notches, as seen in Figure 3.1. 2(a) for the bending and in Figure 3.1. 2(b) for the "shear" type. The signals were recorded in a two-channel monitoring board PCI-2, PAC with a sampling rate of 5 MHz. The threshold was set to 40 dB to avoid ambient noise and the acquired signals were pre-amplified by another 40 dB.

3.1.3.3. Fracture details and FEM analysis

As aforementioned, the target of the study was to develop and passively monitor different fracture modes in mortar specimens. In the simple 3-point bending test, it is easily understood that fracture starts from the bottom due to high tensile stresses. However, concerning the modification of the geometry to test a "mixed" fracture mode, simple FEM analysis was deemed necessary. Two dimensional analysis was conducted for both types of testing for comparison purposes. A free version of commercially available software was used [26]. For the three-point bending simulation under discussion, the model geometry was 160x40 mm, similar to the front view of the specimen. Plain strain conditions were applied. The load was placed at the central point of the top side and support was provided by two points at the bottom side (see Figure 3.1. 3a) at the exact points as dictated by the experiment.

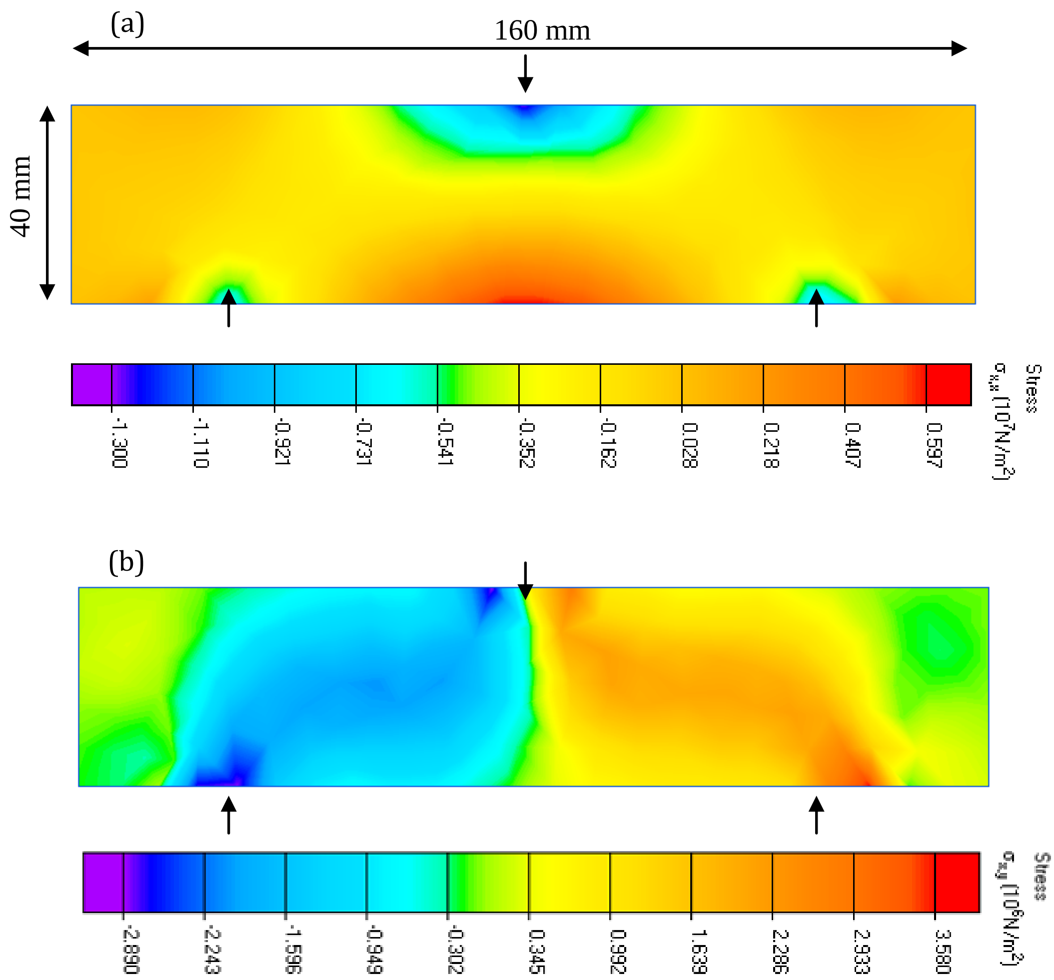

Figure 3.1. 3 *Stress field for three point bending test: (a) normal stress (σxx), shear stress (τxy)*

For the slightly modified geometry intended for the shear-driven fracture, again the front view of the specimen was modeled. In this case the load is applied in a distributed area on the top of the specimen due to a metal tab placed when the material was fresh, while the bottom support is also distributed at two areas (see Figure 3.1. 4a).

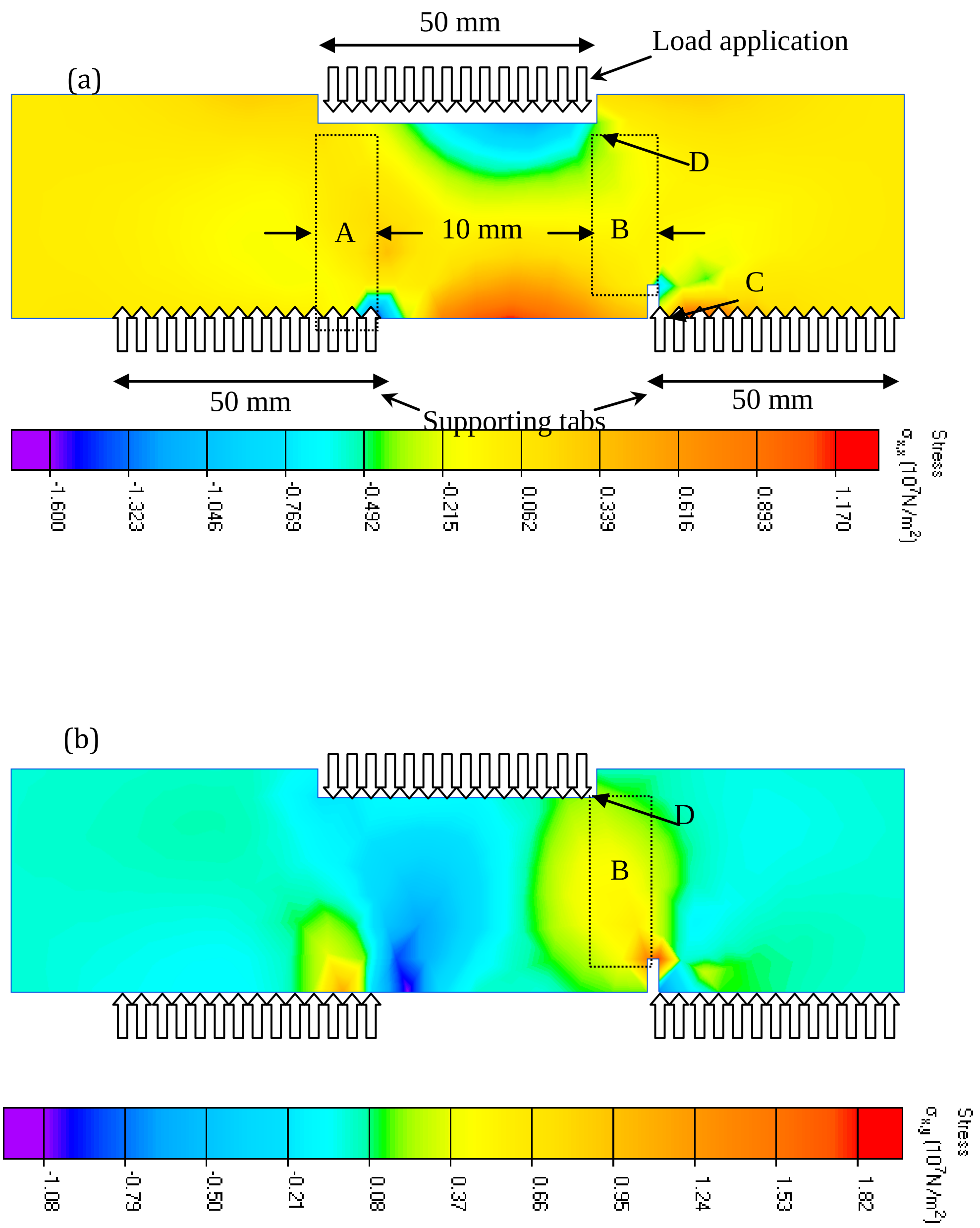

Figure 3.1. 4 *Stress field for the "shear" test: (a) normal stress (σxx), shear stress (τxy)*

The supports were placed in such a way that there is an overlap of opposing forces at the left side (area A in Figure 3.1. 4), while there is a zone of 10 mm without overlapping at the right side between the load and support distributions (area B). The geometry can also be seen in the photograph of Figure 3.1. 2b. This free zone (B) in conjuction with a small notch that was created at the end of the support (point C) led in the fracture of the specimen at this zone. Material elastic constants were indicatively assigned the following values: Elastic modulus 20 GPa and Poisson's ratio 0.2 leading to shear modulus of 8.3 GPa. These values are typical for cementitious materials without however being the only possible values. The geometry was divided into triangular elements with nominal side of 6.5 mm, while the total number of nodes was 163. Other mesh size was also tested (element side of 8 mm) and resulted in very similar stress values with the ones discussed below. Results of the analysis concerning normal and shear stresses are seen in Figures 3.1 (3) and (4) for the two types of specimens. As expected, the normal stresses in the pure bending case, shown in Figure 3.1. 3a, exhibit a positive maximum at the mid span of the bottom, where the specimens actually broke. This happens due to the weak tensile strength of cementitious material. Figure 3.1. 3b shows shear stresses with the same loading condition. Maximum shear stresses are of lower level (approximately half of the corresponding normal), while at the mid-span of the specimen shear stresses change sign, being very close to zero. Therefore, the crack at the center of the specimen can be considered quite close to pure tensile mode.

Concerning the specimen intended for more "shear" fracture, corresponding results are seen in Figure 3.1. 4(a) and (b). Forces and supports were applied by means of tabs instead of contact points. The load application area on top and the left support were overlapped, while there is no overlap between the load application and the support at the right bottom (area B in Figure 3.1. 4a). This led to an unsupported zone available for shearing of the specimen. Figures 3.1 4(a) and (b) show the normal and shear stresses respectively. It is seen that the maximum normal stresses are exhibited away from the notch with the maximum tension near the bottom mid-span point. However, the tip of the notch clearly exhibits maximum shear stresses, as seen in Figure 3.1. 4b, while the shear zone extends to the top in a diagonal direction until the normal angle in point D. Although, low normal stresses may still be applied on the same zone, it can be reasonably argued that the initiation and propagation of the specific crack includes strong shear components which was not the case for the pure bending experiment. Figure 3.1. 5 shows fractured specimens after both types of tests.

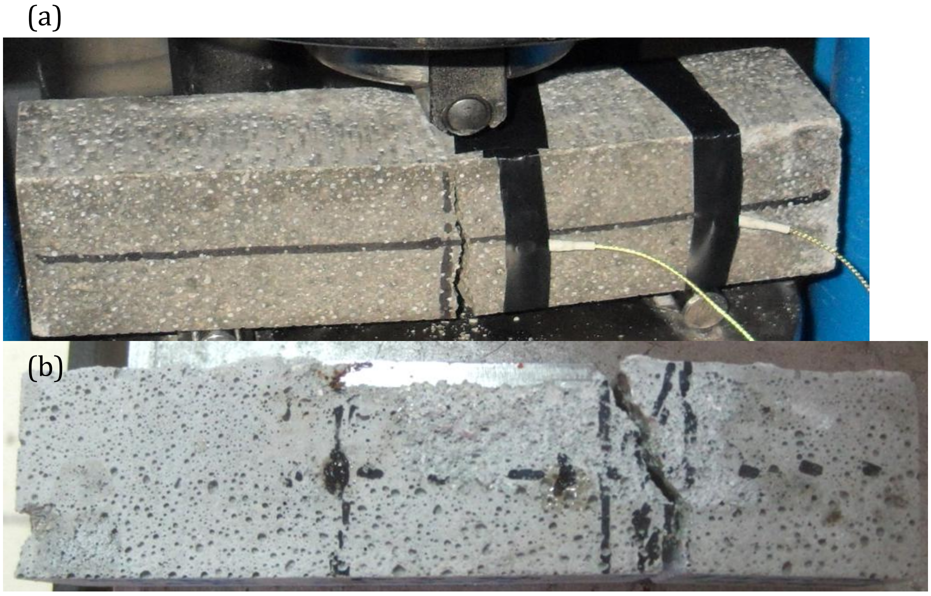

Figure 3.1. 5 *Fractured specimens after (a) bending, (b) shear.*

As the simulation results imply, the specimen tested in pure bending (Figure 3.1. 5a) was fractured at the mid span where maximum tension is exhibited in Figure 3.1. 3a. For the "shear" type of test (Figure 3.1. 5b), the crack extends diagonally from the notch to the top within the zone shear stresses indicated by FEM and being in agreement with the simulation results. Since the cracking events include different constituents of the stress tensor, monitoring by AE is expected to show distinct trends, something presented and analyzed in the following section.

3.1.4. AE results

Results of the acoustic monitoring, concern the total activity and the qualitative features of the waveforms. Figure 3.1. 6a shows the accumulated AE signals (hits) received by the near-by sensors (15 mm from the crack) for typical bending and shear tests.

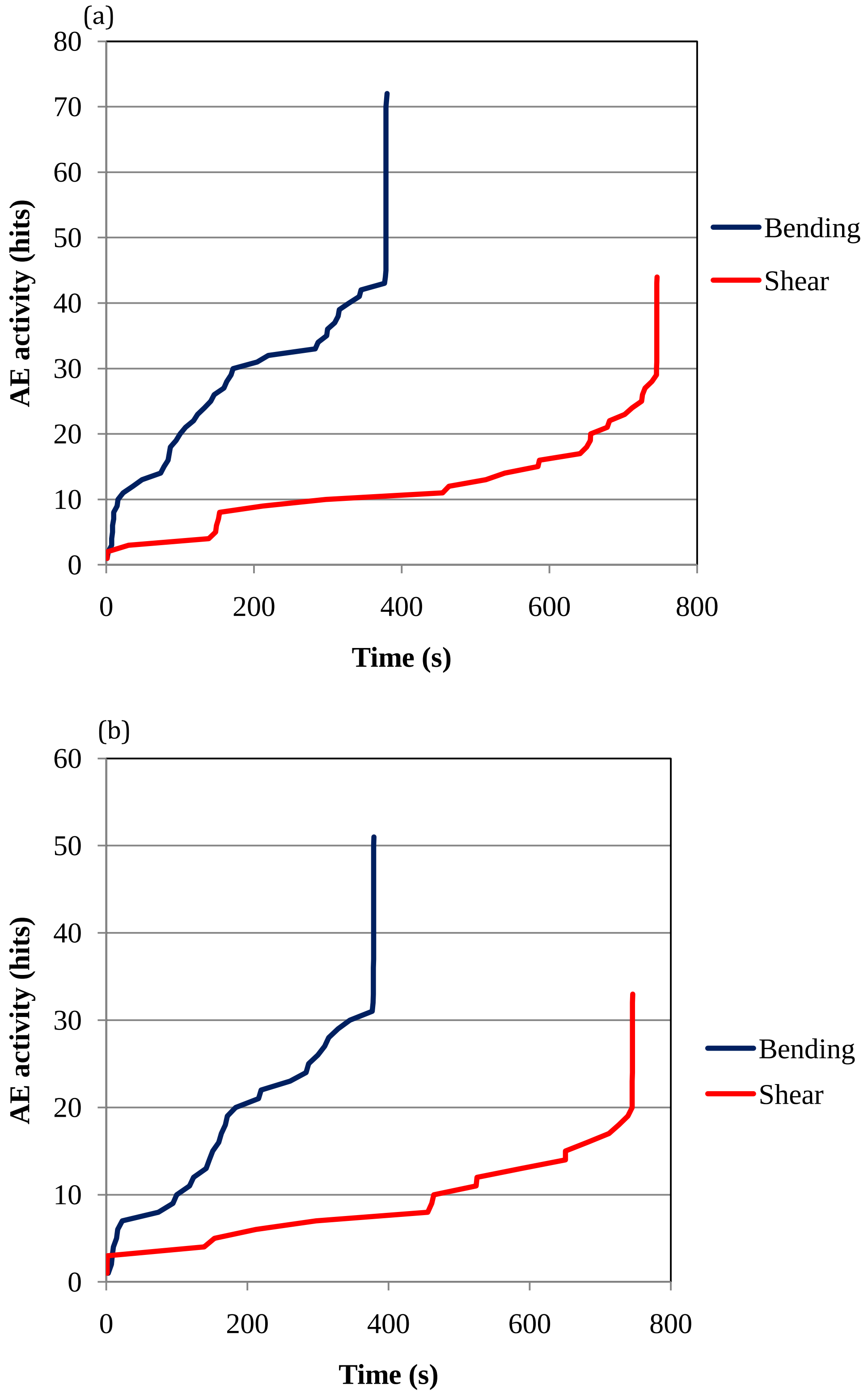

Figure 3.1. 6 *Cumulative AE activity of typical tests (a) 1st sensor (15 mm from the crack), (b) 2nd sensor (55 mm from the crack).*

For both of them the population of hits is built gradually until the moment of final failure where the maximum hit rate is exhibited. The total number of signals is limited below 100 hits. The 2nd sensor (55 mm away from the crack) follows the same behavior with the difference of slightly lower number of hits (Figure 3.1. 6b). This is reasonable due to longer propagation distance which crucially attenuates some of the signals already captured by the 1st receiver, below the threshold level.

Figure 3.1. 7a shows, the RA of the signals received by the 1st sensor for the same experiments.

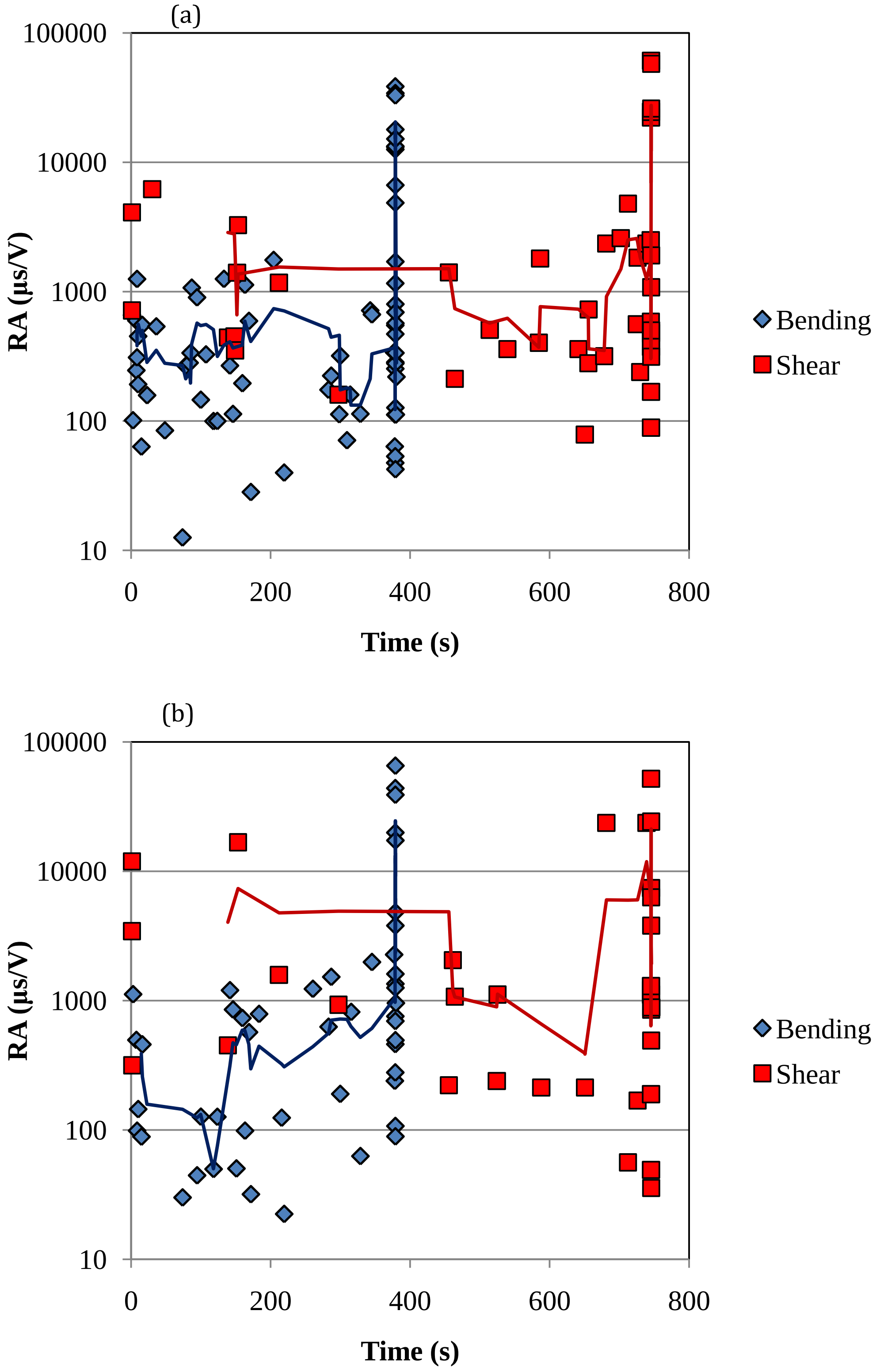

Figure 3.1. 7 *RA vs. Time for different fracture modes as monitored by: (a) 1st sensor (15 mm from the crack), (b) 2nd sensor (55 mm from the crack).*

Concerning the bending mode, RA ranges mainly below 1 ms/V except for the moment of final failure when some RA values of more than 10 ms/V are noted. The specimen under shear on the other hand exhibited some RA values of level higher than 1 ms/V, while at the end it showed a certain increase similar or even higher than the bending case. The solid lines are the moving average of the recent five values in order to show the trends in a more clear way. The corresponding RA values as captured by the 2nd sensor, are seen in Figure 3.1. 7b. Again, the signals coming from the shear experiment exhibit generally higher RA values, as revealed by the moving average lines.

Typical results concerning the AF are included in Figures 3.1 8(a) and (b), for both fracture modes and sensors.

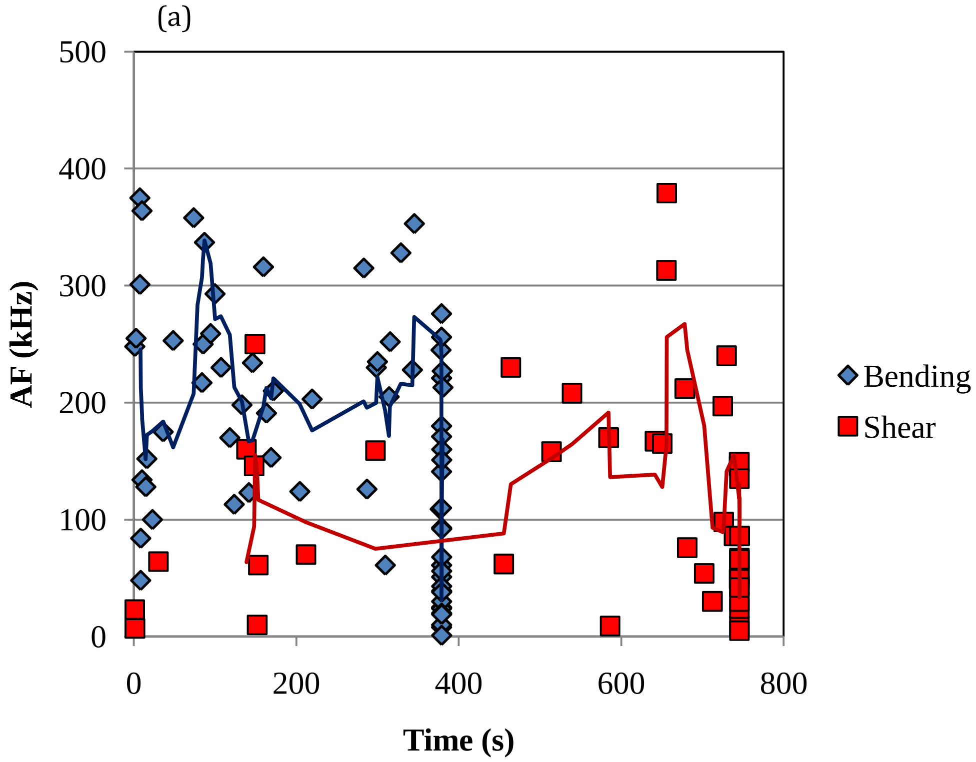

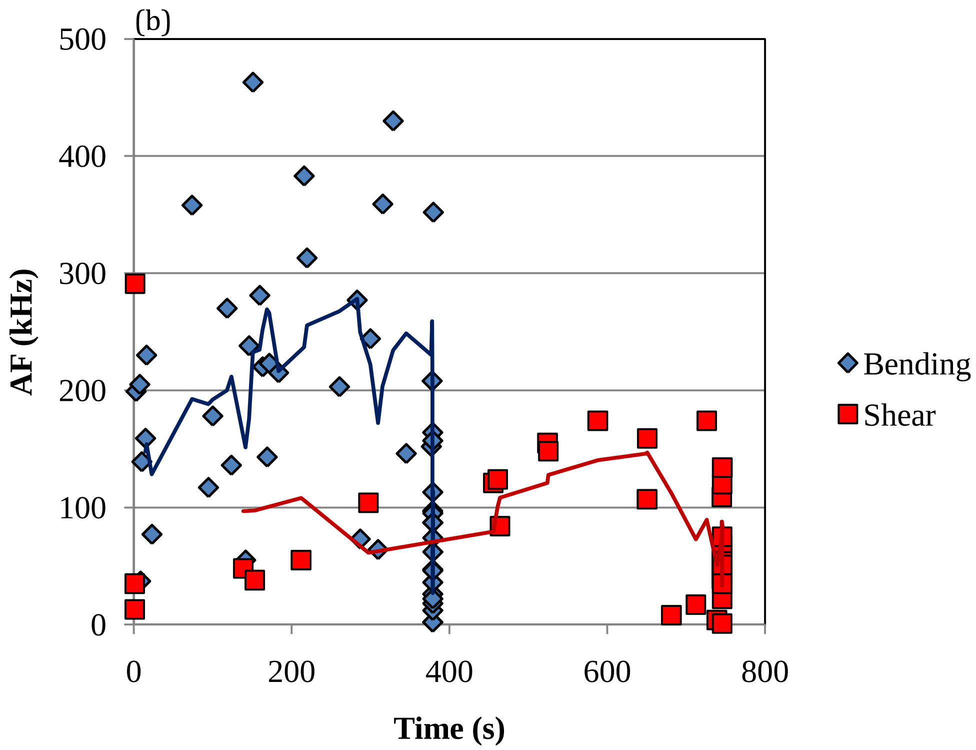

Figure 3.1. 8 *AF vs. Time for different fracture modes as monitored by: (a) 1st sensor (15 mm from the crack), (b) 2nd sensor (55 mm from the crack).*

In this case, the bending type of fracture exhibits higher frequency in average, ranging from 50 kHz to 400 kHz while at failure AF values close to zero are also noted. On the other hand shear mode results in frequencies up to 250 kHz, while at macro-fracture they are limited below 150 kHz. AF measured by the 2nd sensor follows similar trends with the shear being again notably lower than bending (Figure 3.1. 8b). These results are some typical comparisons between pairs of specimens while in the next paragraph the average values of all specimens are discussed.

In the present case, the ambient noise level was low and the applied threshold secured that no external signals are acquired. In order to increase the reliability of the obtained information even more, the following analysis concerns only the “AE events”. This means that for any hit of the first sensor analyzed, another hit was also recorded by the second sensor which belonged to the same source event. Typically for each experiment a number of approximately 20 events were recorded. The AF and RA value of these events are averaged and presented in Figure 3.1. 9.

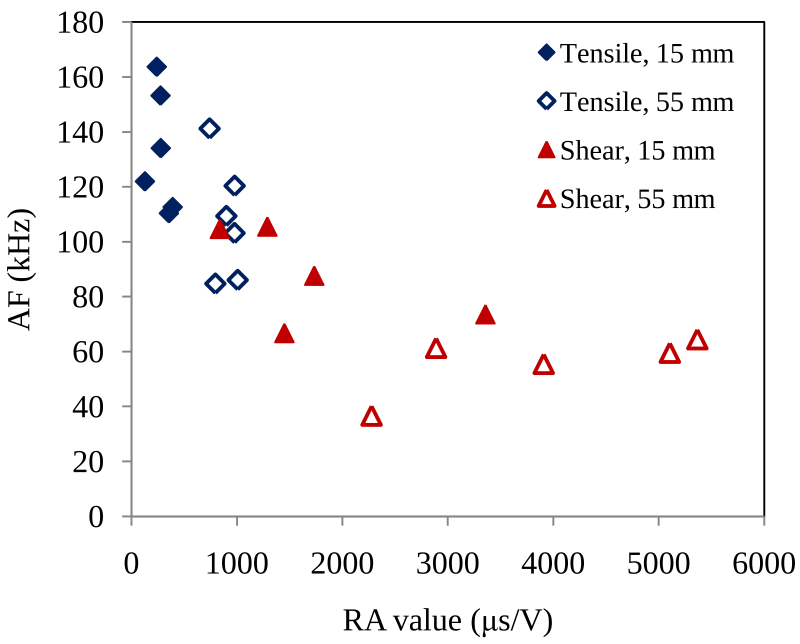

Figure 3.1. 9 *AF vs. RA value for different fracture modes and sensor distances (each symbol is the average of all AE events of each experiment)*

Tensile fracture mode specimens monitored by the 1st sensor, typically exhibit AF between 110 kHz and 160 kHz, while their RA is less than, 500 μs/V in average. Figure 3.1. 9, contains also the corresponding values for the shear type of testing. The average values of AF of the five specimens as measured by the 1st sensor shows a maximum AF of 105 kHz and a minimum RA of 840 μs/V being totally separated from the corresponding population of the bending (tensile) mode as monitored by the sensor at the same distance.

Concerning the same events monitored by the 2nd sensor (at 55 mm) distinct changes are shown. Tensile events exhibit lower frequency (from 80 kHz to 140 kHz) and higher RA, close to 1000 μs/V, compared to the sensor at 15 mm. This is an indication of waveform distortion that occurs in heterogeneous media like cement mortar. Scattering on the boundaries of the microstructure (sand grains, air bubbles) reduces the representative frequency, mainly by more effectively attenuating higher components, while it also elongates the pulse because the energy is redistributed to many random wave paths after each impact and does not arrive in a straight line as would happen in a homogeneous medium [27,28]. Additionally, the sensor at 55 mm exhibits much lower frequency (around 60 kHz) and higher RA values (2000 to 5500 μs/V) than the 1st for the shear mode as well. These indications show that any AE study should be combined with knowledge of wave propagation in the specific material, since a few centimeters of additional propagation between sensor 1 and 2 force noticeable changes.

The above mentioned AE descriptors (AF and RA) are two of the most powerful for discrimination of damage mode [1,4,17]. However, the individual fracture modes result in differences in other AE parameters as well. Figure 3.1. 10 shows the average values of peak frequency (PF) and Amplitude (Amp) for both modes and sensor distances.

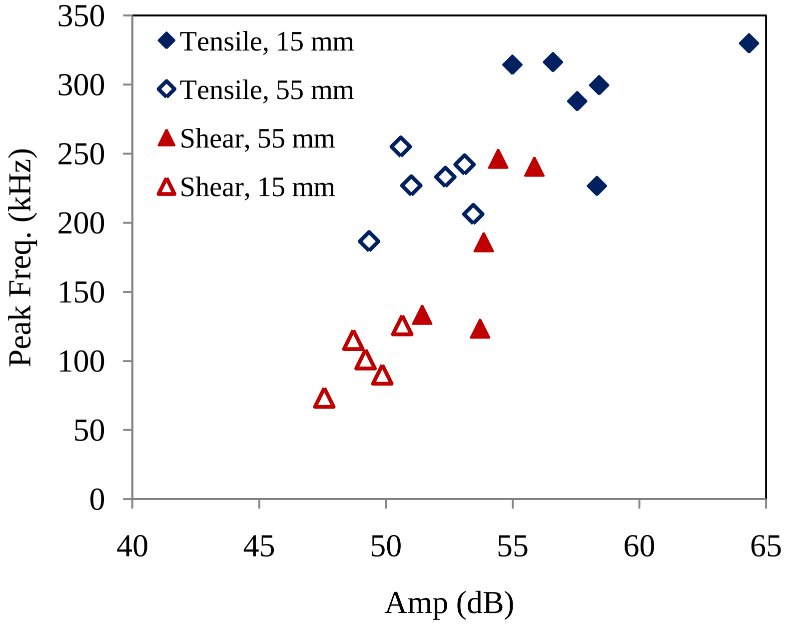

Figure 3.1. 10 *PF vs. Amp for different fracture modes and sensor distances (each symbol is the average of all AE events of each experiment)*

The tensile mode exhibits higher amplitude and peak frequency than shear in average for the same sensor distances. Apart from the effect of fracturing mode, the effect of distance is again highlighted since the sensor at 55 mm obtains much lower amplitude and peak frequencies than the near-by sensor for both cracking modes. Table 3.1. 1 summarizes the average values of basic AE parameters for the two examined fracture modes and propagation distances.

Table 3.1. 1 *Basic AE parameters for different modes and propagation distances to the sensor*

Mode and distance		AF (kHz)	RA (μs/V)	AMP (dB)	P-Freq (kHz)
Tensile (15 mm)	**Average**	**132.4**	**278.4**	**58.4**	**295.2**
	COV	16.5%	33.2%	5.5%	12.5%
Shear (15 mm)	***Average***	***87.6***	***1733.6***	***53.8***	***186.1***
	COV	*18.0%*	*49.7%*	*2.7%*	*27.7%*
Tensile (55 mm)	**Average**	**109.3**	**900.7**	**52.3**	**233.2**
	COV	19.6%	12.2%	3.0%	10.5%
Shear (55 mm)	***Average***	***55.6***	***3908.0***	***49.2***	***101.3***
	COV	*17.8%*	*30.8%*	*2.1%*	*18.2%*

One conclusion from these data concerns the discrepancies in the AE descriptors between the different fracture modes monitored at a standard distance. Shear (or mixed mode) fracture emits signals of lower basic frequency characteristics and amplitude but longer in rise time than tensile. The differences are visible in all parameters but greater changes are seen in RA, for which the values of shear (1734 μs/V) are more than six times higher than tension (278 μs/V). The decrease in amplitude is also large since shear emissions are lower than tensile by almost 5 dB (58.4 dB to 53.8 dB). Additionally, frequency characteristics measured either by the AF or the PF show strong decrease for the shear mode by about 35% compared to tensile events. Overall, the clearly separated averages and the relatively limited variance (presented as standard deviation over average, coefficient of variation, COV) enables quite good separation of the clusters without need to employ pattern recognition approaches. It is seen therefore, that in simple geometries in laboratory conditions, the cracking mode can be reliably monitored by its AE fingerprint.

However, the differences measured by the two sensors show how much the results are dependent on the testing conditions and specifically the distance between the cracks and the sensors. The additional distance of 40 mm between the two sensors forces a decrease of more than 20% in frequency parameters (132 kHz to 109 kHz for tension and 87 kHz to 56 kHz for shear) and an increase by three to four times in RA (278 μs/V to 900 μs/V for tensile and 1734 μs/V to 3908 μs/V for shear). Indeed, scattering is quite strong in this kind of material due to inhomogeneity which distorts the shape of the propagating pulse resulting also in considerable attenuation especially at the higher frequencies. Complimentary to scattering, viscous damping of the material contributes to loss of transmitted energy to heat, resulting in a decrease in amplitude of 5 to 6 dB between the first and second receiver.

3.1.5. Discussion

Combining the information of Table 3.1. 1, an illustration of an AE waveform typical of each mode, as recorded by the sensor at 15 mm is shown in Figure 3.1. 11.

.

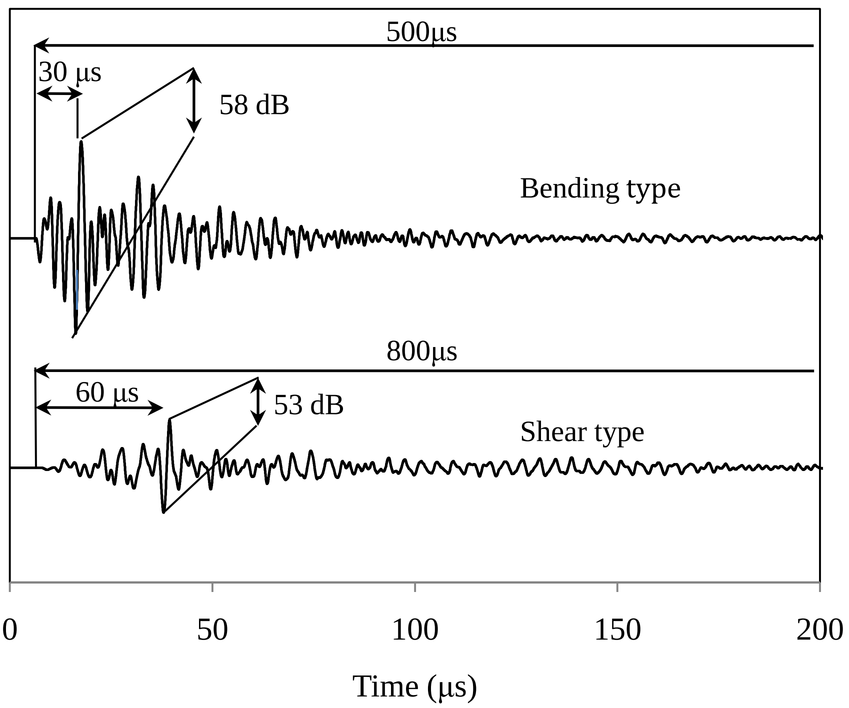

Figure 3.1. 11 *Typical waveforms attributed to different fracture modes (distance 15 mm).*

The "tensile" waveform has an amplitude much higher than shear, while it is also characterized by shorter "rise time" (30 μs compared to 60 μs). Additionally the total duration of a tensile signal is significantly shorter than shear.

The above mentioned results show that the separation of fracture modes is tangible in laboratory conditions. The characterization in real structures would also be tangible if it weren't for the signal distortion and attenuation that occurs in heterogeneous materials. Along with the sensor's response this is another parameter that renders the application of AE case-specific and does not allow fully exploiting its potential in real structures [29]. If distortion is not taken into account, tensile signals monitored at longer distance (55 mm) may well be overlapped with shear signals received at 15 mm from the source, see Figures 3.1 (9) and (10). This would prevent from applying characterization in real structures where the distances between cracks and sensors are typically of the order of meters and highlights the importance of incorporating the distance that the wave travelled from the crack tip to the sensor. Fortunately contemporary AE equipment includes software with powerful location algorithms. Therefore, the time delay between acquisition of waveforms of the same event at different positions, leads to calculation of the crack location in real time, enabling an inverse procedure for evaluation of the signal as-emitted by the crack before distortion due to inhomogeneity is accumulated in the as-received by the sensor waveform [16].

Another issue that should be highlighted concerning the specific study is that although cement mortar can be regarded as macroscopically homogeneous concerning the stress analysis, still the material contains grains of average size 2 mm. Therefore, it is reasonable that the crack propagates on the interphase between the matrix and the inclusions and the macroscopically simulated or expected stress fields may somehow differ from the actual in the micro-scale of the grain – matrix interphase. If the material was totally homogeneous then the actual stresses would possibly be closer to the shear stresses simulated. However, this study is focused on cementitious materials, which in any case include sand grains and therefore, this is a realistic way to study modes of fracture in cement-based materials. As a future task experiments on marble specimens are scheduled. Also possible modifications in the geometry will be studied in order to develop pure shear fracture, since currently low level normal stresses are also developed on the tip of the notch. Upgrading the scale of the problem is also being considered in order to facilitate concrete testing.

Finally, the sensors response function should be discussed. The results obtained refer to a specific sensor type. This type may be considered broadband compared to other resonant AE sensors but still its response is far from being flat. Therefore, the waveforms captured are certainly influenced by the sensor “preferences”. The specific values obtained would definitely differ if other pair of sensors had been used in the experiment. However, what is emphasized herein, is the change between the emissions of the different fracture modes and separation distances. All the experiments were conducted by the same pair of sensors so that any distinct trends are attributed directly to the fracture mode and separation distance. In any case, in the field of concrete AE, standardization is currently being attempted [17] meaning that for the proposed type of sensor a similar procedure could be undertaken to establish a database with the AE fingerprints of fracture modes at various propagation distances.

3.1.6. Conclusions

The present experiment deals with the nondestructive monitoring of the fracture process in cementitious materials using the acoustic emission technique. The main aim is to characterize the acoustic signature of fracture modes. For this reason, the tensile and shear fracture mode were investigated. Both types of experiments were conducted using the same loading equipment with slight modifications. Elementary finite element analysis showed that the modifications were actually effective to alter the stress field and shift from the normal tensile stresses (responsible for fracture in three point bending) to dominant shear stress. Monitoring with broadband AE sensors revealed distinct trends for the different fracture modes. Specifically, AE signals from tensile tests exhibit higher amplitude and frequency, while shear modes exhibit longer duration and lower rising angle, as measured by the RA value. The results show that accurate characterization of modes is possible in laboratory based on simple features recorded by a single AE sensor. This would be very beneficial for warning against final failure since, cracking modes generally follow a sequence during fracture. Results also highlight the need to jointly study AE with elastic wave propagation, since an additional distance of a few centimeters alters significantly the frequency content and shape of the acquired waveforms. This is an important parameter that needs to be amended in order to fully exploit the capabilities of AE in laboratory and expand its application for reliable characterization in real structures.

3.1.7. References

1. K. Ohno, M. Ohtsu, Crack classification in concrete based on acoustic emission, Constr Build Mater. 24(12) (2010) 2339–46.
2. D.G. Aggelis, T. Shiotani, S. Momoki, A. Hirama, Acoustic emission and ultrasound for damage characterization of concrete elements, ACI Materials J. 106(6) (2009) 509-514.
3. D.G. Aggelis, D.V. Soulioti, N.M. Barkoula, A.S. Paipetis, T.E. Matikas, Influence of fiber chemical coating on the acoustic emission behavior of steel fiber reinforced concrete, Cement & Concrete Composites 34 (2012) 62–67.
4. D.G. Aggelis, Classification of cracking mode in concrete by acoustic emission parameters, Mechanics Research Communications 38 (2011) 153–157.
5. C.U. Grosse, F. Finck, Quantitative evaluation of fracture processes in concrete using signal-based acoustic emission techniques, Cem Concr Compos 28 (2006) 330–336.
6. M. Shigeishi, M, Ohtsu, Acoustic emission moment tensor analysis: development for crack identification in concrete materials, Construction and Building Materials, 15 (2001) 311-319.
7. T. Shiotani, Evaluation of long-term stability for rock slope by means of acoustic emission technique, NDT&E Int 39(3) (2006) 217–28.
8. T. Shiotani, D. G. Aggelis, O. Makishima, Global monitoring of large concrete structures using acoustic emission and ultrasonic techniques, Journal of Bridge Engineering-ASCE 14(3) (2009) 188-192.
9. C.U. Grosse, M. Ohtsu, Acoustic emission testing, Springer, Heidelberg, 2008.
10. A. Carpinteri, F. Cardone, G. Lacidogna, Energy Emissions from Failure Phenomena:Mechanical, Electromagnetic, Nuclear, Experimental Mechanics 50 (2010) 1235–1243.
11. B-K. Jang, T. Kishi, Mechanical properties of TiNi fiber impregnated CFRP composites, Materials Letters 60 (2006) 518-521.
12. H. Elaqra, N. Godin, G. Peix, M. R'Mili, G. Fantozzi, Damage evolution analysis in mortar, during compressive loading using acoustic emission and X-ray tomography: Effects of the sand/cement ratio, Cement and Concrete Research 37 (2007) 703–713

13. M. Ohtsu, H. Watanabe, Quantitative damage estimation of concrete by acoustic emission, Construction and Building Materials 15 (2001) 217–224.
14. D. Soulioti, N.M. Barkoula, A. Paipetis, T.E. Matikas, T. Shiotani, D.G. Aggelis, Acoustic emission behavior of steel fibre reinforced concrete under bending, Constr Build Mater. 23 (2009) 3532–3536.
15. Y. Lu, Z. Li, W. I. Liao. Damage monitoring of reinforced concrete frames under seismic loading using cement-based piezoelectric sensor, Materials and Structures, 44(7) (2011) 1273-1285.
16. D. G. Aggelis, T. E. Matikas, Effect of plate wave dispersion on the acoustic emission parameters in metals, Computers and Structures 98-99 (2012) 17-22.
17. Ohtsu M. Recommendations of RILEM Technical Committee 212- ACD: acoustic emission and related NDE techniques for crack detection and damage evaluation in concrete: 3. Test method for classification of active cracks in concrete structures by acoustic emission. Mater Struct 43(9) (2010) 1187–1189.
18. K. Van Tittelboom, N. De Belie, F. Lehmann, C. U. Grosse, Acoustic emission analysis for the quantification of autonomous crack healing in concrete, Construction and Building Materials 28 (2012) 333–341.
19. S. Granger, A. Loukili, G. Pijaudier-Cabot, G. Chanvillard, Experimental characterization of the self-healing of cracks in an ultra high performance cementitious material: Mechanical tests and acoustic emission analysis, Cement and Concrete Research 37 (2007) 519-527.
20. M. M. Kuba, D. C. Van Aken, Plastic strain accommodation and acoustic emission during melting of embedded particles, Materials Letters 77 (2012) 89-92.
21. K. Wu, B. Chen, W. Yao, Study of the influence of aggregate size distribution on mechanical properties of concrete by acoustic emission technique, Cement and Concrete Research 31 (2001) 919-923.
22. T.P. Philippidis, V.N. Nikolaidis, A.A Anastassopoulos, Damage characterization of carbon/carbon laminates using neural network techniques on AE signals, NDT&E Int. 31(5) (1998) 329–40.
23. D.G. Aggelis, N.M. Barkoula, T.E. Matikas, A.S. Paipetis, Acoustic emission monitoring of degradation of cross ply laminates, J Acoust Soc Am. 127(6) (2010) EL246-251.

24. D.G. Aggelis, A.C. Mpalaskas, D. Ntalakas, T.E. Matikas. Effect of wave distortion on acoustic emission characterization of cementitious materials, Construction and Building Materials 35 (2012) 183–190.
25. EN 13892-2:2002, Methods Of Test For Screed Materials - Part 2: Determination Of Flexural And Compressive Strength.
26. http://www.quickfield.com/ (Students' QuickField 5.9)
27. M.L. Cowan, K. Beaty, J.H. Page, L. Zhengyou, P. Sheng, Group velocity of acoustic waves in strongly scattering media: Dependence on the volume fraction of scatterers, Physical Review E 58(5) (1998) 6626-6636
28. D.G. Aggelis, T. Shiotani, Experimental study of surface wave propagation in strongly heterogeneous media, Journal of the Acoustical Society of America J. Acoust. Soc. Am. 122 (5), (2007) EL 151-157
29. J.J. Scholey, P.D. Wilcox, M.R. Wisnom, M.I. Friswell, Quantitative experimental measurements of matrix cracking and delamination using acoustic emission, Compos A 41 (2010) 612–23.

3.2. Concrete[3]

3.2.1. Purpose

The characterization of the dominant fracture mode may assist in the prediction of the remaining life of a concrete structure due to the sequence between successive tensile and shear mechanisms. Acoustic emission sensors record the elastic responses after any fracture event converting them into electric waveforms. The characteristics of the waveforms vary according to the movement of the crack tips, enabling characterization of the original mode. In this study fracture experiments on concrete beams are conducted. The aim is to examine the typical acoustic signals emitted by different fracture modes (namely tension due to bending and shear) in a concrete matrix. This is an advancement of a recent study focusing on smaller scale mortar and marble specimens. The dominant stress field and ultimate fracture mode is controlled by modification of the four-point bending setup while acoustic emission is monitored by six sensors at fixed locations. Conclusions about how to distinguish the sources based on waveform parameters of time domain (duration, rise time) and frequency are drawn. Specifically, emissions during the shear loading exhibit lower frequencies and longer duration than tensile. Results show that combination of AE features may help to characterize the shift between dominant fracture modes and contribute to the structural health monitoring of concrete. This offers the basis for in-situ application provided that the distortion of the signal due to heterogeneous wave path is accounted for.

[3] Adapted from “Acoustic emission signatures of damage modes in concrete” Proc. SPIE 9062, Smart Sensor Phenomena, Technology, Networks, and Systems Integration 2014, 90620P (22 April 2014); doi: 10.1117/12.2044750, ISBN 9780819499882.

3.2.2. Introduction

The fracture of structural materials follows a sequence; micro-cracking due to tensile stresses is initially induced and consequently shearing phenomena are observed[1]. Monitoring of the dominant fracture type (tensile/shear) provides information on the structural condition and enables evaluations on its remaining life. Fracture monitoring can be conducted by the acoustic emission (AE) technique, which records the elastic pulses after crack nucleation and propagation incidents. This is done by piezoelectric sensors placed on the surface of the material[2]. Different studies have been published concerning the characterization of the fracture mode [3,4], monitoring of other processes like concrete self-healing [5] and damage evolution [6,7]. Classification results are quite successful under laboratory conditions. Apart from processes like debonding or pull-out that resemble shear motion and can be separated from tensile cracking [3,4], recently shear and tensile fracture of the matrix material itself has been targeted in mortar and granite specimens[8]. In this experiment, the shear and bending modes are directly applied in concrete as an upgrade of the previous study on mortar. The experiments are based on four-point bending. Bending results in a tensile fracture starting from the bottom of the beam. To create shear conditions, a modification to the basic set up was applied, by decreasing the free span at the bottom and leaving only a small zone for fracture. AE was monitored by six sensors (two resonant and four broadband) in both set ups.

Some of the basic parameters of an AE waveform that is recorded by the piezoelectric sensors are the amplitude, A (Volts or dB) and the energy (area under the rectified signal envelope, usually dimensionless). Additionally, the duration (delay between first and last threshold crossings) and rise time, RT (delay between the first threshold crossing and peak amplitude in μs) are connected to the original fracture mode. Frequency content is measured by average frequency, AF, which is the number of threshold crossings over the duration of a signal and the central frequency, CF, which is the centroid of the frequency of the spectrum measured in kHz. In general, RT obtains higher values for shear events, rather than tensile due to the stronger shear wave component excited. Frequency on the other hand is higher for the tensile events [3,4,7,8].

3.2.3. Experimental Details

3.2.3.1. Materials and mechanical testing

One concrete mixture was produced consisting of eleven specimens. The specimens were prismatic beams of size 100x100x400 mm. The aggregates consisted of 56% crushed sand, 13.87% fine gravel and 30.13% coarse gravel with maximum aggregate size 31.5 mm, while the water/cement ratio was 0.70 by mass. The density and the water absorption of the crushed sand were 2601 kg/m3 and 0.98 %, of fine gravel 2621 kg/m3 and 0.75 %, of coarse gravel 2681 kg/m3 and 0.61 % respectively. The cement type was CEMII/A-M(P-LL). The exact mix proportions were as follows: cement (type II 42.5N) 80 kg/m3, cement (type II 32.5N) 200 kg/m3, water 195 kg/m3, crushed sand 1050 kg/m3, fine gravel 260 kg/m3, coarse gravel 565 kg/m3 , retarder - plasticizer (CHEM I) 1.54 kg/m3, retarder - plasticizer (CHEM II) 1.96 kg/m3 . The actual bulk density of concrete was 2359 kg/m3) while the ambient temperature was 25 oC. The workability as measured by the slump test was 11 cm. The specimens were cured in water saturated with calcium hydroxide at 23 ±2 oC. The average compressive strength of three days was fc(3)= 18.0 MPa, of seven days fc(7)= 24.7 MPa and of twenty eight days was fc(28)= 33.8 MPa (with a standard deviation of 3.0 MPa).

To establish the flexural testing of the prismatic beams, the BS EN 12390-5:2000 standard was followed. Four of the prismatic beam specimens were subjected to four-point bending (Figure 3.2. 1a), with a bottom span length of 300 mm. The tests were conducted on a servo-hydraulic Instron Model 5967 (30kN Capacity) and the third point loading was applied to the specimen without eccentricity and torque. The load was applied at a constant rate of 166.7N/sec up to the breaking point. The specimens failed with a vertical crack in the middle of the bottom span, as seen in Figure 3.2. 1 b.

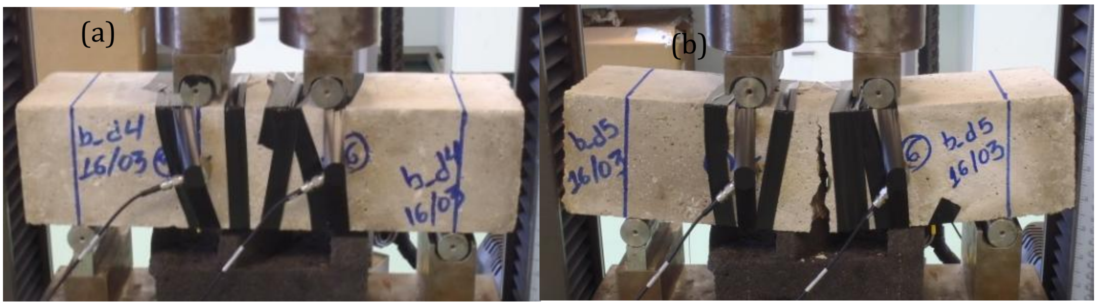

Figure 3.2. 1 *(a) photograph of the prismatic beam specimen for four-point bending testing, (b) Representation of the AE sensors location on the bending specimen (distances in m)*

The setup was modified for the test of the other seven specimens that were intended for the shear mode, a steel tab of length of 140 mm was placed in the center above the specimen when fresh in the mould (Figure 3.2. 2a). This created a reduction in cross section, stress concentration points and enabled the distributed loading on the top side by means of a metallic tab (Figure 3.2. 2b). Additionally two distributed supports at the bottom were used. Although at the four-point bending test, the crack starts from the central point of the bottom side due to the tensile stresses, for the modified test, the metal tabs used for support reduce the free bottom span and leave only a small zone available for shearing at one side of the specimen (left in Figure 3.2. 2b). The load was applied at a constant rate of 166.7Nt/sec to the breaking point.

Figure 3.2. 2 *(a) Concrete beam with reduced cross section for shear testing, (b) test set up for the shear testing.*

A sketch of the test set up for the shear test is seen in Figure 3.2. 3a. It is noted that small notches were applied at the shearing zone to dictate the side of the specimen where fracture would occur. This enabled the placement of the AE sensors close to the fracture surface in order to minimize attenuation effects. Figure 3.2. 3b shows the crack in a typical specimen after fracture in the shear setup.

(a) (b)

Figure 3.2. 3 *(a) Schematic representation of loading and support system at the shear test set up, (b) shear test after fracture, a large crack is visible in the shear zone (see arrow).*

Concerning the developed stress field, it is clear that four-point bending nominally results in pure tension at the bottom of the beam. The modified set up of the "shear" experiment is certainly not as straightforward. Investigation with the finite element method concerning a similar geometry but in smaller scale (40% of the present) revealed that the maximum shear stresses acting on the notch are stronger than the normal [9]. Therefore, it is certain that although the test is not pure shear, it is mixed-mode with stronger shear than normal components.

3.2.3.2. Monitoring technique

AE was monitored by two types of piezoelectric sensors, namely the R15 (Physical Acoustics Corp., PAC) with resonance nominally at 150 kHz, as well as the Pico (PAC) which are considered more broadband with a sensitivity peak around 450 kHz. In total six sensors were applied, namely four Pico and two R15. The signals were pre-amplified by 40 dB and were digitized by a sampling rate of 3 MHz in a PCI-8 board of PAC. In total six sensors were applied at the specimens in both cases of bending and shear tests, namely four Pico and two R15 (see Figure 3.2. 1 for bending and Figures 3.2. 2(b) and 3(b) for shear). The representation with the location of the sensors for both setups is seen in Figures 3.2. (4) a and (b). Grease was applied between the sensors and the specimen's surface to enhance acoustic coupling, while they were secured by tape during the experiment. All signals with amplitude higher than 40 dB (0.01 V) were recorded, while for the analysis, the signals with energy "zero" were disregarded. For location purposes the pulse velocity was measured by pencil lead breaks to the value of 4500 m/s. (Figure 3.2. 5) shows a typical AE waveform. Among many parameters that have been analyzed in AE literature, particular attention in this study is given to RT and AF.

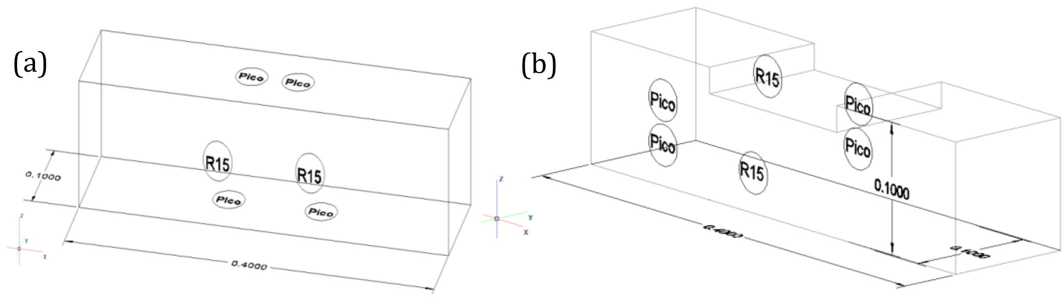

Figure 3.2. 4 *(a) Representation of the AE sensors location on the bending (a) and the shear (b) specimen (distances in m)*

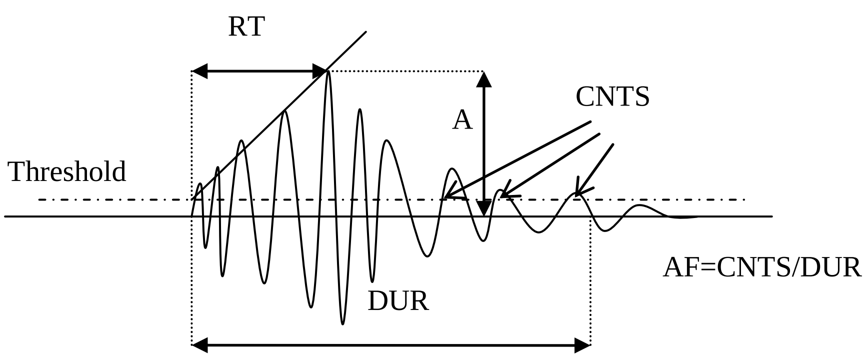

Figure 3.2. 5 *Typical AE waveform with main features.*

3.2.4. Results

Examples of the cumulative AE behavior for both types of fracture are shown in Figure 3.2. 6 (as recorded by the nearest Pico sensor). Figure 3.2. 6 (a) concerns the bending layout. For all specimens there is a scarce AE recording initially followed by a rapidly accumulating stage which signifies the final failure of the specimen. Concerning the shear layout, the AE curves exhibit an additional part of intermediate inclination between the initial and the final part (Figure 3.2. 6b). Three stages could be discerned, one of micro cracking with low number of emissions, the next with evidently more serious cracking development and moderate AE rate and finally the stage of final fracture when the rate of AE is maximum and signifies the end of the experiment due to split of the specimen in two. This is a repeatable trend for all the specimens fracture by the shear layout and shows damage in this case came more gradually as compared to the bending. The population of the acquired signals is comparable with an increase for shear by about 20% in average.

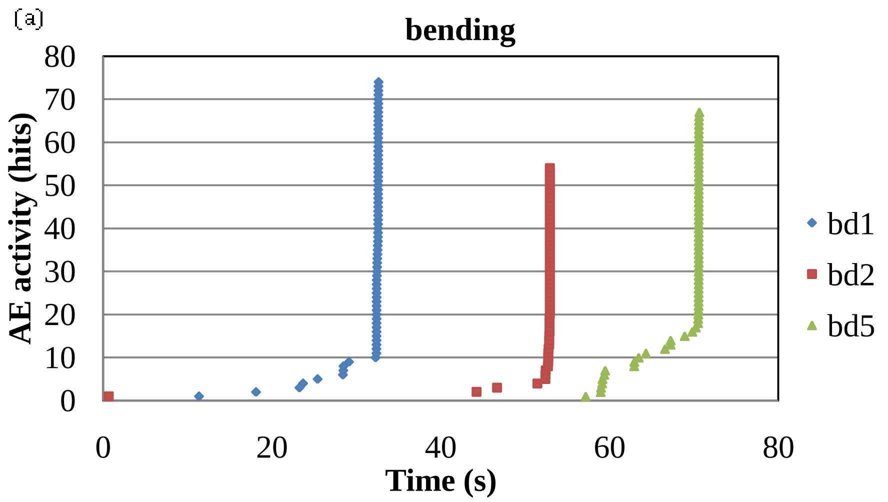

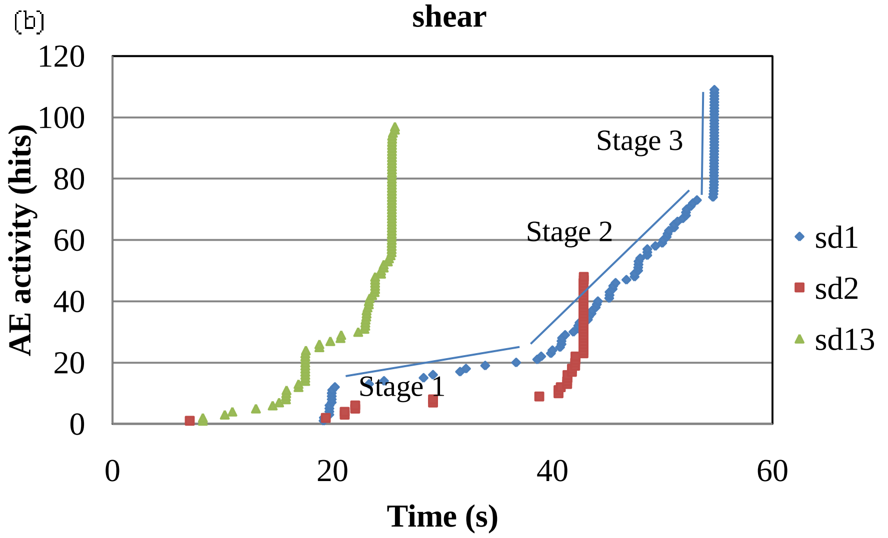

Figure 3.2. 6 *(a) Cumulative AE activity for bending tests in three concrete specimens as recorded by two pico sensors per specimen located at 50 mm diametrically opposite position from the cracking zone. (b) Cumulative AE activity for shear tests in three concrete specimens as recorded by two pico sensors per specimen located at 50 mm diametrically opposite position from the cracking zone.*

Concerning specific AE parameters, Figure 3.2. 7 shows the average frequency vs. rise time for the whole population of AE activity of the bending and shear tests of all the concrete specimens as recorded by the pico sensors. Despite the certain overlap of the numerous points in the AF-RT plane, a strong shift of the shear hits to lower AF and longer RT is evident. This is also shown by the difference between the averages of the two populations (see larger symbols). There is a difference of almost 100 kHz in AF between tensile and shear average values, while the average RT of the shear is again visibly higher than the tensile.

Table 3.2. 1 includes the averages of AF and RT as measured by the broadband and the resonant sensors. The total number of emissions was more than one thousand of hits for both bending and shear cases for all specimens combined. Monitoring with broadband sensors shows the different frequency characteristics, bending produced an average of 281 kHz while shear testing resulted in 192 kHz. Additionally, the RT of shear is 32% longer than bending (747 μs over 563 μs). These trends confirm the corresponding results obtained in mortar and marble [10]. Resonant sensors manage to catch a difference in rise time though it is only 11%, while they do not register systematic changes in frequency.

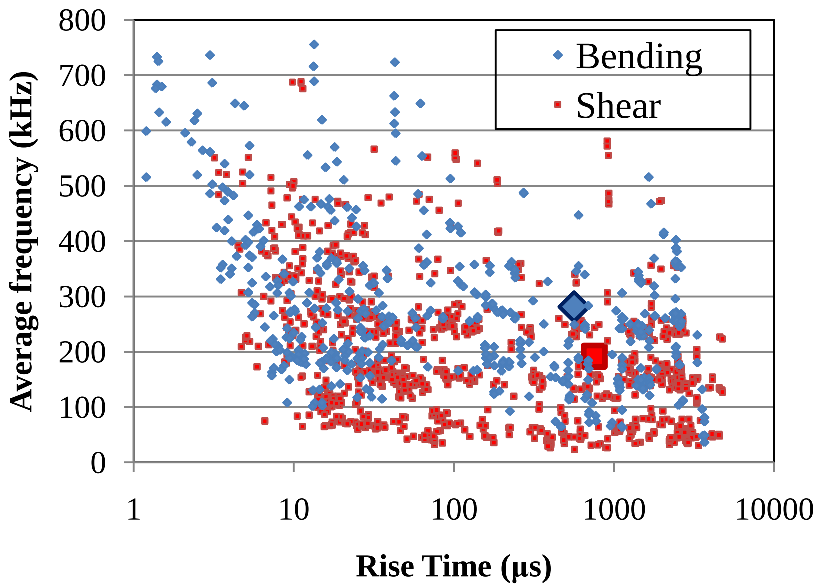

Figure 3.2. 7 *Average frequency vs. rise time for bending and shear tests in all concrete specimens as recorded by all the pico (four) sensors per specimen.*

Table 3.2. 1 *AE parameters for the different fracture modes with two different types of sensor in concrete specimens*

	AF (kHz)	RISE time (μs)
Bending (broadband)	281	563
Shear (broadband)	192	747
Bending (resonant)	210	392
Shear (resonant)	211	436

Despite the large overlap of the data, the differences in averages are very important. The experimental scatter is inherent with AE measurements and comes mainly by the random nature of fracture, since each crack propagation event cannot be identical to the previous of next. This variability is certainly passed into the AE data, something that does not occur for example in ultrasonics, where the excitation may always be identical. However, the analysis of AE does not depend on single hits but on large populations of data. Therefore, trends and average values obtain great significance and are indicative of any shift in the fracture process.

It should be kept in mind that in a heterogeneous medium like concrete, the results always depend on the distance between the cracking sources and the position of the sensors. The texture of the material imposes strong damping and scattering altering the waveform characteristics [11,12]. In this case, the presented results concern the whole number of broadband sensors and therefore, the effect of propagation distance although it is certainly included in the results, does not mask the trends and some differences between the two modes can be seen. However, a more thorough investigation by separating the data to different zones (shorter/medium/longer) propagation distance would clear the differential effect of scattering which is now included in the data.

3.2.5. Conclusions

The present experiment presents the AE behavior of concrete beams under two different fracture modes. Specifically, the beams were subjected to four-point bending and shear stress and their activity was monitored by several AE transducers. Despite the large experimental scatter, which is certainly inherent to the measurement of AE and fracture processes, distinct differences in waveform characteristics were registered. Specifically, bending, which is expressed by tensile stress cracking at the bottom of the beam, exhibited frequency content of emissions nearly 50% higher than shear in average. Additionally, it registered shorter waveforms with much shorter rise time. These changes are important because they can lead to the determination of the active fracture by non destructive and passive AE monitoring. This can help in the study of materials' fracture in controlled conditions, while even in real conditions, the determination of the damage mode will enable the evaluation of the fracture stage and would allow projections on the remaining life span.

3.2.6. References

[1] Ohtsu, M., "Recommendations of RILEM Technical Committee 212- ACD: acoustic emission and related NDE techniques for crack detection and damage evaluation in concrete: 3. Test method for classification of active cracks in concrete structures by acoustic emission," Mater Struct 43(9), 1187–1189 (2010).

[2] Shull, P. J., [Nondestructive evaluation, Theory, Techniques and Applications], CRC Press, New York, (2002).

[3] Aggelis, D.G., "Classification of cracking mode in concrete by acoustic emission parameters," Mechanics Research Communications 38, 153–157 (2011).

[4] Ohno, K., Ohtsu, M., "Crack classification in concrete based on acoustic emission," Constr Build Mater., 24(12), 2339–2346 (2010).

[5] Van Tittelboom, K., De Belie, N., Lehmann, F., Grosse, C. U., "Acoustic emission analysis for the quantification of autonomous crack healing in concrete," Construction and Building Materials 28, 333–341 (2012).

[6] Carpinteri, A., Lacidogna, G., Niccolini, G., Puzzi, S., "Critical defect size distributions in concrete structures detected by the acoustic emission technique," Meccanica 43 (3), 349-363 (2008).

[7] Shiotani, T., "Evaluation of long-term stability for rock slope by means of acoustic emission technique," NDT&E Int 39(3), 217–28 (2006).

[8] Aggelis, D.G., Mpalaskas, A.C., Matikas, T.E., Van Hemelrijck, D. "Acoustic emission signatures of damage modes in structural materials, " Proceedings of SPIE - The International Society for Optical Engineering 8694 , art. no. 86940T (2013).

[9] Aggelis, D.G., Mpalaskas, A.C., Matikas, T.E., "Investigation of different fracture modes in cement-based materials by acoustic emission, " Cement and Concrete Research 48, 1–8 (2013).

[10] Aggelis, D.G., Mpalaskas, A.C., Matikas, T.E., "Acoustic signature of different fracture modes in marble and cementitious materials under flexural load, " Mechanics Research Communications 47, 39– 43 (2013).

[11] Tsinopoulos, S. V., Agnantiaris, J. P., Polyzos, D., "An advanced boundary element/fast Fourier transform axisymmetric formulation for

acoustic radiation and wave scattering problems," J. Acoust. Soc. Am. 105, 1517 (1999).

[12] Vavva, M.G., Protopappas, V.C., Gergidis, L.N., Charalambopoulos, A., Fotiadis, D.I., Polyzos, D., "Velocity dispersion of guided waves propagating in a free gradient elastic plate: Application to cortical bone," J. Acoust. Soc. Am. 125(5), 3414-3427 (2009).

3.3. Marble and comparison with Mortar[4]

3.3.1. Purpose

The present study deals with the examination of the acoustic emission signatures of distinct fracture modes. Tensile and mixed mode cracking is excited in specimens of marble and cement mortar and the acoustic emission behavior is monitored. Tensile cracking incidents show a preference to higher frequencies and shorter waveforms unlike shear events. The results imply that adequate analysis of simple AE features enables the characterization of the current fracture condition of the material and consequently predictions on the remaining safe service life for monolithic, as well as microstructured materials.

3.3.2. Introduction

Fracture of structural materials in most cases follows a sequence, tensile stresses induce initial micro-cracking and later shear phenomena dominate as damage is being accumulated (Ohtsu 2010). Identification of the active damage mode may well provide real time information on the status of the structural integrity of the material and allow predictions on its useful life span. Acoustic emission (AE) is a method suitable for damage monitoring since it utilizes the transient elastic waves after any crack propagation event. AE enables monitoring of crack growth with sensors mounted on the material surface. These sensors record the response after each cracking incident and transform it into electrical voltage due to their piezoelectric nature (Shull 2002). Several laboratory efforts have been published concerning characterization of the cracking mode (Aggelis 2011, Ohno and Ohtsu 2010, Aggelis et al. 2010), monitoring of other processes like healing (Van Tittelboom et al. 2012)

[4] adapted from "Acoustic signature of different fracture modes in marble and cementitious materials under flexural load" published in Mechanics Research Communications, Volume 47, January 2013, Pages 39-43

and progression of damage (Aggelis et al. 2011, Yonezu et al. 2010). However, in most of the cases of fracture monitoring, tensile cracking came from the direct tensile stresses on the matrix material (e.g. lower surface of a concrete beam under bending) while shear phenomena developed not by shear stresses directly on the matrix but by phenomena like frictional pull-out of steel fibers (Aggelis 2011), detachment of reinforcing bars (Ohno and Ohtsu 2010) or delamination between successive plies (Aggelis et al. 2010). In this study the shear cracking due to shear stresses on the matrix is directly targeted and the AE activity is compared to reference tests of tensile fracture on specimens of the same type and size. Two kinds of structural materials are used, namely marble and cementitious mortar. The first is an example of monolithic material while the latter contains microstructure in the size of few mm due to the sand grains. The interphase between the cement matrix and the grains may well dictate the path of the crack despite the external stress field and therefore, the acoustic behavior between fracture of the two material systems (monolithic and microstructural) can be compared. The experiments are conducted on a three point bending set up. Bending produces a fracture due to pure tensile stresses on the bottom surface of the material. With a slight modification of the setup, fracture due to shear stresses was also examined, as will be discussed below. Two AE transducers were used at certain distances from the crack in order to monitor the same AE event on two positions and make additional conclusions on the signal distortion as it propagates through different types of materials (Aggelis et al. 2012, Sause et al 2012). This is important since AE signals, being elastic waves, suffer distortion and amplitude reduction due to scattering and damping. If this is not taken into account it may well result in erroneous conclusions when sensor separation distances are long since the basic characteristics of the waveforms are considerably changed compared to the emitted signal.

AE transducers are piezoelectric, and therefore the amplitude, A of a recorded AE waveform is measured in Volts or dB. Indications of the released -by the fracture event- energy are: the measured area under the rectified signal envelope, simply called “energy” or the “absolute energy” with units of Joule (Zarate et al. 2012). Other important parameters are the duration (delay between first and last threshold crossings), rise time, RT (delay between the first threshold crossing and peak amplitude point in μs) and RA, which is RT over A measured in μs/V. Representative frequency features are the average frequency, AF, which is the number of threshold crossings over the duration of a signal and the peak frequency, PF, which is the frequency of the spectrum with the maximum magnitude, both measured in kHz. It has been shown that RA undergoes a certain increase as the dominant fracture mode shifts from tensile to shear, while frequency indicators undergo strong decrease (Aggelis 2011, Ohno and Ohtsu 2010, Aggelis et al. 2010, Shiotani 2006).

3.3.3. Experimental details

Two types of materials were used, namely cement mortar and marble. The specimens were prismatic of size 40x40x160 mm. Two similar mortar mixtures were produced consisting of six specimens each containing approximately 60 % vol. of sand grains the maximum size of which was 4.75 mm, while the water to cement ratio by mass was 0.55. This led to a density of 2217 kg/m3. Six of the specimens were subjected to three-point bending according to EN 13892-2:2002, see Figure 3.3. 1 (a), with constant rate of loading.

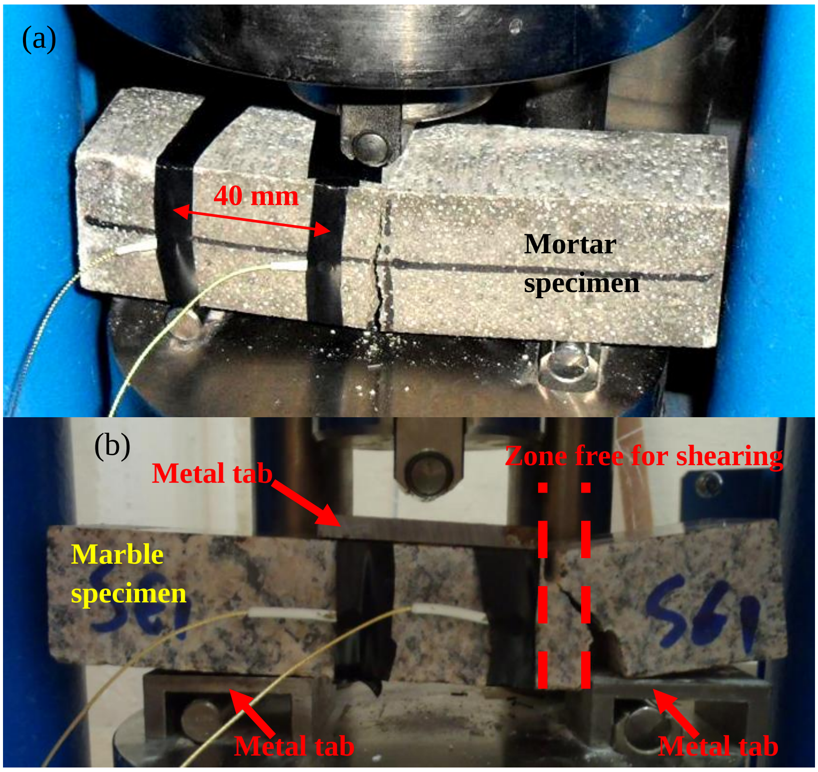

Figure 3.3. 1 *(a) Three point bending test of mortar and (b) shear test of marble with concurrent AE monitoring by two sensors.*

A slight modification was done for the other six specimens that were intended for study of the shear fracture mode. Specifically, a metal tab of length of 50 mm was placed on top center of the specimen, Figure 3.3. 1(b). This was escorted by distributed support at the bottom considerably altering the stress field. While at the three point bending test, the crack is bound to start from the central point of the bottom side due to the tensile stresses, for the modified test, the metal tabs reduce the free bottom span and leave only a small zone available for shear fracture at one side of the specimen (right in Figure 3.3. 1b). The marble specimens were tested on the same experimental set up (three specimens for bending and three for shear.) The specific slab used to cut the specimens was of the "Afyon white" marble type and had a density of 2727 kg/m3. Figures 3.3. 1(a) and (b) show typical specimens after the bending and shear test respectively.

Simple finite element stress analysis was also performed to evaluate the different stress fields for the "shear-like" experiment. It was shown that at the unsupported zone (see Figure 3.3. 1b), the strongest stress component was shear although normal stresses were also developed. Therefore, it can be considered that pure tensile (from three point bending) and shear to mixed-mode fractures can be compared.

AE measurements were conducted via two broadband sensors (Pico of Physical Acoustics Corporation, PAC). Their maximum sensitivity is at 450 kHz while their response from 300 to 600 kHz is with -3dB from the maximum, see also (PAC website). They were attached to the side of the specimen, as seen in Figure 3.3. 1, with grease to enhance acoustic coupling, while they were secured by tape. The first sensor was placed in a horizontal distance of 15 mm from the cracking zone, while the second in 55 mm. The cracking position was secured by notches that were machined on marble specimens. The monitoring board was a two-channel PCI-2 of PAC and the sampling rate was 5 MHz. The threshold and the pre-amplifier gain were both set to 40 dB.

3.3.4. Results

Initially the behavior of representative specimens will be discussed and then the results will be generalized for the whole population of specimens. For both types of fracture tests, the acoustic emission cumulative activity exhibits a type of sigmoidal curve; a number of hits are recorded at an early stage of the experiment, followed by a period of moderate and constant emission rate, as seen in Figure 3.3. 2 a for two marble specimens.

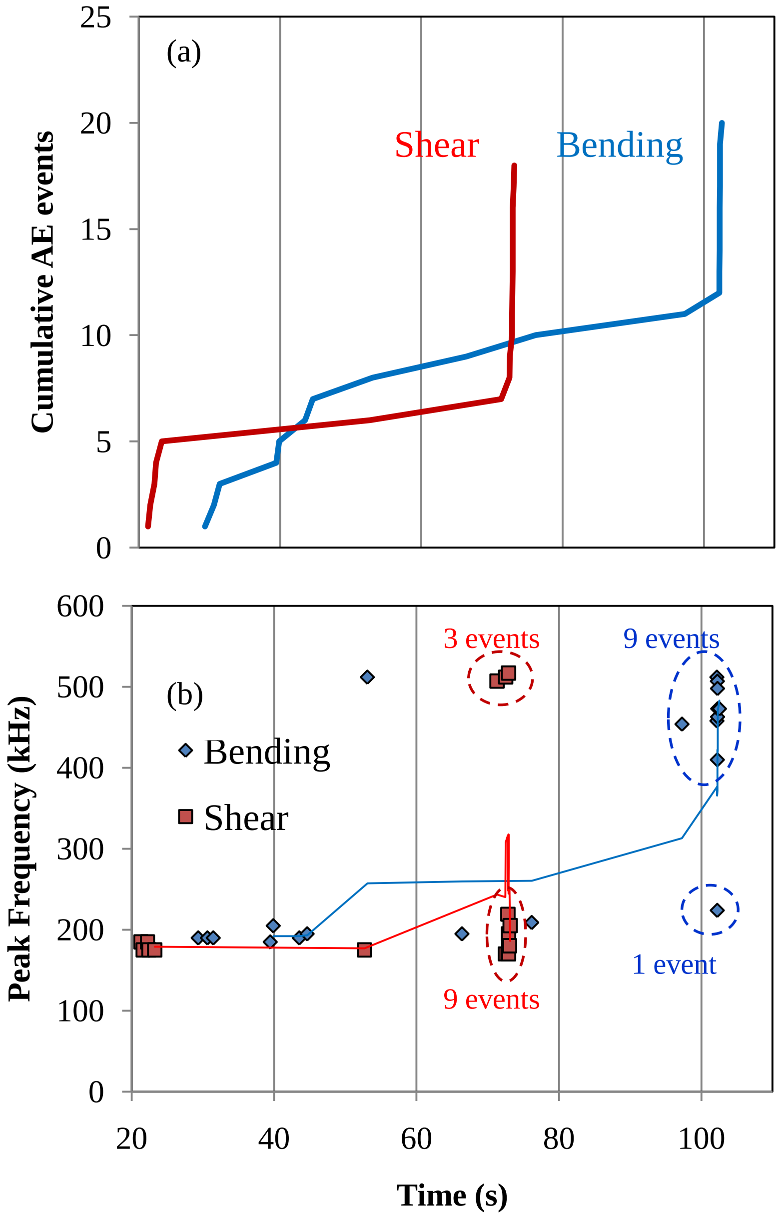

Figure 3.3. 2 *(a) Cumulative events for bending and shear tests in two marble specimens. (b) Peak frequencies for the same events as recorded by the sensor at 15 mm away from the cracking zone. The symbols stand for the PF of the corresponding events, while the solid lines for the moving average of five points.*

The highest AE rate comes with the final fracture and the separation of the specimens in two parts. The cumulative number of events is approximately twenty for this kind of marble specimen. Concerning qualitative characteristics of AE, at the fracture moment of the shear experiment (around 72 s), out of twelve recorded events, only three exhibited peak frequency (PF) around 500 kHz and nine PF around 200 kHz (see Figure 3.3. 2b). On the contrary for the bending experiment and the corresponding moment of macroscopic fracture just after 100 s, out of totally ten recorded events, only one exhibited frequency around 200 kHz and nine between 400-500 kHz. This observation shows that events due to pure tensile stresses show a preference to higher frequencies, while shear or mixed-mode show preference to lower ones. Representative FFT spectra from the two groups of the signals (of higher and lower peak frequency) are seen in Figure 3.3. 3.

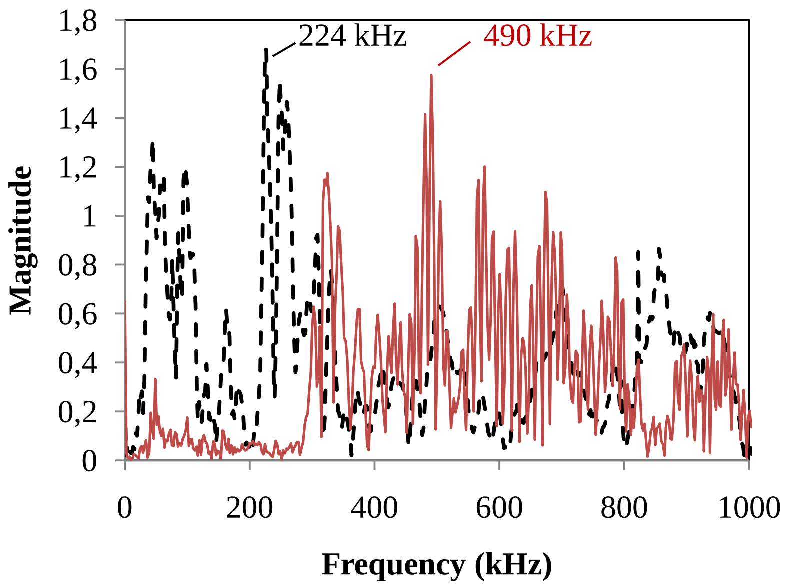

Figure 3.3. 3 *FFT spectra of indicative AE waveforms of lower and higher peak frequencies.*

The first has a peak magnitude at 224 kHz (typical of shear) while the other at 490 kHz which is typical of tensile cracking in this study. Apart from the peak of 224 kHz, the "shear" spectrum exhibits content below 200 kHz while the "tensile" has negligible content below 300 kHz but exhibits random peaks up to 800 kHz.

This trend indicatively depicted for two specimens is generalized for the whole population of the AE events recorded during fracture of the bending and shear specimens. Figure 3.3. 4a shows the correlation plot between PF and rise time (RT) for all the events recorded by the nearest transducer (15 mm from the crack) for the whole population of marble specimens (three for shear and three for bending test).

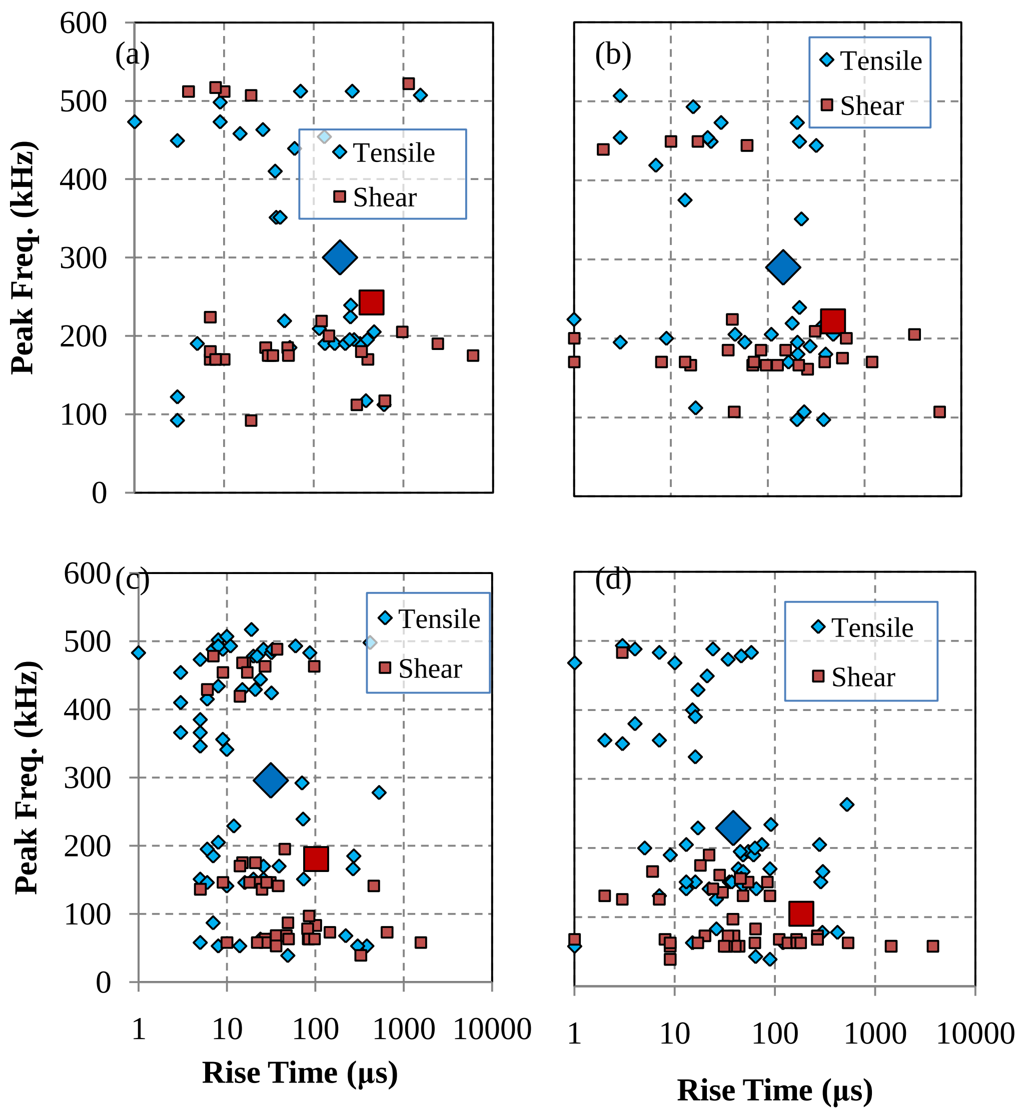

Figure 3.3. 4 *Peak frequency vs. Rise time for all the events recorded in marble by (a) the near sensor, (b) the furthest sensor. (c) and (d) concern events in mortar for the near and the furthest sensor respectively. (Larger symbols of each type stand for the average of the points of the same type).*

For shear fracture only a small portion of the population reaches 500 kHz, while most of the signals are below or around 200 kHz. For the signals coming from bending test the population is approximately equally dispersed in the bands of 100-200 kHz and 400-500 kHz, resulting in an average value of 300 kHz, considerably higher than the 242 kHz of shear, see large symbols in Figure 3.3. 4a. Figure 3.3. 4b shows the same events as captured by the furthest transducer (55 mm away from the crack). The results follow the same general trend while the frequencies are reduced due to the accumulated effect of attenuation of the longer distance. This decrease may seem limited, but considering that it occurs over just 40 mm of additional propagation between the two sensors, it bears great significance for larger specimens and definitely for actual application in structures, as will be discussed later.

The results of Figures 3.3. 4(a) and (b) concern marble material which can be considered macroscopically homogeneous. Similar experiments have been conducted in cementitious materials, as mentioned earlier. These specimens have microstructure in the form of sand grains, air bubble of similar size to the sand grains, as well as capillary porosity. In this case due to the weak cement paste – sand interphase the path of the crack is dictated around grains since they are stiffer than the matrix. Therefore, even though macroscopically a stress situation can be assumed or a stress field calculated, this may well differ from the actual stress condition responsible for the crack propagation around the microstructure. This was the reason to employ both types of materials in this study. Figures 3.3. 4(c) and (d) show the correlation plots between PF and RT for cementitious materials as recorded by the near and the far sensor respectively. The trends only slightly change compared to the behavior of marble. For the nearest sensor (Figure 3.3. 4c) two main groups of points are observed. The higher frequency group (400 – 500 kHz) is much more densely populated by events of the tensile mode than shear, while several events with peak frequencies below 200 kHz are noted for both modes. Concerning the furthest sensor in Figure 3.3. 4d, the shear mode exhibits only one event near 500 kHz while the number of tensile events remains large though certainly reduced compared to the nearest sensor. The drop of average value of PF (see large symbols, especially of the "shear" signals) between the two sensors is more evident for mortar than for marble, something attributed to the more attenuative microstructure of cementitious materials.

Concerning RT the differences are similarly strong with the RT of the shear events being approximately 3 times longer than tensile in average value.

In order to discuss the trends on a firm basis, Table 2.2.3. 1includes the average and coefficient of variation of important AE parameters.

Table 3.3. 1 *Average values of AE parameters.*

Material		Distance from event	Rise Time (μs)	Peak Frequency (kHz)	Amp (dB)
Marble	Tensile	Close (15 mm)	136 (101%)	300.3 (47%)	48.1 (8%)
		Far (55 mm)	144 (71%)	289.6 (48%)	47.9 (8%)
	Shear	Close (15 mm)	439 (263%)	242.8 (56%)	52.8 (13%)
		Far (55 mm)	472 (256%)	221.7 (49%)	51.5 (13%)
Mortar	Tensile	Close (15 mm)	31.3 (191%)	295.5 (57%)	57.9 (12%)
		Far (55 mm)	38.3(135%)	229.2 (62%)	52.6 (11%)
	Shear	Close (15 mm)	102.6 (245%)	180.6 (85%)	53.5 (13%)
		Far (55 mm)	182.9 (320%)	104.9 (68%)	49.2 (13%)

(in parenthesis the coefficient of variation)

Therefore, comparisons can be made between different materials, fracture modes and distances to the crack. The first trend that should be pointed out is that the “shear” events repeatedly exhibit longer RT than the “tensile” for the same material and sensor distance. For marble, the average RT of the tensile mode is around 140 μs while for shear it is almost 440 μs being more than three times longer. The increase is analogous for mortar with the values being in general much shorter than marble (31 μs for tension compared to 103 μs for shear). Concerning frequency characteristic, shear fracture exhibits constantly lower PF than tension (e.g. 243 kHz compared to 300 kHz for marble and 180 kHz compared to 296 kHz for mortar for the nearest sensor).

It is worth to mention that the additional propagation distance of 40 mm has a strong effect on the waveform shape. It increases RT for all materials (6-7% for marbles and up to 75% for mortar). This is related to the microstructure of the material, which exhibits stronger scattering characteristics in cement-based materials. The energy of an ultrasonic pulse propagating through the medium is dispersed in time due to multiple scattering on inhomogeneities (Tsinopoulos et al. 1999) and this has an effect on the duration of the rising part as well as the main frequency content of the signal. Similarly the PF is consistently lower at the 2nd transducer for all cases. The decrease between sensors is again more evident in mortar where PF drops by about 70 kHz, while the decrease in marble is less than or about 20 kHz. The same decreasing trend is noted for amplitude, where events in marble suffer a drop of about 1 dB, while events in mortar lose 4 to 5 dB for the additional propagation of 40 mm, something again attributed to the microstructure of cementitious materials.

For AE waveform features the variation is quite large and especially for the RT the coefficient of variation (standard deviation over the average) is of the order of 100% or more. This is inherent to AE measurements since the amount of crack displacement during each event and the state of the material as damage is being accumulated are continuously changing. This randomness is inevitably transferred to the AE results, in contrast to e.g. ultrasonic measurements where the excitation and the medium through which propagation occurs are usually constant. Completely separating populations of tensile and shear signals would be desirable, however, the fact that the AE parameter averages of tension and mixed mode fracture are quite far apart is of great significance for material science and engineering research, as it enables the correct characterization of shifting trends in real time. It is also very important to mention that this parameter-based approach is easy to perform and requires just a few sensors in order to monitor the process offering therefore the potential for in-situ use in contrast to other laboratory oriented approaches like the moment tensor analysis that requires practically eight sensors for mode classification (Ohno and Ohtsu 2010).

It should be noted that the specific values of AE features and frequencies certainly depend on the response characteristics of the transducers. The specific sensors, although considered broad band, still exercise certain influence on the acquired waveforms. However, since the same set of transducers is used throughout the testing series, any differences can be attributed to the fracture mode or propagation distance. It is shown therefore, that broad band AE sensors can monitor the differences of fracture modes while using other set of transducers, the discrepancies would still be monitored though most likely with different values of AE parameters. It is mentioned that the above trends concern the specific materials tested. Although the AE characteristics depend on the transient displacement of the crack sides dictated by the active fracture mode, the microstructure of the materials is also important and therefore, similarities to other type of structural materials like wood or steel should not be taken for granted.

3.3.5. Conclusions

The present experiment examines the evidence of the AE signature of different fracture modes in cementitious mortar and marble materials under flexural load. This subject exhibits strong interest from the engineering point of view since usually a specific sequence of failure mechanisms is followed in actual fracture. Passive monitoring can reveal the dominant fracture mode and help the estimation of the remaining life of the material. Materials with different microstructure were tested in bending and shear, namely marble as a typical homogeneous material and cement mortar as a material with microstructure on the level of millimeters. Simple alterations on the experimental set up allowed triggering different fracture modes. The results show firm evidence that actually the different fracture modes (tension and mixed mode) exhibit different AE signatures in terms of frequency and waveform shape parameters like the rise time. Shear fracture exhibits lower frequency and longer waveforms in average. Collecting an adequate population of signals may certainly help to distinguish the dominant fracture mode despite the inherent variation on the measurements. A noteworthy detail is that the distance between the cracking source and the sensor is of primary importance, since an additional propagation of 40 mm poses substantial changes in the values of AE features for both materials. . Any AE monitoring should therefore be combined with elastic wave propagation study, since the distortion and attenuation imposed by the medium may well mask the original characteristics of the emitted wave even in small laboratory samples. Future efforts should employ larger concrete specimens and recording of signal by more sensors and longer propagation distances while the testing set up could be improved by the aid of FEM analysis in order to result to pure shear fracture instead of mixed mode.

3.3.6. References

[1] Aggelis, D.G., 2011. Classification of cracking mode in concrete by acoustic emission parameters. Mechanics Research Communications 38, 153–157.

[2] Aggelis, D.G., Barkoula, N.M., Matikas, T.E., Paipetis, A.S., 2010. Acoustic emission monitoring of degradation of cross ply laminates. J Acoust Soc Am., 127(6), EL246-251.

[3] Aggelis D.G., Kordatos E.Z., Matikas T.E. 2011. Acoustic emission for fatigue damage characterization in metal plates. Mechanics Research Communications 38 106–110.

[4] Aggelis, D.G., Mpalaskas, A.C, Ntalakas, D., Matikas T.E., 2012. Effect of wave distortion on acoustic emission characterization of cementitious materials, Construction and Building Materials 35, 183–190.

[5] Ohno, K., Ohtsu, M. 2010. Crack classification in concrete based on acoustic emission. Constr Build Mater., 24(12), 2339–2346.

[6] Ohtsu, M., 2010. Recommendations of RILEM Technical Committee 212-ACD: acoustic emission and related NDE techniques for crack detection and damage evaluation in concrete: 3. Test method for classification of active cracks in concrete structures by acoustic emission. Mater Struct 43(9), 1187–1189.PAC website, http://www.mistrasgroup.com/products/solutions/acousticemission/sensors/

[7] Sause, M.G.R., Müller, T., Horoschenkoff, A., Horn, S., 2012. Quantification of failure mechanisms in mode-I loading of fiber reinforced plastics utilizing acoustic emission analysis, Composites Science and Technology, 72(2),167–174.

[8] Shiotani, T. 2006. Evaluation of long-term stability for rock slope by means of acoustic emission technique. NDT&E Int 39(3), 217–28.

[9] Shull, P. J. (ed.) 2002. Nondestructive evaluation, Theory, Techniques and Applications, CRC Press, New York.

[10] Tsinopoulos S. V., Agnantiaris J. P., Polyzos D. 1999. An advanced boundary element/fast Fourier transform axisymmetric formulation for acoustic radiation and wave scattering problems. J. Acoust. Soc. Am. 105, 1517.

[11] Van Tittelboom, K., De Belie, N., Lehmann, F., Grosse, C. U. 2012. Acoustic emission analysis for the quantification of autonomous crack healing in concrete, Construction and Building Materials 28, 333–341.

[12] Yonezu, A., Arino, M., Kondo, T., Hirakata, H., Minoshima, K., 2010. On hydrogeninduced Vickers indentation cracking in high-strength steel. Mechanics Research Communications 37, 230–234.

[13] Zárate, B.A., Caicedo, J.M., Yu, J., Ziehl, P., 2012. Probabilistic Prognosis of Fatigue Crack Growth Using Acoustic Emission Data, Journal of Engineering Mechanics 138(9), 1101-1111.

3.4. Granite and comparison with Mortar [5]

3.4.1. Purpose

The prediction of the remaining life of a structure can be assisted by the characterization of the current cracking mode. Usually tensile phenomena precede shear fracture. Due to the different movement of the crack sides according to the dominant mode, the emitted elastic energy possesses waveforms with different characteristics. These are captured by acoustic emission sensors and analyzed for their frequency content and waveform parameters. In this study fracture experiments on structural materials are conducted. The goal is to check the typical acoustic signals emitted by different modes as well as to estimate the effect of microstructure in the emitted wave as it propagates from the source to the receivers. The dominant fracture mode is controlled by modification of the setup and acoustic emission is monitored by two sensors at fixed locations. Signals belonging to tensile events acquire higher frequency and shorter duration than shear ones. The influence of heterogeneity is also obvious since waveforms of the same source event acquired at different distances exhibit shifted characteristics due to damping and scattering. The materials tested were cement mortar, as a material with microstructure, and granite, as representative of more homogeneous materials. Results show that in most cases, AE leads to characterization of the dominant fracture mode using a simple analysis of few AE descriptors. This offers the potential for in-situ application provided that care is taken for the distortion of the signal, which increases with the propagation distance and can seriously mask the results in an actual case.

---

[5] Adapted from "Acoustic emission signatures of damage modes in structural materials" Proc. SPIE 8694, Nondestructive Characterization for Composite Materials, Aerospace Engineering, Civil Infrastructure, and Homeland Security 2013, 86940T (16 April 2013); doi: 10.1117/12.2008942

3.4.2. Introduction

Most structural materials follow a sequence while fracturing, initially tensile stresses induce micro-cracking and consequently shear stresses or phenomena become active [5]. Characterization of the damage mode provides real-time information on the structural integrity of the structure and allows estimations on its useful life span. Acoustic emission technique (AE) is capable of damage monitoring since it records the stress waves after any crack propagation event. AE enables monitoring crack development with sensors placed on the surface of the material [8]. Several laboratory efforts have been published relatively to the characterization of the fracture type [3,4], monitoring of other processes like healing [9] and progression of damage [11,3]. Though classification results can be considered quite successful in the laboratory, in most of the cases, tensile cracking came from the direct tensile stresses on the matrix material (e.g. lower surface of a concrete beam under bending) while shear phenomena developed not by shear stresses directly on the matrix but by phenomena like frictional pull-out of steel fibers [3], detachment of reinforcing bars [4] or delamination between successive plies. In this experiment the shear cracking of the matrix due to shear stresses is applied and the AE activity is compared to tests of tensile fracture on similar specimens. Two kinds of structural materials are used, namely granite and cement-based mortar. The first is monolithic material while the latter contains microstructure due to the sand grains and air bubbles. Since the interphase between the cement and the sand grains is weak it dictates the path of the crack without necessarily following the external stress field. Therefore, the acoustic behavior between the two material systems is compared.

The experiments are based on a three-point bending set up. Bending leads to a tensile fracture on the bottom surface of the material. Applying a slight modification of the set up, fracture due to shear stresses was also examined, as will be discussed below. AE was monitored by two sensors at certain distances from the crack and enable conclusions on the signal distortion as it propagates through different types of materials. This is important since AE signals, being elastic waves, undergo distortion and amplitude reduction due to scattering and attenuation. If this is not accounted for it will result in erroneous results especially when sensor separation distances are long.

This is because the characteristics of the waveforms change compared to the emitted signal due to propagation in a heterogeneous medium.

Some important parameters of an AE signal is the amplitude, A, and is measured in Volts or dB. Other descriptors are the energy (area under the rectified signal envelope), the duration (delay between first and last threshold crossings), rise time, RT (delay between the first threshold crossing and peak amplitude in μs) and RA, which is RT over A measured in μs/V. Indicative frequency features are the average frequency, AF, which is the number of threshold crossings over the duration of a signal and the peak frequency, PF, which is the frequency of the spectrum with the maximum magnitude, both measured in kHz. In general RA exhibits strong increases as the fracture mode shifts from tensile to shear, while frequency parameters show decrease [3,4,2,7].

3.4.3. Experimental Details

Two types of materials were used, namely cement mortar and granite. The specimens were prismatic of size 40x40x160 mm. Two similar mortar mixtures were produced consisting of six specimens each containing approximately 60 % vol. of sand grains with maximum size of 4.75 mm. The water to cement ratio by mass was 0.55 and the density of mortar was 2217 kg/m3. Six of the specimens were subjected to three-point bending according to EN 13892-2:2002, see Figure 3.4. 1(a), with constant rate of loading. The setup was modified for the test of the other six specimens that were intended for the shear mode, a metal tab of length of 50 mm was placed in the center above the specimen (Figure 3.4. 1(b)). Additionally two distributed supports at the bottom were used. Although at the three-point bending test, the crack starts from the central point of the bottom side due to the tensile stresses, for the modified test, the metal tabs used for support reduce the free bottom span and leave only a small zone available for shearing at one side of the specimen (right in Figure 3.4. 1(b)). The granite specimens were tested on the same experimental set up and specifically three specimens for bending and three for shear. The granite type was absolute black from

India with a density of 2970 kg/m3. Figures 3.4. 1(a) and (b), show typical specimens after the bending and shear test respectively.

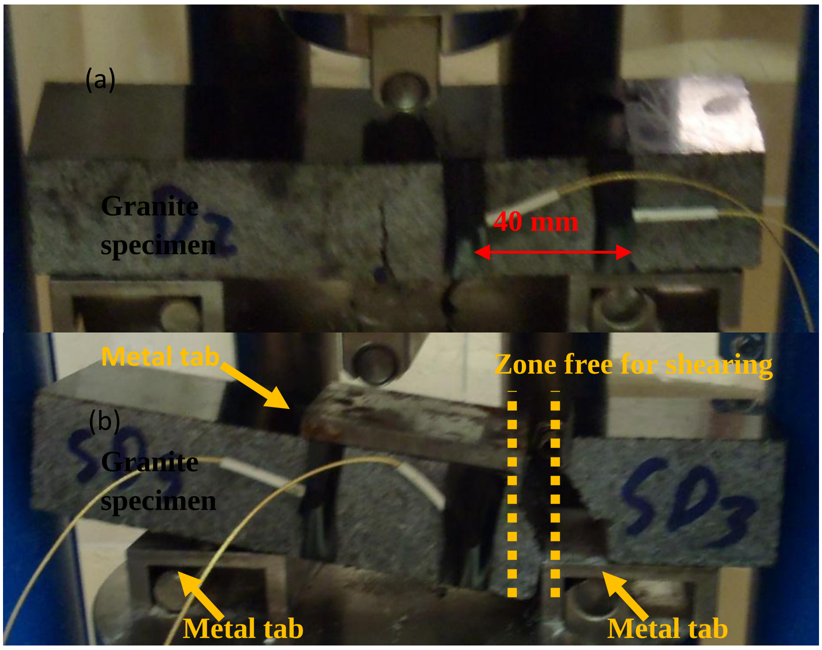

Figure 3.4. 1 *(a) Three point bending and (b) shear test of granite with concurrent AE monitoring by two sensors.*

AE measurements took place with two broadband sensors (Pico, PAC) with good response from 50 kHz to 800 kHz. They were attached on the front side of the specimen as seen in Figure 3.4. 1. Grease was applied between the sensors and the specimen's surface to enhance acoustic coupling, while they were secured by tape during the experiment. The first sensor was placed in a horizontal distance of 15 mm from the cracking zone and the second 40 mm away from the first. The cracking position was secured by notches that were machined on granite specimens. AE signals were acquired on a two-channel PCI-2 of PAC with a sampling rate of 5 MHz. The threshold and the pre-amplifier gain were 40 dB.

3.4.4. Results

For both types of fracture, the acoustic emission cumulative activity (as recorded by the nearest sensor) exhibits a type of sigmoidal curve, as seen in Figure 3.4. 2 for two mortar specimens. These specimens showed approximately fifty hits for shear and seventy hits for bending while the maximum rate of AE recording was at the final fracture, which came at approximately 400 s for bending and 750 s for shear. Concerning specific AE parameters, Figure 3.4. 3(a) shows the RA values of the corresponding hits. Most of the hits from bending test are within 100 and 1000 μs/V, while only at the moment of final fracture some higher values are exhibited. On the contrary, RA values of the shear test lie around the level of 1000 μs/V while at the end even higher values are exhibited. The solid lines in the graph stand for the average of recent five hits in order to show the trend more clearly. Constantly, the line of shear is higher than the bending for the corresponding stage of the experiment. This shows that events due to pure tensile stresses have quite short rise time and attain their maximum peak quite early after their onset. On the other hand shear ones show a different behavior since their RA value is generally higher.

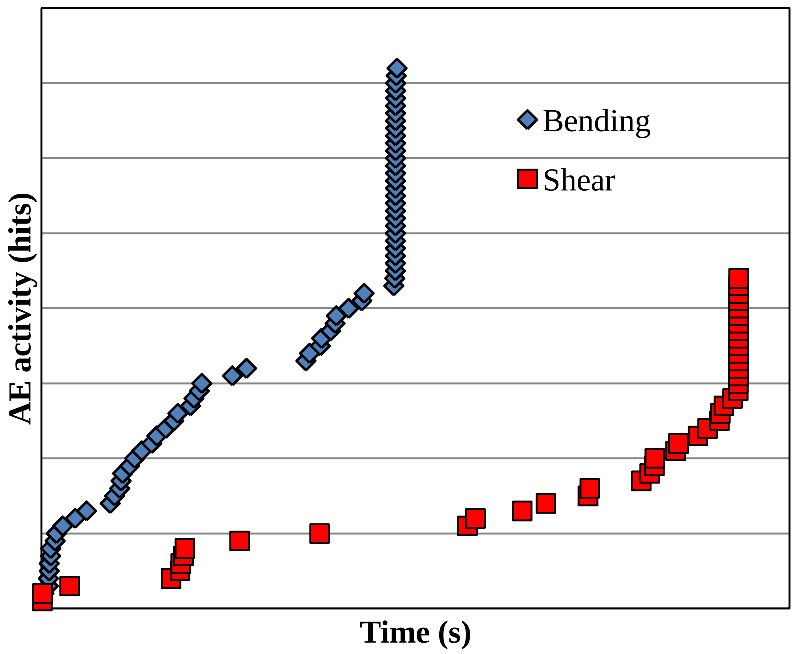

Figure 3.4. 2 *Cumulative AE activity for bending and shear tests in two mortar specimens as recorded by the sensor at 15 mm away from the cracking zone.*

Figure 3.4. 3(b) shows the average frequency of the same specimens. Unlike the RA values seen in Figure 3.4. 3(a), the hits originating from the bending test lie to higher frequency ranges from 100 kHz to 400 kHz than the shear ones which do not pass above 300 kHz. At the end both specimens exhibit low frequency emissions. Again

the moving average (of recent five points) line shows clearly that there is approximately a difference of 100 kHz between bending and shear.

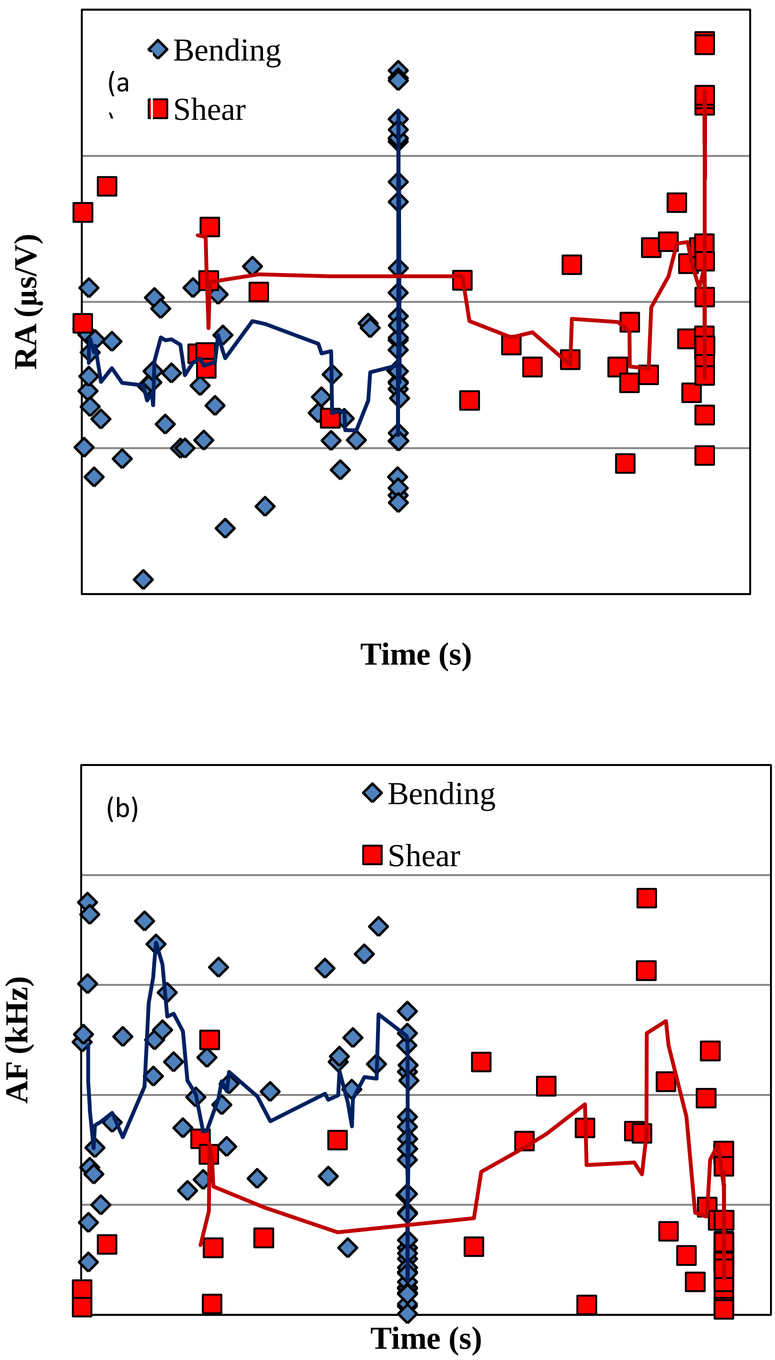

Figure 3.4. 3 *(a) RA values of the AE signals of Fig. 2 and (b) AF of the same signals. The symbols stand for the RA of the corresponding signals, while the solid lines for the moving average of five points.*

In order, to discuss the results in a firm basis, Table 3.4. 1 includes the averages of some important AE parameters of the whole population of hits for both sensors (15 mm away and 55 mm).

Table 3.4. 1 *AE parameters for the different fracture modes and sensor distances in mortar*

	Duration (μs)	Av. Freq. (kHz)	Amplitude (dB)	RA (μs/V)
Bending (15 mm)	554	175	54.6	2966
Shear (15)	600	110	51.5	5434
Bending (55 mm)	509	163	53.8	4276
Shear (55)	693	83	50	5685

Quite strong differences are seen in most of the AE parameters. The AF of shear hits is 40% less than bending for the nearest sensor, while the average amplitude is lower by 3 dB. RA value on the other hand is higher by about 80% and duration is slightly higher. The differences remain for the second sensor although with somehow modified values. Actually despite the short propagation distance, remarkable differences can be seen for the same population of events. Concerning bending the furthest sensor records the hits with a frequency reduced by 12 kHz compared to the first while for the shear the drop is stronger (83 kHz compared to 110 kHz, or 25% decrease). This is due to attenuation which is more intensive for higher frequencies and is due to damping and scattering. The same mechanism is responsible for the decrease in amplitude by about 3 dB between the two receivers. Differences are also noted in other waveform parameters like duration and RA since the nature of the material imposes dispersion as has been shown in materials with microstructure [1,10].

The trends of granite material are similar, Figure 3.4. 4 shows the cumulative AE activity for typical bending and shear tests. In both tests the AE hit rate is increasing smoothly up a point when a high and nearly constant rate is obtained around the moment of fracture. The total population of hits of the nearest sensor is of the order of 150 hits. However, it should be noted that this is not necessarily the case for different granite types examined, some of which exhibited much less activity during fracture. Figure 3.4. 5 shows the RT of the signals of Figure 3.4. 4 for the time window focusing at the end of the experiment. For both specimens RT is quite limited for the earlier part of the experiment while hits with progressively higher RT are exhibited as final failure approaches. It is characteristic though that for the bending test only two hits have RT longer than 2 ms, while for the shear the corresponding number is more than five and some reach close to 7 ms. This is in accordance to the mortar test and shows that for granite similar trends apply concerning the different fracture modes.

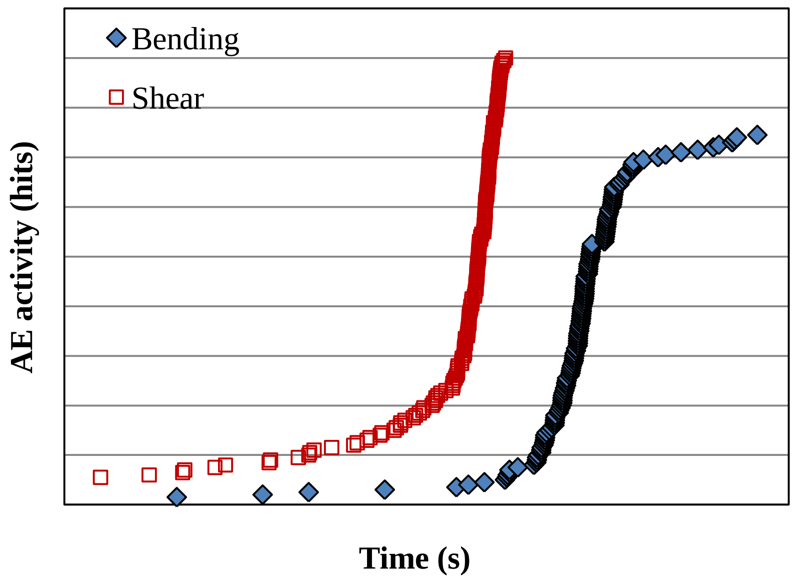

Figure 3.4. 4 *Cumulative AE activity for bending and shear tests in two granite specimens as recorded by the sensor at 15 mm away from the cracking zone.*

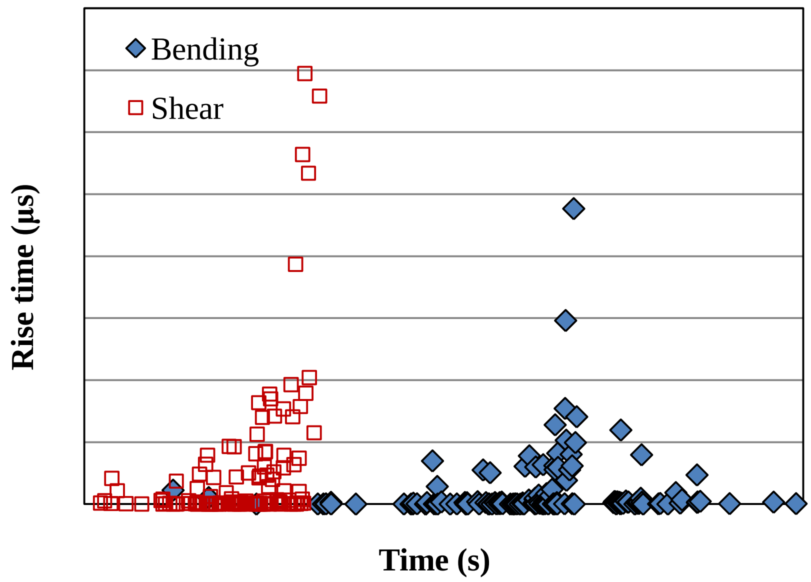

Figure 3.4. 5 *RT values of the AE signals of Figure 3.4. 6 .*

Table 3.4. 2 shows the average values of AE parameters for the whole duration of the tests. Again, the bending signals are shorter in duration and higher in frequency content. The shear test on the other hand exhibits higher RA. Nevertheless, the difference between the two sensors is obvious. The frequency decreases by about 20 kHz for the additional distance of 40 mm between sensor 1 (15 mm from the crack) and 2 (55 mm). The amplitude drops by about 1 dB. Though the differences are strong, they are much less striking than mortar, where frequency dropped by more than 70 kHz for the same distance and the amplitude lost about 2-3 dB. This can be attributed to the texture of the materials, mortar contains microstructure in the form of sand grains, air bubbles and porosity that impose stronger attenuation and dispersion [6]. On the other hand granite is much more homogeneous and therefore, the differences for the same propagation distance is not as high, though they are still strong. This shows that when testing materials with intense microstructure by means of AE, one should be particularly careful for the distance between the crack and the sensors as this may well impose a large percentage of deviation from the original signal as emitted by the sensor.

Table 3.4. 2 *AE parameters for the different fracture modes and sensor distances in granite*

	Duration (μs)	Av. Freq. (kHz)	Amplitude (dB)	RA (μs/V)
Bending (15 mm)	842	123	54.5	4221
Shear (15)	1182	106	54	5176
Bending (55 mm)	554	123	51.9	5738
Shear (55)	1022	103	52.8	6453

The fact that the AE parameter averages of tension and shear (or mixed mode) fracture are quite far apart for each material is of great significance for material science and engineering research, as it enables the correct characterization of shifting trends in real time, even though the variation of AE descriptors is inherently large. It is also important to mention that this parameter-based approach to separate the signals according to the corresponding fracture mode is easy to perform and requires just a few sensors in order to monitor the process. Therefore, it offers the potential for in-situ use.

It should be noted that the specific values of AE features and frequencies certainly depend on the response characteristics of the transducers. The specific sensors, although considered broad band, still exercise certain influence on the acquired waveforms. However, since the same set of transducers is used throughout the testing series, any differences can be attributed to the fracture mode or propagation distance. It is shown therefore, that broad band AE sensors can monitor the differences of fracture modes while using other set of transducers, the discrepancies would still be monitored though most likely with different values of AE parameters.

3.4.5. Conclusions

This experiment presents the measurements on the AE signals of different fracture modes. The subject exhibits strong engineering interest since usually a sequence of fracture mechanisms is followed in material failure. Passive monitoring by AE reveals the dominant fracture mode and enables the evaluation of the remaining life of the material. Materials with different microstructure were tested. Specifically, granite as a typical homogeneous material, and cement mortar as a material with heterogeneity, were examined in bending and shear modes. Modifications on the experimental set up allowed triggering different types of failure. The results show reliable trends that the different fracture modes (tension and shear or mixed mode) exhibit different AE signatures in terms of frequency and waveform shape. Shear events exhibits lower frequency and longer waveforms. Collecting an adequate population of signals helps to discriminate the active fracture mode. Additionally, the distance between the cracking source and the sensor is important, since an additional propagation of 40 mm influences substantially the values of AE features. AE monitoring should therefore, be combined with elastic wave propagation studies in order to avoid masking the characteristics of the emitted wave by the distortion and attenuation of the medium. Future efforts should employ larger concrete specimens and recording of signal by more sensors and longer propagation distances while the testing set up could be improved by FEM analysis in order to result to pure shear fracture instead of mixed mode.

3.4.6. References

[1] Aggelis, D.G., Shiotani, T., " Experimental study of surface wave propagation in strongly heterogeneous media," J. Acoust. Soc. Am. 122(5), 151-157 (2007).

[2] Aggelis, D.G., Kordatos, E.Z., Matikas, T.E., "Acoustic emission for fatigue damage characterization in metal plates," Mechanics Research Communications 38, 106–110 (2011).

[3] Aggelis, D.G., "Classification of cracking mode in concrete by acoustic emission parameters," Mechanics Research Communications 38, 153–157 (2011).

[4] Ohno, K., Ohtsu, M., "Crack classification in concrete based on acoustic emission," Constr Build Mater., 24(12), 2339–2346 (2010).

[5] Ohtsu, M., "Recommendations of RILEM Technical Committee 212- ACD: acoustic emission and related NDE techniques for crack detection and damage evaluation in concrete: 3. Test method for classification of active cracks in concrete structures by acoustic emission," Mater Struct 43(9), 1187–1189 (2010).

[6] Tsinopoulos, S. V., Agnantiaris, J. P., Polyzos, D., "An advanced boundary element/fast Fourier transform axisymmetric formulation for acoustic radiation and wave scattering problems," J. Acoust. Soc. Am. 105, 1517 (1999).

[7] Shiotani, T., "Evaluation of long-term stability for rock slope by means of acoustic emission technique," NDT&E Int 39(3), 217–28 (2006).

[8] Shull, P. J., [Nondestructive evaluation, Theory, Techniques and Applications], CRC Press, New York, (2002).

[9] Van Tittelboom, K., De Belie, N., Lehmann, F., Grosse, C. U., "Acoustic emission analysis for the quantification of autonomous crack healing in concrete," Construction and Building Materials 28, 333–341 (2012).

[10] Vavva, M.G., Protopappas, V.C., Gergidis, L.N., Charalambopoulos, A., Fotiadis, D.I., Polyzos, D., "Velocity dispersion of guided waves propagating in a free gradient elastic plate: Application to cortical bone," J. Acoust. Soc. Am. 125(5), 3414-3427 (2009).

[11] Yonezu, A., Arino, M., Kondo, T., Hirakata, H., Minoshima, K., "On hydrogeninduced Vickers indentation cracking in high-strength steel," Mechanics Research Communications 37, 230–234 (2010).

3.5. Acoustic emission signatures of different fracture modes in plain and repaired granite specimens [6]

3.5.1. Purpose

In this study, bending and shear fracture experiments on healthy and adhesively repaired granite samples with concurrent acoustic emission (AE) monitoring are discussed. AE can characterize the shift between the fracture modes using simple features analysis. It is the first time that such a direct correspondence between the stress field and the results of a monitoring technique emerges for granite. This offers a new insight in the material's behavior especially in relation to complicated geometries where the dominant stress mode is not known a priori.

3.5.2. Introduction

Fracture of structural materials exhibits a typical succession. Micro-cracking due to tension occurs with low to moderate load and later shear phenomena tend to dominate [1]. Defining of the main fracture mode provides information on the fracture process and the structural behavior of the materials and structures. A suitable way to monitor fracture is the acoustic emission (AE) technique. AE utilizes piezoelectric sensors attached on the surface of the material to record the stress waves triggered after crack nucleation and propagation events in analogy to the earthquake activity but in smaller scale [2-4]. Several studies have been published on monitoring of fracture evolution [5-8], monitoring of corrosion [9], healing [10] and creep in granite or other materials [11,12]. AE signals from cracking and debonding have been separated in composite structures, where in addition to the cracking of the matrix material, reinforcement in the form of bars, fibers or patches was detached from the matrix [13-15]. Recently

[6] Adapted from "Acoustic signatures of different damage modes in plain and repaired granite specimens" Proc. SPIE 9439, Smart Materials and Nondestructive Evaluation for Energy Systems 2015, 94390L (March 27, 2015); doi:10.1117/12.2085040

shear and tensile patterns of fracture in the matrix material itself have been targeted in mortar, concrete and marble specimens [16-18]. This section presents the AE activity during bending and shear tests of granite beams in laboratory. Mechanical behavior of granite is of interest in different fields, from restoration of cultural heritage monuments to underground engineering and excavation works [19-21]. AE has been used for monitoring the fracture and localizing the sources [20,21] while ultrasonics for correlations to the damage degree of granite materials [22]. AE total activity and indices like the “b-value” have proven helpful to improve the difficulties in determining the damage level of granite in conjunction with electrical variation measurements [23]. After the test, the specimens were repaired by epoxy resin with polyamide hardener, and loaded to failure a second time under the same mode in order to evaluate the degree of restoration of properties. AE was monitored by two resonant sensors enabling event location and allowing to capture all relevant activity due to material fracture excluding noise. The AE characteristics most sensitive to the changes in the stress field are presented and discussed.

3.5.3. Experimental Details

3.5.3.1. Materials-Repair method

Two types of granite were used, one named Giallo Rusty from China with a density of 2470 kg/m3 and the other named Tropical Black with a density of 2613 kg/m3 from Italy. For convenience the first type will be addressed as G2 and the next as G6. The specimens were prismatic of size 40x30x160 mm. Three of the specimens per granite type were subjected to three-point bending according to EN 13892-2:2002 see (Figure 3.5. 1a). The load was applied at a constant rate of 50 N/s and the loading was automatically terminated at the moment of load drop. The setup was modified for the test of the other three specimens per granite type that were intended for the shear mode: a metal tab of length of 50 mm was placed in the center above the specimen (Figure 3.5. 1b). Although at the three-point bending test, the crack starts from the central point of the bottom side due to the tensile stresses, for the modified test, the metal tabs used for support reduce the free bottom span and leave only a small zone available for shearing which is triggered by notches on both top and bottom sides of the specimen of 5 mm depth (right in Figure 3.5. 1b). In a previous study, static FEM simulations confirmed that shear stresses obtain much higher values than normal at the notch tip [17]. Figures 3.5. 1(a) and (b) show typical granite specimens during the bending and shear test respectively.

(a

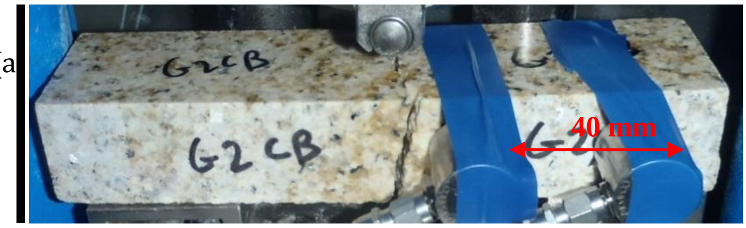

(b)

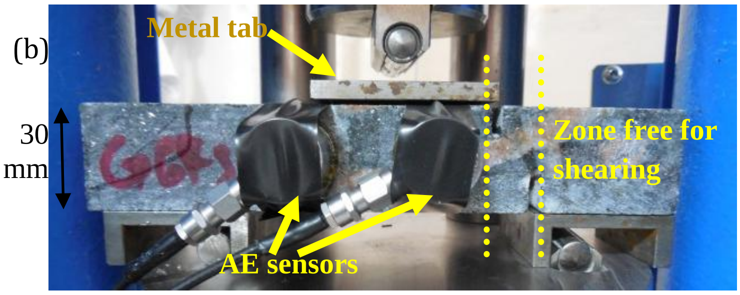

Figure 3.5. 1 *(a) Three point bending and (b) shear test of granite with concurrent AE monitoring by two sensors.*

After bending and shear fracture has occurred all the specimens were repaired in the crack surface with a two-component bonding system based on epoxy resin and hardener named “Epoxol” in its commercial product name. It is a specially formulated, high viscosity two component polyester marble adhesive-putty, used to bond and fill for repair purposes with hardening time of approximately 5-6 hours [24]. The bonding was carefully established so that the original geometry of the specimen was not altered.

3.5.3.2. AE testing

AE monitoring took place by means of two piezoelectric sensors, (R15, Mistras). Their resonance comes at 150 kHz and their positions on the specimens are shown in Figure 3.5. 1. One sensor was placed 15 mm away from the expected crack, which was secured by a notch. The second sensor was placed 40 mm away. Both sensors were positioned at the same side of the crack in order to be able to characterize the distortion of the signals as they propagate for the additional distance of 40 mm. Acoustic coupling was improved by silicon grease between the sensors face and the specimens' surface. AE activity was captured by a two-channel PCI-2 Mistras board with sampling rate of 5 MHz. The threshold was 40 dB, as well as the pre-amplification. A schematic representation of a waveform is seen in Figure 3.5. 2. Some of the main features are the maximum amplitude, A (usually in dB), and the duration (period between the first and the last threshold crossing). The "rise time", RT (which is the time between the first threshold crossing and the point of peak amplitude in μs) is related to the fracture mode of the crack. It has been shown that shear type of failure like debonding of patches, pull-out of fibers and shear matrix cracking induces signals with longer duration and RT, mainly attributed to the higher proportion of transverse elastic waves that are triggered by the parallel motion of the crack tips [13,14,16-18]. Frequency content can be measured by AF (average frequency), which is the total number of threshold crossings divided by the duration while there are other indices based on the spectrum of the FFT.

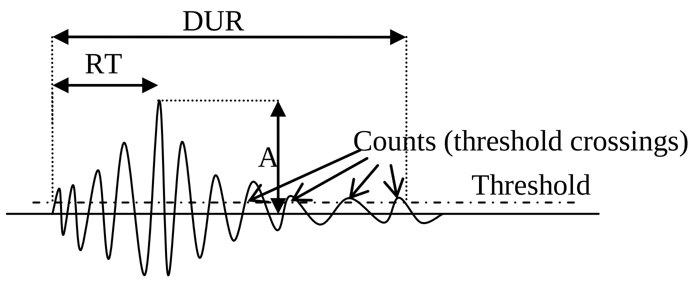

Figure 3.5. 2 *Typical AE waveform and its basic characteristics.*

Before the fracture tests, ultrasonic measurements were conducted on the samples, according to Figure 3.5. 3. They were conducted by the same piezoelectric transducers as the AE monitoring. The electric excitation triggering the pulser was one cycle of 150 kHz. The received signal was digitized with 10 MHz sampling and the first detectable disturbance of the waveform was picked manually. The measurement corresponds to the longitudinal waves which are the fastest type. Pulse velocity was calculated by the length of the specimens (160 mm) over the wave transit time.

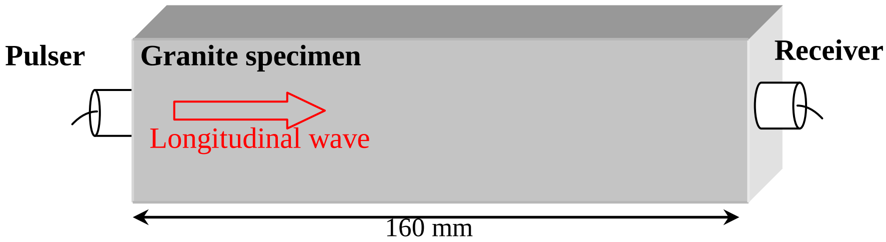

Figure 3.5. 3 *Schematic representation of ultrasonic test with longitudinal waves.*

3.5.4. Results

3.5.4.1. Ultrasonic and Mechanical results

Table 3.5. 1 includes the results of the ultrasonic pulse velocity test. Specimens of type G6 exhibited values close or above 6000 m/s, while G2 lower, around 5000 m/s. This implies higher stiffness for G6. Indeed based on the densities of the materials and the measured wave velocities, the elastic moduli values are between 60 and 70 GPa for type G2 and around 90 GPa for type G6, as seen in Table 3.5. 1. The maximum loads for both bending and shear tests for the intact and the repaired version of the specimens are included in Table 3.5. 2. The intact Tropical Black (G6) specimens exhibited steadily higher bending load which is in accordance with its higher ultrasonic pulse velocity. In the shear test, there is again a difference in favor of G6 in average (approximately 1 kN), but with overlap between the populations. Concerning reloading after repair, all specimens maintained their initial fracture surface and for the bending test there is a noticeable restoration of approximately 50-75% of the initial strength. For the shear, the restoration is much lower between 30-40%. This is for both types of granite indicating that after repair by epoxy, the material is more susceptible to shear, while for bending the order of load that can be carried is quite restored to the "virgin" state, though not completely. Photographs of typical specimens after fracture are seen in Figure 3.5. 4.

Table 3.5. 1 *Pulse velocities and elastic moduli for both granite types*

Type	Specimen	Pulse velocity (m/s)	Elastic modulus* (GPa)
Giallo Rusty	G2AB	4969	61.0
	G2BB	5333	70.3
	G2CB	5031	62.6
Tropical Black	G6AB	5735	85.9
	G6BB	6084	96.7
	G6CB	6061	96.0

*Elastic modulus E, was calculated through relation $E=\rho C^2$, where ρ is density and C the pulse velocity.

Table 3.5. 2 *Maximum load for two granite types for both test modes*

Type	Specimen	Bending (kN)		Strength Restoration (%)	Specimen	Shear (kN)		Strength Restoration (%)
		Healthy	Repaired			Healthy	Repaired	
Giallo Rusty	G2AB	3.626	2.303	63.5	G2DS	5.491	1.513	27.6
	G2BB	3.883	1.882	48.5	G2ES	3.626	1.395	38.5
	G2CB	3.836	2.759	71.9	G2FS	4.074	1.138	27.9
Tropical Black	G6AB	5.286	3.527	61.8	G6DS	4.222	1.576	37.3
	G6BB	4.89	2.989	51.1	G6ES	7.209	2.152	29.9
	G6CB	4.444	2.287	73.8	G6FS	4.771	1.693	35.5

Last letter "B" in the codenames denotes "bending" and "S" denotes "shear".

Figure 3.5. 4 *Typical specimens after fracture (a) bending, (b) shear.*

3.5.4.2. Acoustic emission activity-Bending test

Before presenting the differences of AE descriptors based on the mode of test, the curves of the cumulative AE events activity vs. time can be seen in Figure 3.5. 5. These curves reveal the rate of nucleation/propagation of cracks and help to assess the time or load during which most of the damage is occurring. The left column concerns bending of three healthy specimens and right concerns the reloading of the same specimens after repair by epoxy. The depicted activity concerns the "events" and not the whole number of recorded AE hits. Specifically, by applying two sensors, it was possible to activate "linear localization". Practically, by the time delay between acquisitions of two successive signals by the two sensors, the actual location of the source can be calculated. Localization makes use of the ultrasonic pulse velocity that was measured beforehand. This way, the activity concentrated in a zone of 10 mm around the crack was isolated in the specific analysis. This serves two purposes: one is to eliminate possible sources of noise that may contribute to the overall recorded activity but they are not actually due to the fracture in the intended mode and location. The second is to avoid contributions by the attenuation and dispersion of the material: isolating the origin of the events in a narrow zone of 10 mm, it is sure that the path of propagation was very similar for all the different events until being recorded by the sensor. Therefore, possible influence by attenuation and material heterogeneity is kept to a minimum. The information presented in this analysis comes from the sensor closer to the crack in order, as aforementioned, to clear the waveforms from effects of distortion from the additional propagation of 40 mm, even though the distance is quite short.

The plots start at time zero when the central loading point touched the specimen. This contact resulted in a small number of hits, but not in events as it did not originate from the fracture zone and it was not related to the fracture process. After a period (A) of silence indicating no cracking activity due to negligible stresses, a few events were recorded (point B). Another plateau followed (C) and at point D a moderate activity started to be noted, continuing throughout period E. Finally, there is an increase of AE rate (stage F) leading to the final fracture of the specimen. All healthy specimens seem to follow a more or less similar pattern of AE activity. The only remark is that stage "E" for the specimen G2CB exhibits much less activity than the other two specimens. These plateaus in the AE activity have been observed in compression experiments of granite as well [25], and more specifically, two zones of “avalanche-like” activity interrupted by a long period of acoustic silence. This is related to initial micro cracking which is restrained, while the material accumulates elastic energy before mechanisms of larger scale become active.

The behavior of the same specimens at reloading after repair does not seem as uniform and cannot be described with the same stages. This is not surprising as the homogeneity of the material has been irreversibly changed leading to stronger experimental scatter between different samples. Indicatively, the second specimen (G2BB repaired) did not even exhibit a plateau once the emissions started at 31 s, while the last specimen (G2CB repaired) exhibited a large plateau between 35 and 55 s. On the other hand, the first specimen (G2AB repaired) had a stage of moderate activity.

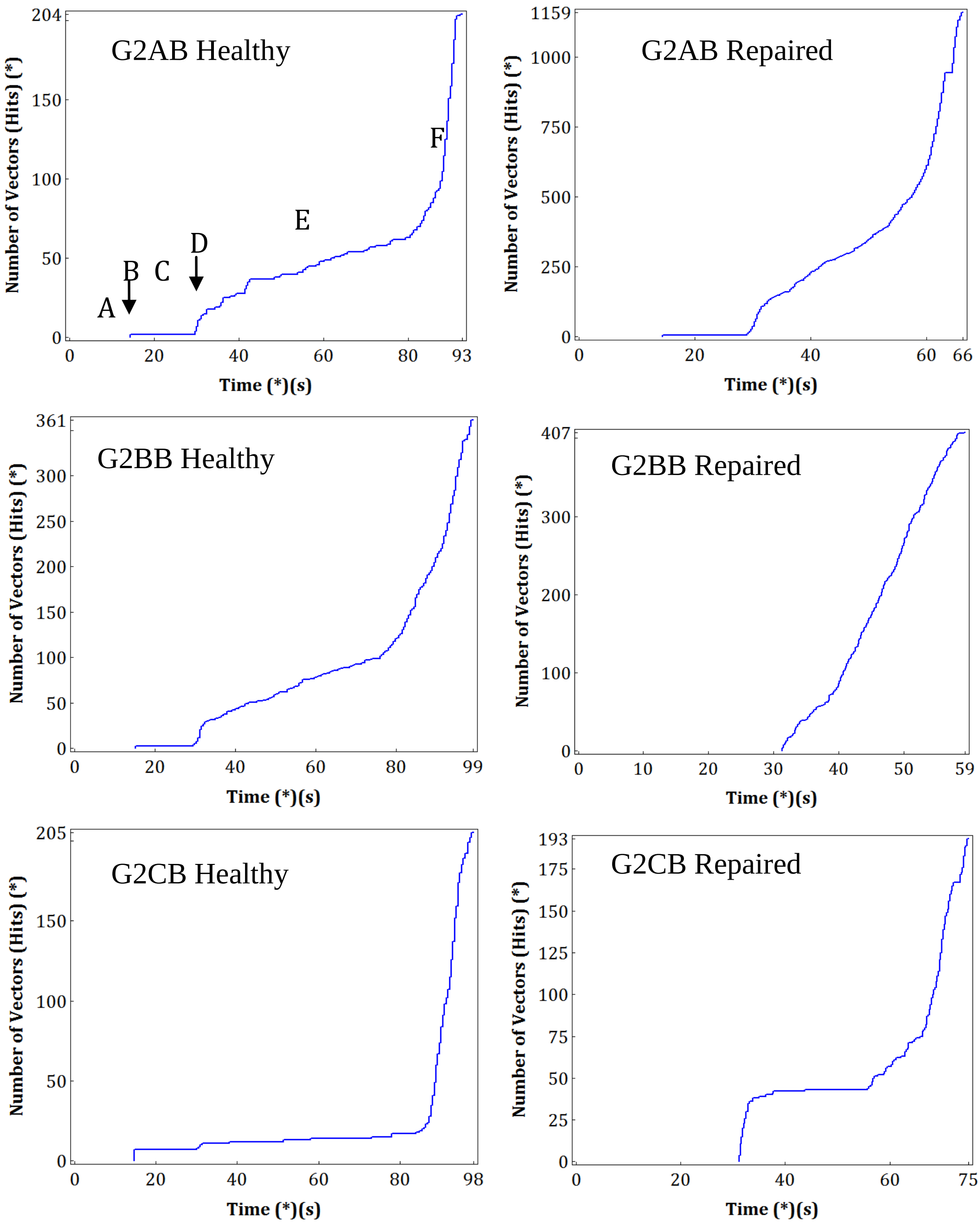

Figure 3.5. 5 *Accumulated AE activity of granite G2 vs. time for the bending test: left healthy, right repaired specimens.*

The behavior of specimens from granite type G6 is shown in Figure 3.5. 6.

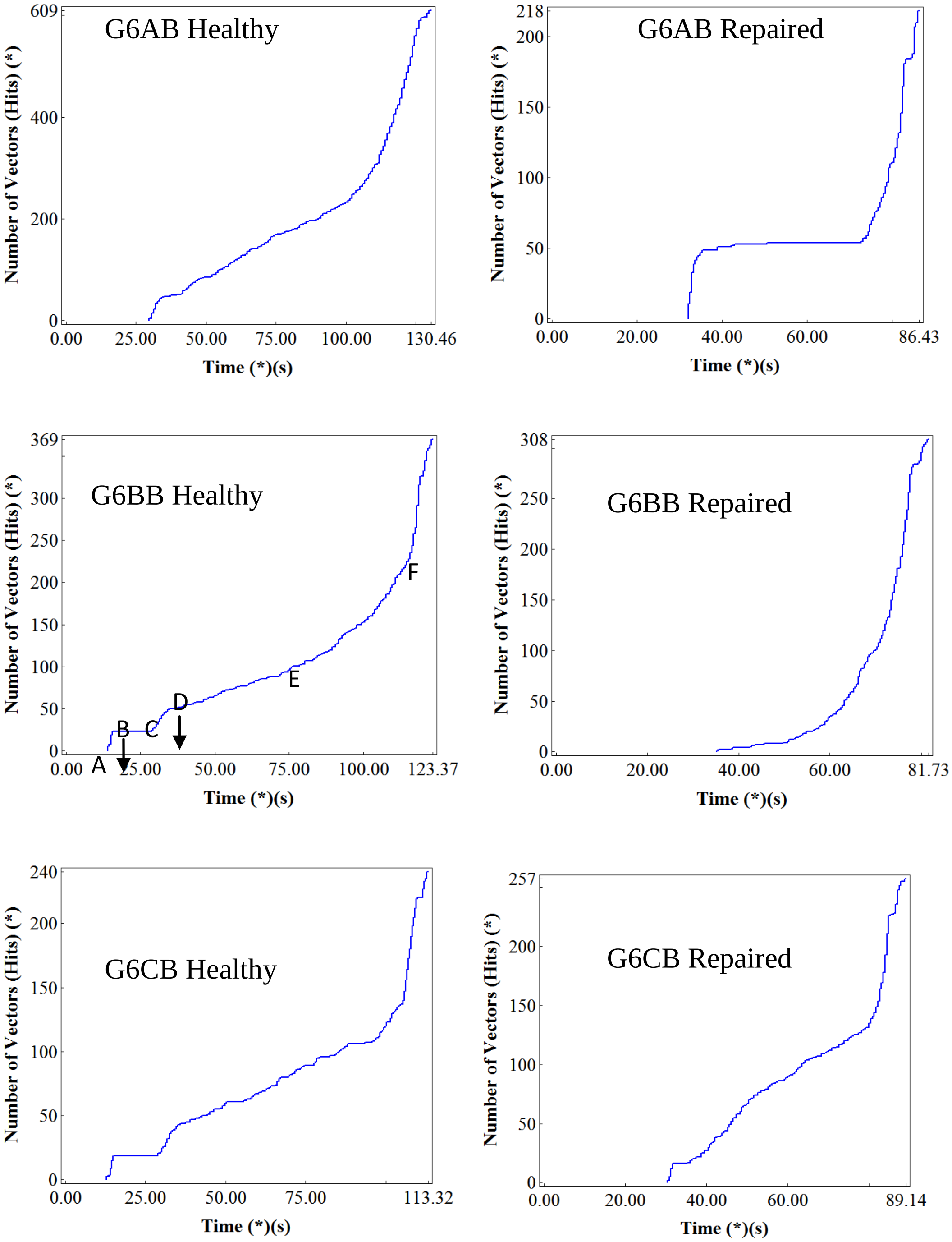

Figure 3.5. 6 *Accumulated AE activity of granite G6 vs. time for the bending test: left healthy, right repaired specimens.*

For the specimens of this granite type the same succession of stages seems to hold (especially the two last healthy specimens). Concerning the repaired, again there is not a unique trend, as the first specimen exhibited a long silence plateau, the second an exponential increase of AE and the last, a stage of moderate activity instead of plateau or exponential increase. One detail that can be mentioned is that the initial plateau was slightly longer for the repaired specimens than the healthy in both categories. For the repaired version of the specimens this silent period was between 30 and 40 s, while for the healthy it was equal or shorter than 25 s. This can be attributed to the elasticity of the epoxy resin which is one order of magnitude lower than elastic modulus of granite. Therefore, under a certain displacement rate, it can strain for longer period of time before emitting acoustic signals due to irreversible cracking.

3.5.4.3. Acoustic emission activity – Shear test

The corresponding AE activity for specimens G2 tested in shear is shown in Figure 3.5. 7. The behavior of the intact specimens is shown at the left. All specimens exhibited a continuous line once the activity starts, without plateaus like the corresponding bending tests. It seems that shear micro-cracking was continuous without periods of stress build-up as was the case for bending. For the repaired specimens at the right of, Figure 3.5. 7, the whole duration was shorter since the specimens failed at much lower load. The initial period of silence remains of the same order followed by a more or less linear path until failure.

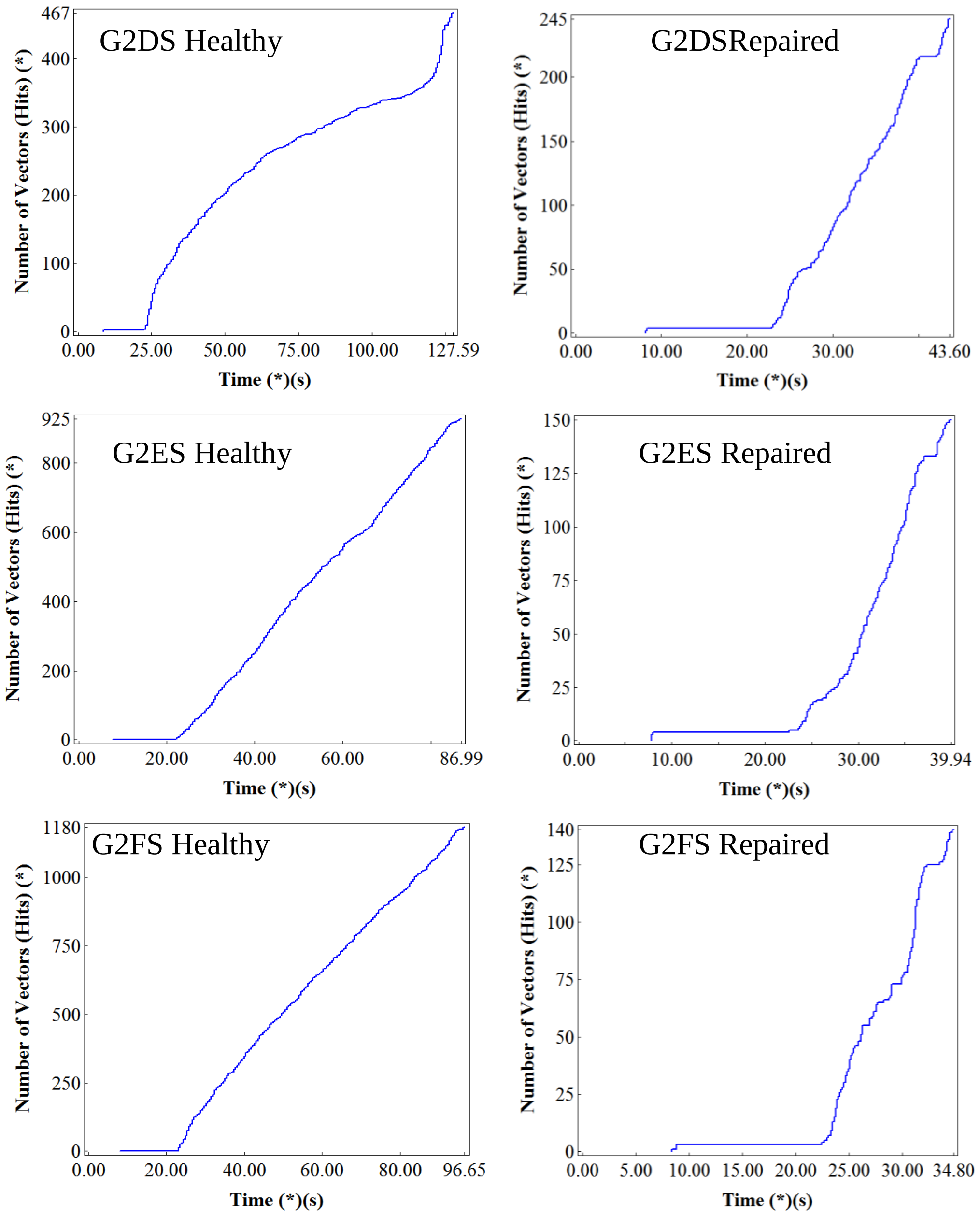

Figure 3.5. 7 *Accumulated AE activity of granite G2 vs. time for the shear test: left healthy, right repaired specimens.*

The AE behavior of granite G6 is shown in Figure 3.5. 8. The trends remain similar for the healthy specimens, with the AE activity building up in a more or less linear way until failure. In this case, the repaired specimens showed a more uniform behavior, including an initial plateau, an increase of the rate followed by a slight decrease before the rise of the slope up to failure. The linear development to failure was not followed by the repaired specimens.

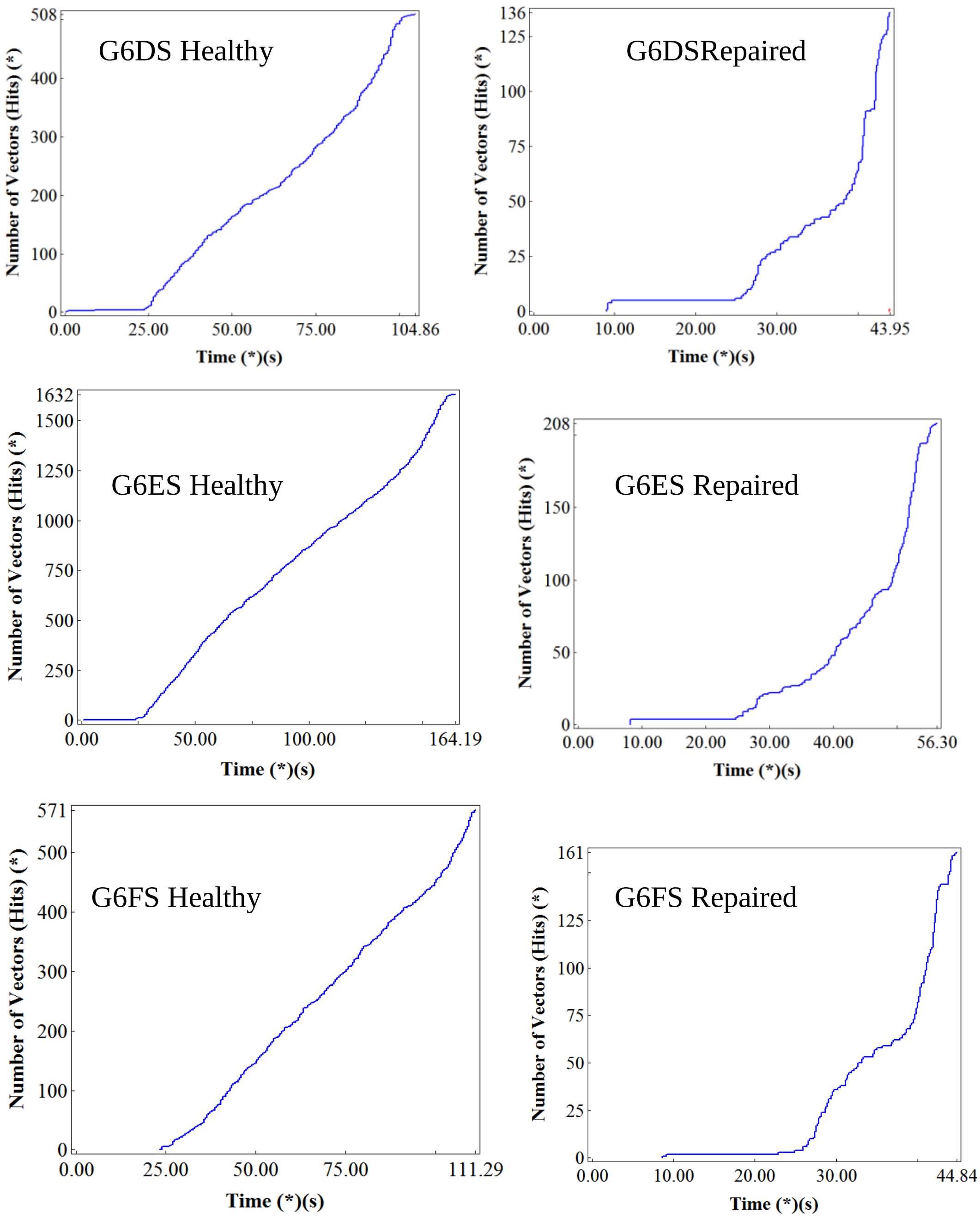

Figure 3.5. 8 *Accumulated AE activity of granite G6 vs. time for the shear test: left healthy, right repaired specimens.*

3.5.4.4. AE waveform parameters analysis

Apart from the total activity, AE parameters shed light in the fracture process and specifically have been used to characterize the fracture mode [26-28]. Therefore, it is deemed very important to check the values of AE parameters as it has been shown that they are sensitive to the different type of loading and the resulting fracture pattern. Of particular importance in this study is the rise time, RT, as shown in Figure 3.5. 2, which showed the most drastic changes between the two fracture modes. In order to analyze the development of the AE parameters during loading, indicative parts of the whole population were isolated as shown in Figure 3.5. 9. One part was taken during the early stage of the loading when the AE rate was still moderate (below 50% of ultimate, class 1, green) and the second just before final failure when the AE recording rate was much faster (class 2, blue).

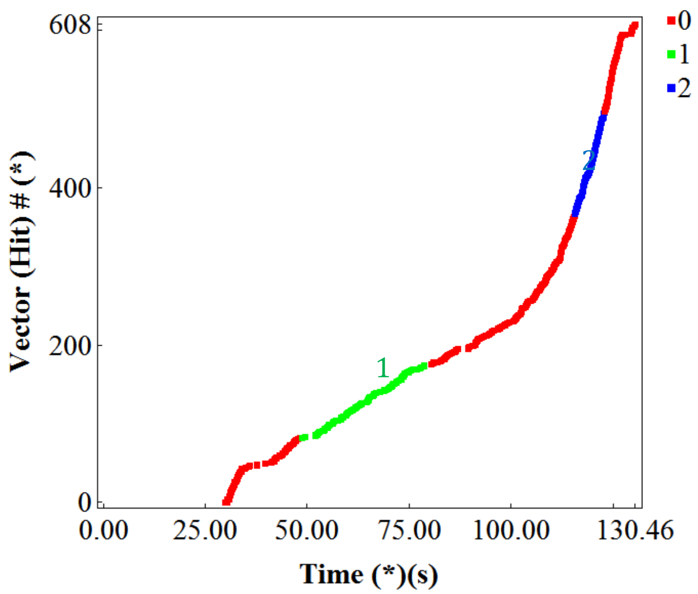

Figure 3.5. 9 *Cumulative history of events and indicative class separation using the Noesis software [29].*

The populations from all three specimens of each type were added together to produce a larger database of AE signals, received at initial loading stages (class 1) and before failure (class 2) separately for bending and shear loading. Figure 3.5. 10, shows the density distribution of the values of RT of the early class 1 for bending and shear of granite G2 (top) and G6 (bottom). Concerning bending of G2, most of the RT values are below 40 μs, having a peak at 20 μs. For the shear type of loading, the distribution moves to higher values up to 100 μs, while there is also a small peak at 180 μs. The picture is quite similar for granite G6; bending load results in RT mostly below 40 μs, while the corresponding distribution for shear extends up to 200 μs. This is a very direct indication of the influence of the stress tensor (normal-shear) to the AE exhibited during fracture and has never been measured in granite so far. In addition to the whole distributions as depicted in Figure 3.5. 10, the averages of the populations are very indicative; Bending of G2 and G6, results in average values of RT of 45.1 μs and 42.5 μs respectively, while for the shear tests the corresponding average RT values are 210.8 μs and 229.7 μs, being four to five times higher. The reason can be related to the different wave modes (longitudinal or transverse) that are triggered by the motion of the crack sides under the dominant mode [30]. This enables the assessment of the type of stresses acting on the material by passive AE monitoring of the initial loading stage without inducing serious damage in the material (e.g. 50% of maximum load or even less).

For the repaired version of the specimens things do not seem to change considerably (see right of Figure 3.5. 10). For both material types, bending RTs are limited up to 40-60 μs, while shear ones extend to 200 μs or more. This shows that the intended fracture mode is followed even after repair confirming that AE is a suitable technique for passive characterization of the stress built-up and fracture accumulation. It should be mentioned that apart from the populations up to 300 μs which are shown in the graphs, there are systematic differences in the higher regimes. Specifically, for the bending tests of both granites, only 2% of the RT population is included above 300 μs, while for shear this percentage is 10% leaving a substantial part of the population to higher values. This behavior of higher RT values corresponds to the different stress field, which as aforementioned targeted the shear type of failure and has been seen in materials like mortar and concrete [16,17]. Measuring the waveform parameters enables conclusions on the fracture mode simply using one sensor (essentially the 2nd is for noise removal in this case), while a more elaborate approach would be the moment tensor analysis (MTA) that requires multiple sensors. Though the results of MTA are quite detailed [31], application may not be practical in all situations since the number of at least six sensors is necessary for recording of each AE event.

It is interesting to note that these differences in the activity of class 1 were obtained much earlier than final fracture, before the load bearing capacity of the specimens has been compromised. Therefore, it is possible that after suitable study, a proof test with simultaneous recording by AE can reveal the dominant stress component as well as indicate the suitability of the repaired material to withstand the same loading pattern.

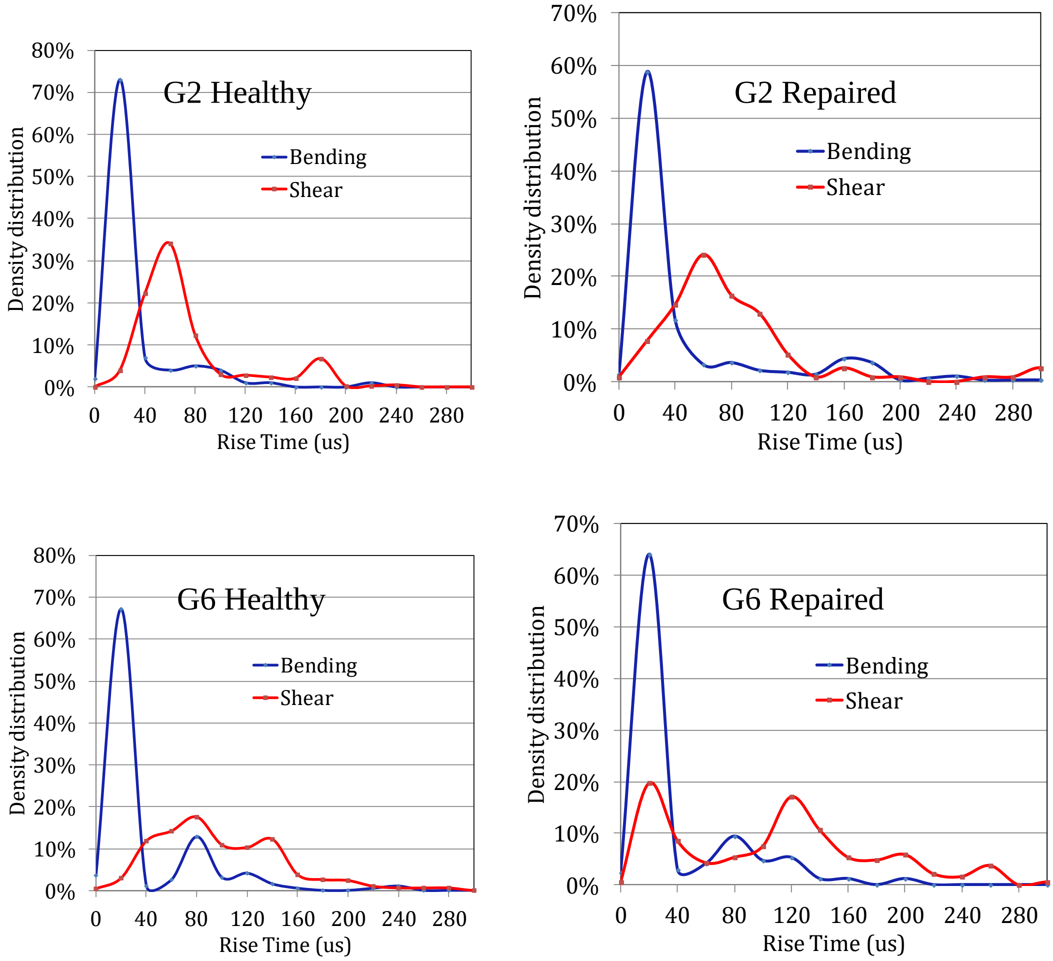

Figure 3.5. 10 *Density distributions of RT for AE populations at moderate load (class 1)*

The behavior of the AE populations at higher load (class 2) is shown in Figure 3.5. 11. It is interesting to see that the differences between bending and shear in this case are much smaller. For granite G2, the density distribution of shear RT values has its peak at the same point (i.e. up to 20 μs) but is wider reaching to values up to 200 μs. For G6 the distributions are essentially the same. This finding shows that after the initial micro-cracking is developed according to the different fracture mode (bending or shear), at the final stage of loading the material fractures nearly in the same way independent of the type of loading. This behavior, although should be further investigated, it has been evidenced in similar media where the regime near the load peak "is characterized by a strong strain localization, independent of the actual failure mechanism" and the energy dissipation is "a surface-dominated phenomenon, analogously to the tensile behavior" [5,32]. Most of the systematic differences therefore, are seen in the early behavior, while later fracture resembles tensile behavior, which justifies the low RT values during high load even in the shear test. It will be interesting to use FEM to simulate the stress field during fracture, in order to reveal how the dynamic stress tensor changes after the crack initiation, relatively to the initial stress field revealed by static simulations [17]. The repaired specimens' behavior is similar, with the "shear" distributions peaking at the same point but usually expanding to slightly higher values than "bending". The above show that simple analysis can reveal the preliminary fracture mechanism and the tendencies that will be followed throughout loading. Experimental scatter is inherent with AE and therefore, it is almost impossible to completely separate the data hit by hit regarding their origin. However, taking into account an indicative group, the relative shifts can be well identified and shed light in the damage process since, as shown the population distributions are quite different.

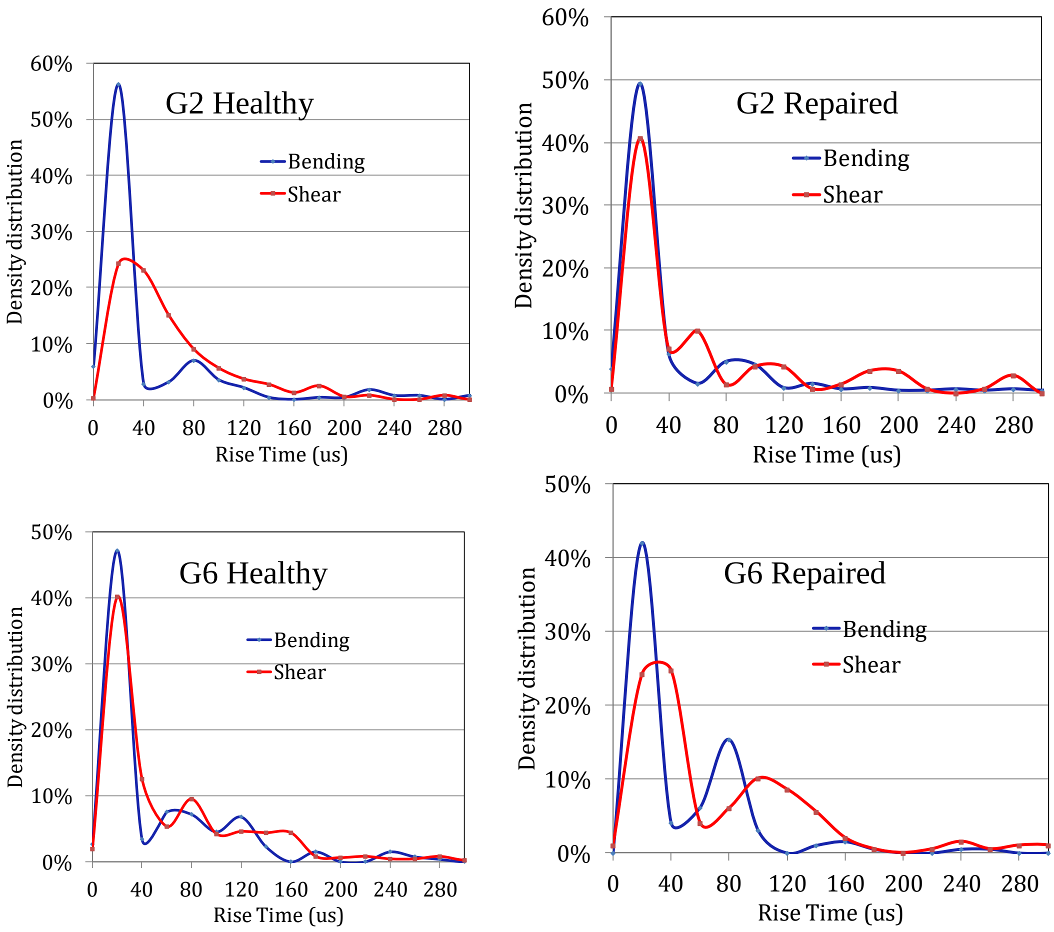

Figure 3.5. 11 *Density distributions of RT for AE populations at high load (class 2)*

3.5.5. Discussion

In this section some specific issues are discussed after the basic results were presented. The first point concerns the characterization of the fracture mode. This characterization is based on the initial static stress field as simulated by FEM analysis. For the so-called “shear” experiment, the ratio between shear and normal is more than 10 at the point of the notch [17]. Therefore, it is highlighted that although shear stress is high, this is not pure shear. We use the term “shear” for simplicity to denote mixed mode with stronger shear components. It is also highlighted that the microstructure of the material may well change the conditions of crack propagation from what is macroscopically calculated even in the static case, let alone the dynamic crack propagation. The present manuscript considers the initial “macroscopic” static loading conditions and not how the fracture process develops after crack initiation. From the moment the fracture starts, the process zone is affected “by the stess field generated by the fracture itself” [32] and simulations become much more difficult and would need more details to yield reliable results. Thus, it is certain that the stress field is dynamic and changes continuously after each crack propagation event compared to the initial static field. However, due to the different starting points of fracture (strong normal in the one experiment and strong shear in the other), there are still considerable changes in the fracture behavior as monitored by the AE parameters.

In the “shear” experiment, in order for the fracture to be developed in the specific intented way, the notches were necessary. After breaking some specimens it was made clear that notches were important to achieve the fracture in the predefined zone. Else, several specimens were fractured again near the middle, where the shear stresses are lower and normal are higher. By making the notches, the cross section is reduced in the targeted zone and the fracture zone is dictated to occur at the point where shear stresses are higher. Thus the comparison between the bending and “shear” test is possible. Additionally the notches were essential for the placement of the AE sensors. In order to be able to collectively study all experiments, the distance between the fracture zone and the sensors should be similar. Else if the location of crack was random, due to attenuation and distortion of the signal, a few additional cm would not allow studying the signals as one group. In order to check only the effect of fracture mode, it was necessary to fix the other parameters (like propagation distance between source and receiver) so that they do not crucially influence our result. The first sensor was in all case 2 cm from the zone of the crack. The second was another 4 cm away. The reason that both sensors were at the same side, is that it gives the opportunity in the near future to check the AE parameters in terms of their additional propagation distance from one to the other receiver. Since all sources are from the same side of the sensors, this additional distance can be useful for characterizing how the AE parameters change by the additional propagation of 40 mm (between the two receivers).

Concerning the difference in the cumulative AE behavior between shear and bending it is difficult to state a specific reason. Failure under the shear loading registers a nearly constant AE rate until failure. The reason is difficult to conclude from this experimental study. Literature does not help since previous works do not target two distinct tests like herein, but a single test type was performed (usually compressive) which leads to all different fracture events (tension, shear, mixed). In most of the cases these modes coexist [5,23,31,33]. This behavior seems to be a finding to be explored further.

3.5.6. Conclusions

This section describes and discusses the fracture behavior of two granite types under different modes. Tests were accompanied by ultrasonic assessment before loading and acoustic emission monitoring during loading. The two granite types exhibited quite consistent behavior either in bending or shear exhibiting the similar trends in AE cumulative history and AE parameter values. This cannot be said for the adhesively repaired version of the specimens during the second loading as each specimen behaved in a unique way. Apart from the fact that ultrasonic pulse velocity is considerably higher for higher strength granite, the basic conclusions are mentioned below:

i) The characteristics of AE waveforms are directly sensitive to the loading pattern (bending or shear). When preliminary damage is building up during moderate shear loading, AE signals have much longer RT than the corresponding bending damage. This direct correspondence between the stress field and the AE waveform parameters has not been explored in granite before. It allows to get information on the fracture very early in loading and before serious damage starts to be inflicted.

ii) Shear loading produces a more continuous acoustic activity compared to bending. This implies that while bending damage resumes after periods of silent stress build-up, the shear goes on without serious “plateaus”.

iii) Repair by means of epoxy in between the crack faces, restores the load bearing capacity up to 70% for bending and up to 40% for shear loading.

iv) Repaired specimens exhibit longer initial silent periods in bending. This behavior is attributed to the elasticity of epoxy which allows straining longer before starting to have irreversible damage than granite itself.

This study shows that passive monitoring by AE can provide information on the stress field and the fracture pattern which cannot be provided by other nondestructive techniques. The research continues with several other types of granite as well as marble materials. The effect of attenuation due to damping will be studied through the results of multiple sensors, something that could help to upgrade the test to larger geometries.

3.5.7. References

[1] M. Ohtsu, Recommendations of RILEM Technical Committee 212- ACD: acoustic emission and related NDE techniques for crack detection and damage evaluation in concrete: 3. Test method for classification of active cracks in concrete structures by acoustic emission, Mater Struct 43(9) (2010) 1187–1189.

[2] C.U. Grosse, M. Ohtsu, Acoustic emission testing, Heidelberg: Springer, 2008.

[3] S. Mindess, Acoustic emission methods. In: Malhotra VM, Carino NJ, editors. CRC handbook of nondestructive testing of concrete. Boca Raton (FL): CRC, 2004.

[4] R. Vidya Sagar, B.K. Raghu Prasad, R.K. Singh, Kaiser effect observation in reinforced concrete structures and its use for damage assessment, Archives of Civil and Mechanical Engineering 15 (2015) 548–557.

[5] A. Carpinteri, M. Corrado, G. Lacidogna, Heterogeneous materials in compression: Correlations between absorbed, released and acoustic emission energies, Engineering Failure Analysis 33 (2013) 236–250.

[6] H. Elaqra, N. Godin, G. Peix, M. R'Mili, G. Fantozzi, Damage evolution analysis in mortar, during compressive loading using acoustic emission and X-ray tomography: Effects of the sand/cement ratio, Cement and Concrete Research 37 (2007) 703–713.

[7] D.A. Lockner, J.D. Byerlee, V. Kuksenko, A. Ponomarev, A. Sidorin, Quasi static fault growth and shear fracture energy in granite, Nature 350 (1991) 39–42.

[8] B. Goszczynska, G. Swit, W. Trampczynskin, A. Krampikowska, J.Tworzewska, P.Tworzewski Experimental validation of concrete crack identification and location with acoustic emission method, Archives of Civil and Mechanical Engineering I2 (2012) 23–28.

[9] Y. Kawasaki, T. Wakuda, T. Kobarai, M.Ohtsu, Corrosion mechanisms in reinforced concrete by acoustic emission, Construction and Building Materials 48 (2013) 1240–1247.

[10] E. Tsangouri, D. G. Aggelis, K. Van Tittelboom, N. De Belie, D. Van Hemelrijck, Detecting the activation of a self-healing mechanism in concrete by acoustic emission and digital image correlation, The Scientific World Journal (2013) Article number 424560, http://dx.doi.org/10.1155/2013/424560.

[11] L. Chen, C.P. Wang, J.F. Liu, Y. M. Liu, J. Liu, R. Su, J. Wang, A damage-mechanism-based creep model considering temperature effect in granite, Mechanics Research Communications 56 (2014) 76– 82.

[12] E. Verstrynge, L. Schueremans, D. Van Gemert, M. Wevers, Monitoring and predicting masonry's creep failure with the acoustic emission technique, NDT&E International 42 (2009) 518–523.

[13] K. Ohno, M. Ohtsu, Crack classification in concrete based on acoustic emission, Constr Build Mater 24(12) (2010) 2339–2346.

[14] D.G. Aggelis, S. Verbruggen, E. Tsangouri, T. Tysmans, D. Van Hemelrijck, Characterization of mechanical performance of concrete beams with external reinforcement by acoustic emission and digital image correlation, Construction and Building Materials 47 (2013) 1037–1045.

[15] C. Grosse, H. Reinhardt, T. Dahm, Localization and classification of fracture types in concrete with quantitative acoustic emission measurement techniques, NDT & E International 30(4) (1997) 223-230.

[16] A.C. Mpalaskas, I. Vasilakos, T.E. Matikas, H.K. Chai, D.G. Aggelis, Monitoring of the fracture mechanisms induced by pull-out and compression in concrete, Engineering Fracture Mechanics 128 (2014) 219–230.

[17] D.G. Aggelis, A.C. Mpalaskas, T.E. Matikas, Investigation of different fracture modes in cement-based materials by acoustic emission, Cement and Concrete Research 48 (2013) 1–8.

[18] D.G. Aggelis, A.C. Mpalaskas, T.E. Matikas, Acoustic signature of different fracture modes in marble and cementitious materials under flexural load, Mechanics Research Communications 47 (2013) 39– 43.

[19] A. Moropoulou, K. Polikreti, V. Ruf, G. Deodatis, San Francisco Monastery, Quito, Equador: characterisation of building materials, damage assessment and conservation considerations, Journal of Cultural Heritage 4 (2003) 101–108.

[20] L. Chen, J.F. Liu, C.P. Wang, J. Liu,R. Su, J. Wang, Characterization of damage evolution in granite under compressive stress condition and its effect on permeability, International Journal of Rock Mechanics & Mining Sciences 71 (2014) 340–349.

[21] T. Ishida, Acoustic emission monitoring of hydraulic fracturing in laboratory and field, Construction and Building Materials 15 (2001) 283-295.

[22] C. Cerrillo, A. Jiménez, M. Rufo, J. Paniagua, F.T. Pachón, New contributions to granite characterization by ultrasonic testing, Ultrasonics 54 (2014) 156–167.

[23] D. Lockner, The Role of Acoustic Emission in the Study of Rock Fracture, lnt. J. Rock Mech. Min. Sci. & Geomech. Abstr. 30(7), (1993) 883-899.

[24] Neotex SA, "Technical data sheet," < http://www.neotex.gr/frontoffice/portal.asp?cpage=NODE&cnode=122&clang=1 >, (accessed 2/2015).

[25] A. Chmel, I. Shcherbakov, A comparative acoustic emission study of compression and impact fracture in granite, International Journal of Rock Mechanics & Mining Sciences 64 (2013) 56–59.

[26] T. Shiotani, Y. Oshima, M. Goto, S. Momoki, Temporal and spatial evaluation of grout failure process with PC cable breakage by means of acoustic emission, Construction and Building Materials, 48 (2013) 1286-1292.

[27] S. Shahidan, R. Pulin, N. Muhamad Bunnori, K.M. Holford, Damage classification in reinforced concrete beam by acoustic emission signal analysis, Construction and Building Materials 45 (2013) 78–86.

[28] T. Watanabe, S. Nishibata, C. Hashimoto, M. Ohtsu, Compressive failure in concrete of recycled aggregate by acoustic emission, Construction and Building Materials 21 (2007) 470–476.

[29] http://www.pacndt.com/index.aspx?go=products&focus=Software/noesis.htm

[30] D. Polyzos, A. Papacharalampopoulos, T. Shiotani, D. G. Aggelis, Dependence of AE parameters on the propagation distance, Journal of Acoustic Emission 29 (2011) 57-67.

[31] L. Jian-po, L. Yuan-hui, X. Shi-da, X. Shuai, J. Chang-yu, Cracking mechanisms in granite rocks subjected to uniaxial compression by moment tensor analysis of acoustic emission, Theoretical and Applied Fracture Mechanics 75 (2015) 151–159.

[32] D.C. Jansen, S.P. Shah, Effect of length on compressive strain softening of concrete, J Eng Mech 123 (1997) 25–35.

[33] [33] D. E. Moore and D. A. Lockner The role of microcracking in shear-fracture propagation in granite, Journal of Structural Geology, 17(1), (1995) 95-114.

Chapter 4. Fracture induced by pull-out and compression in concrete[7]

4.1. Purpose

In-situ characterization of strength is of paramount importance for concrete engineers. To get an estimation of the compressive strength, slightly destructive tests are conducted on the surface of the material. One is the LOK test (pull-out) which offers a reliable estimation of compressive strength. The developed stress field is quite complicated and researchers have argued about the nature of the fracture mechanism. In the present study, acoustic emission (AE) is applied during both compression and pull-out experiments on concrete cubes. Results show that the two damage modes emit different AE signatures, with compression leading to higher frequencies and pull-out to longer signal durations, while the finite element method (FEM) is used to analyze the stress field. Identification of the active damage mode in real time is beneficial in order to assess the condition of integrity of concrete in structures by nondestructive monitoring.

4.2. Introduction

The issue of structural integrity assessment is of primary concern nowadays, due to the aging of existing infrastructure. Effective monitoring and maintenance schemes are sought for in order to characterize the damage status and select the proper repair methodology. One of the factors that can provide valuable information about the structural condition is the dominant fracture mode. This is because in engineering structures the failure procedure follows a succession of modes starting from (micro-)

[7] Adapted from “Monitoring of the fracture mechanisms induced by pull-out and compression in concrete” Engineering Fracture Mechanics, Volume 128, September 2014, Pages 219-230

cracking of the matrix material and leading eventually to catastrophic shear phenomena like delaminations, detachment of reinforcing bars or fiber pull-out. The dominant mode can possibly be characterized after fracture tests when the cracked surface is investigated with Scanning Electron Microscopy (SEM) [1,2]. However, it would be of great importance to characterize the fracture mode in real time. On this respect the acoustic emission (AE) technique has shown the potential to provide crucial information on the damage mode in a non-invasive and real time fashion. This has been demonstrated in many fields, ranging from metals [2-4], composites [5,6], rock [7], as well as cementitious materials [8,9]. The present work is concerned with the comparison of AE signatures during two different widely used fracture tests of concrete that lead to different failure modes, specifically the compression test and the “LOK” test.

The compression test is generally applied on cubes or cylindrical specimens. The maximum load over the cross section area is termed as “compressive strength” due to the nominally compression stress field that is developed and is the most significant engineering property of concrete [10]. However, the actual field may be more complex, influenced by the friction between the rigid metal plates and the concrete specimen that tends to expand laterally. In order to be able to evaluate as close as possible the compressive strength in-situ, different slightly destructive test have been developed. These tests cause minor damage on the surface of concrete and therefore, they do not compromise structural performance. One of the most widely applied tests is the pull-out test, the first reference on which can be found in 1938 [11]. It involves a metallic insert which is cast into fresh concrete with the aim of pulling it out when the material hardens. This is mainly for checking the compliance with concrete strength regulations, while drilled-hole methods are also applicable for estimations on an existing structure. The advantage of such a test is that it immediately supplies a result on the “strength” of the material on the spot, without the need to extract cores saving time and resources, while the surface disruption caused is certainly smaller than sampling a cylindrical core. When the insert is extracted, a cone of concrete is also pulled out of the specimen or structure, meaning that the result depends on strength properties of the material, making the test a reliable assessment of strength [12,13]. However, the exact failure mechanism is not clear, while different researchers have worked on the subject with sometimes contrasting studies as to the strength property that dominates failure [14,15]. What should be generally accepted is that LOK results in a non-uniform three dimensional field with strong shearing components, which certainly differs from the stress field of the standard compressive test.

In this study the compression and pull-out test (in the form of LOK) are used to study the acoustic emission signature of different damage modes while the results are escorted by a finite element analysis on the developed stress field. To the authors' knowledge it is the first time AE monitoring during the LOK test is presented. Preliminary results on pullout of reinforcing bars out of concrete have been published [16] after the pioneering work of Ohtsu et al. in a different pull-out setup of hook anchors [17] Concerning compression on sampled cores, the AE activity has been used to evaluate the status of the bulk material and damage development [18,19]. Among others, the AE behavior is related to compressive strength, cracking development during bending as well as fracture energy [18-20] while recently AE events have been correlated to the creep behavior of concrete [21]. This is a part of a series of ongoing studies concerned with the identification of the dominant fracture mode in concrete based on the parameters of the emitted AE signals [22,23]. Previously it has been shown that the stage of matrix micro-cracking has distinct AE signature than the fiber pull-out stage in steel fiber reinforced concrete (SFRC) in terms of frequency (e.g. average frequency, AF) as well as other waveform parameters like "RA value" [8,22]. Additionally bending and shearing of mortar beams resulted in distinct differences with shear fracture emitting lower frequencies and longer AE waveforms [23]. In the above mentioned works the differences between the AE characteristics show the potential to identify the dominant fracture mode at least in controlled laboratory conditions using simple schemes based on a few AE parameters. Characterization of the active damage mode in real time is of great importance for the field, in order to supply information and basically warning against final failure, while it bears significance for material science studies, since it can help to characterize the type of damage that the material is susceptible to and contribute to a better design. This is the first step in an effort to apply characterization in real structures after of course other parameters like the wave attenuation and distortion due to microstructure are accounted for [23,24].

4.3. Experimental Details

4.3.1. Materials

One concrete mixture was produced consisting of fourteen specimens. There were two types of cubical specimen size: one was 200 x 200 x 200 mm and the other was 150 x 150 x 150 mm. Two of the larger specimens were produced, one for conducting the LOK test and the other for compression. Twelve specimens of 150x150x150 mm size were also produced for measuring the average compression strength per age: three days (three specimens), seven days (three specimens) and twenty eight days (six specimens). The aggregates consisted of 56% crushed sand, 13.87% fine gravel and 30.13% coarse gravel with maximum aggregate size 31.5 mm, while the water/cement ratio was 0.70 by mass. The density and the water absorption of the crushed sand were 2601 kg/m3 and 0.98 %, of fine gravel 2621 kg/m3 and 0.75 %, and of coarse gravel 2681 kg/m3 and 0.61 % respectively. The exact mix proportions were as follows: cement (type II 42.5N) 80 kg/m3, cement (type II 32.5N) 200 kg/m3, water 195 kg/m3, crushed sand 1050 kg/m3, fine gravel 260 kg/m3, coarse gravel 565 kg/m3 , retarder - plasticizer (CHEM I) 1.54 kg/m3, retarder - plasticizer (CHEM II) 1.96 kg/m3 . The actual bulk density of concrete was 2359 kg/m3 while the ambient temperature at mixing was 25 0C. The workability as measured by the slump test was 11 cm. The specimens were cured in water saturated with calcium hydroxide at 23 ±2 0C. The average compressive strength of three days was fc(3)= 18.0 MPa, of seven days fc(7)= 24.7 MPa and of twenty eight days was fc(28)= 33.8 MPa with a standard deviation of 3.0 MPa.

4.3.2. Compression and LOK test

Compression and LOK tests were conducted at the age of 28 days. Concerning compression, the load was applied on the 200x200x200 mm specimen at a constant rate of 0.3375 MPa/s until fracture and the test was automatically terminated at the moment of load drop. The compressive strength was 30.8 MPa.

The LOK test is generally applied to provide a reliable measurement of the actual strength of concrete mainly in newly cast structures in accordance with the pullout test method described in ASTM C900, or EN 12504-3 [25,26]. The steel disc (diameter of 25 mm) is cast at a depth of 25 mm into concrete, either by attaching it to the formwork before placing concrete or by inserting it manually into fresh concrete, see Figures 4. 1 (a) and (b) shows the fresh specimen after placing the insert, which is attached to the red buoyancy cup.

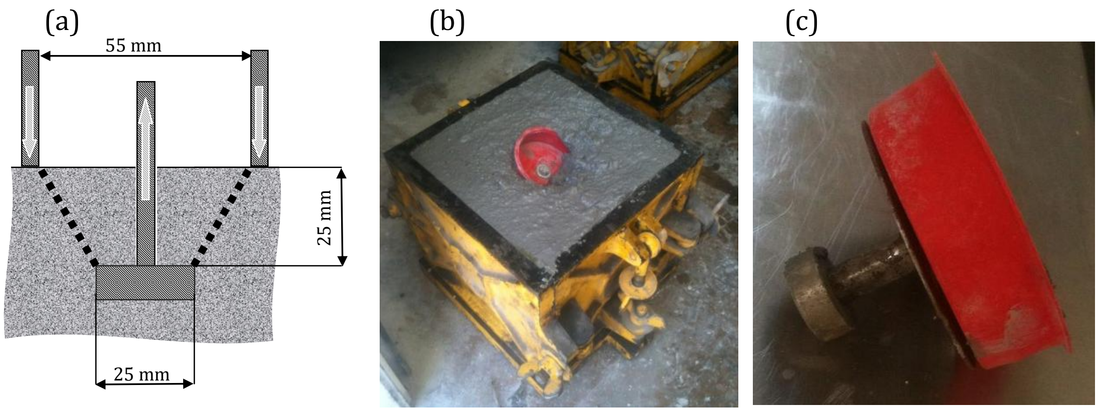

Figure 4. 1 *a) Schematic cross section of cast-in-place LOK-TEST insert, b) LOK-TEST insert placed in fresh concrete, (c) close up of the insert and the floating cup.*

In practice the axis of the insert is slightly inclined relatively to the surface. Figure 4. 1(c) shows the insert and buoyancy cup system in more detail. After hardening, the steel disc is pulled against a 55 mm diameter pressure ring bearing on the surface similarly to Figure 4. 1 (a) and the required force to pull the insert out is measured. The material in the strut between the disc and the counter pressure ring is subjected to a complex stress pattern. The pullout force is strongly correlated to the compressive strength [27].

Unlike the compression test, the loading rate for the LOK test cannot be constant because it is handled by a hydraulic jack driven by human hand thus, the loading rate is approximately 0.5 ±0.2 kN/s [25]. As the insert is being pulled out, a conical fragment of the material is extracted. The compressive strength can be evaluated from established calibration curves [27]. The pull out load measured during the specific LOK test was 25.1 kN corresponding to a compressive strength of 31.9MPa. More details about the geometry and the whole procedure of LOK test can be found in literature [12,13,27].

4.3.3. AE monitoring

AE was monitored by two types of piezoelectric sensors, namely the R15 (Physical Acoustics Corp., PAC) with resonance nominally at 150 kHz, and the Pico (PAC) which are considered more broadband with a sensitivity peak around 450 kHz. In total six sensors were applied, specifically four Pico and two R15. The signals were pre-amplified by 40 dB and were digitized by a sampling rate of 3 MHz in a PCI-8 board of PAC. In both cases of compression and LOK tests the four Pico were attached near the top surface of the cube and the two R15 in opposite corners near the bottom, see Figure 4. 2.

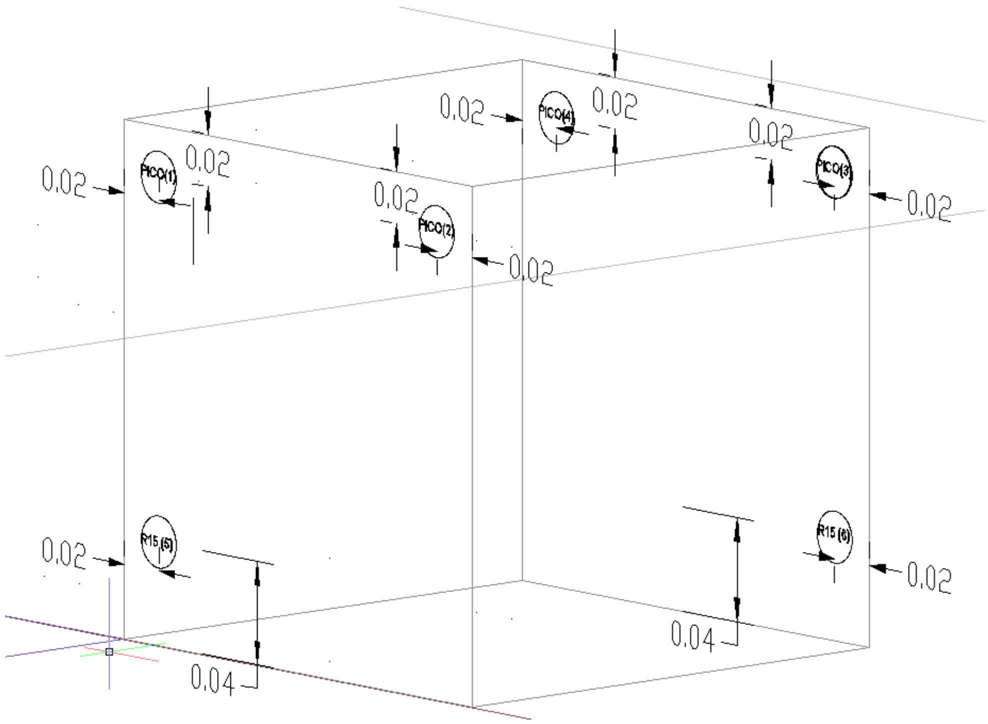

Figure 4. 2 *Representation of the AE sensors location on the cube (distances in m).*

All signals with amplitude higher than 40 dB (0.01 V) were recorded, while for the analysis, the signals with energy "zero" were disregarded. For location purposes the pulse velocity was measured by pencil lead breaks to the value of 4500 m/s.

Figure 4. 3, shows a typical AE waveform. Among many parameters that have been analyzed in AE literature, this illustration focuses on the RA value, which is the ratio of Rise Time (μs) over Amplitude (V) [8,22,28,29].

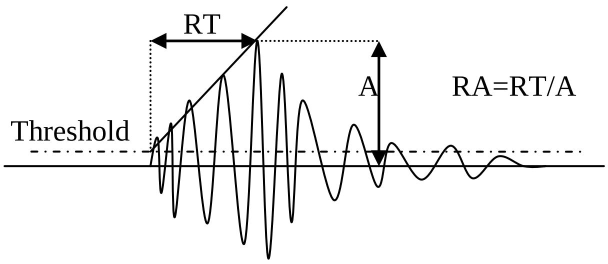

Figure 4. 3 *Typical AE waveform*

Additionally, peak frequency (PF) is the frequency with the maximum magnitude after fast Fourier transform of the time domain signal. These are the parameters that will be discussed in the results, while other indicators of frequency, like average or central frequency show similar trends.

4.4. Results

4.4.1. AE hits

The gravity in this study is given on some of the qualitative parameters of AE but introductory the cumulative population of individual signal (hits) will be discussed. Since two types of sensors with different characteristics were used, it is deemed essential to present the results separately for each type. Comparison of their behaviors is essential since the broadband type are better-suited for more detailed but laboratory-scale studies, while the resonant ones are fit for in-situ application. Figure 4. 4(a) shows the cumulative activity for the LOK test.

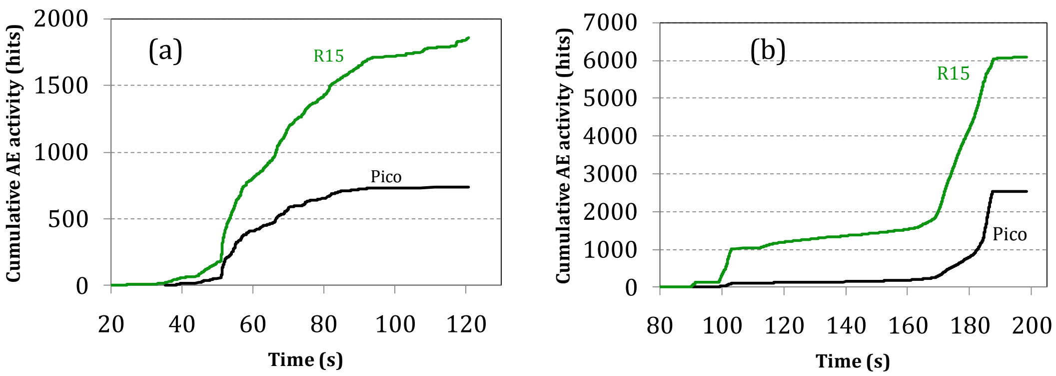

Figure 4. 4 *Cumulative activity for (a) the LOK test and (b) the compression test as recorded by the different sensor types.*

Initially the activity is gradually building up until about 50 s, when a sharper increase is noted. This is the moment of maximum pull-out load. Consequently the rate of the recorded activity decreases exhibiting an asymptotic behavior. The resonant sensors reasonably acquire much higher number of emissions, even though they are two compared to four broadband sensors. Concerning the rate of the emissions, although the moment of peak load can be determined (as mentioned around 50 s) further comments cannot be done due to the fact that the rate of loading is not constant, as it is hand driven by a hydraulic jack. Figure 4. 4 (b) shows the corresponding activity for the compression test. The trends are quite different with a quick increase (at 100 s) followed by a nearly constant (but not negligible) rate for approximately a minute. Afterwards, the activity for both sensor types increases as the final fracture stage of the specimen has started. Again resonant sensors exhibit more than double activity compared to the broadband ones.

Concerning qualitative features, which are the focuses of this study, Figure 4. 5 (a) shows the peak frequency (PF) of the hits as measured by the broadband sensors for both loading configurations.

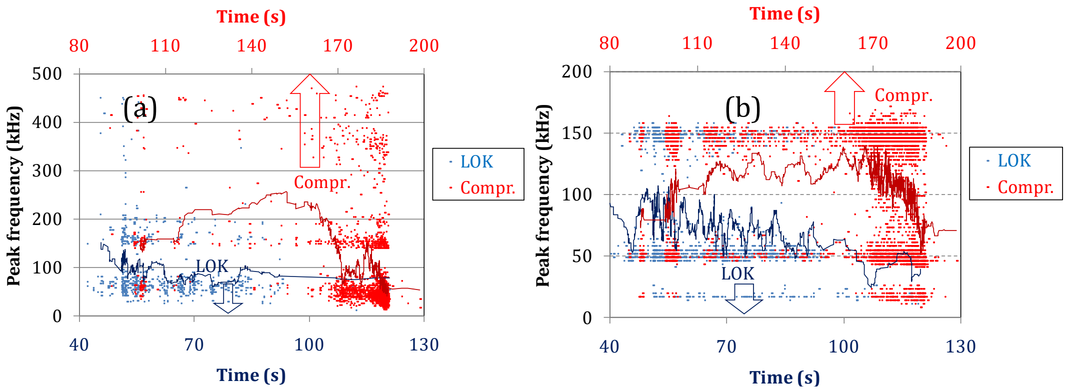

Figure 4. 5 *Peak frequency history for different loading patterns as recorded by (a) the Pico sensors and (b) the R15 sensors. Lines are moving averages of 50 successive points.*

Starting from the hits generated during the LOK test (Figure 4. 5a) it can be seen that the population can be divided in three major parts, one below 100 kHz, one between 100 kHz and 200 kHz and another smaller part with PF higher than 200 kHz. Specifically, the majority (75%) of the hits exhibit PF lower than 100 kHz, 20% is between 100 kHz and 200 kHz and only 5% scatterers in the highest band above 200 kHz.

For the compression test, the same general classification holds with the difference that the third part of the population with frequency higher than 200 kHz is more densely populated than the LOK test, while the other bands are apparently weakened. Specifically from the total number of hits received by the Pico sensors during the compressive failure process up to 160 s, 30% have peak frequency below 100 kHz, 42% between 100 and 200 kHz and 28% PF higher than 200 kHz, which indicates a considerable shift to high frequencies compared to the LOK test. The sliding average lines which are also included in, Figure 4. 5 (a) show that for the period of stable micro-cracking (up to 160 s for the compression test) the “compressive” signals constantly exhibit higher frequency as an average than the LOK since the line fluctuates around 200 kHz, while for the LOK it is around 100 kHz.

It is mentioned that concerning the compression test, the above analysis of qualitative features are based on the AE population recorded up to 160 s when a stable cracking was being recorded. After that, the final stage of fracturing started during which, the cube was severely cracked while parts of the surface layer were detached (see Figure 4. 6).

Figure 4. 6 *Concrete cube after final failure under the compressive test.*

Due to the obvious disruption of the continuity of the medium, no correlation of the received waveform with the actual emitted signal can be supported for that stage and this is why the signals of the final part of the compression loading (after 160 s) are not taken into account for parameter analysis rather than only the cumulative activity graphs presented earlier.

For the same experiment the two resonant sensors showed two main bands (see Figure 4. 5b), below and above 100 kHz. Due to the resonance of the sensors, signals of higher frequencies were not recorded. The LOK test exhibited 75% of the population under 100 kHz and 25% above, while for the compression the majority of the hits is above 100 kHz, specifically 56% and the rest 44% below. The differences between the moving average lines as seen in Figure 4. 5 (b) are still clear despite the resonant behavior of the sensors, i.e. the LOK line fluctuates around 75 kHz while the compression line around 120 kHz.

Another parameter that has been used for classification of AE signals based on their fracture mode is the RA value. The RA history for both tests based on the Pico sensors is shown in Figure 4. 7.

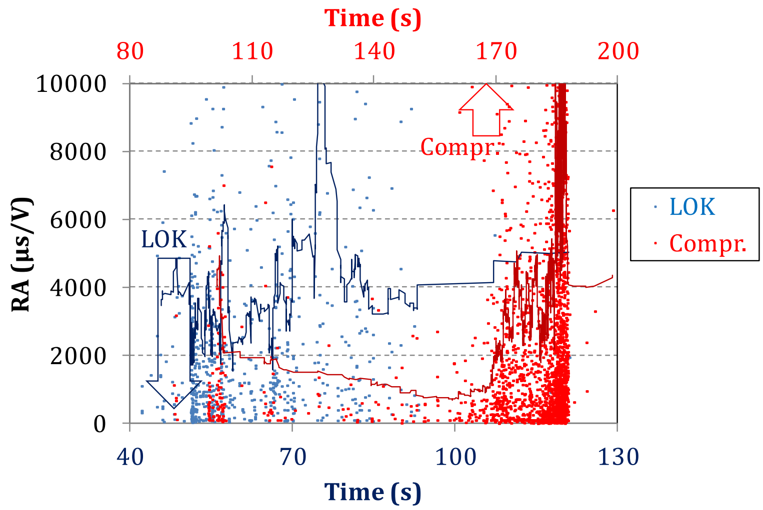

Figure 4. 7 *RA-value history for different loading patterns as recorded by the Pico sensors. Lines are moving averages of 50 successive points.*

The moving average line shows clearly that before the last stage of large scale fracture, the compression signals' RA lies in values approximately half or less than the signals of LOK, something that is in correspondence with previous results concerning matrix cracking and fiber pull-out of SFRC [8,22]. Results of RA based on the signals of R15 are not discussed as they did not exhibit strong trends.

4.4.2. AE events

The number of sensors (totally six) mounted on the specimens allowed to map the AE sources in three-dimensional space. When different sensors acquire signals within a limited time window, these are classified in an acoustic emission "event", which is the source fracturing incident that results in the individual signals recorded by the different receivers. By the time delay between acquisition of the signals at the different positions and provided that the elastic wave velocity of the material is known, the location of the source cracking event can be calculated [30,31]. Results of this analysis are presented below with discussion of the limitations. Figure 4. 8 (a) shows the location of AE sources for the LOK test.

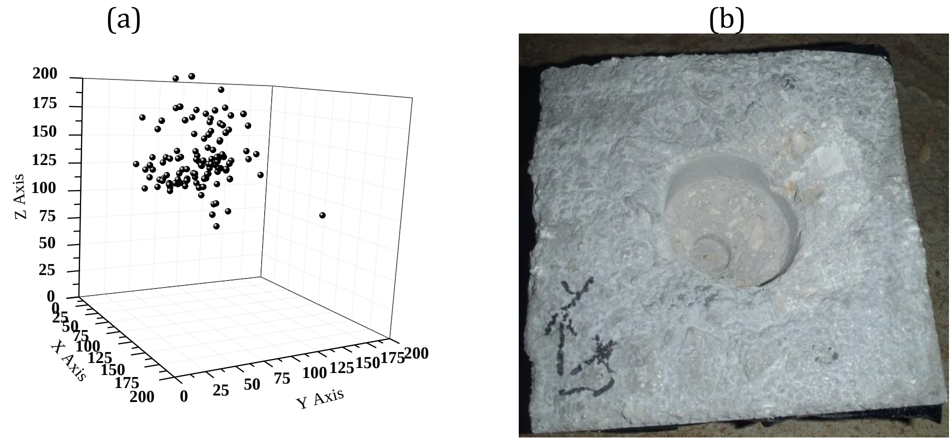

Figure 4. 8 *(a) Location of AE sources for the LOK test and (b) photograph of the specimen after LOK test. The depth of the conical hole is 50 mm. The units are in mm.*

The sources are located at the upper half of the cube. Specifically almost the whole population rests above the height of Z=120 mm, averaging at 150 mm which actually corresponds to the depth of the insert (50 mm below the top surface of the cube). The empty volume after the cone was extracted is seen in Figure 4. 8 (b), having a depth of 50 mm which is the depth that the metal disc was inserted during casting of the concrete cube. It is admitted that the accuracy of the AE sources location cannot be absolute as it depends on the sensor size relatively to the propagation distances as well as the heterogeneity of the medium [30,31]. In the specific case the insert is fixed to the plastic buoyancy cup (see Figure 4. 1) which reaches the surface of the cube, creating –in terms of wave propagation- a large void near the top surface of 50 mm diameter. Therefore, when a cracking incident occurs, the straight path is not available for propagation to each one of the sensors. This condition worsens as the cracking system between the insert and the surface is formed increasing the volume of the material which cannot support un-deviated wave propagation. This renders results of location approximate, still under these conditions, the results of Figure 4. 8 (a) appear satisfactory.

Figure 4. 9, shows the corresponding location results for the compression test.

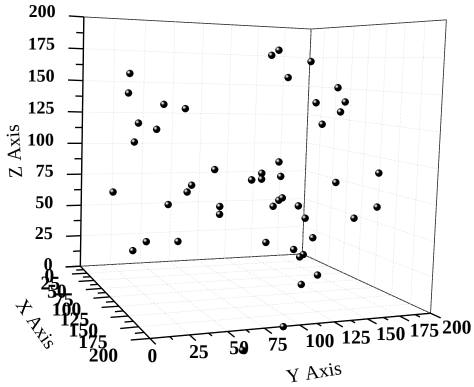

Figure 4. 9 *Location of AE sources for the compression test.*

The sources in this case may be more dispersed in the volume of the cube, something reasonable due to the nominally uniform stress field but the results are not even as satisfactory. The reason is mainly that after the major cracking events, the whole volume of the medium loses its continuity and most of the emissions do not reach the required number of five sensors in order to be qualified as “events”. This is why a relatively small number of events are shown on the graph of Figure 4. 9 corresponding to testing times before 170 s. After that moment the AE activity continued resulting to extensive number of individual AE hits as shown in Figure 4. 5 and Figure 4. 7. However, this activity could not be received by the required number of sensors to be geometrically located so it does not appear in the events plot.

This can also be seen in Figure 4. 10 where the RA history based on the broadband (a) and the PF based on the resonant (b) are plotted based on the events.

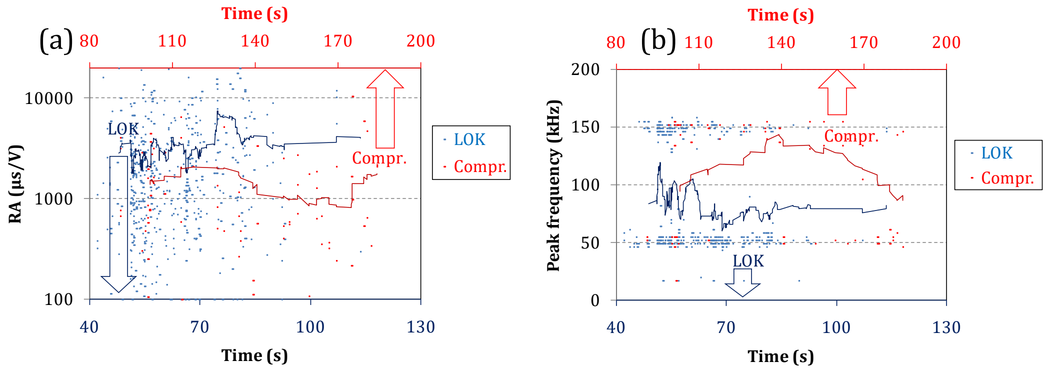

Figure 4. 10 *(a) RA history for different loading patterns based on the qualified events, as recorded by the Pico sensors and (b) peak frequency for different loading patterns based on the qualified events, as recorded by the R15 sensors. Lines are moving averages of successive 30 hits.*

The trends shown in Figure 4. 10 (a) are quite similar with the whole hit population discussed above and shown in Figure 4. 7. Additionally, the PF results from the resonant –based again on the events - show the same trends as the whole population of hits, with the average line of signals from compression being between 100 kHz and 150 kHz, while the LOK signals exhibit averages below 100 kHz. It is characteristic that from the dense population of hits at the last stage of the compression experiment (shown in Figure 4. 5 and Figure 4. 7) most of them are individual due to the severely cracked texture of the material at this stage and are not qualified as events. Therefore, the points of Figure 4. 10 are much less dense at the end.

4.4.3. Finite element model

The finite element method (FEM) is usually applied for stress analysis of static problems [32], [42]. It was used to investigate the stress field involved in the LOK test, while a previous effort was published in the 1980s [15] aiming at predicting the cracking system for the same test. In the present case, FEM was used to determine the level and the area of influence of the shear as well as the normal stresses. For this purpose, a three dimensional model of the concrete specimen was generated according to the dimensions used in the experimental process (see section 2.2). Tetrahedral solid elements of the Lagrangian formulation with four nodes, one integration point and linear displacement interpolation functions were used. The quality of the mesh was evaluated through a mesh convergence test based on the strain energy of concrete. The refinement of the mesh was based on the h-refinement process [33]. The mesh convergence analysis provided the result that an element size of 2 mm guarantees the necessary accuracy of the solution without significant increase of the computational time. To reinforce the stability of the numerical analysis an implicit integration scheme was selected. The concrete specimen was considered as linear elastic material with Young's modulus of 40 GPa and Poisson's ratio of 0.2, which is sufficient for the purpose of this study, i.e. to analyze the stress field developed due to the LOK insert pull out force. It is mentioned that the actual microstructure of concrete including aggregates, sand grains, air voids and porosity down to the size of μm could not be simulated due to the several millions of elements that would be required, number that renders the simulation unrealistic. In any case this is a static stress simulation while the microstructure would play important role in the simulation of the propagation of cracks, the path of which could be influenced by the interphase between the paste and aggregates. Dynamic fracture simulations have also been studied in different cases recently to reproduce the generation of AE events and predict the subsequent developments of cracks in concrete and other materials based on some assumptions concerning the elastic/plastic behavior of the material [34-36]. The steel disk, as well as the counter-pressure ring, were simulated as rigid bodies since they are much stiffer than concrete and their deformations are of no interest. For the execution of the numerical analysis the commercial finite element software ABAQUS/CAE 6.10 was used. Finally, all the calculations performed on an Intel Core i7 processor at 2.50 GHz. [42].

Figure 4. 11, illustrates the mesh used for the concrete specimen (a) as well as the assembly and the loading conditions applied (b).

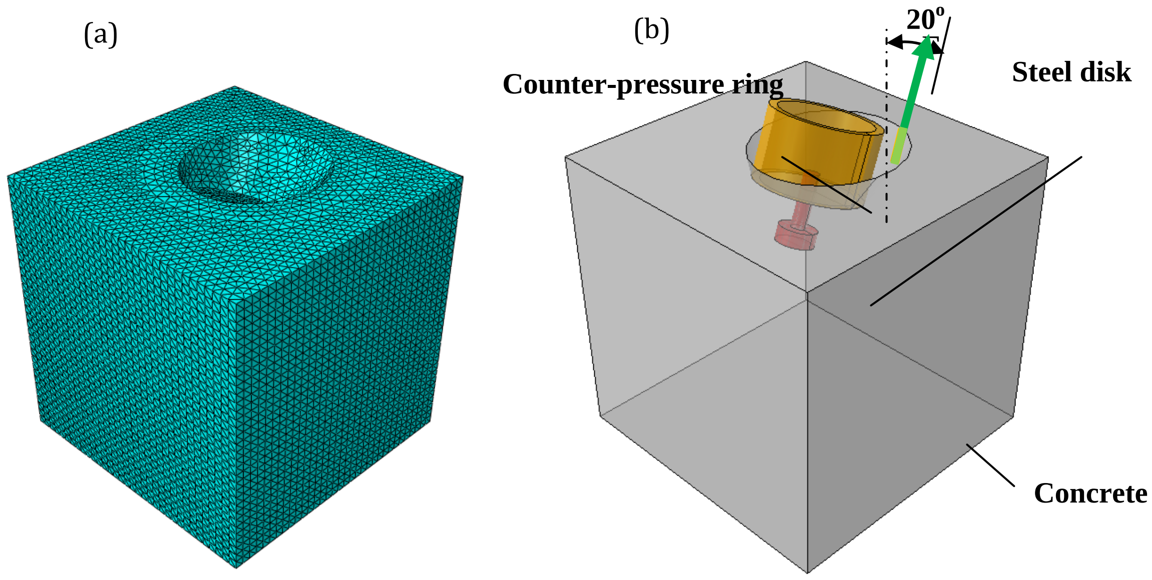

Figure 4. 11 *Finite element mesh with elements of 2 mm (a) and assembly with loading conditions (b)*

A pull force with magnitude of 25 KN was applied on the LOK-TEST insert for calculation of the developed stress field. The angle of the force with respect to the vertical edges of the specimen was 20^{o} as in the experiment. The counter-pressure ring with inner diameter of 55 mm was placed concentric with the disk on the surface of concrete. Concrete surfaces are free of constraints and therefore, the loading conditions are limited to the pulling force and the reaction of the counter-pressure ring. The results of the analysis are plotted relatively to the central cross section of the cube [42]..

Figure 4. 12, shows the distribution of the normal stress σyy (at the loading direction) in the plane of section A-A.

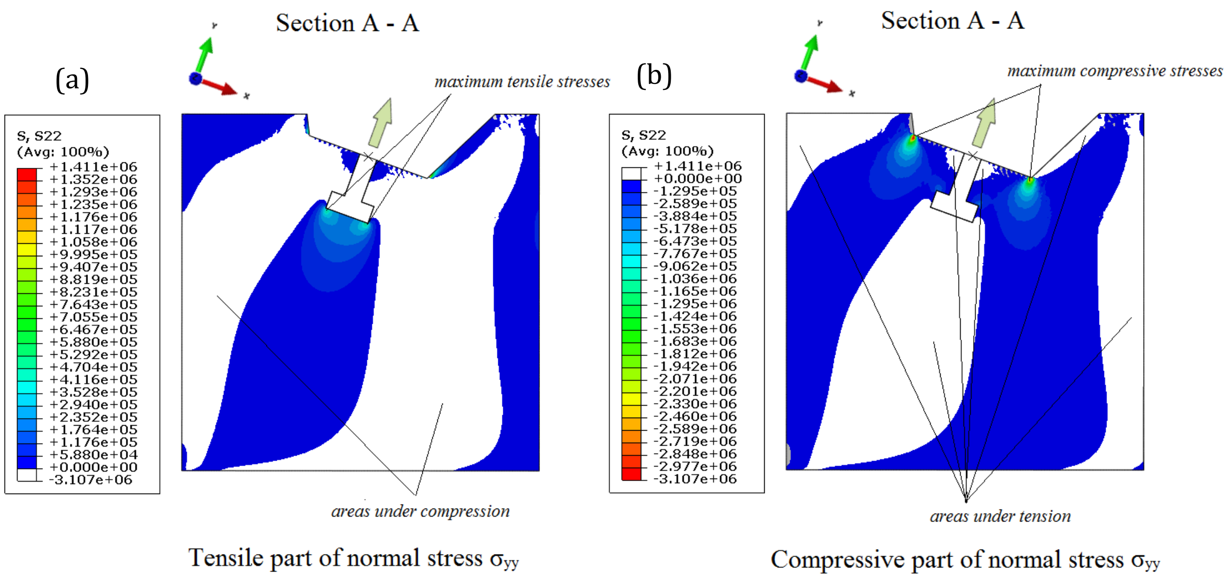

Figure 4. 12 *Distribution of the normal stress component σyy. Decomposition into a tensile (a) and a compressive part (b).*

To determine the areas under tension and compression, the stress component is decomposed into a tensile (Figure 4. 12a) and a compressive part (Figure 4. 12b). The maximum value belongs to compressive stress just below the reaction ring (see Figure 4. 12b). Perpendicular stresses (σxx, vertical to the loading direction) are of much lower value and their presentation is not deemed important [42]..

Figure 4. 13(a) presents the distribution of the shear stress component σxy in terms of absolute values.

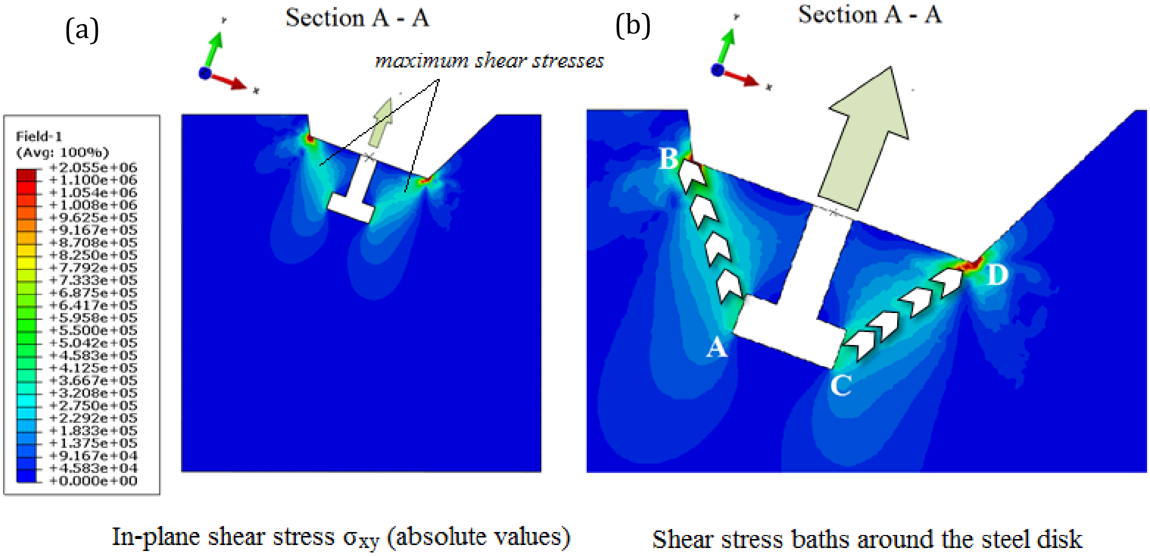

Figure 4. 13 *(a) Distribution of the in-plane shear stress component σxy, (b) focus on the area of the insert.*

Considerable shear stresses are observed in paths AB and CD, as seen in Figure 4. 13(b) [42].. Notice that these paths form a conical perimeter around the LOK insert that coincides with the final area of fracture observed during the experimental process.

To provide a more clear visualization of the stress mechanism that is developed during the test, the ratio of the in-plane shear component to the normal stress component is computed in terms of absolute values. Figure 4. 14 (a) presents the areas where the value of the ratio σxy/σyy is greater than 1.2. These are areas dominated by shear stresses.

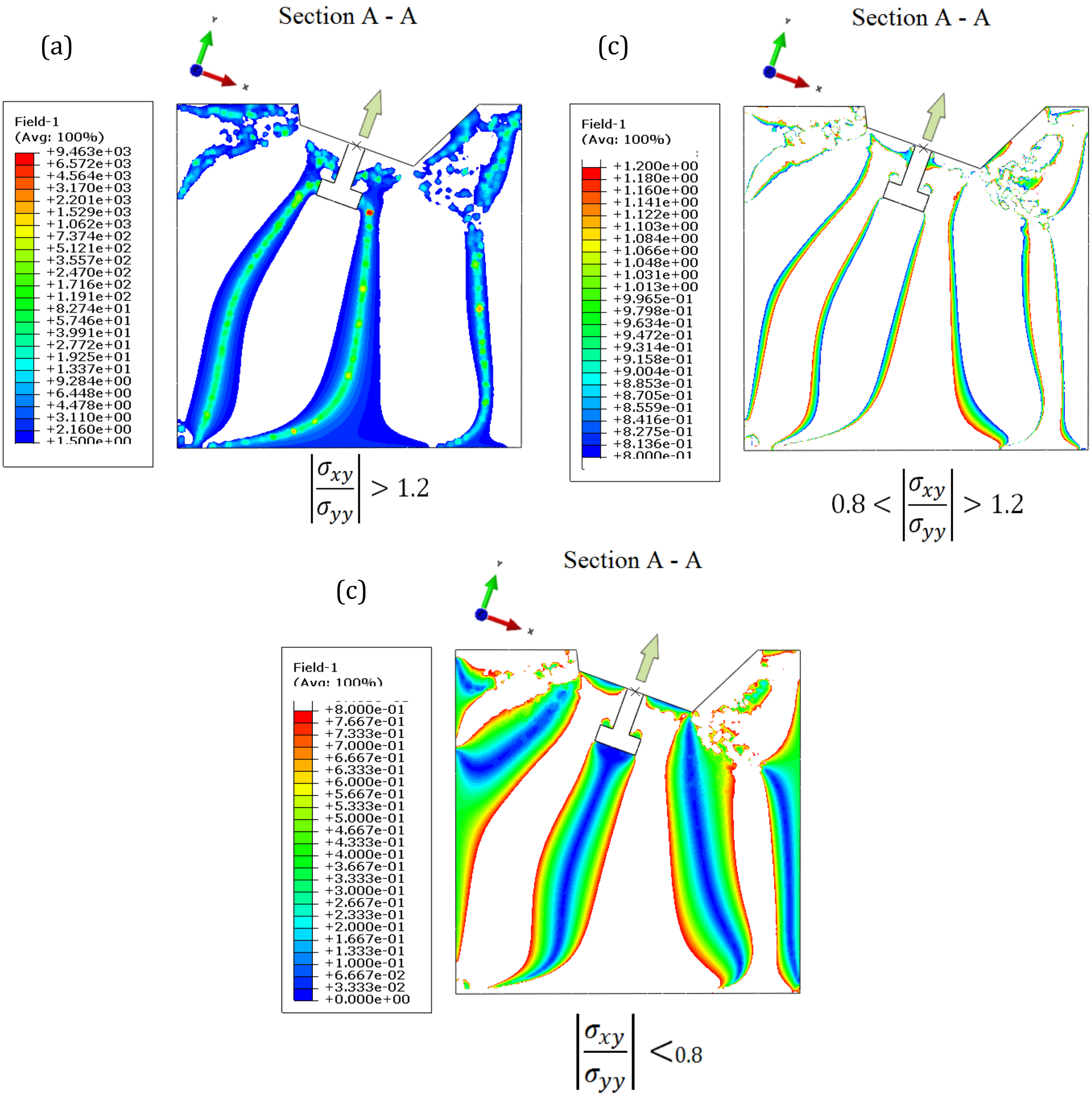

Figure 4. 14 *Areas of influence of shear stresses (a), combination of shear with normal stresses (b) and normal stresses (c).*

Figure 4. 14 (b) shows the areas where the ratio is between 0.8 and 1.2. The characteristic of these areas is that the normal and the shear stresses are acting simultaneously with approximately the same order of magnitude. Finally, Figure 4. 14 (c) shows the areas where the ratio is less than 0.8. In these areas shearing has a minor effect and the major stress mechanism are due to normal stresses. It can be seen that in contrast to the traditional compression test where fracture is (nominally)

caused from purely compressive stresses, in the LOK test the effect of shearing to fracture is of extreme importance.

This is highlighted in Figure 4. 15 which provides a representation of the stress ratios in the area around the steel disk, where the absolute value of stresses is high, neglecting areas away from the insert where stresses are negligible.

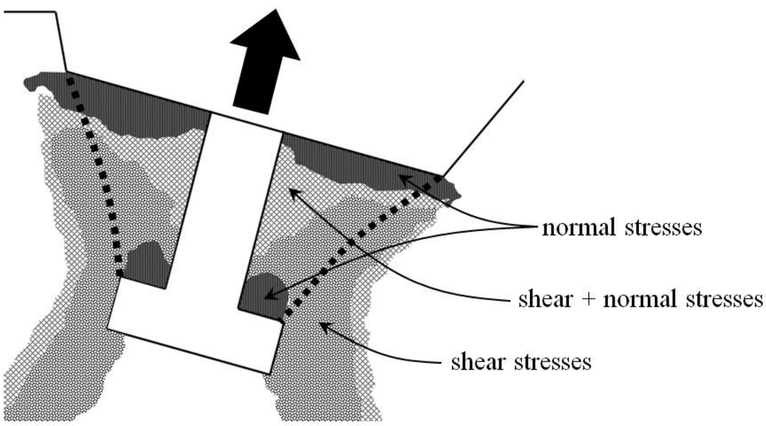

Figure 4. 15 *Stress mechanism acting on the areas around the steel disk.*

The thick dot lines represent the fracture path that has been experimentally observed. Purely normal stresses are limited on the concrete surfaces around the steel axis as well as on small areas around the upper surface of the steel disk insert. Areas along the fracture paths are dominated by high shearing stresses ($\sigma xy/\sigma yy>1.2$). Finally, transition areas characterized from shear and normal stresses of similar magnitude are observed between areas under pure normal stresses and areas under shearing.

4.5. Discussion

As the results of the FEM analysis demonstrate, the stress field initially developed during the LOK test combines both normal (tension and compression) and shear stresses. On the conical fracture surface, which is of great interest, strong shear stresses appear while their absolute values are higher than the normal stress at the same area. This mechanism substantially differs from the one involved in the concrete compression test where fracture is nominally caused by compressive stresses with absence of shearing. In an earlier study of AE during pull-out with different boundary conditions (absence of confinement ring) [17], the application of moment tensor analysis concluded that tensile stresses contributed strongly to fracture. However, in the present case, the existence of the confinement ring in the LOK test obviously increases the shear components as indicated by FEM and the AE parameters, leading to a more mixed mode of failure.

In this case, the FEM simulation model was not expanded to follow fracture rather than the initial elastic stress field [42].. The reason is that it in the present stage it would be premature to conduct reliable prediction for the fracture of concrete with such complicated microstructure. Air bubbles, porosity, and fine sand grains would require an ultra fine mesh unrealistically increasing the computation power. Additionally, the macroscopic fracture is the result of interaction of several parameters; interphasial strength between the different components (paste-sand, paste-aggregates), strength of paste and aggregate, as well as local stress concentration factors in the microstructure which altogether induce more uncertainty than clarifying the results. The main aim of the present study was focused on quantifying the differences in AE emitted from a nominally uniform compressive stress field, and the pull-out field which certainly includes strong shear components as verified by the analysis of the initial stress field. Though different stress fields may be expected to emit AE signals of different characteristics, before these are quantified in laboratory-controlled studies, the trends cannot be possibly exploited in situ. In this experiment this quantification is attempted as a first step towards acoustic structural health monitoring. Investigating the AE signatures of different fracture modes in concrete will contribute in interpreting the trends in real time monitoring applications. Therefore, the condition severity will be possibly evaluated based on shift of simple AE parameters as the ones described in the manuscript, indicating the shift between the different dominant fracture mechanisms.

From the experimental part of the study it is clearly concluded that the normal stresses of the compression test result in higher frequencies and lower RA values of AE signals than the shearing of LOK, as measured by two types of sensors. Specifically, compressive stresses result in double value of emitted frequencies than shear in average (approximately 200 kHz over 100 kHz). RA values exhibit similar differencies between the two tests, with the pull-out emitting double values. Still, the specific values of AE parameters assigned to the different modes may not necessarily hold for other specimen geometries or structures. Peak frequencies recorded by the broadband sensors in Figure 4. 5 (a) would more likely be downshifted for larger specimens and longer propagation distances, with compressive signals maintaining their relatively higher frequency than shear in any case. The reason is connected to the conditions of wave propagation through concrete. It is well known that propagation of elastic waves through heterogeneous media is both attenuative and dispersive [37-39]. This certainly changes the parameters of the waveform from their emission at the tip of the crack until acquisition at the sensor. Distortion and attenuation is active even in small scale influencing the AE signals. This is a matter of great significance when qualitative waveform parameters of the signals are of interest and is treated separately by the authors both by experiments and simulations [40,41]. In this case due to the finite size of the specimens as well as the same positioning of the sensors around all the edges of the cubes for both types of loading, it is assumed that the influence does not crucially mask the observed trends.

It is also worth to mention that using broadband sensors, differences in waveform parameters as well as frequency are readily available between the LOK and compressive test. As has been shown in previous studies broadband sensors are quite suitable for detecting various sources. However, even with resonant sensors, the discrepancies between loading patterns could be distinguished, something important for in-situ application where resonant sensors are preferred due to their higher sensitivity.

4.6. Conclusions

The acoustic emission behavior during different fracture tests on concrete is examined in this section. Two tests were conducted in order to apply different stress conditions on concrete cubes. The basic modes targeted are compression in the standard compressive test and shear during the insert pullout in the form of the LOK test. As FEM analysis indicates, the latter results in a complex state of stress including strong shearing components that overpass normal ones at the area of fracture. The resulting trends show distinct behaviors allowing discrimination of the AE signal populations from the two fracture modes. Fracture due to strong shearing stress components emits waves with longer duration and lower frequency than compression. The passive characterization of the cracking mode can prove very beneficial for structural health monitoring operations as it supplies information that cannot be yielded by any other technique. Discrimination of the modes is accomplished by a few AE parameters which is very encouraging for in-situ application. Apart from this, the analysis can assist material characterization studies in laboratory as it reveals the sensitivities of the material at different stress states.

4.7. References

1. Z. Shen, X. Yang, Z. Zhang, L. Cui, T. Li, Microstructure and failure mechanisms of refill friction stir spot welded 7075-T6 aluminum alloy joints, Materials & Design 44 (2013) 476–486.
2. A. Shanyavskiy, M. Banov, The twisting mechanism of subsurface fatigue cracking in Ti–6Al–2Sn–4Zr–2Mo–0.1Si alloy, Engineering Fracture Mechanics 77 (2010) 1896–1906.
3. Z. Han, H. Luo, J. Cao, H. Wang, Acoustic emission during fatigue crack propagation in a micro-alloyed steel and welds, Materials Science and Engineering A 528 (2011) 7751– 7756.
4. B. Zárate, J. Caicedo, J. Yu, P. Ziehl, Probabilistic Prognosis of Fatigue Crack Growth Using Acoustic Emission Data, J. Eng. Mech., 138(9) (2012) 1101–1111.
5. M. Iwamoto, Q-Q. Ni, T. Fujiwara, K. Kurashiki, Intralaminar fracture mechanism in unidirectional CFRP composites Part I: Intralaminar toughness and AE characteristics, Engineering Fracture Mechanics 64 (1999) 721-745.
6. E. Maillet, N. Godin, M. R'Mili, P. Reynaud, G. Fantozzi, J. Lamon, Damage monitoring and identification in SiC/SiC minicomposites using combined acousto-ultrasonics and acoustic emission, Composites: Part A 57 (2014) 8–15.
7. C.-S. Kao, F.C.S. Carvalho, J.F. Labuz, Micromechanisms of fracture from acoustic emission, International Journal of Rock Mechanics and Mining Sciences, 48(4) (2011) 666–673.
8. D. G. Aggelis, Classification of cracking mode in concrete by acoustic emission parameters, Mechanics Research Communications 38 (2011) 153–157.
9. A. Farhidzadeh, S. Salamone, B. Luna, A. Whittaker, Acoustic Emission Monitoring of a Reinforced Concrete Shear Wall by b-value Based Outlier Analysis, Structural Health Monitoring: an International Journal 12(1) (2013) 3-13.
10. A. M. Neville, Properties of concrete, Pearson Education Limited, Essex, England 2011.
11. B. G. Skramtajev, Determining concrete strength for control of concrete in structures J. Am. Concr. Inst. 34 (1938) 285-303.
12. N.J. Carino, Pullout Test, chapter 3 in "Handbook on Nondestructive Testing of Concrete", V.M. Malhotra and N. J. Carino Eds., CRC Press, Boca Raton, FL, (1991) 39-82.
13. J. H. Bungey and S. G. Millard, Partially destructive strength tests, chapter 4 in "Testing of Concrete in Structures", Chapman & Hall, Glasgow, 1996.
14. H. Krenchel, S. P. Shah, Fracture analysis of the pullout test, Materials and Structures 18(108) (1985) 439-446.

15. A.K. Hellier, M. Sansalone, N. J. Carino, W. C. Stone, A. R. Ingraffea, Finite-element analysis of the pullout test using a nonlinear discrete cracking approach, J. Cement, Concr. Aggregates 9(1) (1987) 20-29.
16. C. U. Grosse, F. Finck, Quantitative evaluation of fracture processes in concrete using signal-based acoustic emission techniques, Cement & Concrete Composites 28 (2006) 330–336
17. M. Ohtsu, M. Shigeishi, H. Iwase, Proceedings of the Japan Society of Civil Engineers 408/V-11 (1989) 177-186.
18. T. Watanabe, S. Nishibata, C. Hashimoto, M. Ohtsu, Compressive failure in concrete of recycled aggregate by acoustic emission, Construction and Building Materials 21 (2007) 470–476.
19. I. Iturrioz, G. Lacidogna, A. Carpinteri, Experimental analysis and truss-like discrete element model simulation of concrete specimens under uniaxial compression Engineering Fracture Mechanics 110 (2013) 81–98.
20. H. Cifuentes, B. L. Karihaloo, Determination of size-independent specific fracture energy of normal- and high-strength self-compacting concrete from wedge splitting tests, Construction and Building Materials 48 (2013) 548–553.
21. P. Rossi, J-L. Tailhan, F. Le Maou, L. Gaillet, E. Martin, Basic creep behavior of concretes investigation of the physical mechanisms by using acoustic emission, Cement and Concrete Research 42 (2012) 61–73.
22. D.G. Aggelis, D.V. Soulioti, E.A. Gatselou, N.-M. Barkoula, T.E. Matikas, Monitoring of the mechanical behavior of concrete with chemically treated steel fibers by acoustic emission, Construction and Building Materials 48 (2013) 1255–1260.
23. A. Carpinteri, G. Lacidogna, F. Accornero, A.C Mpalaskas, T.E. Matikas, D.G. Aggelis, Influence of damage in the acoustic emission parameters, Cement & Concrete Composites 44 (2013) 9–16.
24. M. Treiber, J-Y. Kim, J. Qu, L. J. Jacobs, Effects of sand aggregate on ultrasonic attenuation in cement-based materials, Materials and Structures 43 (2010) 1–11.
25. ASTM C900 Standard Test Method for Pullout Strength of Hardened Concrete.
26. EN 12504-3 Testing concrete in structures - Part 3: Determination of pull-out force.
27. Claus Germann Petersen, LOK-TEST and CAPO-TEST pullout testing, twenty years experience, Non-Destructive Testing in Civil Engineering Conference in Liverpool, U.K., April 8-11th, 1997, The British Institute of Non-Destructive Testing (http://www.germann.org/TestSystems/LOK-TEST/lok_and_capo_test_correlation.pdf, accessed 1/2014)
28. K. Ohno, M. Ohtsu, Crack classification in concrete based on acoustic emission, Construction and Building Materials 24 (2010) 2339–2346.
29. Shahiron Shahidan, Rhys Pulin, Norazura Muhamad Bunnori, Karen M. Holford, Damage classification in reinforced concrete beam by acoustic

emission signal analysis, Construction and Building Materials 45 (2013) 78–86

30. S. G. Shah, J.M. Chandra Kishen, Fracture behavior of concrete–concrete interface using acoustic emission technique, Engineering Fracture Mechanics 77 (2010) 908–924
31. B. Schechinger, T. Vogel, Acoustic emission for monitoring a reinforced concrete beam subject to four-point-bending. Construct Build Mater 21(3) (2007) 483–90.
32. S. Swaddiwudhipong, P. E. C. Seow, Modelling of steel fiber-reinforced concrete under multi-axial loads, Cement and Concrete Research 36 (2006) 1354–1361.
33. O.O. Ochoa, J. N. Reddy, Finite element analysis of composite laminates, Kluwer Academic Publishers (1992).
34. S. Invernizzi, G. Lacidogna, A. Carpinteri Particle-based numerical modeling of AE statistics in disordered materials, Meccanica, 48(1) (2013) 211-220.
35. A. Carpinteri, S. Invernizzi, G. Lacidogna. Historical brick-masonry subjected to double flat-jack test: Acoustic Emissions and scale effects on cracking density. In: Construction and Building Materials 23 (2009) 2813-2820.
36. I. Iturrioz, G. Lacidogna, A. Carpinteri, Acoustic emission detection in concrete specimens: Experimental analysis and lattice model simulations, International Journal of Damage Mechanics, 23 (2014), 327-358.
37. M.G. Vavva, V.C. Protopappas, L. N. Gergidis, A. Charalambopoulos, D.I. Fotiadis, D. Polyzos, Velocity dispersion of guided waves propagating in a free gradient elastic plate: Application to cortical bone, J. Acoust. Soc. Am. 125(5) (2009) 3414-3427.
38. J.F. Chaix, V. Garnier, G. Corneloup, Ultrasonic wave propagation in heterogeneous solid media: Theoretical analysis and experimental validation, Ultrasonics 44 (2006) 200–210.
39. W. Punurai, J. Jarzynski, J. Qu, K.E. Kurtis, L.J. Jacobs, Characterization of entrained air voids in cement paste with scattered ultrasound, NDT&E International 39 (2006) 514–524.
40. D. G. Aggelis, T. Shiotani, A. Papacharalampopoulos, D. Polyzos. The influence of propagation path on acoustic emission monitoring of concrete, Structural Health Monitoring, 11(3) (2012) 359-366.
41. D.G. Aggelis, A.C. Mpalaskas, D. Ntalakas, T.E. Matikas, Effect of wave distortion on acoustic emission characterization of cementitious materials, Construction and Building Materials 35 (2012) 183–190.
42. A.C. Mpalaskas, I. Vasilakos, T.E. Matikas, H.K. Chai, D.G. Aggelis, Monitoring of the fracture mechanisms induced by pull-out and compression in concrete, Engineering Fracture Mechanics 128 (2014) 219–230.

PART B DAMAGE INVESTIGATION ON CEMENT-BASED ELEMENS APPLYING ELASTIC WAVE APPROACHES

Chapter 5. Effect of artificial damage in cement-based materials [8]

5.1 Purpose

In the present experiment cementitious material with simulated damage is examined as to its mechanical and fracture properties. Nondestructive monitoring techniques are applied in an effort to establish or improve correlations with the simulated damage content and the failure load. Specifically, the specimens are ultrasonically interrogated before fracture, while during fracture their behavior is monitored by acoustic emission. Scattering theory seems adequate to explain the experimental ultrasonic behavior showing that modern approaches should incorporate the heterogeneity instead of considering the material macroscopically homogeneous. Apart from the strong correlations between wave velocity and damage content in the form of light inclusions, specific acoustic emission parameters show good correlation not only to simulated damage content but also to the ultimate bending load. Overall, the suitability of ultrasonic parameters to investigate damage and of acoustic emission parameters to correlate with failure load are discussed, while the influence of material's heterogeneity on the distortion of the signals is also discussed.

5.2 Introduction

Reliable nondestructive evaluation (NDE) of material condition is a prerequisite for successful structural health monitoring (SHM). Wave propagation, commonly referred to as ultrasonic testing (UT) offers this nondestructive nature along with certain advantages. One of the strongest advantages is that wave velocity is directly connected to the elastic constants [1]. In most of the cases concrete can be considered macroscopically homogeneous and hence without large error, the elastic and shear moduli can be calculated. Additionally, numerous empirical correlations have already

[8] Adapted from "Mechanical and fracture behavior of cement-based materials characterized by combined elastic wave approaches" Construction and Building Materials, Volume 50, 15 January 2014, Pages 649-656

been proposed between elastic wave velocity (mainly longitudinal) and strength, being quite valuable for on-site evaluations [2]. Quite recently the heterogeneity of concrete and other materials have started to be considered in order to explain more accurately phenomena like dispersion and attenuation [3-7]. Aggregates, porosity and especially air bubbles or damage in the form of cracking or light inclusions act as scatterers deflecting the wave beam. This introduces excessive scattering attenuation, and imposes a frequency dependent velocity behavior, as will be discussed.

Another utilization of elastic waves is in the framework of acoustic emission (AE) studies. In this case, no external wave excitation is applied but the elastic waves are emitted by fracture incidents inside the material under loading [8]. These waves carry information on the source of the fracture events and after recording and suitable study, characterization of the damage stage and mode is possible, especially in laboratory conditions [9-12]. However, due to their elastic nature, acoustic emission waves are similarly influenced by the heterogeneity of the medium, as any ultrasonic wave. Therefore, their energy, frequency content and general waveform shape changes as they propagate from the source to the receiver which is usually placed on the material’s surface. Analysis of the AE parameters can well be used to characterize the damage process of brittle materials but simultaneously, care should be taken for the scattering influence on the signals [13, 14].

In the present study both elastic wave techniques are applied in the characterization of cementitious mortar. Different volume contents of light nearly-spherical grains are included to simulate micro-cracking that could be the result of thermal damage. The spherical size of the inclusions make them suitable to simulate the randomly oriented micro-cracks as has been shown in cementitious and other material [15-18]. The material is ultrasonically interrogated in order to check the effect of inclusion content on the measured velocity of both longitudinal and surface wave modes. The density of the expanded polystyrene grains used as simulated damage, is an order of magnitude lower than the density of mortar, resulting in a strong acoustic impedance mismatch with the matrix, while the scattering contribution of sand grains is considered weak due to similar stiffness and density to the cement matrix. The results are compared with the prediction of scattering formulation of the problem of cavities inside an elastic matrix showing that the existence of damage is responsible for the observed behavior. Furthermore, and since strength is the most important property of a material from the engineering point of view, the specimens are fractured and their AE behavior is monitored. The effect of simulated damage is very strong on the AE signals as well, since several monotonic and innovative correlations are observed between AE parameters and damage content. Additionally, specific AE parameters exhibit strong correlations to the bending tensile strength since the latter is firmly connected to the fracture events occurring inside the material which give rise to the recorded emissions. Although the empirical relation between ultrasound and (mainly compressive) strength is well known, there is no theoretically justified relation between the elastic constants and strength. Strength depends on fracture mechanisms acting at the tip of cracks even in the micro-level which are not possible to critically affect wave propagation of elastic wave lengths several orders of magnitude longer. On the other hand even the smallest fracturing event emits an amount of energy that can trigger its acquisition by the AE transducers. Therefore, parameters evolving from UT and AE testing are related to both mechanical and fracture properties. After proper combined study, the different techniques may act complimentarily in evaluation of different parameters related to the material's performance, like heterogeneity content and failure load.

5.3 Experimental Details

5.3.1. Materials and testing

Seven different mortar mixtures were produced consisting of three specimens each. One was plain mortar (PM, including cement sand and water) and the others additionally included 1.5%, 2.5%, 5.0%, 7.5%, 10.0% and 12.5% (vol.) of light nearly-spherical expanded polystyrene inclusions (see Figure 5. 1) acting as voids.

Figure 5. 1 *Particles used as simulated damage*

The average inclusions size was 3.9 mm as measured from a population of twenty particles. Sand grains were of 4.75 mm maximum size, while the water to cement ratio was 0.70 by mass. The density and the water absorption of the sand were 2500 kg/m3 and 2.44% respectively. The exact mix proportions of PM were as follows: cement type (II 42.5 N) 440 kg/m3, water 308 kg/m3, sand 1364 kg/m3, super-plasticizer 4.5 kg/m3. For mortar with simulated damage the corresponding amount of inclusions was added in the mixer to account for the prescribed volume content, while the other parameters were modified accordingly so that to keep water to cement and sand to cement ratios constant. An idea of the microstructure at the scale of the inclusions, air bubbles and grains is shown in the photograph of Figure 5. 2 where the cross section of a specimen with 12.5% inclusions is included.

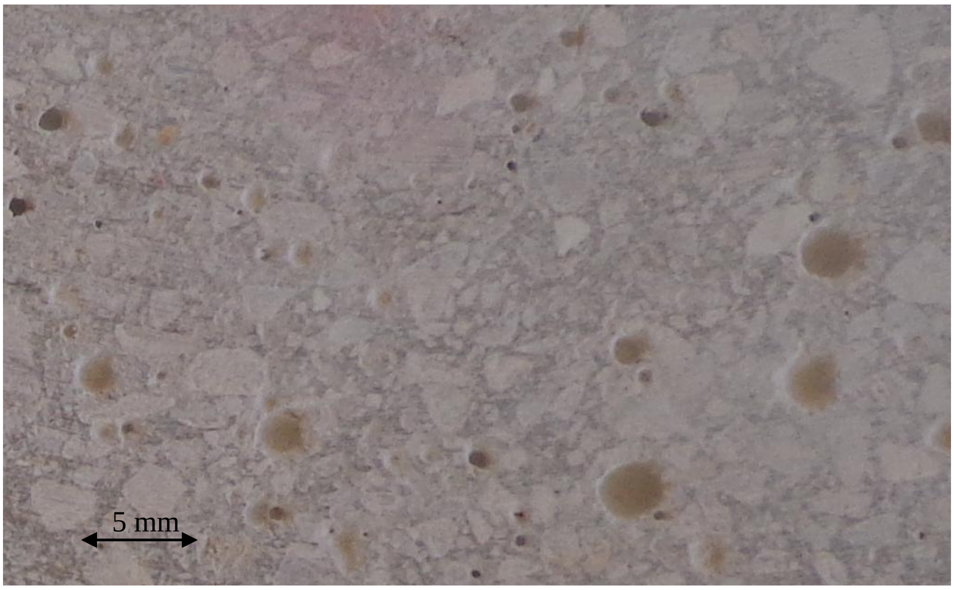

Figure 5. 2 *Photograph of cross section for a mortar specimen with 12.5% of inclusions.*

No conglomeration of inclusions was noticed in any of the specimens after saw cutting at the end of the experiments.

The specimens were cured in water for 28 days prior to nondestructive and destructive testing. Their size was 40 x 40 x 160 mm and they were eventually subjected to three-point bending according to EN 13892-2:2002 (Figure 5. 3a).

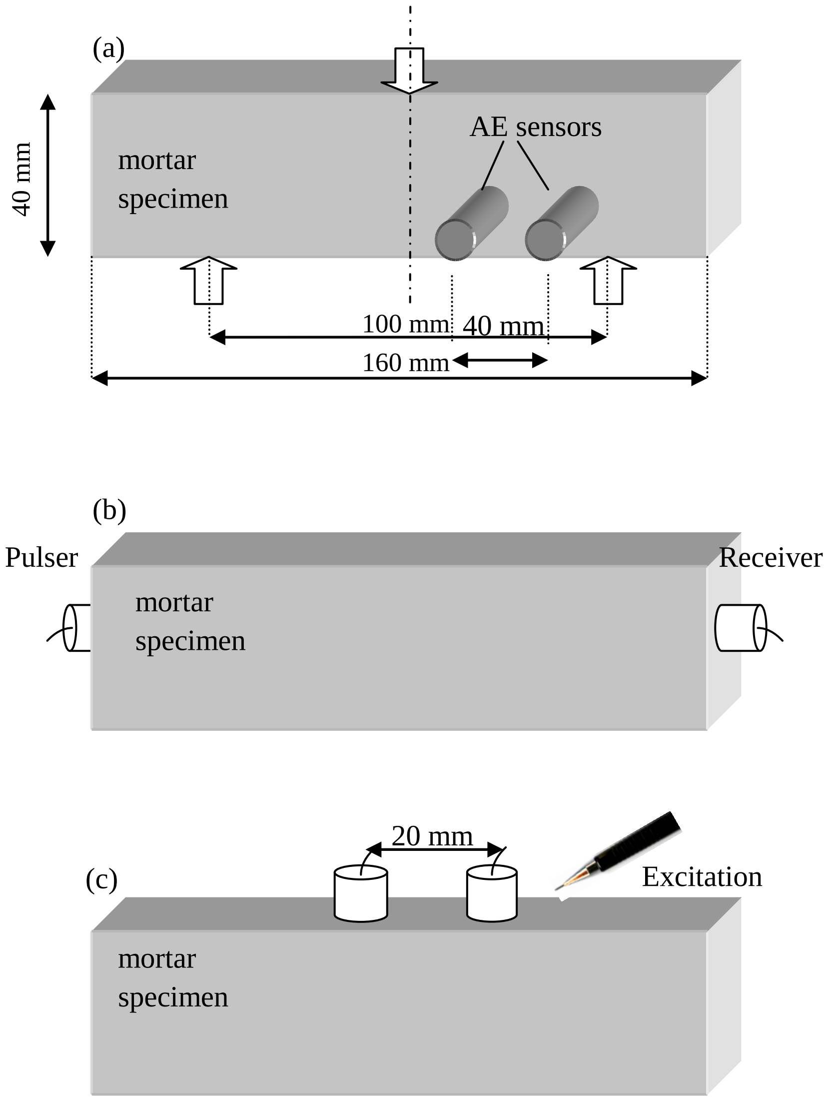

Figure 5. 3 *Schematic representation of (a) three point bending test with AE monitoring, (b) ultrasonic test with longitudinal waves, and (c) ultrasonic test for surface waves.*

The load was applied at a constant rate of 50 N/s until fracture and the loading was automatically terminated at the moment of load drop. Table5. 1 includes main physical and mechanical properties of the different materials.

Table 5. 1 *Basic physical and mechanical properties of the mixes (average of three specimens)*

Mix name	Inclusions content (vol.%)	Density (kg/m^3)	Max. bending load (kN)	Longitudinal velocity (m/s)	Rayleigh velocity (m/s)	Elastic* modulus (GPa)
A	0	1969	2.92	3693	1960	24.4
B	1.5	1941	2.67	3684	1966	24.7
C	2.5	1821	2.55	3684	1891	22.6
D	5	1959	2.75	3582	1854	22.5
E	7.5	1914	2.36	3569	1893	22.6
F	10	1921	3.01	3545	1848	22.4
G	12.5	1880	2.22	3390	1729	18.9

**Calculated from the longitudinal wave velocity and density.*

5.3.2. Nondestructive monitoring

As to AE monitoring, which was conducted during the bending test, two AE sensors (Pico, PAC) were attached to the front side of the specimen as seen in Figure 5. 3 (a). They are considered quite broadband with central frequency of 500 kHz. Roller bearing grease was used for acoustic coupling, while the sensors were secured by the use of tape during the experiment. The horizontal distance between the sensors was 40 mm and the first was placed at the horizontal distance of 15 mm from the center where the crack was expected, as seen in Figure 5. 3 (a). The sensors were placed from the same side of the specimen, in order to be able in future to correlate the AE values with the travelled distance between the source crack (mid span) and the sensor. The signals were recorded in a two-channel monitoring board PCI-2, PAC with a sampling rate of 5 MHz. The threshold was set to 40 dB in order to avoid ambient noise and the acquired signals were pre-amplified by 40 dB.

Before the fracture test, the specimens were also ultrasonically examined both through the thickness (longitudinal mode) and on the surface (Rayleigh mode). The measurements were conducted by acoustic emission transducers (R15, PAC) which exhibit maximum sensitivity around 150 kHz and have a diameter of 15 mm. For the longitudinal wave examination (see Figure 5. 3 (b)), the electric pulse fed to the transducer acting as pulser was one cycle of 150 kHz. The received signal was pre-amplified by 40 dB and digitized with a sampling rate of 10 MHz. Noise level was low and therefore, pulse velocity was measured by the first detectable disturbance of the waveform (onset). Due to the finite number of specimens (seven mixes of three specimens each) the onset was manually picked. The first disturbance corresponds to the longitudinal waves which are the fastest type. The length of the specimens (160 mm) over the pure wave transit time (after sensor delay effects are excluded) resulted in the pulse velocity for each measurement.

Concerning the Rayleigh mode, the excitation was introduced by a pencil lead break and the response at two positions on the surface was recorded again by R15 sensors (see Figure 5. 3 (c)). Although the onset of the Rayleigh wave cannot be determined as it is masked by the faster longitudinal wave, the velocity is measured by a reference peak of Rayleigh in both waveforms which is much stronger than longitudinal [19-21].

Theoretical prediction

Due to the strong acoustic impedance mismatch between the stiff cementitious matrix and the light inclusions, and the relation between the applied wave length and inclusion size as will be discussed later, scattering is the first reasonable approach to explain the wave behavior of this material. Specifically the impedance of the mortar matrix is approximately 8 MRayl (with pulse velocity 4000 m/s and density of 2000 kg/m3). For the inclusions, pulse velocity values were not found in literature while their density is less than 100 kg/m3). In order to investigate the influence of the light inclusions on ultrasonic parameters, the simple multiple scattering theory of Waterman and Truell [22] is employed, which is an advancement of the model proposed by Foldy [23]. Application of this theory to concrete is well documented in literature [3, 4, 24, 25] so only a short introduction will take place herein.

A pulse propagating in a particulate composite or material with cavities undergoes both dispersion and attenuation due to its interaction with the embedded particles. According to the above mentioned model, this wave dispersion and attenuation is represented by a frequency-dependent complex wavenumber, k, which is expressed in terms of the particle concentration, φ, and the forward, f(0), and the backward far-field, f(π) scattering amplitudes:

$$\left(\frac{k}{k_c}\right)^2 = 1 + \frac{3\varphi}{k_c{}^2 R^3} f(0) + \frac{9\varphi^2}{4k_c{}^4 R^6}\left[f^2(0) - f^2(\pi)\right] \tag{1}$$

where in the above equation, R is the size of the scatterer and kc is the wave number of the matrix.

The scattering amplitudes f(0) and f(π) are taken from the solution of the single particle wave scattering problem where a plane wave of given frequency impinges upon a particle/cavity suspended in the matrix. The single scattering parameters required are evaluated by means of the corresponding analytical expressions provided by Ying and Truell [26]. Using this formulation, the problem of a longitudinal plane wave impinging on a spherical obstacle is dealt with, taking into account the continuity of displacements and stresses on the scatterer–matrix interface. A schematic representation of the two addressed problems is depicted in Figure 5. 4 (a) for single and Figure 5. 4 (b) for multiple scattering.

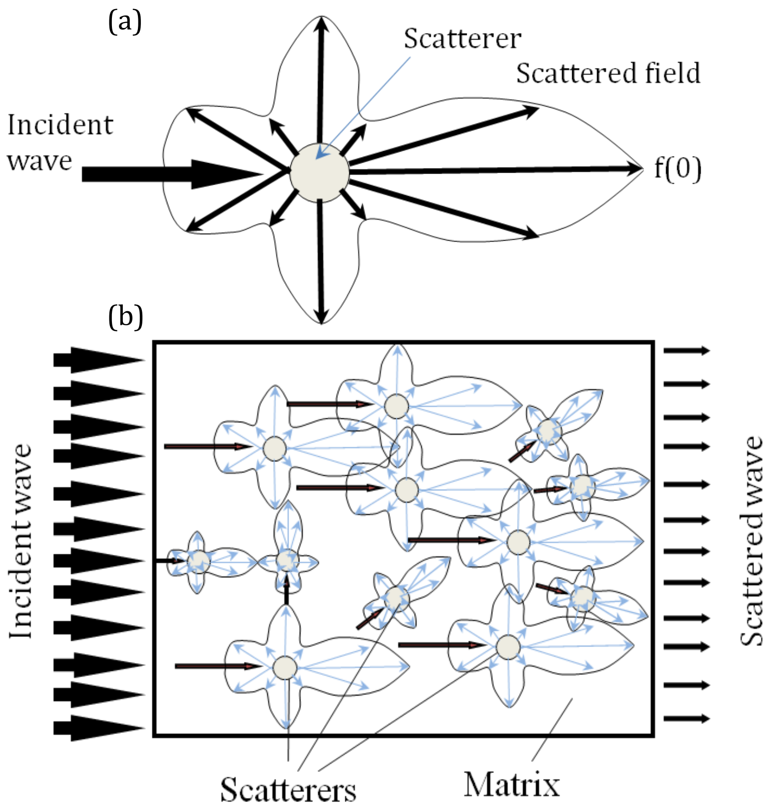

Figure 5. 4 *(a) Scattering on a single void and (b) scattering on a matrix with randomly distributed voids.*

The velocity of the scattered wave is of interest, while the incident wave is a monochromatic wave with user-selected frequency. Practically the procedure is repeated for as many frequencies the user selects. In this case results up to 400 kHz were obtained. For each different radial frequency ω, the complex wave number, k, is calculated through (1) and the phase velocity is derived from the real part of the wave number, k:

$$k = \frac{\omega}{c} + i\alpha \qquad (2)$$

while the attenuation coefficient α is the imaginary part.

For the specific calculations the elastic modulus used for the cement matrix is 24.4 GPa as measured by ultrasonic test in plain material, while the measured density of the same reference material is 1969 kg/m3. The size of the scatterers used for the theoretical calculations was 3.9 mm, as mentioned earlier. Concerning their mechanical properties, the light particles were considered as cavities (bulk, shear moduli and density near zero).

Figure 5. 5, shows the phase velocity vs. frequency curves for different percentages of inclusions.

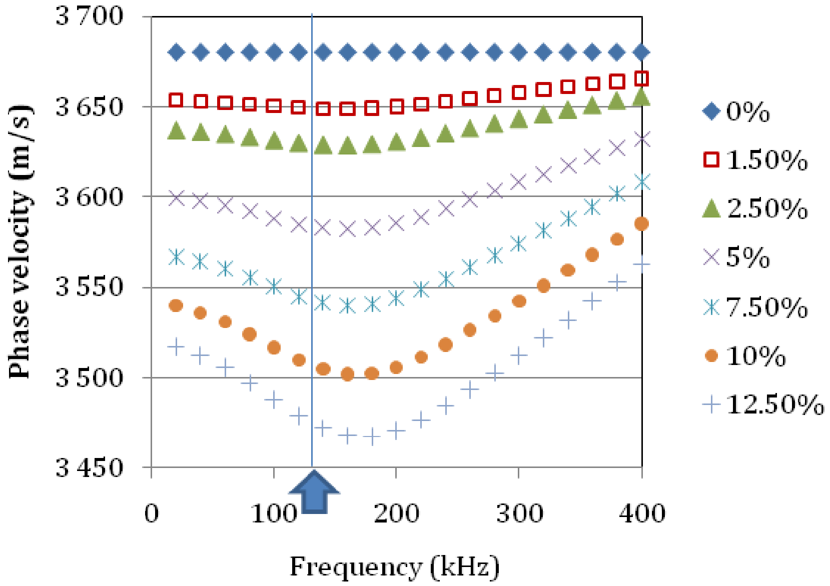

Figure 5. 5 *Theoretical phase velocity vs. frequency curves for mortar with different volume content of cavities.*

As expected in scattering media, the dispersion curve is not a horizontal line; specifically it exhibits a minimum below 200 kHz. This minimum is more intense as the inclusion content increases. This is typical behavior of porous media [27] and the frequency of the minimum is defined by the typical size of the voids. In this case the local minimum of velocity is exhibited at the frequency of 160 kHz, where the wavelength (λ) is approximately 23 mm and the product of wavenumber (k=2π/λ) times the inclusion size (R) is approximately equal to one:

$$k * R = \left(\frac{2\pi}{\lambda}\right) * R = 1.06 \qquad (3)$$

In this regime (k*R≈1) the scattering interactions are strong [28]. This is another reason that the scattering model is used, as opposed for example for k*R tending to zero, where the wavelength is orders of magnitude longer than the characteristic size of heterogeneity and homogeneous approaches are able to provide reasonable results. These results are compared to the experimental ones in the next section. It is mentioned that in similar media, approaches focusing on the incoherent part of the wave have also shown the potential to characterize distributed damage in the form of air voids or micro cracking taking into account diffuse ultrasound and late wave arrivals [29,30].

5.4 Experimental Results

5.4.1. Ultrasonics

Figure 5. 6 (a). shows the experimental longitudinal wave velocity vs. the inclusion content.

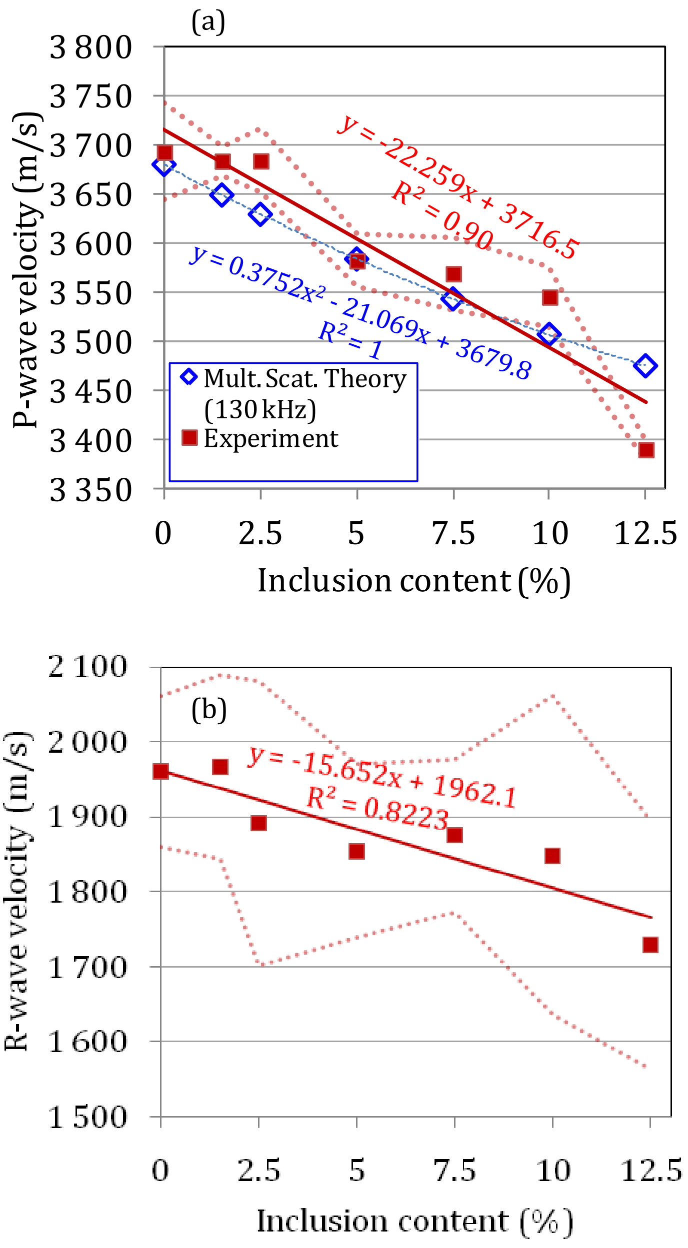

Figure 5. 6 *Wave velocity vs. inclusion content: (a) longitudinal, and (b) Rayleigh waves.*

For plain material, the velocity is close to 3700 m/s a value quite usual for sound cementitious materials. For damage content up to 2.5% the velocity seems little influenced, while for higher content the velocity clearly decreases down to 3390 m/s. The red solid squares stand for the average of three specimens, while the dot lines represent the standard deviation. The velocity decrease incurred by damage is of the order of 10%. On the same graph, the theoretical values of longitudinal phase velocity are plotted, as taken for the frequency of 130 kHz from Figure 5. 5 (see arrow on horizontal axis of Figure 5. 5). This frequency is selected as the closest to the peak frequency of the received experimental signals (120-140 kHz). The agreement between the theoretical phase velocity and the experimental pulse velocity is good showing that the wave behavior of damaged concrete can be well simulated by scattering on material with cavities and the scattering contribution of sand is relatively negligible. This agreement shows that scattering should be used to explain the wave behavior of damaged cement-based materials in more detail than homogeneous approaches. As an example from Table 5.1, if the macroscopically homogeneous approach is followed for material G, the effective elastic modulus would be calculated at 18.9 GPa (given its wave velocity of 3390 m/s and its density of 1880 kg/m3). However, in reality this velocity measured at 130 kHz is the result of the existence of 12.5% of cavities of size 3.9 mm inside a cement matrix of 24.4 GPa, as shown by scattering theory.

In a theoretical basis (i.e. the scattering model in this case) when all but one parameters are fixed (size of scatterers, elastic properties, applied frequency etc.) and only the value of volume content varies, there is one wave velocity value that corresponds to one specific volume content of scatterers (R2=1 in Figure 5. 6 (a)). Therefore, a simple inversion would lead to deterministic results; i.e. by knowing the wave velocity, the volume content would be calculated. When experiment is concerned, due to several “random” parameters this inversion cannot provide similarly accurate results, so some differences in the theoretical and experimental curves of Figure 5. 6 arise (experimental R2<1). Still in laboratory conditions most of the parameters can be controlled. So in the present case, since the volume fraction of scatterers is of interest, other mix design parameters like cement type, water to cement ratio, aggregate to cement ratio, aggregate size distribution are kept constant. Therefore, a quite satisfactory inversion can be conducted despite the possible random experimental parameters that concern mixing, small differences in air content etc. Under controlled conditions these inversions are possible. For example in the specific case, velocity values less than 3500 m/s indicate scatterer volume content of more than 10%. On the other hand velocities higher than 3650 m/s correspond to scatterer content lower than 5%. This characterization is certainly rough compared to the theoretical one-to-one inversion, but in an actual situation it would be very helpful and would contribute to the identification of the most vulnerable parts of a member given that other material parameters are similar (which is normal for a concrete belonging to the same batch).

The experimental surface (Rayleigh) wave velocity is depicted in Figure 5. 6 (b). Similarly to longitudinal, it exhibits a certain decrease with damage increase. The R-wave velocity exhibits a drop of more than 11% for inclusion-rich material showing that the influence of damage is at least equal in the Rayleigh mode, while the experimental scatter is also enhanced. Each dot is the average of twelve measurements on each type of material.

Scattering is a suitable way to explain the correlations between wave parameters and inclusion content since the wave physically propagates through the material and each inclusion/cavity leaves its fingerprint on the wave front. On the other hand, correlations with strength cannot be taken for granted, as the fracture of a material is a much more stochastic process. This is shown in Figure 5. 7 where the correlation of wave velocities vs. average load sustained on the bending test is depicted (“a” for longitudinal and “b” for Rayleigh).

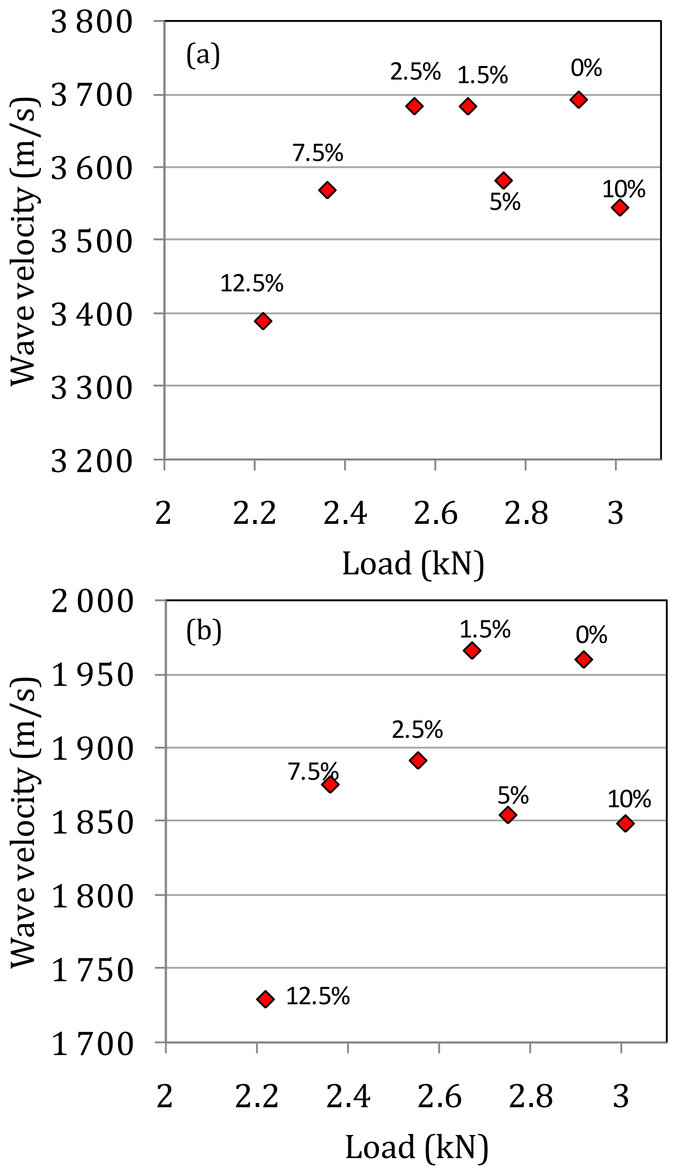

Figure 5. 7 *Wave velocities vs. maximum bending load: a) longitudinal, b) Rayleigh (percentages on graph denote inclusion content).*

While most of the classes follow a reasonable trend, two of them (containing 5% and 10% of inclusions) exhibited a higher failure load than material with fewer inclusions and in overall they result in a non monotonic curve. Only the 12.5% material exhibits constantly lower strength and wave velocities of both modes.

An idea of the experimental scatter of the strength data is given in Figure 5. 8, which depicts the load of all twenty one specimens (three for each class).

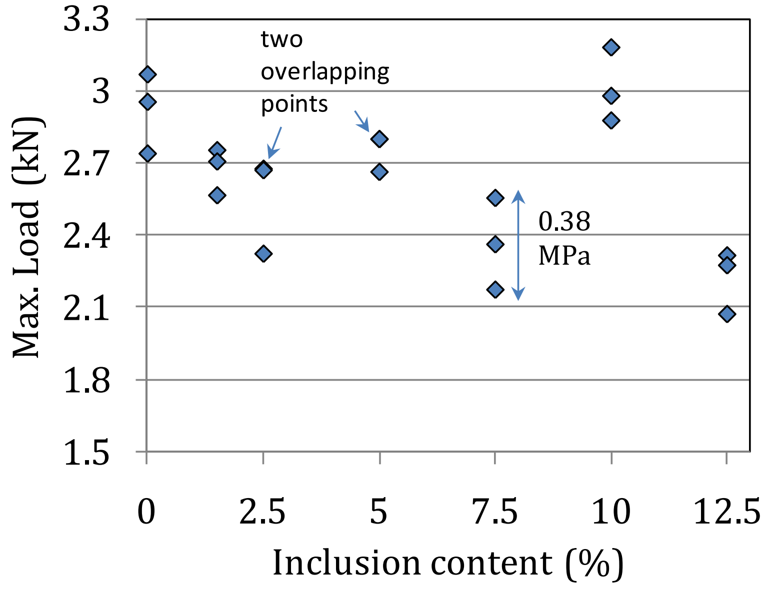

Figure 5. 8 *Maximum load vs. inclusion content for all mortar specimens.*

The range of values for each class is typically around 0.3 MPa and the maximum range is 0.38 MPa for the 7.5% inclusion content. While a general decreasing trend is seen as the inclusion content increases, the trend cannot be regarded as monotonic since the 10% class exhibits the highest load bearing capacity in average. This is not unfamiliar to cementitious materials and mixtures, due to the inherent large variation of properties and mixing conditions. Although conglomeration of inclusions was not the case, it may have resulted by local variations on the amount of light inclusions. In the three point bending configuration, the maximum bending moment is exhibited in the mid-span. Therefore, the maximum load registered is a combination of the applied load, and the amount of reduction of the effective central vertical cross section due to the inclusions. Though the bending moment is sure to obtain its maximum value in the mid span due to geometry, the uniform reduction of the load bearing cross sections cannot be guaranteed, leading to some variability on the resulted maximum load. The fact that the 10% mortar surprisingly exhibited the highest load could have led to the decision to repeat the mix for this inclusion percentage. This would be the case if the only aim of the work was the correlation between ultrasonic velocity and inclusion content. However, one of our aims was to examine the possible correlation between AE parameters to failure load. Therefore, from this point of view there are seven classes of materials with different values of failure load and different AE parameters that exhibit the correlations which will be described later. Due to the physical existence of the inclusions that act as cavities, the wave velocity is influenced showing the corresponding decreasing trend of Figure 5. 6. However, due to the more complicated behavior at fracture, the existence of the total amount of light inclusions cannot guarantee the expected strength relatively to the more or less densely inclusion-populated specimens.

5.4.2. Acoustic emission results

At the moment of main fracture the tensile stresses at the bottom exceed the strength of the matrix material. The emitted signals from the fracture are recorded and their parameters analyzed. As aforementioned, frequency and waveform parameters are used for characterization of the severity of the process. Specifically the following parameters are discussed herein: central frequency, defined as the centroid of the spectrum after fast Fourier transform (FFT) of each recorded waveform, measured in kHz and RA value which is inverse of the “rising angle” of the waveform and is defined as the ratio of rise time over the amplitude (μs/V) [9,10,12]. Additionally, the number of threshold crossings (counts) are of interest, while energy related parameters are also included since they have proven useful in monitoring of real structures [31]. In the present case RMS (root-mean-square – square root of the average of the squares of all points of a waveform) and ASL (the average signal level defined as the average amplitude of samples of the rectified signal [32]) are applied. Figure 5. 9 (a), shows the maximum central frequency exhibited during the fracture of the specimens vs. the inclusion content.

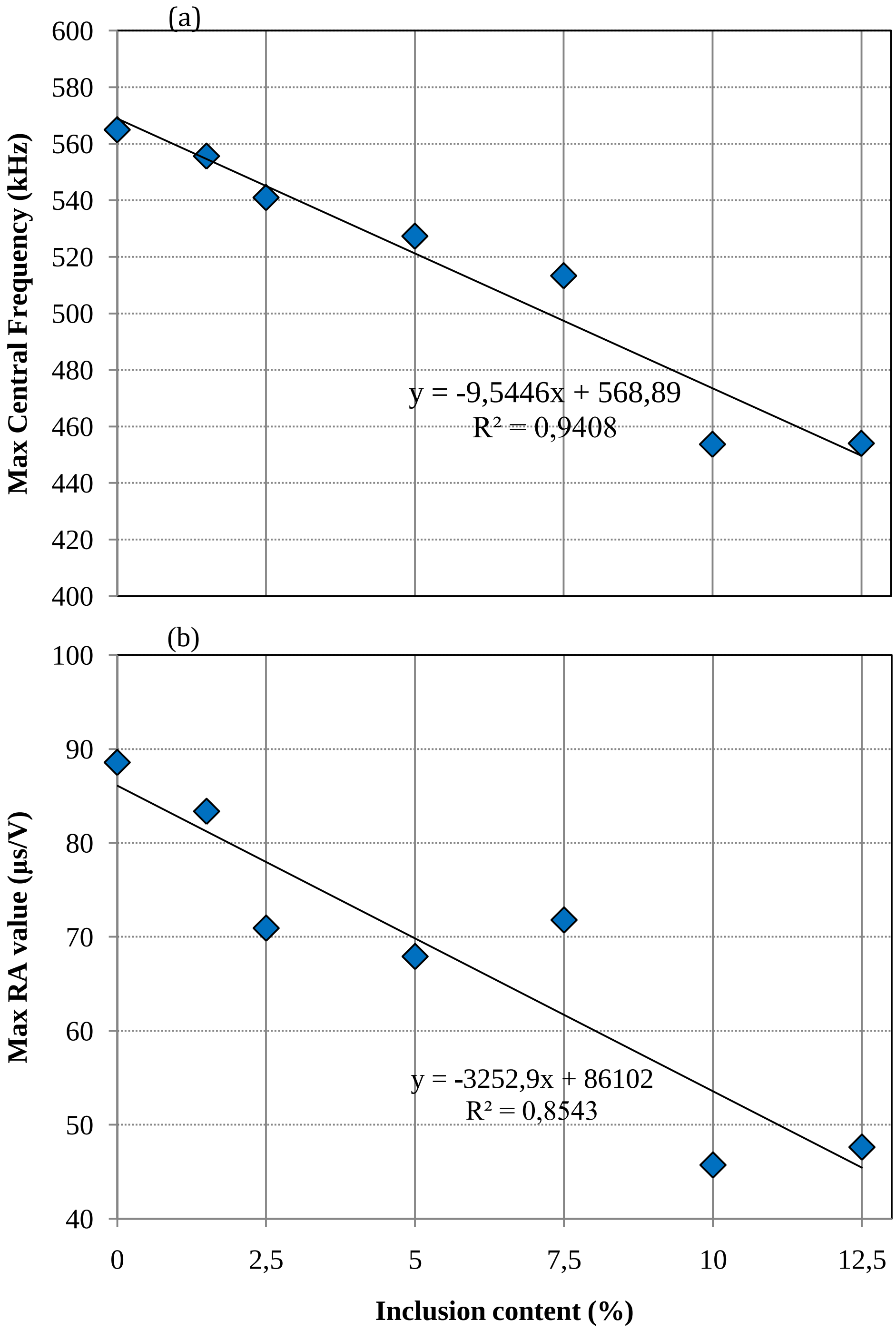

Figure 5. 9 *AE parameters at the moment of fracture vs. the damage (inclusion) content of the material: (a) central frequency, (b) RA.*

This feature monotonically decreases as inclusions increase and is characteristic of their scattering action. Actually the material of the specimens which is fractured under the bending load is the same mortar matrix regardless of the inclusion content. Therefore, a typical AE event should not systematically differ from specimen to specimen. Though the emissions from the fracture of the matrix are reasonable to be similar, the scattering action of the inclusions will certainly influence their propagation. Results of Figure 5. 9 (a), show that the frequency received after a matrix crack may well differ by more than 100 kHz (20%) depending on the inclusion content of the material.

Additionally, the maximum RA recorded is seen in Figure 5. 9 (b). In general, RA value exhibits maxima at the moment of main crack formation [9,10] and it is related to the severity of the incident. In this case although, as mentioned earlier, the fracture events are not expected to differ in their source, the received signals exhibit a decreasing trend of RA as damage increases. This is again a result of the scattering action of the inclusions, which influences the amplitude of the signals, their duration and rise time and most of the waveform parameters possibly posing serious problems in AE classification as will be discussed.

As also examined for the ultrasonic parameters, correlations between AE parameters and failure load were sought. Since the failure load does not necessarily follow the increase of inclusion content, AE parameters well correlated to inclusions are not expected to correlate in the same way to the failure load. However, correlations exist, though not for the same AE indices which were found well correlated to simulated damage. These parameters are relative to the emitted energy, namely ASL and RMS, see Figure 5. 10 (a) and (b) respectively.

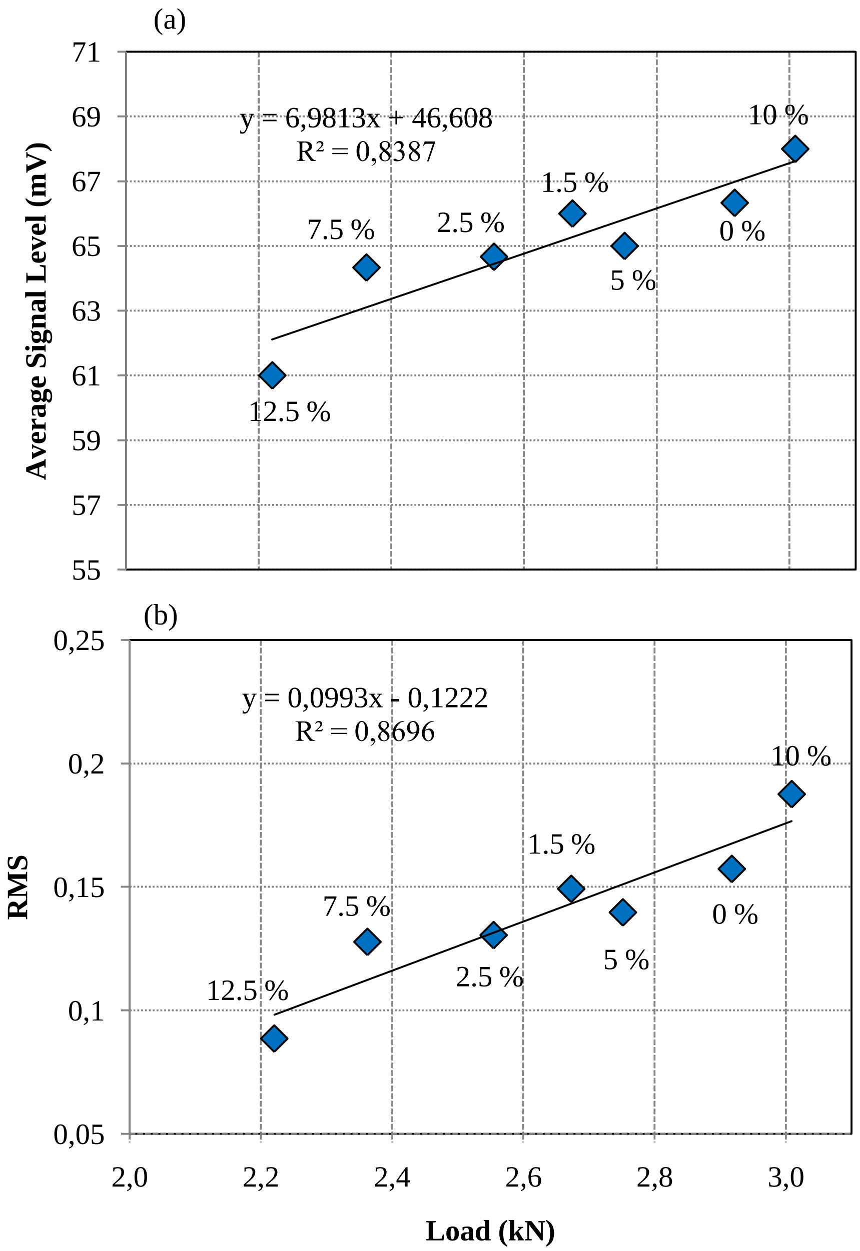

Figure 5. 10 *(a) Average signal level and (b) root-mean-square vs. maximum load (percentages on graph*

The straight curve fitting is just indicative of the clear increasing trend, showing that as the maximum load of the specimens increases, so do these AE energy indicators recorded by the sensors. This is reasonably connected to the released energy at fracture which depends on the load level. It is indicative that the RMS of the AE signals increases by a factor of two for material with the highest failure load (3.01 kN) compared to the lowest (2.22 kN). The same parameters are not similarly well correlated to the percentage of inclusions, showing that some parameters are suitable for correlation with existing damage or heterogeneity while others are more indicative of strength properties.

5.5 Discussion

In general, ultrasonic velocities are more successfully linked to inclusion content while AE energy parameters are linked to the failure load. However, due to their elastic nature, AE signals exhibit strong dependence on the inclusion content as well, mainly seen through RA value and central frequency. From the reported correlations of this study it seems that the strongest one is between the wave velocity and inclusion content, since the trend is monotonic with a correlation coefficient R^2 higher than 0.9. Concerning failure load though, AE energy-related parameters seem to yield also strong correlations (R^2 just below 0.9). However, it would be premature to classify the different descriptors according to their characterization strength from this series of laboratory measurements. This mainly goes for the AE parameters, which are more sensitive than pulse velocity to the experimental conditions (sensor types, coupling, distance between crack and sensor). The importance is that AE parameters can be used in conjunction with slightly destructive tests, like the pull-out or drilling in order to supply extra correlations with the load bearing capacity of a material in a structure. So far several models have been proposed for compressive strength estimation based on ultrasonic pulse velocity and rebound hammer. Most of these provide relatively good results but they leave a substantial zone of uncertainty related to the specific material. Possible addition of another parameter (of the AE family this time) in a multiple parameter model will hopefully increase the accuracy provided by pulse velocity and is an area that needs serious future effort.

Although it can be argued that ultrasonic properties are physically related to elastic modulus, there is no certain relation between elasticity and strength (tensile, bending or compressive) so as to expect a robust correlation between UT results and failure load. In several cases, as already mentioned in the introduction, correlations may have emerged but these are empirical, while there is no proved physical connection between elasticity and the failure load of the specimen. Elastic modulus is the incremental resistance of a material to strain in the elastic region, while strength is defined by fracture criteria and the role of the material's microstructure (certainly smaller than the ultrasonic wavelength of some cm) is imperative. Therefore, it is reasonable that correlations to any type of strength should be sought for in the family of AE parameters, while existent damage in the form of cracks, voids, or inclusions which certainly influences the overall elastic properties should be better described by ultrasound propagation. In the specific case, the AE parameters are related to the bending strength of the material.

It is significant to highlight that up to a large extent the AE parameters depend on the texture of the material and not solely on the source. Despite the fact that AE sources are the same in all specimens since fracture starts from tensile cracks on the mortar matrix, several strong monotonic trends are noticed between AE parameters and damage content. This is particularly important since AE parameters are used for crack classification concerning the dominant fracture mode (tensile, mixed-mode or shear [9,12,33]). In any specific crack classification scheme the values of AE parameters including frequency indicators and RA are used to classify the events according to their source. Therefore, the differences presented due to heterogeneity can mislead characterization and misclassify the data.

The understanding of the different role of the two techniques is of paramount importance since it opens the direction for evaluating not only the content of damage which is one of the main goals of structural health monitoring but also the estimation of failure load which is the most crucial parameter for a load bearing construction.

5.6 Conclusions

This is a study of combined elastic wave techniques on cementitious material with simulated damage. The main objective is to help in establishing tools for detailed assessment of the material's condition. Wave velocity can be quite accurately used to correlate to the damage content in the form of light spherical-like inclusions. Experiments are supported well by scattering theory, the results of which are in very good agreement for the experimental frequencies. Additionally, the load bearing capacity of the specimens was tested. Though ultrasonic parameters do not exhibit similarly strong correlations with the ultimate load, specific parameters of AE seem to correlate better. This is reasonable since the ultimate load depends on the fracture incidents which are monitored through the emitted acoustic waves. Energy related parameters of AE reveal quite strong correlations directly to bending strength implying that apart from ultrasonic velocity which has been used for empirical correlations with strength, AE should be studied complimentarily in order to improve the rough estimations of strength offered by ultrasonic velocity.

5.7 References

1. Naik TR, Malhotra VM, Popovics JS, The ultrasonic pulse velocity method. In: Malhotra VM, Carino NJ, (eds) Handbook on nondestructive testing of concrete. Boca Raton: CRC Press; 2004.
2. Popovics S. Analysis of the concrete strength versus ultrasonic pulse velocity relationship. Materials Evaluation 2001;59(2):123-130.
3. Chaix JF, Rossat M, Garnier V, Corneloup G. An experimental evaluation of two effective medium theories, for ultrasonic wave propagation in concrete. J. Acoust. Soc. Am. 2012;131(6):4481-4490.
4. Aggelis DG, Polyzos D, Philippidis TP. Wave dispersion and attenuation in fresh mortar: theoretical predictions vs. experimental results. Journal of the Mechanics and Physics of solids 2005;53:857–883.
5. Treiber M, Kim JY, Qu J, Jacobs LJ. Effects of sand aggregate on ultrasonic attenuation in cement-based materials. Materials and Structures 2010;43:1–11.
6. Vavva MG, Protopappas VC, Gergidis LN, Charalambopoulos A, Fotiadis DI, Polyzos D. Velocity dispersion of guided waves propagating in a free gradient elastic plate: Application to cortical bone. J. Acoust. Soc. Am. 2009;125(5):3414-3427.
7. Tsinopoulos, S.V., Polyzos, D., Beskos, D.E. Static and dynamic BEM analysis of strain gradient elastic solids and structures. CMES - Computer Modeling in Engineering and Sciences 2012;86(2), 113-144.
8. Grosse CU, Ohtsu M Acoustic emission testing. Springer; 2008.
9. Aggelis DG. Classification of cracking mode in concrete by acoustic emission parameters. Mechanics Research Communications 2011;38:153–157.
10. Farid Uddin AKM, Numata K, Shimasaki J, Shigeishi M, Ohtsu M. Mechanisms of crack propagation due to corrosion of reinforcement in concrete by AE-SiGMA and BEM. Construction and Building Materials 2004;18:181–188.
11. Carpinteri A, Cardone F, Lacidogna G. Energy emissions from failure, phenomena: mechanical, electromagnetic, nuclear. Experimental Mechanics 2010;50:1235–43.
12. Ohtsu, M. Recommendations of RILEM Technical Committee 212-ACD: acoustic emission and related NDE techniques for crack detection and damage

evaluation in concrete: 3. Test method for classification of active cracks in concrete structures by acoustic emission, Mater. Struct. 2010;43(9):1187–1189.

13. Schechinger B, Vogel T. Acoustic emission for monitoring a reinforced concrete beam subject to four-point-bending. Construction and Building Materials 2007;21:483–490.
14. Aggelis DG, Mpalaskas AC, Ntalakas D, Matikas TE. Effect of wave distortion on acoustic emission characterization of cementitious materials, Construction and Building Materials 2012;35:183–190.
15. Chaix JF, Garnier V, Corneloup G. Ultrasonic wave propagation in heterogeneous solid media: Theoretical analysis and experimental validation, Ultrasonics 2006;44:200–210.
16. Aggelis DG, Momoki S. Numerical simulation of wave propagation in mortar with inhomogeneities. American Concrete Institute Materials Journal, 2009;106(1):59-63.
17. Tsinopoulos SV, Polyzos D, Paipetis SA. Wave propagation in randomly cracked polymers, International Symposium COMP 95, Corfu, Greece, 1995.
18. Lu Y, Liaw PK. Effects of particle orientation in silicon carbide particulate reinforced aluminum matrix composite extrusions on ultrasonic velocity measurement. J. Comp. Mat. 1995;29:1096-1116.
19. Abraham O, Piwakowski B, Villain G, Durand O. Non-contact, automated surface wave measurements for the mechanical characterisation of concrete. Construction and Building Materials 2012;37:904-915
20. Qixian L, Bungey JH Using compression wave ultrasonic transducers, to measure the velocity of surface waves and hence determine dynamic modulus of elasticity for concrete. Constr Build Mater 1996;4(10):237–42.
21. Aggelis DG, Shiotani T. Experimental study of surface wave propagation in strongly heterogeneous media, J. Acoust. Soc. Am. 2007;122(5):EL 151-157.
22. Waterman PC, Truell R. Multiple scattering of waves. J. Math. Phys. 1961; 2, 512–537.
23. Foldy L. L., The multiple scattering of waves, Phys. Rev. 67, 107–119, 1945.
24. Punurai W, Jarzynski J, Qu J, Kurtis KE, Jacobs LJ, Characterization of entrained air voids in cement paste with scattered ultrasound, NDT&E International 2006;39:514–524.

25. M. Molero, I. Segura, M.G. Hernández, M.A.G. Izquierdo, J.J. Anaya, Ultrasonic wave propagation in cementitious materials: A multiphase approach of a self-consistent multiple scattering model, Ultrasonics 51 (2011) 71–84.
26. Ying CF, Truell R. Scattering of a plane longitudinal wave by a pherical obstacle in an isotropically elastic solid. J. Appl. Phys. 1956;27, 1086–1097.
27. Sayers CM, Dahlin A. Propagation of Ultrasound Through Hydrating Cement Pastes at Early Times. Advanced Cement-Based Materials 1993;1:12-21.
28. Chekroun, M., Le Marrec, L., Abraham, O., Durand, O., Villain, G. Analysis of coherent surface wave dispersion and attenuation for non-destructive testing of concrete, Ultrasonics 49 (2009) 743–751.
29. Chi-Won In, R. Brett Holland, Jin-Yeon Kim, K. E. Kurtis, L. F. Kahn, L. J. Jacobs, Monitoring and evaluation of self-healing in concrete using diffuse ultrasound, NDT&E International57(2013)36–44.
30. D. P. Schurra, Jin-Yeon Kim, K. G.Sabra, L. J. Jacobs, Damage detection in concrete using coda wave interferometry, NDT & E International 44 (2011) 728–735.”
31. Shigeishi, M., Colombo, S., Broughton, K.J., Rutledge, H., Batchelor, A.J., Forde, M.C. Acoustic emission to assess and monitor the integrity of bridges, Construction and Building Materials 2001;15,35-49
32. Kaewwaewnoi W, Prateepasen A, Kaewtrakulpong P. Measurement of Valve Leakage Rate using Acoustic Emission, Proceedings of The ECTI'05, pp. 597-600, May 12-13, Pataya, Chonburi, Thailand 2005.
33. Ohno K., Ohtsu M, Crack classification in concrete based on acoustic emission, Construction and Building Materials 2010;24:2339–2346.

Chapter 6. Effect of real damage (fire) in concrete

6.1 Purpose

The mechanical behavior of concrete after extensive thermal damage is studied in this experiment. After being exposed to direct fire action at temperatures of 700 ^{o}C and 850 ^{o}C, specimens were subjected to bending and compression in order to determine the loss of strength and stiffness in comparison to intact specimens. Nondestructive monitoring techniques were also applied in the form of ultrasonics (ultrasonic pulse velocity, UPV) and acoustic emission (AE). Apart from the good-but well known-correlation of UPV to strength (bending and compressive), strong correlations are noticed between UPV and absorbed fracture energy. Additionally, AE parameters based mainly on the energy of the emitted signals after cracking events, show similar or –in certain cases- better correlation with the mechanical parameters and temperature. This demonstrates the sensitivity of AE to the fracture incidents which eventually lead to the fracture of the material and it is encouraging for potential use in-situ, where it could provide indices with additional characterization capacity concerning the mechanical performance of concrete after fire.

6.2 Introduction

Concrete structures under service conditions are normally exposed to temperatures below 100^{o}C. Only in the event of accidental situations (fire) the temperature of the material may increase to several hundred ^{o}C. Even in these cases, after a fire has finished, the concrete structure will often remain standing which gives the opportunity to repair the structure if it is economically feasible, rather than demolishing and reconstructing [1]. However, for these cases it is essential to know the mechanical and physical behavior of the material after having sustained high temperatures in order to allow assessment of the residual strength and performance capacity in general [2]. Concrete generally exhibits good resistance to thermal loads. This is due to its low thermal conductivity which also provides a barrier for thermal protection of the reinforcing steel [3]. However, elevation to high temperatures of the order of several hundred ^{o}C or even 1000^{o}C can well compromise its mechanical performance. This is due to a combination of reasons including chemical decomposition of structural substances and thermal micro-cracking due to the different expansion coefficients of its constituents. Finally there is spalling, which results from increase of the pore pressure and from temperature gradients due to which, the hot surface layers tend to separate and spall from the cooler interior. This exposes deeper layers of concrete to the elevated temperatures and accelerates deterioration. Once the reinforcing bars are also exposed, they conduct heat and accelerate the action of high temperature [4-7]. Therefore, reliable assessment of the mechanical properties of concrete after exposure to high temperatures is a crucial issue in order to decide if the structure can be repaired and how [1,8].

Elastic waves have been used in order to provide characterization of the structural condition of concrete materials and structures. Ultrasonic pulse velocity (UPV) depends on the elastic properties and void content of concrete supplying valuable correlations to strength and evaluations of the interior condition [9,10]. Furthermore, acoustic emission (AE) detects the elastic waves due to cracking events occurring within the volume of the material allowing a reliable monitoring of its fracture process. AE indices are used to correlate to strength, damage content, while they also help to characterize the dominant damage mode [11-13].

In the field of thermally damaged cementitious materials although a unique relationship between the maximum sustained temperature and strength cannot be found, several studies have shown that the remaining strength (compressive, flexural or tensile) reduces from 50% to 80% for temperatures at 800^{o}C or higher [14-18], while the strength of the concrete-steel bond reduced dramatically at 450 ^{o}C [19]. Elastic modulus decreases in a similar way [4,8] while toughness or the capacity of the material to absorb energy during fracture is also decreased by a factor of two or more [8]. Along with the drop of strength the material after thermal damage exhibits higher ductility [4,8,20]. Ultrasonic pulse velocity has been used to evaluate the thickness of the fire-damaged concrete layer in-situ [21] and estimate the remaining strength [22], since it is quite sensitive to the drop of material stiffness induced by the elevated temperatures [3,5,23]. Wave attenuation measured in the first MHz range was shown to significantly increase as a function of the sustained temperature [24-26] while dispersion curves at the same frequency range exhibit a large shift to lower velocity levels for temperatures below or slightly above 500^{o}C [25,26]. Nonlinear wave techniques have also been used to monitor progressive thermal damage [25,27].

The use of AE is certainly more limited concerning thermally damaged material. AE has been used to monitor the cracking behavior of various materials due to exposure in open flames [28]. Specifically for concrete it was shown that thermal micro-cracking causing recordable AE is not induced below the temperature of 180^{o}C [4]. In another study, strong number of AE events were recorded as the temperature rose from 500^{o}C to 750^{o}C [29], while the AE results were used for the development of models for prediction of the spalling behavior. Additionally, when thermally loaded concrete was mechanically tested, it emitted AE energy in a slower pace in agreement with the more ductile texture that allows considerable increase of maximum strain [4]. It was also shown that the width of the fracture process zone, measured by AE location increases for thermally damaged material [20]. Finally, AE of concrete specimens with metal bars under constant axial load on the rebar with increasing temperature up to 600^{o}C has indicated long ago that the technique is sensitive to the deterioration of bonding quality after fire [1].

In this study concrete specimens were subjected to direct fire action, instead of elevated temperatures in an oven that is usually the case. This kind of experiment is not easily conducted due to the specialized necessary equipment, chamber, as well as safety precautions. In our case the facility of a brick manufacturing industry was used. After being exposed to as high temperatures as 850^{o}C, the concrete specimens were ultrasonically interrogated and mechanically tested in bending and compression with simultaneous AE monitoring. Important conclusions are drawn with respect to the mechanical behavior of concrete after fire. The combined results of the monitoring methods and the mechanical properties obtained show that incorporation of parameters from both AE and UPV techniques may lead to more precise characterization of remaining strength after severe thermal damage.

6.3 Experimental Details

6.3.1. Materials and mechanical loading

One concrete mixture was produced consisting of sixteen specimens. Half of the specimens were prismatic beams of size 100x100x400 mm for conducting four-point bending test and half were cubes of size 150x150x150 mm for compression testing. The aggregates consisted of 56% crushed sand, 13.87% fine gravel and 30.13% coarse gravel with maximum aggregate size 31.5 mm, while the water/cement ratio was 0.70 by mass. The density and the water absorption of the crushed sand were 2601 kg/m3 and 0.98 %, of fine gravel 2621 kg/m3 and 0.75 %, of coarse gravel 2681 kg/m3 and 0.61 % respectively. The cement type was CEMII/A-M(P-LL). The exact mix proportions were as follows: cement (type II 42.5N) 80 kg/m3, cement (type II 32.5N) 200 kg/m3, water 195 kg/m3, crushed sand 1050 kg/m3, fine gravel 260 kg/m3, coarse gravel 565 kg/m3 , retarder - plasticizer (CHEM I) 1.54 kg/m3, retarder - plasticizer (CHEM II) 1.96 kg/m3 . The actual bulk density of concrete was 2359 kg/m3) while the ambient temperature was 25^{0}C. The workability as measured by the slump test was 11 cm. The specimens were cured in water saturated with calcium hydroxide at 23 $\pm 2^{0}$C. The average compressive strength of three days was fc(3)= 18.0 MPa, of seven days fc(7)= 24.7 MPa and of twenty eight days was fc(28)= 33.8 MPa (with a standard deviation of 3.0 MPa).

Thermal damage needs specialized equipment and is not always an easy task to accomplish. In this case, the fire loading was conducted in a specialized facility. Six of the bending and six of the compression specimens were exposed to fire action. The fire damage process took place in a furnace of a brick industry and the specimens were exposed in direct fire, from every side, except from the side that they laid down. Half of the specimens were exposed to fire with maximum temperature of 850^{o}C and the other of 700^{o}C. The fire developed gradually to maximum temperature for 12 hrs and the temperature was held constant for 8 hours. After that, the temperature gradually reduced for about 12 hours. Photographs of typical bending and compression specimens after fire exposure are seen in Figure 6. 1 where spalling is obvious.

Figure 6. 1 *Typical specimens after fire exposure.*

Six of the prismatic beam specimens (two healthy, two exposed at 700^{o}C and two at 850^{o}C) were subjected to four-point bending (Figure 6. 2 a), with a span length of 300 mm.

(a) (b)

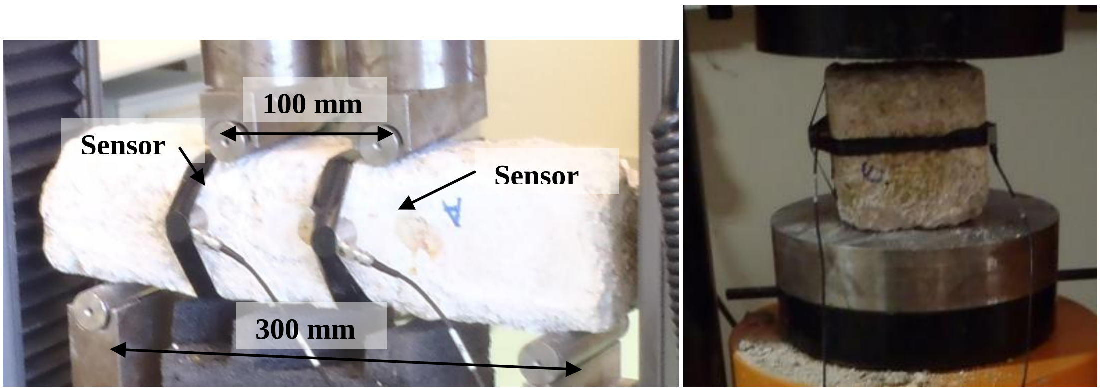

Figure 6. 2 *(a) Prismatic beam specimen after fire damage subjected to four-point bending with AE monitoring, (b) Cubic specimen after fire damage subjected to compressive test.*

The tests were conducted on a servo-hydraulic Instron Model 5967 (30kN capacity). The loading and support system was designed in accordance with BS EN 12390-5:2000 and the third point loading applied to the specimen without eccentricity and torque. The displacement rate was 0.12 mm/min.

A number of seven specimens were subjected to compression, see Figure 6. 2b. The load rate was 0.3375 MPa/s

6.3.2. Monitoring techniques

AE was monitored by two resonant piezoelectric sensors, namely the R15 (Physical Acoustics Corp., PAC) with resonance nominally at 150 kHz, see Figure 6. 2a. The signals were pre-amplified by 40 dB and were digitized by a sampling rate of 3 MHz in a PCI-8 board of PAC. It is mentioned that for the healthy specimens a number of four small broadband Pico sensors were additionally applied, but this was not possible for the rough texture of the fire-damaged. Therefore, the analysis is limited in this case to the results of the sensitive R15 sensors. Grease was applied between the sensors and the specimen's surface to enhance acoustic coupling, while they were secured by tape during the experiment, see Figures 6. 2 (a) and (b). All signals with amplitude higher than 40 dB were recorded, while for the analysis, the signals with energy “zero” were disregarded. Some of the most important parameters of a received waveform are the amplitude (A), which is related to the intensity of the cracking event and energy (ENE) which is the area under the rectified signal envelope and is again connected to the energy released by the crack [30]. These, along with the accumulated hit activity are analyzed in the next sections offering strong correlations to the mechanical parameters.

Pulse velocity was measured with a commercial device (PUNDIT), see Figures 6. 3 (a) and (b) for testing of a prismatic and a cubic fire damaged specimen respectively.

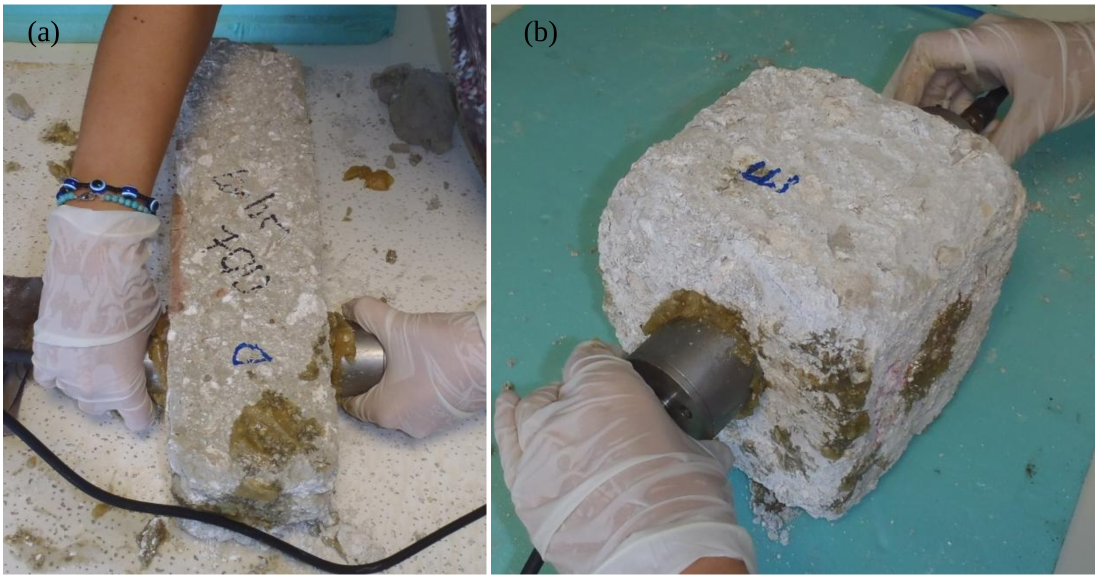

Figure 6. 3 *UPV measurements in (a) bending specimen, (b) compression specimen after fire damage.*

The frequency of excitation was 54 kHz while the transit time through the known thickness of the material was recorded. Three measurements were taken at different vertical wave paths for bending specimens and two for compression ones. The results were averaged for each specimen.

6.4 Results

The basic properties of the specimens are shown in Table 3.2. 1 and Table 3.2. 2 for bending and compression specimens accordingly.

Table 6. 1 *Basic properties for concrete specimens in bending*

Code	**Temperature (^oC)**	**Mass reduction (%)**	**Max. load (kN)**	**Toughness* (J)**	**UPV (m/s)**
A	850	37	1.265	0.985	1839
D	850	23	1.319	0.778	1778
E	700	20	2.128	0.817	1959
F	700	21	2.238	0.829	1988
G	20	0	11.855	2.351	4619
H	20	0	8.581	1.601	4565

*As measured by the load-extension curve

Table 6. 2 *Basic properties for concrete specimens in compression*

Code	**Temperature (^oC)**	**Mass reduction (%)**	**Strength (MPa)**	**UPV (m/s)**
A	850	24	1.69	1942
B	850	25	1.47	1086
C	700	12	1.85	1403
D	700	19	4.96	1455
E	700	21	2.85	1938
G	20	0	36.55	4490
H	20	0	34.19	4179

A great reduction in maximum load and toughness, accompanied by severe mass reduction due to spalling is noted for the bending specimens. The situation is quite similar for the compression specimens. Additionally, the exposure to 850^oC results in lower mechanical properties than 700 ^oC. These trends are accompanied by the corresponding strong decrease of UPV that is of the order of 60-70% compared to the intact specimens. The results are analytically presented and discussed separately for bending and compression below.

6.4.1. Bending

Figure 6. 4 shows indicative curves of load vs. extension for typical specimens.

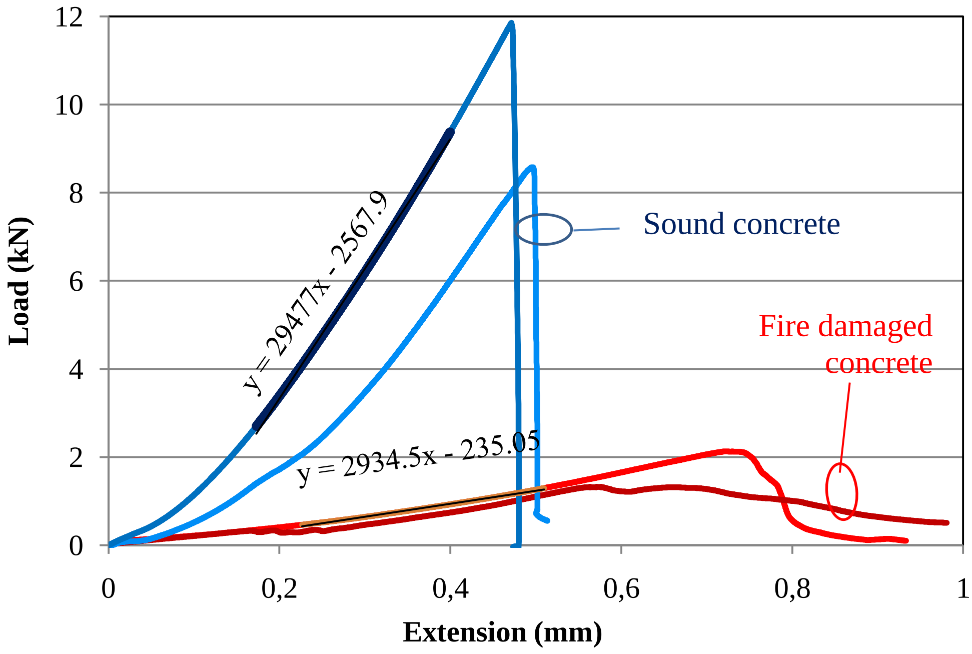

Figure 6. 4 *Load vs. extension curves for concrete beams. The fire damaged specimens were subjected to 850oC.*

Apart from the obvious decrease of ultimate load bearing capacity of the fire-damaged specimens (decrease of approximately 80% compared to the intact beams), a certain increase in ductility is noticed in terms of extension at peak load. While the intact beams are fractured at a load cell extension of 0.5 mm, the extension at load drop for the fire-damaged reaches even 0.8 mm. The load drop is much smoother than the one of sound beams. Apparently the stiffness is also diminished as seen by the different slopes of the load – extension curves. The slope of the fire-damaged is approximately one tenth of the sound specimens. It is mentioned that since the extension is measured by the displacement of the load cell and not the mid-span deflection of the specimen, projections to actual Young's modulus are not conducted. The more ductile nature of the material after fire damage can also be seen in Figure 6. 5, where the specimen has not split in two parts even after the termination of the experiment.

Figure 6. 5 *Bending specimen after the four-point bending test. A large crack is visible (see arrow).*

The AE activity in terms of recorded hits for indicative specimens is shown in Figure 6. 6 along with the load histories. Figure6. 6 (a) and (b) concern fire damaged specimens.

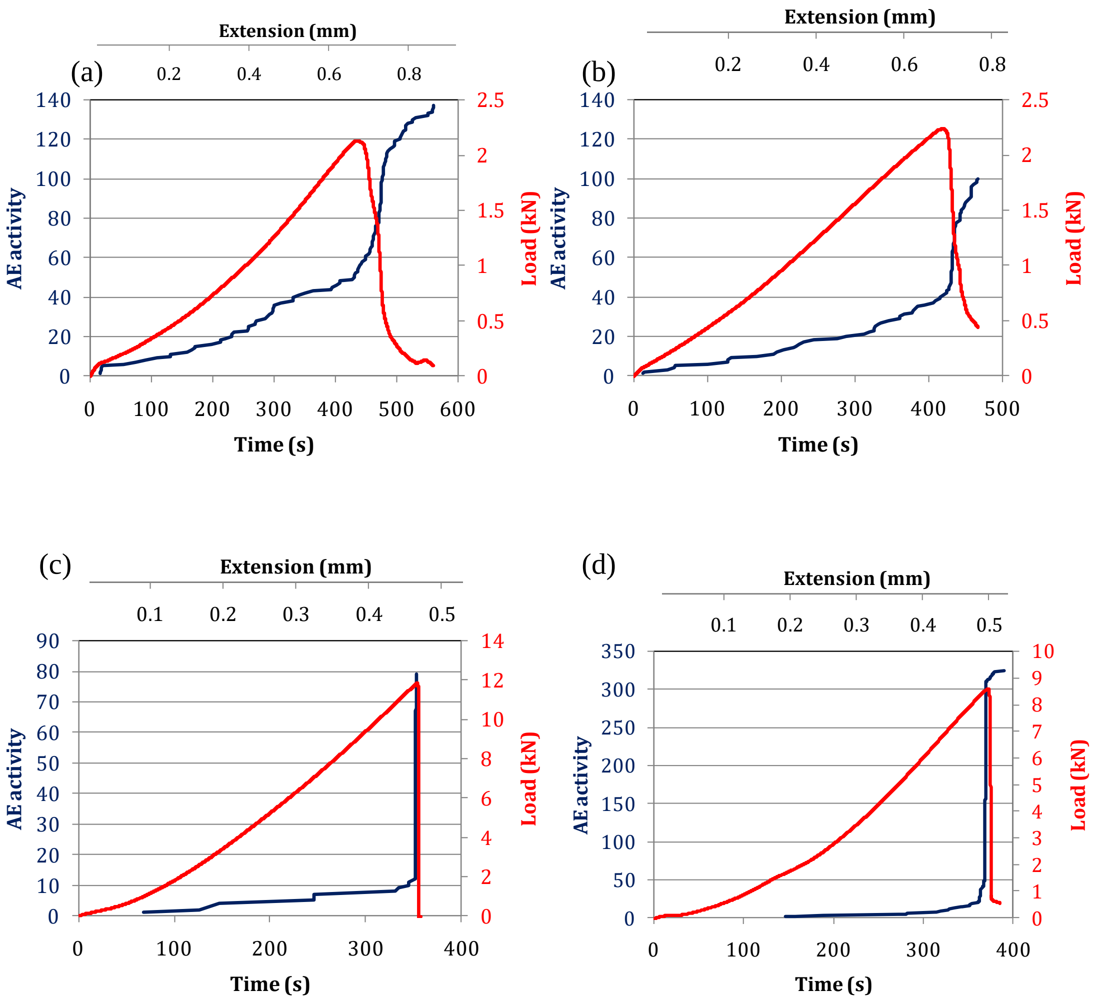

Figure 6. 6 *AE activity and bending load history for specimens sustained fire damage at 850 oC (a) and (b) and intact specimens (c) and (d).*

It is seen that AE activity starts quite early, while the rate of incoming signals increases at the point of load drop. On the other hand, for sound specimens, the load drop at the moment of main failure is much sharper (see Figures 6. 6 (c) and (d)), since the specimen fails catastrophically in two parts. The AE curve of these specimens reveals negligible activity at early stages of loading while continuous emissions are recorded after 70% of the maximum load. At the moment of load drop there is a vertical slope of the accumulated AE activity curve which shows that almost all the energy is emitted at that time. Focusing again on the concrete directly exposed to fire action, the specimens did not split in two after the load drop, while the continuation of AE recording even after the maximum load, confirms the more plastic nature of the material after fire [3,20]. Concerning the moment of main failure, the maximum rate of acquisitions which was noticed at the load drop moment was approximately 3 hits/s for fire damaged, while it was ten times higher for intact specimens.

Concerning concentrated information from all the bending specimens, interesting correlations are noted between mechanical properties and parameters obtained by NDT techniques (AE and UPV). Figure 6. 7 shows the relation between the bending load and pulse velocity.

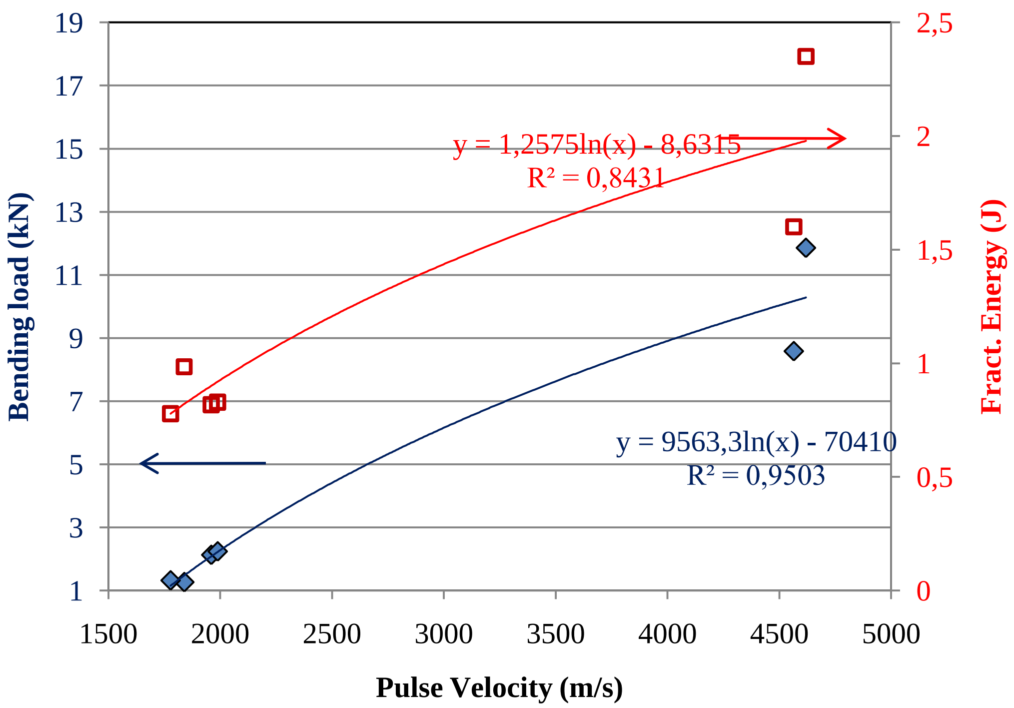

Figure 6. 7 *Bending load and fracture energy vs. UPV of concrete specimens.*

The two sound specimens which did not sustain any fire load exhibited the two highest values of bending load, while exhibiting the highest UPVs (above 4500 m/s). On the other hand, fire damaged specimens revealed a decrease of the order of 90% in strength escorted by a decrease of around 60% of UPV. The situation is similar for the absorbed energy as measured by the area under the load-extension curve. Though it cannot be considered the same as fracture toughness (which would require accurate deflection and not load cell extension measurement) it is quite indicative of the work consumed for the failure of the specimens. Again the specimens that sustained fire damage exhibited a significant drop of fracture energy, in this case of the order of 60%). The larger drop of strength as a percentage relatively to absorbed energy has been also reported in [8] but in compression mode. The fitting lines and correlation coefficients are indicative and are supplied for completeness while for robust and mathematically significant correlations more specimens would be necessary.

Looking into the AE family of descriptors quite strong (or even stronger) correlations emerge. Figure 6. 8 shows the corresponding graphs of bending load and fracture energy vs. the cumulative energy of AE.

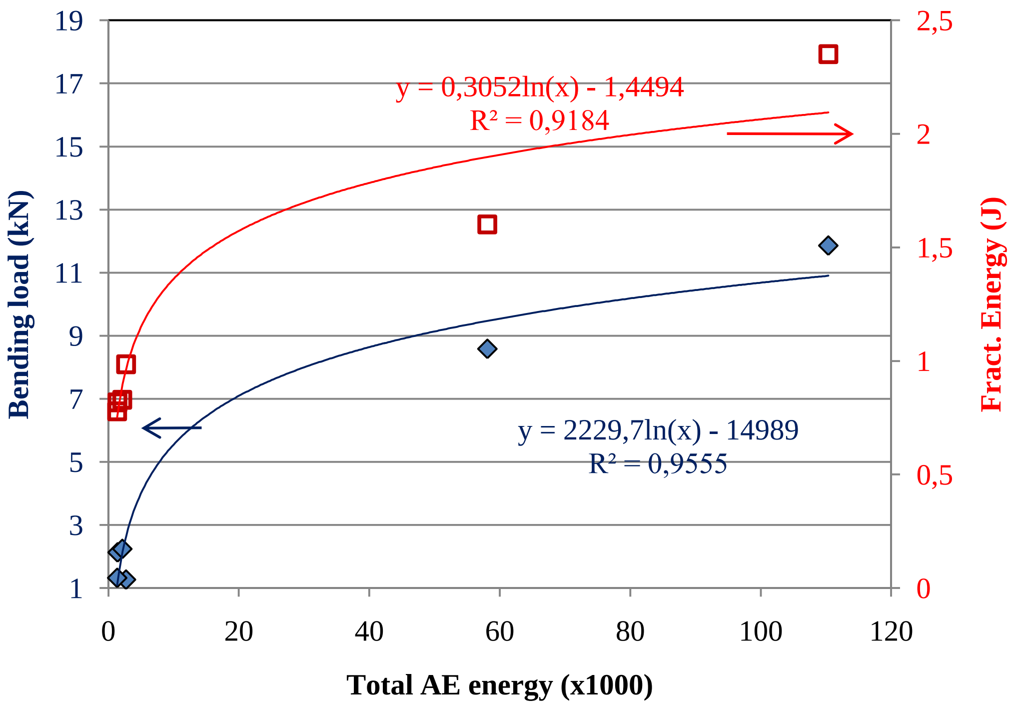

Figure 6. 8 *Bending load and fracture energy vs. total AE energy of concrete specimens.*

The logarithmic fitting exhibits again high correlation coefficient. AE energy for the fire damaged is limited to a few percent of the AE recorded by the sound specimens, which relates well with the drop of mechanical properties. It is also indicative that the AE energy seems sensitive not only to the existence or not of the fire damage but also to the fluctuations of the mechanical properties within each class. Specifically, concerning the intact specimens, the one with the highest bending load (11.9 kN) exhibited approximately double AE energy compared to the second highest (8.6 kN). Fire-damaged specimens emitted AE energy one to two orders of magnitude lower. The correlation of AE energy to the absorbed fracture energy is almost similarly good, which is reasonable bearing into mind that AE is a part of the fracture energy. This, along with the similarly strong or even stronger correlation coefficients of AE energy to the mechanical data than UPV shows that AE descriptors can also be used to enhance the estimations of strength that is being attempted with the UPV so far, as will be discussed in a next section.

The drop of mechanical properties seems to follow the maximum temperature increase, as shown in Figure 6. 9.

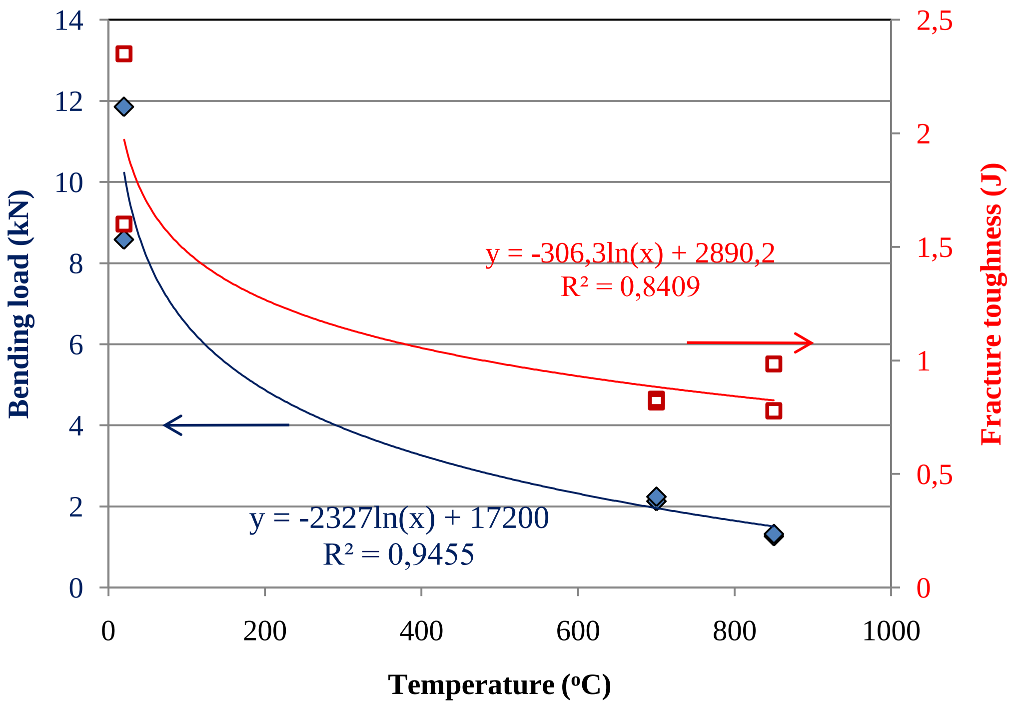

Figure 6. 9 *Bending load and fracture energy vs. maximum sustained temperature of bending concrete specimens.*

Especially the load exhibited quite consistent values being reduced by 79% and 88% for temperatures of 700 ^{o}C and 850 ^{o}C respectively. The fracture energy on the other hand, showed some fluctuations for the 850^{o}C, but still exhibited a quite consistent curve to temperature. The corresponding dependence of NDT parameters on the temperature are shown in Figure 6. 10.

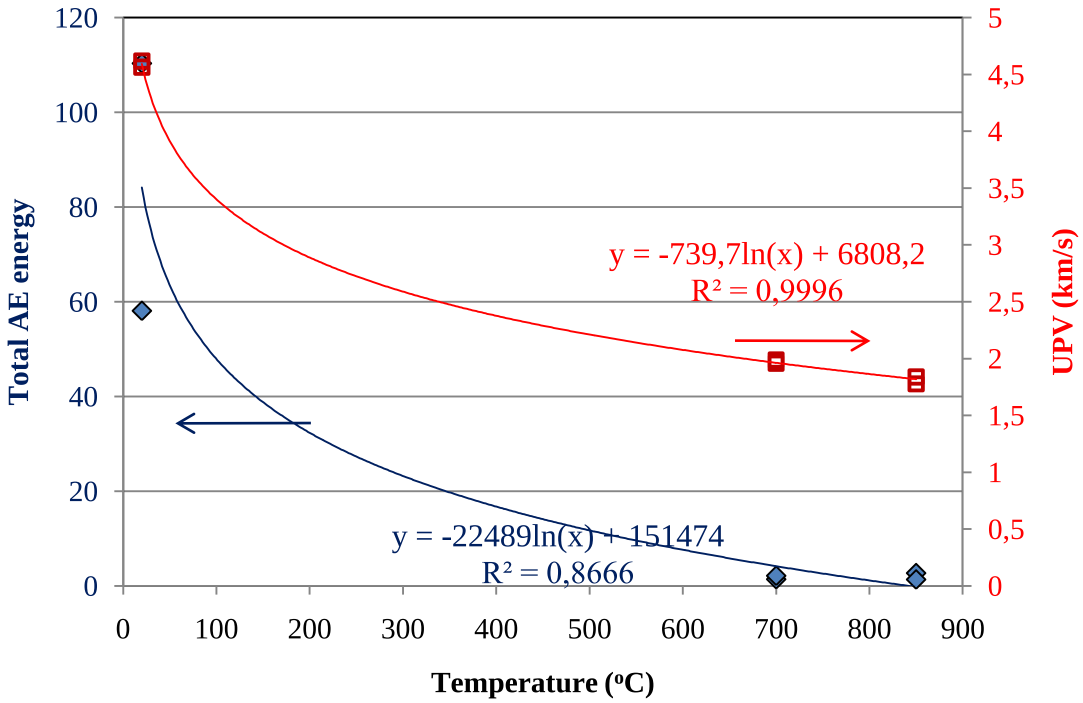

Figure 6. 10 *Total AE energy and UPV vs. maximum sustained temperature of bending concrete specimens.*

While the total AE energy emitted by the specimens during bending shows a good correlation of R2=0.87, the correlation of UPV is almost absolute.

6.4.2. Compression

Results exhibit similar trends for the compression loading. Correlations concerning the compressive load and NDT results (UPV and total AE energy) can be seen in Figure 6. 11.

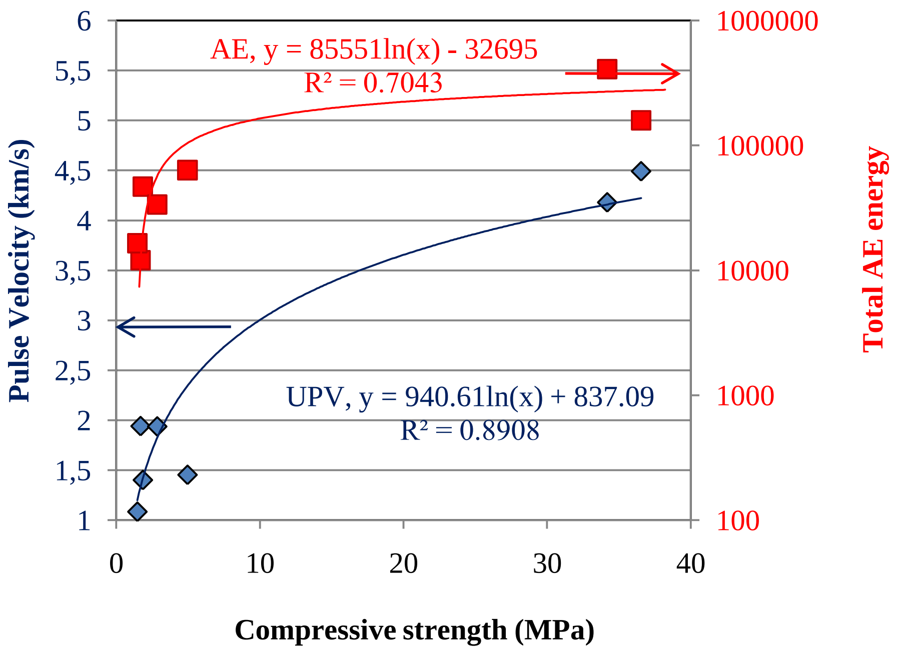

Figure 6. 11 *UPV and total AE energy vs. compressive strength.*

The fire loading induced a huge drop of more than 90% on strength escorted by a drop of 60% in pulse velocity and approximately 90% in recorded AE energy.

In the specific case, other parameters of AE were more representative of the strength, as seen in Figure 6. 12.

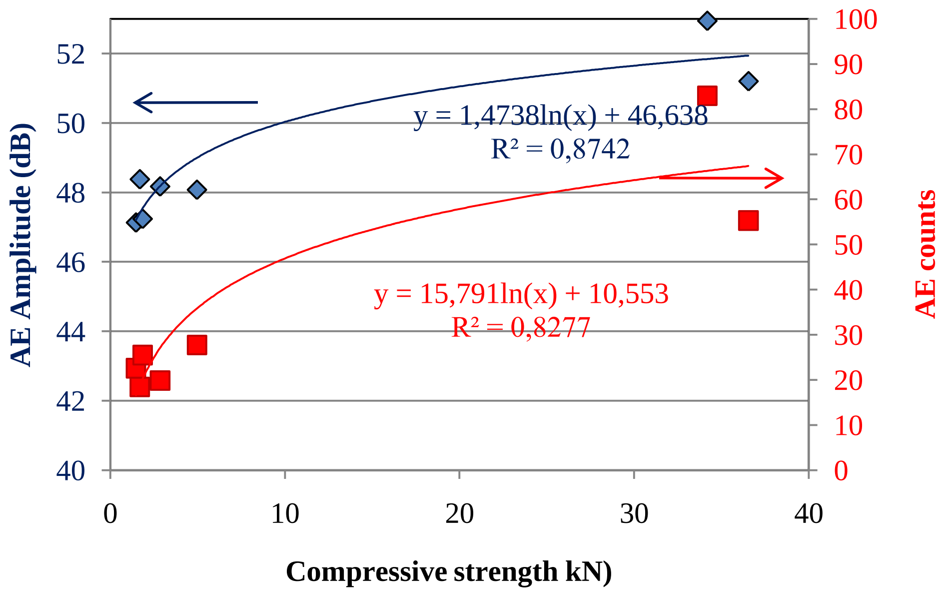

Figure 6. 12 *AE amplitude and AE counts vs. compressive strength.*

Specifically, the average amplitude of AE emissions seems to be well correlated to the compressive strength. In fire damaged concrete the recorded signals are approximately 4 dB lower in average than the ones in sound material, which is connected to the intensity of the original crack propagation incidents. This is reasonably related to the texture of the material which changes from brittle to plastic with the fire damage, as has already been seen by the load-extension curves. The amplitude of the acquired signals certainly depends on the crack tip displacement during any crack opening moment. Therefore, for a brittle material it is reasonable that the amount of energy recorded at each step is higher than a ductile one. Of course it should always be kept in mind that the AE signals are elastic waves which are prone to damping. Therefore, a part of the amplitude reduction between sound and fire damaged should be related to increasing attenuation after fire, as has been seen in related studies [24-26]. However, still this is an effect of deterioration induced by the fire damage which indirectly affects the AE measurements. Correlations with the absorbed energy were not possible since deflection was not monitored in the compression test.

Quite strong is the correlation of the AE threshold crossings ("counts" in AE terminology) and the final strength. Material with normal strength (above 30 MPa) exhibited more than double number of counts compared to the fire damaged. Counts do not have a direct physical connection to material properties like pulse velocity does; however, it is one of the first parameters to provide empirical correlations with strength [31]. Large number of counts show longer recorded waveforms and is also related to less attenuation of the material.

Figure6. 13, shows the relation of compressive strength with the sustained temperature.

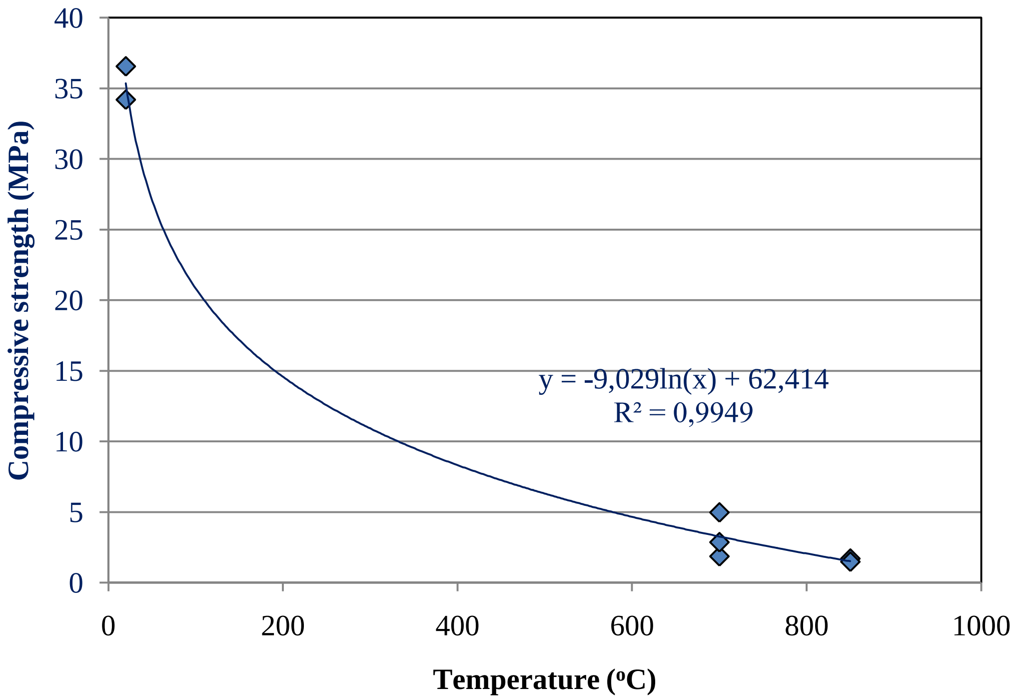

Figure 6. 13 *Compressive strength vs. maximum sustained temperature.*

The relation seems quite strong while a drop in average strength can be seen even for the specimens burnt at 850 ^{o}C relatively to the 700 ^{o}C. The compressive strength drops by 95% as a result of exposure to 850 ^{o}C of direct flames, while for the 700 ^{o}C the percentage of reduction is between 85% and 94%.

Similarly for bending, correlations with temperature are noted for monitoring parameters in compression specimens. Figure6. 14, shows the correlation of AE amplitude and UPV with the maximum fire temperature.

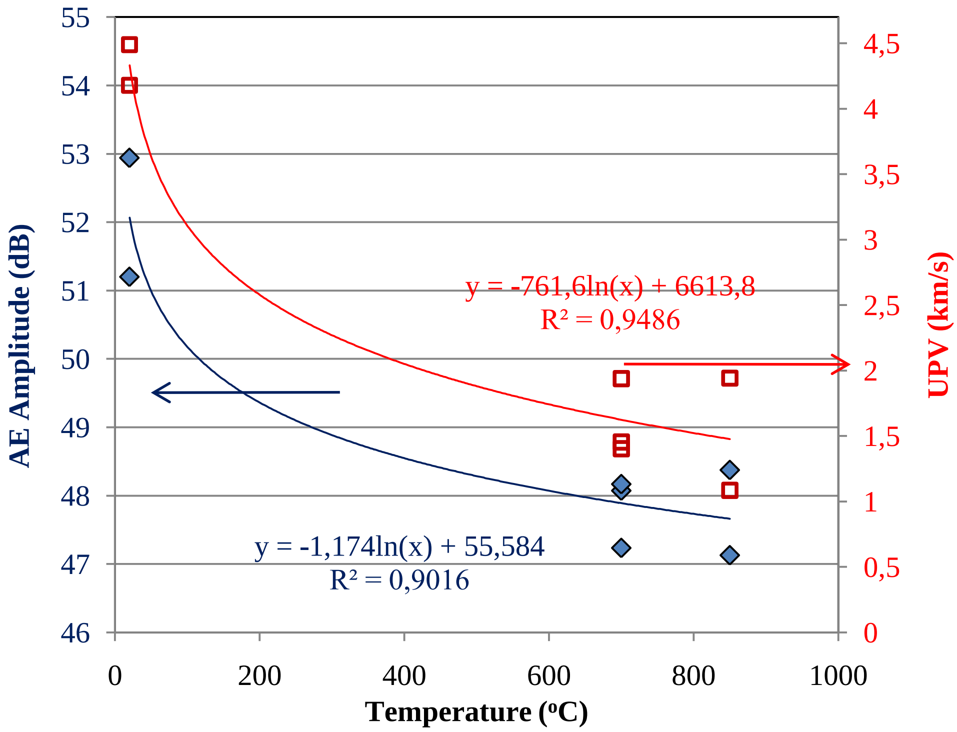

Figure 6. 14 *Total AE energy and UPV vs. maximum sustained temperature of bending concrete specimens.*

Both parameters exhibit a quite strong correlation with the sustained temperature. Although it is certain that the increase of temperature has a deterioration effect on the material's quality, the curve would benefit by addition on intermediate temperatures between 20^{o}C and 700^{o}C.

6.5 Discussion-Conclusion

The assessment of concrete materials and structures after fire is a very important safety issue. In that respect, any assessment parameter that can be drawn may act complementarily to the visual inspection which always supplies the initial and crucial information.

To create a statistically reliable database, exposure to different temperatures and for different durations would be desirable. Although a new series of experiments is already prepared for this purpose, the focus herein is the investigation of novel monitoring parameters as to their characterization power over fire-damaged concrete quality that could act complementarily to the UPV, which is a traditional and established parameter for strength estimation. UPV can be directly connected to elasticity and empirically to strength. The well-known correlations seem to hold for the case of this study as well. Use of ultrasound can easily discern between sound and fire-damaged concrete, while it is proven sensitive to changes in the sustained temperature. However, one aspect that has not been sufficiently studied, is the correlation between the mechanical properties of fire-deteriorated concrete and the AE behavior. In the framework of this study, quite strong correlations emerge. Parameters related to the emitted energy during the fracturing events, as well as waveform descriptors, like the number of threshold crossings show similarly good correlation with the mechanical properties related to strength (in bending and compression) and absorbed energy (in bending). Practically, these parameters can be obtained in conjunction with some slightly destructive tests that are always necessary for in-situ assessment. As an example AE can be measured while drilling for assessment of the thickness of the deteriorated layer [32,33]. AE will change considerably as the drill penetrates deeper into stiffer material with less thermal damage. Alternatively AE can work in conjunction with other type of slightly destructive test like the pull out [34]. The energy released during fracture incidents will vary significantly as shown in the present study depending on the existence or not of fire damage. Based on the presented correlations, inclusion of AE in the armory of NDT for concrete assessment, can provide additional parameters, the characterization capacity of which concerning the remaining strength after fire damage is similar or even better to UPV.

6.6 References

1. R. Royles, P. D. Morley, Acoustic emission and bond degradation in reinforced concrete due to elevated temperatures, Materials and Structures, 17(3) (1984) 185-191.
2. Recommendation of RILEM TC 200-HTC: Mechanical concrete properties at high temperatures-modelling and applications, Materials and Structures, 40 (9) (2007), 841-853.
3. J. P. C. Rodrigues, L. Laím, A. M. Correia, Behaviour of fiber reinforced concrete columns in fire, Composite Structures, 92 (2010) 1263–1268.
4. M.J. Heap, Y. Lavallée, A. Laumann, K. U. Hess, P.G. Meredith, D.B. Dingwell, S. Huismann, F. Weise, The influence of thermal-stressing (up to 1000 oC) on the physical, mechanical, and chemical properties of siliceous-aggregate, high-strength concrete, Construction and Building Materials, 42 (2013) 248–265.
5. P. Kalifa, G. Chéné, C. Gallé. High-temperature behaviour of HPC with polypropylene fibres from spalling to microstructure. Cem Concr Res, 31 (2001) 1487–99.
6. M. Colombo, R. Felicetti, New NDT techniques for the assessment of fire-damaged concrete structures, Fire Safety Journal, 42 (2007) 461–472.
7. A.M. Neville, Properties of concrete, Longman, Essex, England,1995.
8. C.S. Poon, Z.H. Shui, L. Lam, Compressive behavior of fiber reinforced high-performance concrete subjected to elevated temperatures, Cement and Concrete Research, 34 (2004) 2215–2222.
9. D.M. McCann, M.C. Forde. Review of NDT methods in the assessment of concrete and masonry structures. NDT&E Int., 34(2) (2001) 71–84.
10. T.R. Naik, V.M. Malhotra, J.S. Popovics, The ultrasonic pulse velocity method, In: V.M. Malhotra, N.J. Carino (eds), CRC handbook of nondestructive testing of concrete. CRC Press, Boca Raton, 2004.
11. C.U. Grosse, M. Ohtsu, Acoustic emission testing, Springer, Heidelberg, 2008.
12. M. Ohtsu, Recommendation of RILEM TC 212-ACD: acoustic emission and related NDE techniques for crack detection and damage evaluation in concrete: test method for classification of active cracks in concrete structures by acoustic emission. Mater Struct , 43(9) (2010) 1187–1189.

13. D. G. Aggelis, Classification of cracking mode in concrete by acoustic emission parameters, Mechanics Research Communications, 38 (2011) 153–157.
14. C.S. Poon, S. Azhar, M. Anson, Y.L. Wong, Strength and durability recovery of fire-damaged concrete after post-fire-curing, Cement and Concrete Research, 31 (2001) 1307–1318.
15. M. Husem, The effects of high temperature on compressive and flexural strengths of ordinary and high-performance concrete, Fire Safety Journal, 41 (2006) 155–163.
16. J. Xiao, H. Falkner, On residual strength of high-performance concrete with and without polypropylene fibres at elevated temperatures, Fire Safety Journal. 41 (2006) 115–121
17. J. R. Correia, A. M. Marques, C. M. C. Pereira,J. de Brito, Fire reaction properties of concrete made with recycled rubber aggregate, Fire and Materials 36(2) (2012) 139–152.
18. L.T. Phan, N.J. Carino, Effects of test conditions and mixture proportions on behavior of high-strength concrete exposed to high temperatures. ACI Mater, 99 (2002) 54–66.
19. P. D. Morley and R. Royles, The Influence of High Temperature on the Bond in Reinforced Concrete, Fire Safety Journal, 2 (1979/80) 243 – 255.
20. S. Cattaneo, L. Biolzi, Assessment of Thermal Damage in Hybrid Fiber-Reinforced Concrete, Journal of Materials in Civil Engineering, 22(9) (2010) 836-845.
21. O. Abraham, X. De´robert Non-destructive testing of fired tunnel walls: the Mont-Blanc Tunnel case study. NDT&E International, 36(2003) 411–8.
22. E. Tatsis, N. Zoidis, C. Vlachopoulos, T. Matikas, A. Gotzamanis, Visual inspection and evaluation using NDT testing methods of industrial building after fire, Proceedings of the 5th Conference on Emerging Technologies in NDT , 2012, pp. 131-135.
23. S. Masse, G. Vetter, P. Boch, Non-Destructive Ultrasonic Evaluation of Thermal Damage in Cementitious Materials, Key Engineering Materials, Vol. 206 – 213 (2002) 1907-1912.
24. J. Chaix, V. Garnier, G. Corneloup, Concrete damage evolution analysis by backscattered ultrasonic waves, NDT & E International, 36(7) (2003) 461-469.

25. H.J. Yim, J. H. Kim, S.J. Park, H.G. Kwak, Characterization of thermally damaged concrete using a nonlinear ultrasonic method, Cement and Concrete Research, 42(11) (2012) 1438-1446.
26. J. F. Chaix, V. Garnier, G. Corneloup, Ultrasonic wave propagation in heterogeneous solid media: Theoretical analysis and experimental validation, Ultrasonics, 44 (2006) 200–210.
27. C. Payan, V. Garnier, J. Moysan, P.A. Johnson, Applying nonlinear resonant ultrasound spectroscopy to improving thermal damage assessment in concrete Journal of the Acoustical Society of America, 121 (4) (2007) 125-130.
28. W. Grosshandler, M. Jackson, Acoustic Emission of Structural Materials Exposed to Open Flames, Fire Safety Journal 22 (1994) 209-228.
29. C. U. Grosse, J. Ožbolt, R. Richter, G. Periškić, Acoustic emission analysis and thermo-hygromechanical model for concrete exposed to fire, J. Acoustic Emission, 28 (2010) 188-203
30. M. Ohtsu, Recommendations of RILEM Technical Committee 212- ACD: acoustic emission and related NDE techniques for crack detection and damage evaluation in concrete: 3. Test method for classification of active cracks in concrete structures by acoustic emission. Mater Struct, 43(9) (2010) 1187-1189.
31. Vary, Acousto-ultrasonics. An update, ASTM Special Technical Publication (1077) , 1991, pp. 95-104.
32. R. Felicetti, The drilling resistance test for the assessment of fire damaged concrete, Cement & Concrete Composites, 28 (2006) 321–329.
33. K. Iwaki, A. Hirama, K. Mitani, S. Kaise, K. Nakagawa, A quality control method for shotcrete strength by pneumatic pin penetration test, NDT&E International, 34 (2001) 395-403.
34. C. G. Petersen, LOK-TEST and CAPO-TEST pullout testing, twenty years experience, Non-Destructive Testing in Civil Engineering Conference in Liverpool, U.K., April 8-11th, 1997, The British Institute of Non-Destructive Testing (http://www.germann.org/TestSystems/LOK-TEST/lok_and_capo_test_correlation.pdf,accessed 1/2013)

Chapter 7. Effect of real damage (fire) in Reinforced concrete

7.1. Purpose

The mechanical behavior of Reinforced concrete after extensive thermal damage is studied in this experiment. Bending and compression specimens of Reinforced concrete were produced and exposed to direct fire action at temperatures of 700 ^{o}C and 850 ^{o}C, in order to determine the loss of strength and stiffness in comparison to intact specimens. The mechanical tests could not been executed because of the extensive damage of the fired damaged specimens and the change of the shape due to spalling. Nondestructive monitoring techniques were not been able to applied too in the form of ultrasonics (ultrasonic pulse velocity, UPV) and acoustic emission (AE) because of the extensive damage of the fired damaged specimens due to spalling.

7.2. Experimental Details

7.2.1. Materials and mechanical loading

The same concrete mixture with the plain fired damaged concrete specimens witch was studied in the previews chapter was produced consisting of sixteen specimens. The specimens for bending were reinforced by two steel rebar reinforcement of 14mm diameter each. The specimens for compression were reinforced by four steel rebar reinforcement of 14mm diameter each. Half of the specimens were prismatic beams of size 100x100x400 mm for conducting four-point bending test and half were cubes of size 150x150x150 mm for compression testing. The aggregates consisted of 56% crushed sand, 13.87% fine gravel and 30.13% coarse gravel with maximum aggregate size 31.5 mm, while the water/cement ratio was 0.70 by mass. The density and the water absorption of the crushed sand were 2601 kg/m3 and 0.98 %, of fine gravel

2621 kg/m3 and 0.75 %, of coarse gravel 2681 kg/m3 and 0.61 % respectively. The cement type was CEMII/A-M(P-LL). The exact mix proportions were as follows: cement (type II 42.5N) 80 kg/m3, cement (type II 32.5N) 200 kg/m3, water 195 kg/m3, crushed sand 1050 kg/m3, fine gravel 260 kg/m3, coarse gravel 565 kg/m3 , retarder - plasticizer (CHEM I) 1.54 kg/m3, retarder - plasticizer (CHEM II) 1.96 kg/m3 . The actual bulk density of concrete was 2359 kg/m3) while the ambient temperature was 25^0C. The workability as measured by the slump test was 11 cm. The specimens were cured in water saturated with calcium hydroxide at 23 $\pm 2^0$C. The average compressive strength of three days was fc(3)= 18.0 MPa, of seven days fc(7)= 24.7 MPa and of twenty eight days was fc(28)= 33.8 MPa (with a standard deviation of 3.0 MPa).

Thermal damage needs specialized equipment and is not always an easy task to accomplish. In this case, the fire loading was conducted in the same specialized facility like the plain concrete specimens studied in the previews chapter. Six of the reinforced concrete bending and six of the reinforced concrete compression specimens were exposed to fire action. The fire damage process took place in a furnace of a brick industry and the specimens were exposed in direct fire, from every side, except from the side that they laid down. Half of the specimens were exposed to fire with maximum temperature of 850^oC and the other of 700^oC. The fire developed gradually to maximum temperature for 12 hrs and the temperature was held constant for 8 hours. After that, the temperature gradually reduced for about 12 hours. Photographs of typical reinforced concrete bending and reinforced concrete compression specimens after fire exposure are seen in Figure 7. 1 where the excessive spalling is obvious.

Figure 7. 1 *Damaged reinforced concrete specimens after fire exposure.*

7.3. Discussion-Conclusion

Due to extensive spalling of the fired damaged Reinforced bending and compression specimens both the mechanical tests and the Nondestructive monitoring techniques in the form of ultrasonics (ultrasonic pulse velocity, UPV) and acoustic emission (AE), were not been able to applied because the extensive damage leads to the change of the shape of the fired damaged specimens. The study should be repeated with different lower max temperatures this time so as to investigate the influence of fired damage in steel rebar reinforcement in concrete structures.

Chapter 8. Final conclusions and suggestions for future work

8.1. Final conclusions

This study involved the development of a methodology for evaluating the structural integrity of reinforced concrete elements especially with innovative Non-Destructive Evaluation (NDE) techniques mainly acoustic emission and ultrasonics.

The main aim is to characterize the acoustic signature with the passive monitoring of different fracture process in cementitious and others materials. Ultrasound was also applied on these different materials and damage scenarios.

In Chapter 2 has been studied the propagation of elastic wave pulses within material with microstructure. The investigation includes AE parameters which are used for characterization of the fracturing properties of materials, instead of the classical wave speed and attenuation which are related to mechanical and physical properties. Due to the heterogeneity of concrete, the waveforms are continuously distorted as the wave propagates away from the source. This results in significant shift of the original content when the pulses are recorded by the receiver. Experiments in specimens of mortar show that an additional propagation distance of a few cm affects the calculated values by orders of magnitude. RA increases by three to four times while frequency decreases by about 30%. This strong influence would not allow the use of any laboratory-based criterion in-situ. Simulations were also conducted in order to expand to different materials and higher frequencies. They showed even higher influence of inhomogeneity on the propagating wave

In 3.1 session of Chapter 3 has been studied the fracture process in cementitious materials (mortar) with the use of the acoustic emission technique. Monitoring with broadband AE sensors revealed distinct trends for the different fracture modes. Specifically AE signals from tensile tests exhibit higher amplitude and frequency, while shear exhibit longer duration and lower rising angle, as measured by the RA value. The results show that accurate characterization of modes is possible in laboratory based on simple features recorded by one AE sensor.

In 3.2 session of Chapter 3 has been studied the AE behavior of concrete beams under two different fracture modes. Specifically, the beams were subjected to four-point bending and shear and their activity was monitored by several AE transducers. Despite the large experimental scatter which is certainly inherent to the measurement of AE and fracture processes distinct differences in waveform characteristics were registered. Specifically, in bending fracture mode, which is expressed by tensile stress cracking at the bottom of the beam, exhibited frequency content of emissions nearly 50% higher than shear in average. Additionally, it registered shorter waveform with much shorter rise time.

In 3.3 session of Chapter 3 has been studied the AE behavior of Materials with different microstructure that were tested in bending and shear, namely marble as a typical homogeneous material and cement mortar as a material with microstructure on the level of millimeters. Simple alterations on the experimental set up allowed triggering different fracture modes. The results show firm evidence that actually the different fracture modes (tension and mixed mode) exhibit different AE signatures in terms of frequency and waveform shape parameters like the rise time. Shear fracture exhibits lower frequency and longer waveforms in average.

In 3.4 session of Chapter 3 has been studied the comparison in the AE behavior between another pair of materials with different microstructure. Specifically granite, as a typical homogeneous material, and cement mortar as a material with heterogeneity were examined in bending and shear. Modifications on the experimental set up allowed triggering different types of failure. The results show reliable trends that the different fracture modes (tension and shear or mixed mode) exhibit different AE signatures in terms of frequency and waveform shape. Shear events exhibits lower frequency and longer waveforms. Collecting an adequate population of signals helps to discriminate the active fracture mode. Additionally, the distance between the cracking source and the sensor is important, since an additional propagation of 40 mm influences substantially the values of AE features.

In 3.5 session of Chapter 3 has been studied the fracture behavior of two granite types under different modes. Tests were accompanied by ultrasonic assessment before loading and acoustic emission monitoring during loading. Apart from the fact that ultrasonic pulse velocity is considerably higher for higher strength granite, the basic conclusions are mentioned below:

- The characteristics of AE waveforms are directly sensitive to the loading pattern (bending or shear). When preliminary shear damage is building up during moderate loading, AE signals have much longer RT than the corresponding bending damage. This direct correspondence between the stress field and the AE waveform parameters has not been explored in granite.
- Shear loading produces a more continuous acoustic activity compared to bending. This implies that while bending damage resumes after periods of silent stress build-up, the shear goes on without serious "plateaus".
- Repair by means of epoxy in between the crack faces, restores the load bearing capacity up to 70% for bending and up to 40% for shear loading.
- Repaired specimens exhibit longer initial silent periods in bending. This behavior is attributed to the elasticity of epoxy which allows straining longer before starting to have irreversible damage than granite itself.

In Chapter 4 has been studied the acoustic emission behavior during different fracture tests on concrete. Two tests are used as means to apply different stress conditions on concrete cubes. The basic modes targeted are compression in the standard compressive test and shear during the insert pullout in the form of the LOK test. As FEM analysis indicates, the latter results in a complex state of stress including strong shearing components that overpass normal ones at the area of fracture. The resulting trends show distinct behaviors allowing discrimination of the AE signal populations from the two fracture modes. Fracture due to strong shearing stress components emits waves with longer duration and lower frequency than compression.

In Chapter 5 has been a combined study of elastic wave techniques on cementitious material with simulated damage. The main objective is to help in establishing tools for detailed assessment of the material's condition. Wave velocity can be quite accurately used to correlate to the damage content in the form of light spherical-like inclusions. Experiments are supported well by scattering theory, the results of which are in very good agreement for the experimental frequencies.

Additionally, the load bearing capacity of the specimens is tested. Though ultrasonic parameters do not exhibit similarly strong correlations with the ultimate load, specific parameters of AE seem to correlate better. This is reasonable since the ultimate load depends on the fracture incidents which are monitored through the emitted acoustic waves. Energy related parameters of AE reveal quite strong correlations directly to bending strength implying that apart from ultrasonic velocity which has been used for empirical correlations with strength,

In Chapter 6 has been studied the investigation of novel monitoring parameters as to their characterization power over fire-damaged concrete quality that could act complementarily to the UPV, which is a traditional and established parameter for strength estimation. UPV can be directly connected to elasticity and empirically to strength. The well-known correlations seem to hold for the case of this study as well. Use of ultrasound can easily discern between sound and fire-damaged concrete, while it is proven sensitive to changes in the sustained temperature. However, one aspect that has not been sufficiently studied, is the correlation between the mechanical properties of fire-deteriorated concrete and the AE behavior. In the framework of this study, quite strong correlations emerge. Parameters related to the emitted energy during the fracturing events, as well as waveform descriptors, like the number of threshold crossings show similarly good correlation with the mechanical properties related to strength (in bending and compression) and absorbed energy (in bending)

In Chapter 7 has been studied the influence of fire-damage in Reinforced concrete. Due to extensive spalling of the fired damaged Reinforced bending and compression specimens both the mechanical tests and the Nondestructive monitoring techniques in the form of ultrasonics (ultrasonic pulse velocity, UPV) and acoustic emission (AE), were not been able to applied because the extensive damage leads to the change of the shape of the fired damaged specimens. The study should be repeated with different lower max temperatures this time so as to investigate the influence of fired damage in steel rebar reinforcement in concrete structures.

8.2. Suggestions for future work

The passive characterization of the cracking mode with the acoustic emission technique can prove very beneficial for structural health monitoring operations as it supplies information that cannot be yielded by any other NDE technique. Discrimination of the modes is accomplished by a few AE parameters which is very encouraging for in-situ application. Apart from this, the analysis can assist material characterization studies in laboratory as it reveals the sensitivities of the material at different stress states. On the other hand, results highlight the need to jointly study AE with elastic wave propagation since the distortion and attenuation imposed by the medium even in an additional distance of a few centimeters alters significantly the frequency content and shape of the acquired waveforms by masking the original characteristics of the emitted wave even in small laboratory samples. This distance between the cracking source and the sensor is of primary importance, since an additional propagation of 40 mm poses substantial changes in the values of AE features especially for heterogeneous materials.

Future efforts should employ larger concrete specimens and recording of signal by more sensors and longer propagation distances while the testing set up could be improved by the aid of FEM analysis in order to result to pure shear fracture instead of mixed mode. This is an important parameter that needs to be amended in order to fully exploit the capabilities of AE in laboratory and expand reliable characterization in real structures.

In monolithic structures, passive monitoring by AE can provide information on the stress field and the fracture pattern which cannot be provided by other non-invasive techniques. These materials (granite and marble) are adequate to highlight the effect of pure stress field in AE without serious influence of the microstructure on the wave propagation and the fracture itself. The effect of attenuation due to damping will be studied through the results of multiple sensors, something that will help to upgrade the test to larger geometries.

In general passive monitoring with the Acoustic Emission technique should be studied complimentarily in order to improve the rough estimations of strength offered by ultrasonic velocity. Especially in fire damaged concrete evaluation the energy released during fracture incidents will vary significantly depending on the existence or not of fire damage. Based on the presented correlations, inclusion of

AE in the armory of NDT for concrete assessment can provide additional parameters, the characterization capacity of which concerning the remaining strength after fire damage.

Publications

Scientific papers in peer-reviewed journals

1. Effect of wave distortion on acoustic emission characterization of cementitious materials ,Construction and Building Materials, Volume 35, October 2012, Pages 183-190 D.G. Aggelis, A.C. Mpalaskas, D. Ntalakas, T.E. Matikas.
2. Acoustic signature of different fracture modes in marble and cementitious materials under flexural load, Mechanics Research Communications 47 (2013) 39-43. D. G. Aggelis, A. C. Mpalaskas, T. E. Matikas.
3. Influence of damage in the acoustic emission parameters, Cement and Concrete Composites 44 (2013) 9-16, A. Carpinteri, G. Lacidogna, F. Accornero, A. Mpalaskas, T.E. Matikas, D. G. Aggelis.
4. Investigation of different fracture modes in cement-based materials by acoustic emission, Cement and Concrete Research, accepted 2013. D. G. Aggelis, A. Mpalaskas, T. E. Matikas..
5. Fracture Mode Identification in Cementitious Materials using Supervised Pattern Recognition of Acoustic Emission Features, Construction and Building Materials, in press 2014 10.1016/j.conbuildmat.2014.05.015, A. Farhidzadeh, A.C. Mpalaskas, T.E. Matikas, H. Farhidzadeh, D.G. Aggelis.
6. Mechanical and fracture behavior of cement based materials characterized by combined elastic wave techniques, Construction and Building Materials 50 (2014) 649–656, A.C. Mpalaskas, O. Thanasia, T. E. Matikas and D. G. Aggelis.
7. Monitoring of the fracture mechanisms induced by pull-out and compression in concrete, accepted, Engineering Fracture Mechanics, 2014, A. C. Mpalaskas, I. Vasilakos, T. E. Matikas, D. G. Aggelis.
8. 13 - Acoustic monitoring for the evaluation of concrete structures and materials Acoustic Emission and Related Non-Destructive Evaluation Techniques in the Fracture Mechanics of Concrete, 2015, Pages 269-286, D.G. Aggelis, A.C. Mpalaskas, T.E. Matikas
9. List of contributors Acoustic Emission and Related Non-Destructive Evaluation Techniques in the Fracture Mechanics of Concrete, 2015, Pages ix-x F. Accornero, D.G. Aggelis, L. Calabrese, A. Carpinteri, A. Deraemaeker, C. Dumoulin, M. ElBatanouny, F. Grondin, K. Izuno, G. Karaiskos, Y. Kawasaki, G.

Lacidogna, L. Linzer, A. Loukili, A. Manuello, T.E. Matikas, L. Mhamdi, A.C. Mpalaskas, G. Niccolini, K. Ohno, T. Okamoto, et al.

Scientific papers in peer-reviewed conferences proceedings

1. Acoustic emission signatures of damage modes in structural materials, SPIE Smart Structures/NDE, 10-14 March 2013, San Diego, USA, D. G. Aggelis, A.C. Mpalaskas, T. E. Matikas, D. Van Hemelrijck.
2. A study on the identification of different fracture modes in cementitious materials by simple acoustic emission parameters. Structural Faults and Repair 2012, 3-5 July 2012, Edinburgh, UK , D. G. Aggelis, A. Mpalaskas, T. E. Matikas.
3. Monitoring of fracture in fire-damaged concrete using acoustic emission, The 6th Kumamoto International Workshop on Fracture, Acoustic Emission and NDE in Concrete – KIFA-6, 17-18/9 2013, A.C. Mpalaskas, T. E. Matikas, D. G. Aggelis.
4. Acoustic emission signatures of damage modes in concrete, Proc. SPIE 9062, Smart Sensor Phenomena, Technology, Networks, and Systems Integration 2014, 90620P (22 April 2014); doi: 10.1117/12.2044750, ISBN 9780819499882, D. G. Aggelis, A.C. Mpalaskas, T. E. Matikas, D. Van Hemelrijck.